On Metal Speciation and Bioavailability in the Biosphere via Estimation of Metal-Ligand Thermodynamic Properties

by

Apar Prasad

A Dissertation Presented in Partial Fulfillment
of the Requirements for the Degree
Doctor of Philosophy

Approved October 2019 by the
Graduate Supervisory Committee:

Everett Shock, Chair
Kevin Redding
Ryan Trovitch

ARIZONA STATE UNIVERSITY

December 2019

ABSTRACT

Due to analytical limitations, thermodynamic modeling is a lucrative alternative for obtaining metal speciation in chemically complex systems like life. However, such modeling is limited by the lack of equilibrium constant data for metal-complexation reactions, particularly for metal-organic species. These problems were ameliorated estimating these properties from 0-125°C for ~18,000 metal complexes of small molecules, proteins and peptides.

The estimates of metal-ligand equilibrium constants at 25°C and 1 bar were made using multiple linear free energy relationships in accordance with the metal-coordinating properties of ligands such as denticity, identity of electron donor group, inductive effects and steric hindrance. Analogous relationships were made to estimated metal-ligand complexation entropy that facilitated calculation of equilibrium constants up to 125°C using the van't Hoff equation. These estimates were made for over 250 ligands that include carboxylic acids, phenols, inorganic acids, amino acids, peptides and proteins.

The stability constants mentioned above were used to obtain metal speciation in several microbial growth media including past bioavailability studies and compositions listed on the DSMZ website. Speciation calculations were also carried out for several metals in blood plasma and cerebrospinal fluid that include metals present at over micromolar abundance (sodium, potassium, calcium, magnesium, iron, copper and zinc) and metals of therapeutic or toxic potential (like gallium, rhodium and bismuth). Metal speciation was found to be considerably dependent on pH and chelator concentration that can help in the selection of appropriate ligands for gallium & rhodium based anticancer

drugs and zinc-based antidiabetics. It was found that methanobactin can considerably alter copper speciation and is therefore a suitable agent for the treatment of Wilson Disease. Additionally, bismuth neurotoxicity was attributed to the low transferrin concentration in cerebrospinal fluid and the predominance of $Bi(OH)_3^0(aq)$. These results demonstrate that metal speciation calculations using thermodynamic modeling can be extremely useful for understanding metal bioavailability in microbes and human bodily fluids.

ACKNOWLEDGMENTS

This project would not have been possible without the help of several people. Firstly, I would like to thank my advisor, Prof. Everett Shock, for providing me with the idea of metal speciation in bodily fluids and supporting me up to its fruition. His multi-disciplinary approach inspired me to look beyond the conventional boundaries of chemistry, geochemistry, microbiology and medicine. I would forever be grateful to him for my time at Arizona State University. I would also like to thank my committee members- Prof. Kevin Redding for helpful discussions of protein chemistry and honest feedback on the relevance of my work; and Prof. Ryan Trovitch for scientific and professional advice on inorganic chemistry. I would also like to extend my gratitude to Prof. Chad Borges who pointed out the error in my copper speciation simulations and shared his insights on metal toxicity. Their support and guidance immensely helped in the completion of this project.

My project was substantially buoyed by periodic scientific discussions with my peers. I would especially like to thank Kirtland Robinson for his conversations and insights on thermodynamics- a topic most scientists refrain from indulging in. Suggestions made by Grayson Boyer had a direct impact on the trajectory of this project. I am indebted to Dr. Jeff Dick and Brian St Clair for invaluable help during my comprehensive exam. I would also like to thank Alta Howells and Tania Miguel Trabajo for their ideas and suggestions on microbiology. This research was directly or indirectly enhanced by other members of GEOPIG- James Leong, Charlene Estrada, Tucker Ely, Peter Canovas, Kristin Johnson, Alysia Cox, Kris Fecteau, Vince Debes, Lindsey Howe

and Jordyn Robare. I would also like to thank my friends from outside research that helped me get through the graduate school life- Karan Syal, Pranav Chandra, Tamal Mukherjee, Vijeyta Sharma, Pankaj Chabra, Harshad Surdi, Pradyumna Muralidharan, Vaishnavi Govindarajan and Raghuraj Hathwar.

Finally, I would like to thank my family for their unconditional love and support. My parents Swami Dayal Prasad and Jyotirmayi Prasad have made countless sacrifices that allowed me to pursue this obsession of truth. My brother Shikhar Srivastav stood by me during the toughest of times and without him, I would have been lost. My sister-in-law Tanya Gupta Srivastav has been a source of joy and happiness ever since she has entered the family. This dissertation is as much theirs as it is mine.

TABLE OF CONTENTS

Page

CHAPTER Page

CHAPTER Page

APPENDIX Page

LIST OF TABLES

Table Page

LIST OF FIGURES

Figure Page

Figure Page

Figure Page

Figure Page

CHAPTER 1
INTRODUCTION

1.1 Essential Metals, Toxic Metals and Metal Speciation

Metals are indispensable to life. They act as centers for catalytic activity in enzymes, impart stability to protein structure and drive signaling and energy transfer in cells (Lehninger et al. 2004). In fact, considering the essential role they play, it may be argued that metals bring organic chemistry to life. However, metals are also associated with toxic activity. Lead poisoning, for example, is considered one of the prominent factors that brought down the Roman civilization (Delile et al. 2014 and Delile et al. 2017). More recently, lead poisoning has been associated with the rise of violent crime in the US from 1970-1990 (Nevin 2000) and with civilian deaths in Flint, Michigan (Hanna-Atisha et al. 2016 and Masten et al. 2016). Due to this dual nature, metals have attracted the attention of chemists and biologists for centuries.

However, classifying a metal as 'essential' or 'toxic' may be problematic (Templeton 2015). For example, manganese is a required cofactor for numerous enzymes essential for life and has a recommended daily intake of 0-10 mg/day (Institute of Medicine 2001). Conversely, $MnCl_2$ has an LD_{50} (lethal dose for 50% of population) value of 350-420 mg/kg in rats (ATSDR 2012). Thus, the same metal may be essential at one dosage but toxic at another, consistent with the old Paracelsian adage 'sola dosis facit venenum' (the dose makes the poison). Moreover, research over the last 40 years has shown that metal bioavailability is dependent on the chemical form/specimen of the metal. For example, the insoluble forms of nickel like Ni_3S_2 and NiO have much higher

cytotoxicity compared to the soluble forms like $NiCl_2$ and $NiSO_4$ (Apostoli et al. 2006 and Sunderman et al. 1988). Additionally, different soluble forms of metal have varying degrees of bioavailability with free metal ions and neutral, lipophilic complexes considered to be more bioavailable than charged, chelated forms of metal (Levina et al. 2017). Therefore, in order to understand the beneficial and toxic effects of metals on life, the knowledge of metal speciation is essential.

1.2 Obtaining Metal Speciation

Metal speciation in a system may be obtained using analytical techniques or using thermodynamic modeling. However, analytical techniques are extremely limited in measuring metal speciation for complex chemical systems (Kiss et al. 2017). On the other hand, thermodynamic modeling can calculate metal speciation at equilibrium for any complexity of system within seconds if the associated equilibrium constants are known. However, the lack of equilibrium constant data for metal-organic complexes severely limits the applicability of thermodynamic modeling in biological systems (Kiss et al. 2017 and Wilke et al. 2017). As biological systems are exceptionally diverse, experimentally obtaining equilibrium constants for all metal-ligand complexes in such a system is an extremely expensive and time-consuming strategy. Alternatively, researchers in the past few decades have used linear free energy relationships to fulfill the gaps in metal-ligand equilibrium constants (Irving & Rossotti 1956, Hancock & Marsicano 1976, Hancock & Marsicano 1978, Martell & Hancock 1996, Carbonaro & Di Toro 2007 and Atalay et al. 2013). These relationships are based on the simple assumption that the relative stability of cations for one ligand is proportional to the

relative stability of cations for a similar ligand. The simplicity and high applicability of this approach motivated us to extend these estimates to the ligands commonly found in biological systems including low molecular mass ligands like lactate and high molecular mass ligands like human serum albumin.

1.3 Estimating Metal-Ligand Stability Constants

In the second chapter, we explore the applicability of this approach for 220 monovalent oxygen ligands including carboxylates, phenols and inorganic acids. Monovalent oxygen groups are the most prevalent metal-coordinating groups found in nature and an understanding of their metal-coordination thermodynamics would be extremely useful to account for metal speciation and distribution on Earth's crust. As metal-hydroxide and metal-acetate equilibrium constants have been measured for several cations at 25°C and 1 bar, hydroxide and acetate have been used as proxy ligands to estimate equilibrium constants for ~16,000 metal-monovalent oxygen ligand complexes. The slopes and intercepts of these linear free energy relationships have been explained based on steric effects, inductive effects and denticity. Analogous relationships have been obtained for metal-ligand complexation entropy that have facilitated equilibrium constant calculations from 0-125°C. A similar approach has been employed in Chapter 3 to estimate metal-ligand equilibrium constants for ~50 ligands prevalent in blood plasma and microbial growth media. However, different proxy ligands were employed to estimate equilibrium constants of chemically diverse ligands varying in electron donor groups and denticity such as dicarboxylates, vitamins, amino acids, peptides and proteins. Entropy estimations analogous to those ion Chapter 2 enabled calculation of equilibrium

constants from 0 to 125°C. This temperature range corresponds to the known temperature limits of living organisms and thus, may be used to obtain metal speciation in the biosphere.

1.4 Metal Speciation Calculations in Microbial Growth Media and Human Bodily Fluids

In order to investigate the biological implications of our predictions, we used these equilibrium constants to perform speciation calculations of previously reported microbiology studies in Chapter 4. Thermodynamic models of metal speciation have been employed in microbiology and geobiology for over 40 years (Sunda & Guillard 1976, Sunda & Ferguson 1983, Sunda & Huntsman 2000, Unsworth et al. 2006 and Sierra et al. 2017). Early investigations on relationship between metal speciation and microbial toxicity suggested that only the free metal ion is bioavailable, giving birth to the free ion activity model (FIAM) (Morel et al. 1979). However, subsequent research suggested that low molecular weight complexes of metal may also be bioavailable (Poldoski et al. 1979, Pärt & Wikmark 1984 and Daly et al. 1990). The present scientific consensus is that in addition to the free metal ion, metal-ligand complexes of low molecular mass ligands (like citrate) and high molecular mass ligands (like the protein human serum transferrin) are also taken up by living cells via different uptake mechanisms (Levina et al. 2017). However, in our survey of the microbiology literature, we found a few studies where conclusions regarding the relationship between metal speciation and bioavailability were made without appropriate metal speciation calculations or experiments (Laube et al. 1980 and Ahsanullah & Florence 1984). We therefore calculated metal speciation for two of

these studies utilizing equilibrium constants from the previous chapters and those for which experimental results were available in the literature. Our simulations revealed that incorrect conjectures were made in these studies due to improper metal speciation assessment. We have performed similar calculations for some currently used growth media compositions evaluating the dependence of pH and chelator concentration on metal speciation.

In Chapter 5, we have investigated the medicinal implications of our equilibrium constant by calculating metal speciation for 10 biologically relevant metals in human bodily fluids. Metal speciation calculations in human bodily fluids are generally performed for very simple systems with a handful of metals, low molecular mass ligands and proteins (May et al. 1976, May et al. 1977, Kiss et al. 2009, Enyedy et al. 2015, Wilke et al. 2017). In our speciation calculations, we have included ~50 ligands present in blood plasma at >1 μM concentration including proteins like transferrin, albumin and ceruloplasmin and peptides like glutathione. This is the most comprehensive speciation model of blood up to the best of our knowledge. In the chapter, we have also made predictions regarding the anticancer activity of gallium and rhodium-based drugs, the antidiabetic activity of zinc-based antidiabetics and neurotoxicity of bismuth. It may be worth noting that rhodium and bismuth speciation has been obtained almost entirely from estimation of our equilibrium constants. We encourage further investigation in experimental verification of rhodium and bismuth speciation and of the associated equilibrium constants with proteins, peptides and low molecular mass ligands. Other suggestions for future directions have been summarized in Chapter-6.

CHAPTER 2

METAL-LIGAND THERMODYNAMICS IN THE BIOSPHERE-ESTIMATING STABILITY CONSTANTS AND ENTROPIES FOR REACTIONS BETWEEN AQUEOUS METAL IONS AND MONOVALENT OXYGEN-BEARING LIGANDS

2.1 Introduction

From the naturally occurring lactic acid to the artificially synthesized epilepsy drug valproic acid, low molecular mass ligands are integral parts of modern biochemistry, environmental geochemistry, and geobiology. Similarly, many metal ions like calcium, iron, copper and zinc are integral to the functioning of cellular processes while others like cadmium and lead can be toxic even at low concentrations. Almost all organic ligands bond with metal ions via their oxygen, nitrogen or sulfur atoms affecting bioavailability through metal speciation, which is a direct function of metal-ligand thermodynamic properties. However, the thermodynamic measurements for such complexes are far from complete and in a world of constantly increasing pharmaceuticals and anti-microbial drugs, there is a pressing need for alternatives to protracted experimental measurements that may be expensive and time-consuming. This motivated us to estimate stability constants (log K_{ML}) and standard entropy changes ($\Delta S°_{ML}$) at 25°C and 1 bar for metal complexation reactions with monovalent oxygen-bearing (O^-) ligands. These estimates facilitate metal speciation calculations for systems like microbial growth media and all aqueous geochemical and geobiological systems within the biologically relevant temperature range up to 125°C.

In addition to the high abundance of oxygen on the planet, its prevalence among metal-bonding ligands reflects its reactivity. The highly electronegative nature of oxygen

predisposes it to take up the negative charge on the ligand following the loss of a proton akin to a weak acid or strong alcohol. We have focused on monovalent oxygen ligands here as such molecules are generally seen in high abundance within Earth's aqueous systems and are likely to be of biological relevance. Ligands like lactate, ascorbate and phosphate are integral components of blood plasma and many microbial growth media (Sunda and Guillard, 1976; Geigy, 1981; Jackson and Byrne, 1996; Kim et al., 2012). Other O^- ligands like silicate, bicarbonate and acetate are commonly found in hot springs and oilfield brines (Willey et al., 1973; Shock, 1998; Amend et al. 2003, Shock and Canovas 2010). Studying such ligands may also be useful in the context of metal association with polymeric ligands like proteins and humic substances which may have monovalent acidic or phenolic side-chains.

We developed ligand-specific linear free energy relations (LFER) and analogous entropy correlations to estimate stability constants and entropies of association for metal complexes of monovalent oxygen ligands using corresponding thermodynamic properties of metal-acetate or metal-hydroxide complexes. A linear relationship was also obtained between the protonation constant (pK_a) and protonation entropy for several monovalent oxygen ligands like carboxylates and phenols. These relationships enabled the estimation of metal-ligand stability constants from 0-125°C within 1 log unit when only the ligand pK_a is known.

We compiled our dataset of experimental measurements from original papers while critically evaluating the data. As suggested from the title of this work, our estimation strategy is based on chemical properties of the electron-donating atom of the ligand. While some previous work has alluded to this strategy (Hancock and Marsicano,

1978; 1980; and Hancock, 1997), we chose to use the best proxy ligand for which most data was available. This approach was picked on observing that the predictive ability of correlations decreased as the ligands differed on moving from the negatively charged oxygen to other parts of the ligand, thus revealing a simple chemical basis. Our work also shows that some of the previously held notions about denticity may need revision and explain why different estimation strategies need to be employed for different O^- ligands.

Equilibrium speciation calculations are routinely used to determine the elemental distribution of a system and due to the limitations of analytical techniques (Levina et al., 2017), they are often the only option available. Such simulations are particularly accurate in studying complex formation and protonation as these processes are extremely fast and hence equilibrium can be reached within seconds (Tipping, 2002). Thus, our estimates of equilibrium constants of these complexation reactions can be directly applied to study metal or ligand speciation in any aqueous system within 0 to 125°C, i.e., the whole biosphere.

2.2 Definitions and data evaluation

The reactions studied in this work can be generalized by the following equation:

$$M^{y+} + L^{-} = ML^{y-1} \quad (1)$$

where *M* refers to the metal ion of charge *y*+ and *L* indicates the monovalent O^- ligand. Each such reaction has a corresponding overall standard state equilibrium constant, K_{ML}, and entropy change of the reaction, $\Delta S°_{ML}$.

The standard state equilibrium constant (generally given in the logarithmic form as log K_{ML}) is generally obtained upon measuring the stoichiometric constants over

multiple concentrations and extrapolating to zero ionic strength (I). Many scientific investigations, however, report stoichiometric constants at a single ionic strength (generally 0.15 or 0.7 for applications in blood or seawater, respectively). We extrapolated these data to zero ionic strength using the B-dot equation which is an extended Debye-Hückel equation (Helgeson, 1969). While the B-dot equation was primarily devised to deal with inorganic species, we found that the equation worked extremely well for organic species when extrapolating data at $I \leq 0.5$ and occasionally for higher ionic strength. It should be noted that this is the same equation employed by the equilibrium speciation software EQ3/6 (Wolery, 2010). Thus, no extrapolation errors would be made upon using the modified equilibrium constant at the original ionic strength with EQ3/6 or other codes that employ the B-dot equation Reports that explicitly defined the terms and conditions were preferred over ill-defined reports and those with extreme disparity of data were discarded in accordance with the guidelines as outlined in Martell & Smith, 1974; 1976; 1982; Smith & Martell 1975;1977; Smith & Martell, 1977; 1989; Pettit, 1984; Kiss et al., 1991; Berthon, 1995.

Standard states

In aqueous thermodynamics, the standard state refers to unit activity of the solute in a hypothetical one molal solution referenced to infinite dilution. In terms of the parameters reported in experiments, this state refers to an ionic strength of zero. Such a state is impossible to measure experimentally; standard state thermodynamic properties are either obtained upon extrapolating a series of low concentration solutions to infinite dilution or using theoretical approaches like the B-dot equation.

2.3 Estimation strategy

2.3.1 Stability constants

Numerous researchers have developed multiple LFERs to estimate metal-ligand stability constants. These relations are built on assumptions that the metal-ligand interaction is a function of the ligand pK_a (Irving and Rossotti, 1956; Carbonaro & Di Toro, 2007; Carbonaro et al., 2011; Atalay et al., 2013), the electrostatic potential of the metal ion as determined by the ratio of charge^2 to ionic radius (Davies, 1951), ligand electronegativity (Van Uitert et al., 1953) or Gibbs energy of metal ion formation (Shock & Koretsky, 1993; 1995; Prapaipong et al., 1999). However, these correlations are far from perfect and often have serious outliers or limited applicability. Thus, there is a need to create a set of LFERs with greater accuracy and extended applicability.

The correlations in earlier models reveal that metal-ligand thermodynamic properties are complex functions of several factors including: the type of ligand electron-donor atom, ligand denticity, chelate-ring size, ligand preorganization, inductive effects, steric effects, metal ionic radius, metal coordination number and the charge of metal or ligand. The majority of these factors can be attributed to the ligand, which suggests that ligand-based correlations may yield estimation methods of lower uncertainty. Consideration of multiple estimation strategies revealed that correlating properties of metal complexes for a ligand with those of a structurally similar proxy ligand minimizes variability among estimated thermodynamic properties. Thus, our strategy for the estimation of metal-ligand stability constants could be summed up as – pick the closest proxy ligand with the most data. The challenge is to understand what could be meant by 'the closest proxy ligand'. Ideally, the closest proxy ligand would adopt the same metal coordination geometry as that of the ligand of interest. Such a correlation would have an

intercept of zero and the slope would be a function of the inductive effects of the respective ligand sidechains as indicated by the corresponding pK_a values. However, ligand sidechains often sterically hinder the metal-ligand interaction or additionally coordinate with the metal ion. Such interactions are likely to produce negative and positive intercepts, respectively. By the same argument, ligands with a negative charge of 1 on an oxygen atom can be expected to behave similarly.

Analysis of the stability constant literature for monovalent oxygen ligands shows that there are abundant experimental stability constants for metal-hydroxide and metal-acetate complexes, which guided our decision to use acetate and hydroxide as the closest proxy ligands to investigate multiple monovalent oxygen ligands together. While metal-acetate LFERs were successful for most carboxylates, metal-hydroxide correlations were more successful for alcohols and inorganic monovalent oxygen ligands, as described below. Choosing between acetate and hydroxide as the proxy ligand is based on the structure of the ligand and tested with the applicability of the LFER (*i.e.*, considering slope, intercept, and correlation coefficient).

Experimental values of the dissociation constant, pK_a, are available for almost all compounds that produce O^- ligands. As a result, we included protonation constants along with the metal stability constants in our correlations, which enhanced individual correlations and considerably expanded our estimation capabilities. We also found that a substantial number of $\log K_{ML}$ measurements are available for only a few ligands. Thus, we have divided the ligands into the following categories (1) ligands with many $\log K_{ML}$ data, (2) ligands with few $\log K_{ML}$ data, (3) ligands with no $\log K_{ML}$ data.

2.3.2 Entropy of association

Compared to stability constants, many fewer attempts have been made to estimate standard-state entropy changes ($\Delta S°_{ML}$) for metal-ligand reactions (Cobble, 1953a; 1953b; Hinchey & Cobble, 1970; Shock and Koretsky, 1993; 1995, Sverjensky et al., 1997; Prapaipong et al., 1999; Prapaipong and Shock, 2001). This is understandable as there are limited $\Delta S°_{ML}$ data in the literature. As the previous attempts included only a few O^- ligands, there was considerable scope for making new estimates.

Our entropy estimation strategies are completely analogous to our stability constant estimation strategies mentioned above; we have correlated metal-ligand $\Delta S°_{ML}$ values against values of metal-acetate and metal hydroxide $\Delta S°_{ML}$. This approach differs from that employed in previous papers from this research group in which metal-ligand $\Delta S°_{ML}$ values were correlated with the third-law entropies of the metal ions. Thus, yet another motivation behind our work was to compare the two strategies. As our correlations possess a lower uncertainty (±2 cal $(mol\ K)^{-1}$ vs. ± 5 cal $(mol\ K)^{-1}$ obtained with correlations presented in previous papers, we believe these new correlations will yield more accurate estimates.

2.4 Estimating stability constants at 25°C and 1 bar

2.4.1 Ligands with many $logK_{ML}$ data

Among the O^- ligands, the most measurements of $logK_{ML}$ are for hydroxide and acetate with 69 and 52 values, respectively. While both are O^- ligands, acetate can coordinate in a bidentate fashion owing to resonance between its two carboxyl oxygens compared to the monodentate character of hydroxide. Thus, hydroxide is a close proxy ligand to estimate metal-acetate stability constants owing to the similarity in overall charge and the abundant supply of $logK_{ML}$. A correlation between the two datasets was

obtained (Fig. 1) which demonstrated that metal-acetate stability constants could be estimated from metal-hydroxide stability constants within ±0.5 log units, on the order of experimental uncertainty . The slope is close to the ratio of the respective pK_a values and the slightly positive intercept is in accordance with the bidentate nature of acetate. Theoretically, the intercept for LFER with hydroxide for O^- ligands should be zero and for polydentate O^- ligands should increase in increments of $\log_{10}(55.5)$ or 1.74 (Adamson, 1954; Martell & Hancock, 1996). The $\log_{10}(55.5)$ factor can be derived from a dimensionless expression of the equilibrium constant and refers to the molality of 1 kg of pure water. This phenomenon has been investigated thoroughly for analogous amines and is known as the 'chelate effect' (Hancock & Marsicano, 1976). While the intercept here (0.37) is considerably less than 1.74, the repeated appearance of such intercepts for carboxylate vs. hydroxide LFERs (in detail below) suggests that there is a partial bidentate character to these ligands due to the chelate effect. The error bars in this figure correspond to the experimental uncertainties reported in the original papers. As can be seen in the figure, the correlation is within ± 0.5 log units of the stability constants for all the 44 ionic species. Similar uncertainties exist for other correlations. For consistency, we have used the limit of ± 0.5 log units as the target of estimation in our correlations, which is on the order of experimental uncertainty. It is important to note that a slope of greater than 1 in any acetate or hydroxide correlation (discussed below) can enhance this uncertainty, so we have worked to avoid steep slopes. Note also that the ultimate purpose of these correlations is to create a foundational framework that has wide-ranging applications. These correlations have been created using measurements of hundreds of

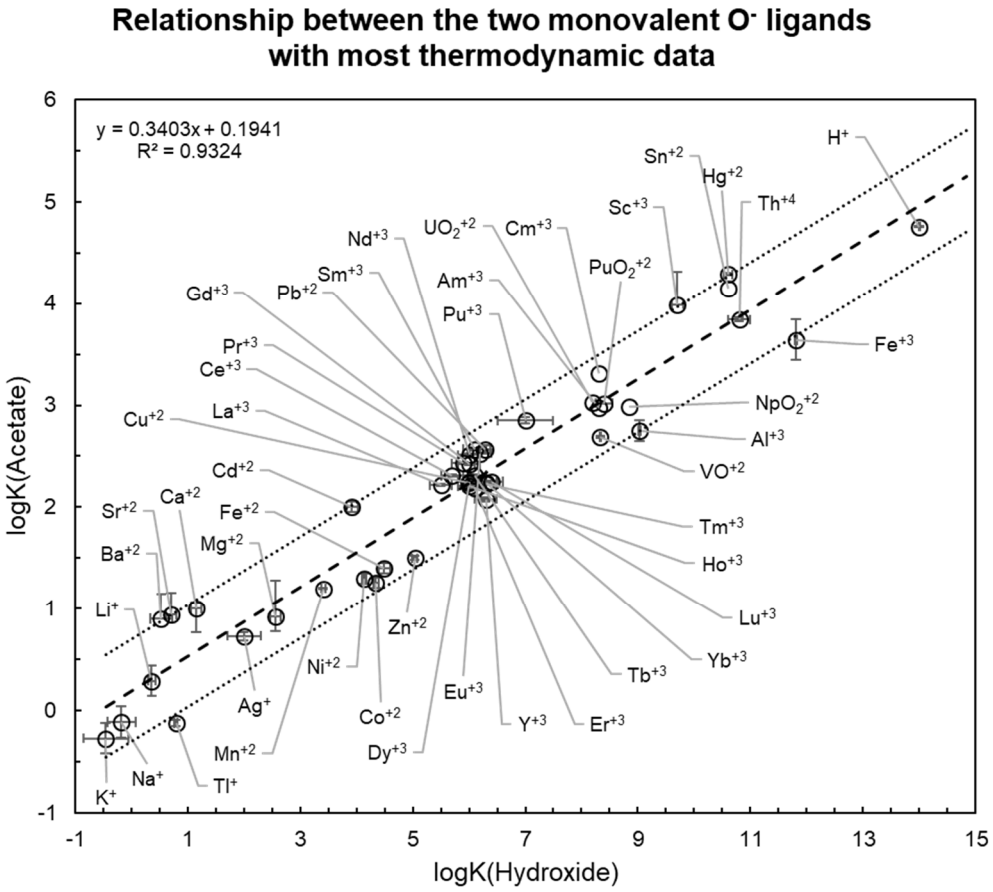

Fig 1. LFER between acetate and hydroxide stability constants with 44 metal ions and proton. Error bars correspond to uncertainties in experimental measurements from one study (straight) or the range of experimental measurements from multiple studies (*italicized*). Error bars are absent for some metal ions as they weren't reported in the original report. The dashed line is the trendline (equation on top) and the dotted lines represent the estimation uncertainty of ± 0.5 log units which is of the order of experimental measurements. As can be seen from the figure, all points lie within the estimation uncertainty.

scientific reports which are bound to have random variability. The consistent applicability of these correlations to a variety of ligands supports the utility of this approach.

In aqueous solution a ligand coordinates with a metal ion via its functional groups that have high electron density (Martell & Hancock 1996). Therefore, the interaction of a metal ion with a mono-alkyl carboxylate like propanoate can be expected to be similar to that with acetate. This is the case as shown in Fig. 2 where an LFER between metal-propanoate complexes and metal-acetate complexes has both slope and R^2 close to 1 and an intercept close to 0. This LFER allows estimates of stability constants of 20 additional metal-propanoate complexes with substantial accuracy (as the number of experimentally constrained metal-acetate stability constants is 52 while that for metal-propanoate complexes is 32). Additionally, a slightly weaker relationship was also obtained between stability constants of metal-propanoate vs. metal-hydroxide complexes. While the values of slope and R^2 displayed on the figure are expected, the intercept differs substantially from 0. One possibility for the non-zero intercept arises from resonance, if both the oxygens of the propanoate have a partial negative charge and hence both groups participate in the interaction with a metal ion. As explained above, the theoretical intercept for a bidentate O^- ligand with hydroxide should be 1.74. While the intercept here (0.47) is considerably less, the repeated appearance of such intercepts for carboxylate vs. hydroxide LFERs (in detail below) suggest that there is indeed a partial bidentate character to these ligands. Nonetheless, as there are more experimentally determined association constants for hydroxide complexes than for acetate complexes, an additional 17 estimates for metal-propanoate complexes are possible with the LFER shown in Fig. 2, albeit with greater uncertainty compared to the acetate-based estimates.

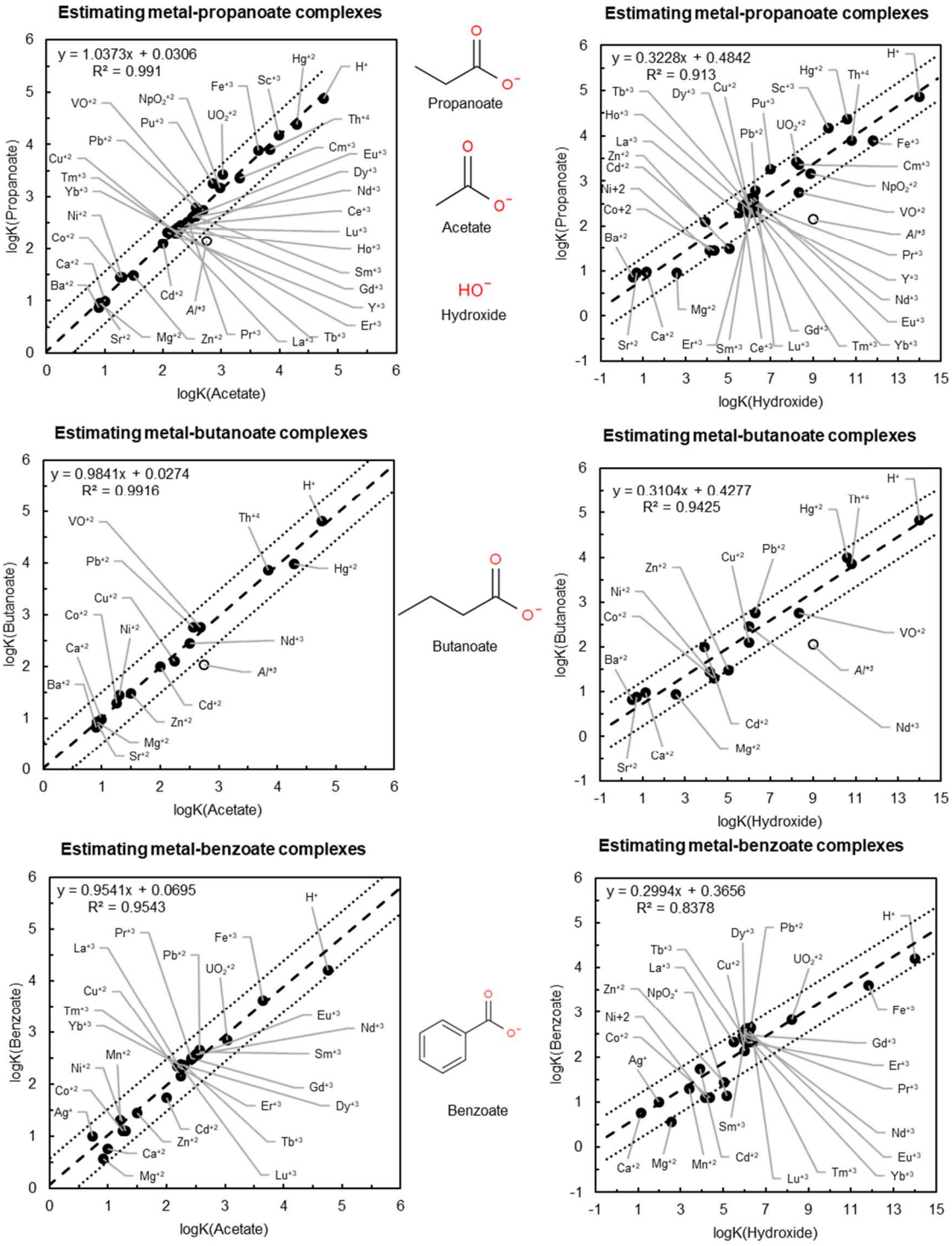

Fig 2. LFERs for carboxylic acids with different side groups (contd.)

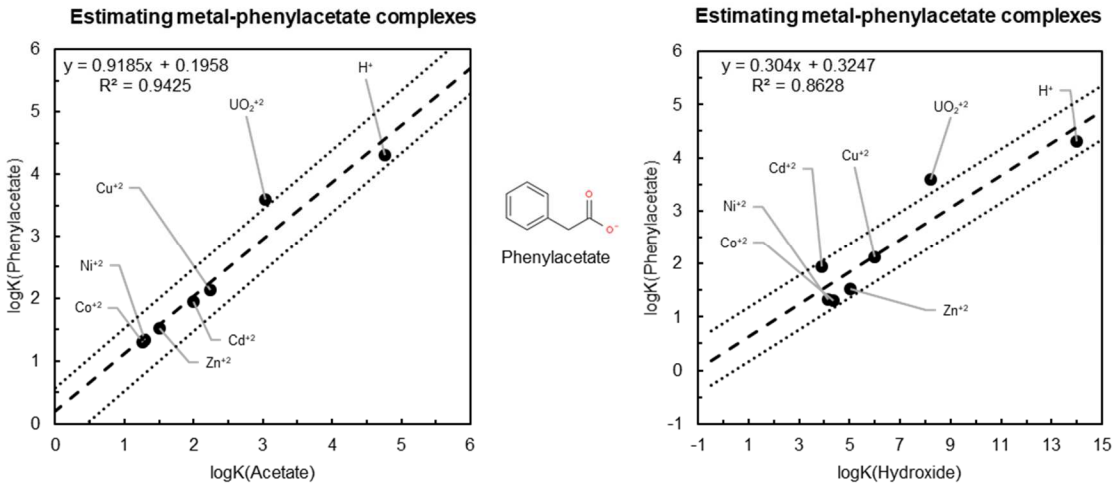

Fig 2. (contd.) LFERs for carboxylic acids with different side groups

As in the case of propanoate, the butanoate vs. acetate LFER exhibits both slope and R^2 close to 1 and an intercept of 0 (Fig. 2), and the corresponding parameters for the hydroxide correlation shown in Fig 2d are almost identical to those for propanoate. To investigate the involvement of aromatic groups in the metal-ligand coordination, we correlated benzoate and phenylacetate complexes in the same manner and found LFER results, shown in Figs 2, to be similar to those for propanoate and butanoate. This suggests that it is predominantly the carboxylate group in benzoate that interacts with metal ions in aqueous solution.

Analogous plots for nitroacetate, chloroacetate, bromoacetate and iodoacetate in Fig 3 reveal the consequences of inductive effects on LFER correlations built on acetate and hydroxide. Nitro-, chloro-, bromo- and iodo- are electron-withdrawing groups that can reduce the charge density at the carboxylate oxygens, and weaken interactions with metal ions or proton resulting in slopes less than unity. This effect appears to be larger for nitroacetate and smaller for the halogenated carboxylates. Note that the slopes are similar for the three correlations between halogen-substituted ligands and acetate. While intercepts differ among the halogen-substituted ligands, we suspect that the variability in intercepts can be explained by the relative lack of data for bromoacetate and iodoacetate.

As shown in Fig 4, correlations for isobutanoate and pivalate exhibit significantly lower intercepts compared with the ligands discussed above. While $\log K_{ML}$ data for these ligands are considerably lower than those for acetate, the pK_a values are almost identical. This suggests that there are steric effects at play. Perhaps the existence of multiple methyl groups at the alpha carbon of the respective ligands sterically hinders the metal-ligand bond thereby reducing its strength. The reason this is not seen in the case of the proton-ligand

interaction may be due to the smaller ionic radius of the proton making the proton-ligand interaction equivalent to that for acetate.

Taken together, Figs. 2, 3 and 4 illustrate deviations from ideality in LFERs. While additional coordinating groups increase the intercept (as seen in the hydroxide correlations of Fig. 2), steric effects decrease the intercept of the correlation due to the presence of non-coordinating groups close to the metal-ligand coordination sphere (as seen in Fig. 2), inductive effects can increase or decrease the slope of the correlation using the ligand pK_a as a guide (as seen in Fig. 3). Given the complexity and diversity of organic moieties, all these factors can be at play together in varying degrees for some ligands. We found this to be the case in some of the more structurally complicated monovalent oxygen ligands discussed next.

As can been seen in the correlations for ascorbate, aceturate, acetoxyacetate, cyanoacetate, lactate and pyruvate (Fig. 5), the intercepts fall between 0 and 1.74 – the theoretical intercepts for monodentate and bidentate ligands, respectively. Rather than a binary distribution between these intercept values, we found a gradation that increases from 0.19 for ascorbate to 1.06 for pyruvate. As an LFER correlation for homo-dentate ligands like acetate and propanoate has an intercept close to zero, as shown in Fig 2, these departures suggest that the associated side-chains of the ligands in Fig. 5 interact variably with the metal ions.

Even though ascorbate does not have a carboxylate group, its log K_{ML} data correlate closely with those for acetate while with hydroxide the correlation yields a slope

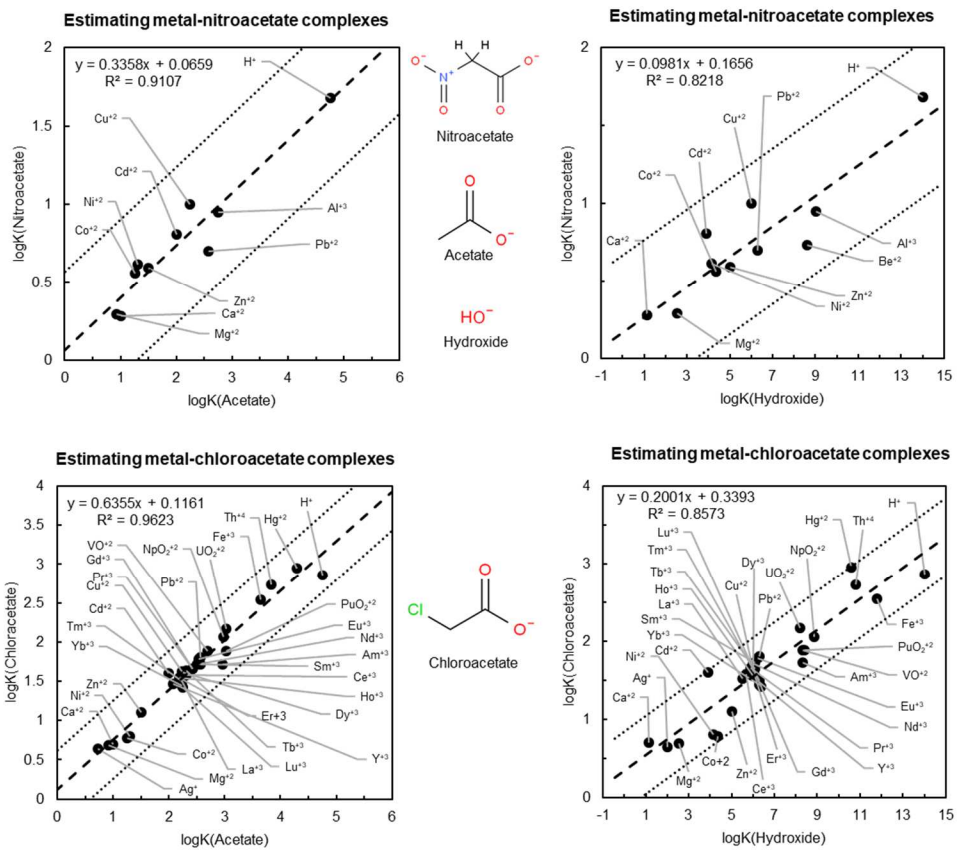

Fig 3. LFERs for carboxylic acids exerting significant inductive effects (contd.)

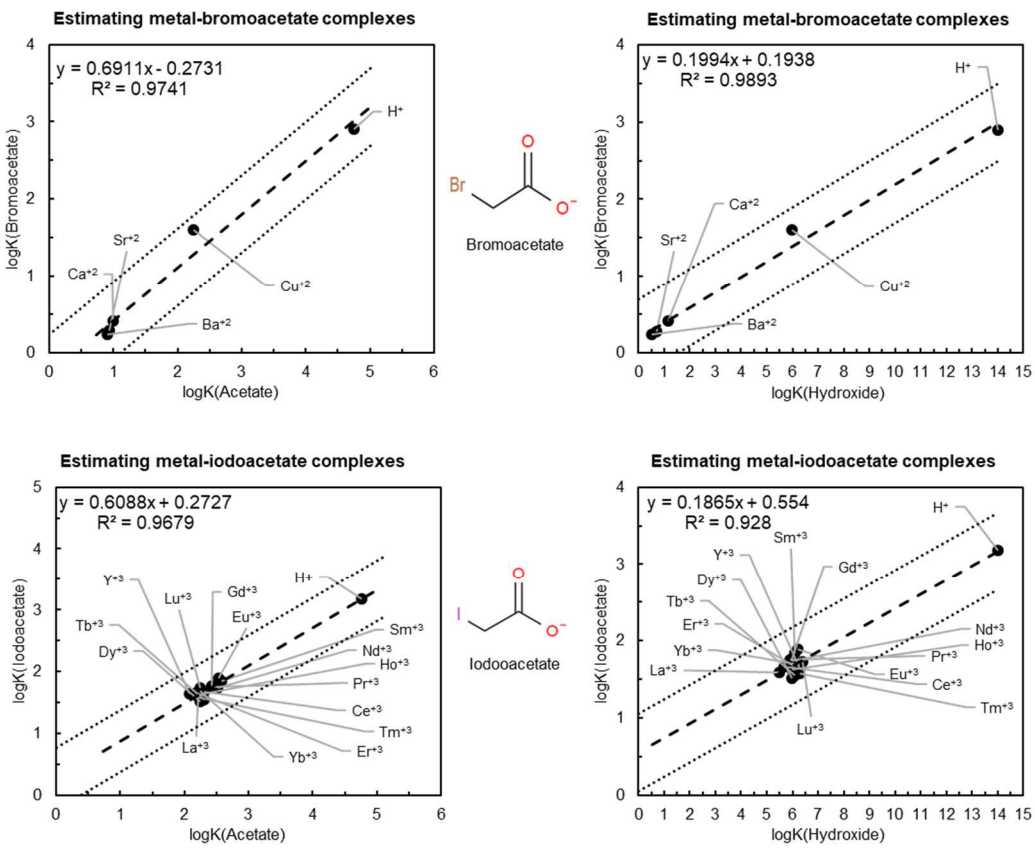

Fig 3. (contd.) LFERs for carboxylic acids exerting significant inductive effects

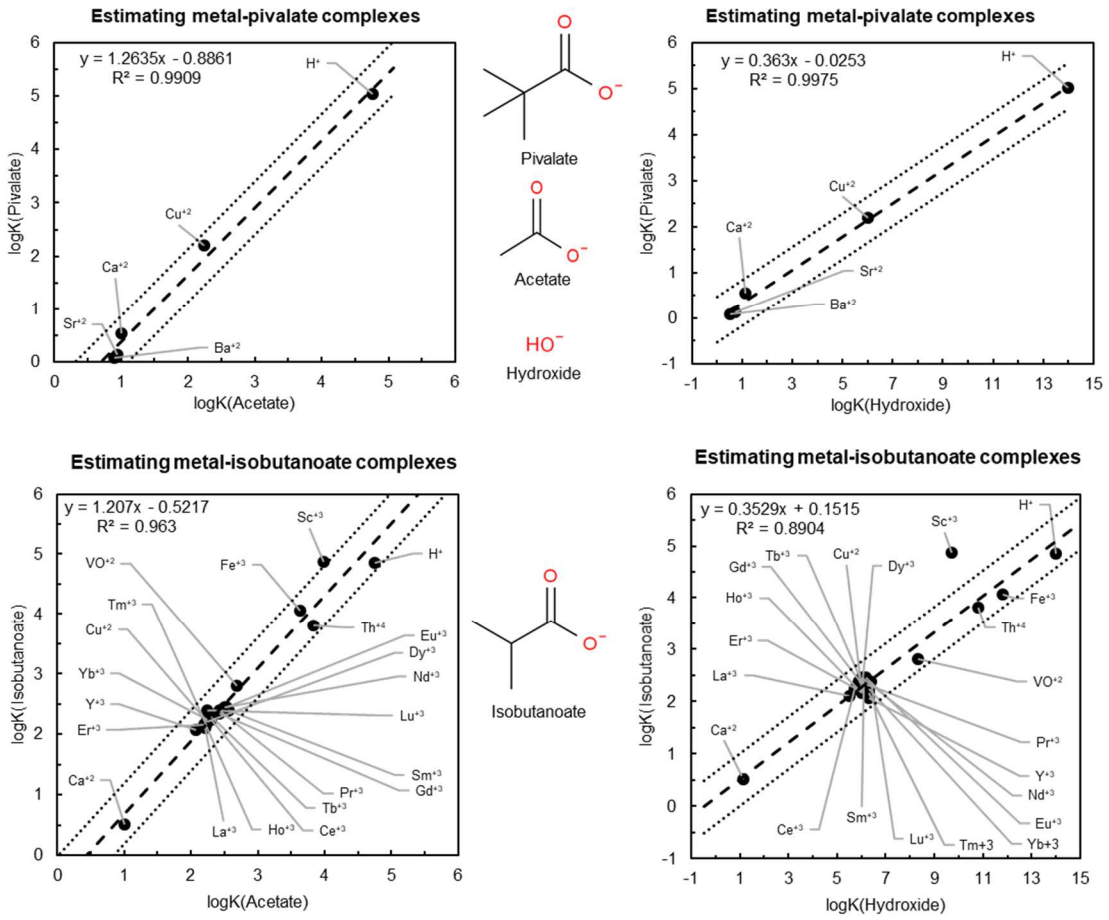

Fig 4. LFERs for carboxylic acids exerting significant steric effects

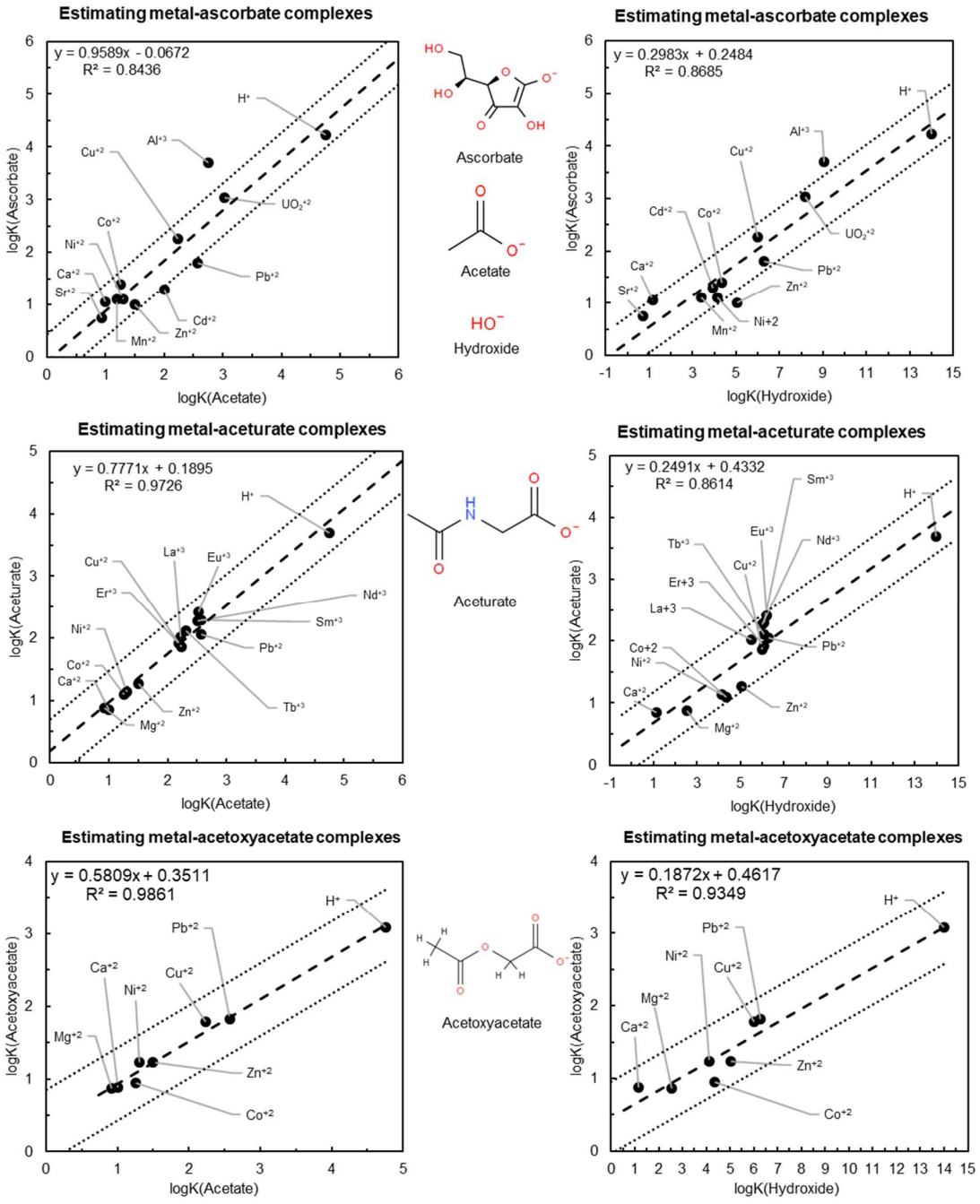

Fig 5. LFERs for monovalent oxygen ligands with additional coordinating functional groups with increasing additional denticity (contd.)

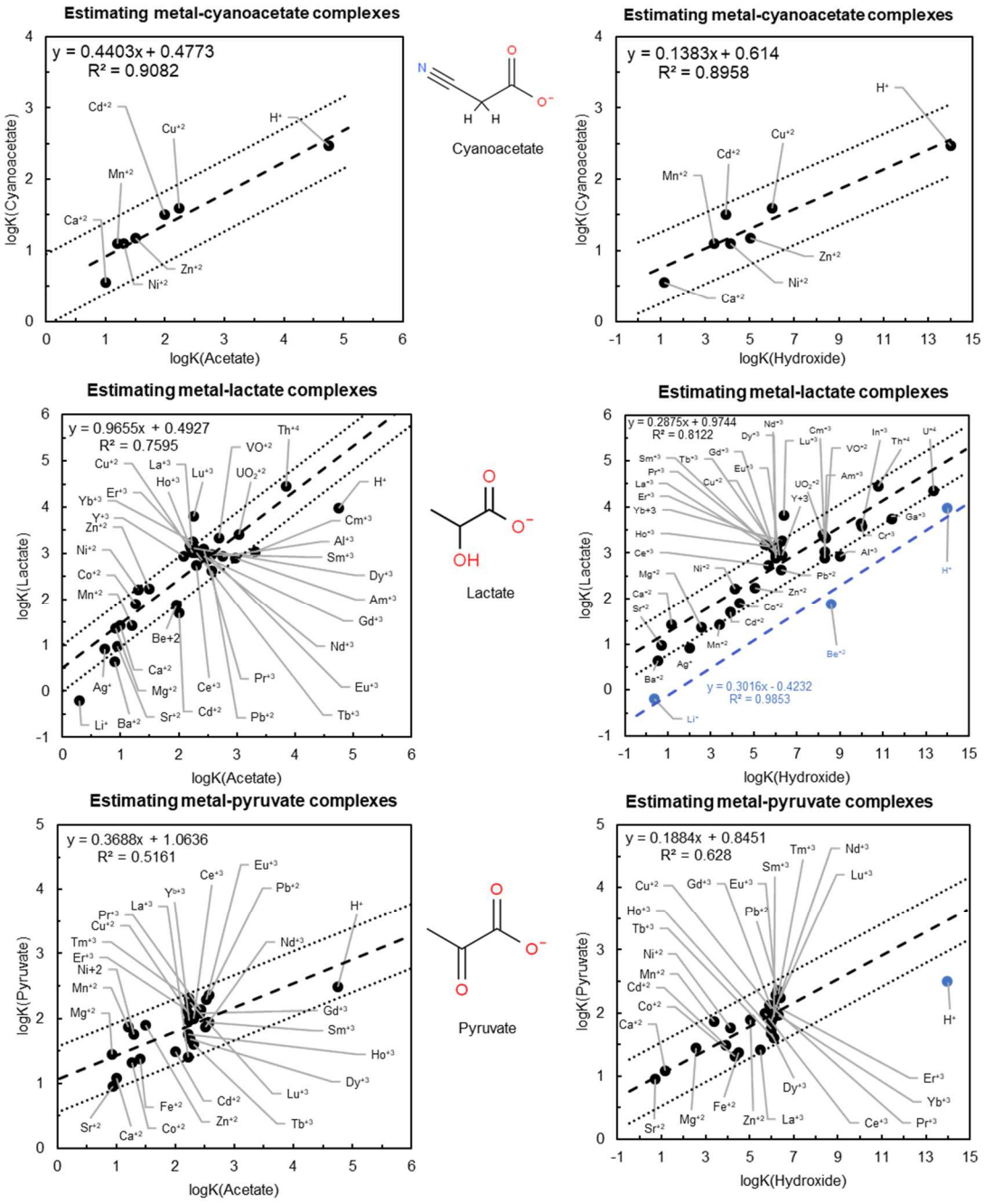

Fig 5. (contd.) LFERs for monovalent oxygen ligands with additional coordinating functional groups with increasing additional denticity

and intercept akin to other carboxylates. The intercepts for aceturate are slightly higher than those for ascorbate, perhaps due to the presence of an oxygen at the gamma position, but lower than those for acetoxyacetate, which has an additional oxygen at the beta position. The influence of the position and nature of these additional functional groups can be seen in the correlations of cyanoacetate, lactate and pyruvate. While cyanoacetate has a cyano-group at the beta position, lactate has a hydroxyl group at the alpha position and pyruvate has a carbonyl oxygen at the alpha position. If the close proximity of other functional groups to the carboxylate group generates a fluidity in the concept of dentition it could explain why lactate and pyruvate have higher intercepts. In addition, the lactate vs hydroxide LFER reveals an influence of metal ionic radius as the small metal ions Be^{+2} and Li^{+}, together with H^{+} (all Lewis acids), fall below the trend owing perhaps to their inability to coordinate with the alpha-hydroxyl group.

Formate and bicarbonate are two monovalent oxygen ligands with the carboxylate group but without the C-C bond. As the alkyl group is an electron-donating group, the lack of the C-C bond is perhaps the reason why the formate vs. acetate LFER (Fig. 6) has a lower slope. As the coefficient of determination (R^2) for the hydroxide correlation was higher than the acetate correlation, we used metal-hydroxide stability constants to estimate metal-formate $\log K_{ML}$. Ba^{+2} and Sr^{+2} were avoided in the correlation as the original report had excessively high stability constants for multiple ligands (Nancollas, 1956). It is worth noting that these metals plot on the correlation if the acetate stability constants from the same paper are used, suggesting a systematic bias. The intercepts of bicarbonate LFERs are lower than expected despite the presence of an additional metal-

coordinating group (the hydroxyl group). Maybe the very close proximity of these metal-coordinating groups is to explain for these observations.

Analogous correlations for monovalent oxygen ligands without the carboxylate group like phenol, borate and silicate show that hydroxide is a closer proxy ligand than acetate (Fig. 7). While this makes structural sense, hydroxide correlations also exhibit much lower slopes than the acetate correlations, consistent with the high pK_a values of these ligands, which is a positive contribution to the accuracy of these estimates. While the negative intercept for the phenol correlation may stem from the higher steric hindrance of the phenyl group, the positive intercepts of borate and silicate may result from the presence of additional hydroxyl groups on the ligand.

While a similar observation was made for nitrite, these LFERs for dihydrogenphosphate ($H_2PO_4^-$) and iodate (Fig. 8) reveal a different phenomenon. The measured pK_a values for these ligands were considerably smaller than expected from the trendline and we suggest that this may be due to the presence of additional metal-coordinating oxygens that increase the strength of the metal-ligand bond but can't do the same for the proton due its smaller size.

2.4.2 Ligands with limited $logK_{ML}$ data

The number of ligands with limited $logK_{ML}$ data far exceeds that for which abundant data exist. This is particularly true for copper-carboxylate complexes and ferric-phenol complexes. In many cases regressing the scant LFER data generates slope and intercept values that are unlike those obtained from more complete datasets. Using such regression results would likely induce large uncertainties in estimated values. To circumvent this problem, we regressed the LFER data by setting the intercept to zero and

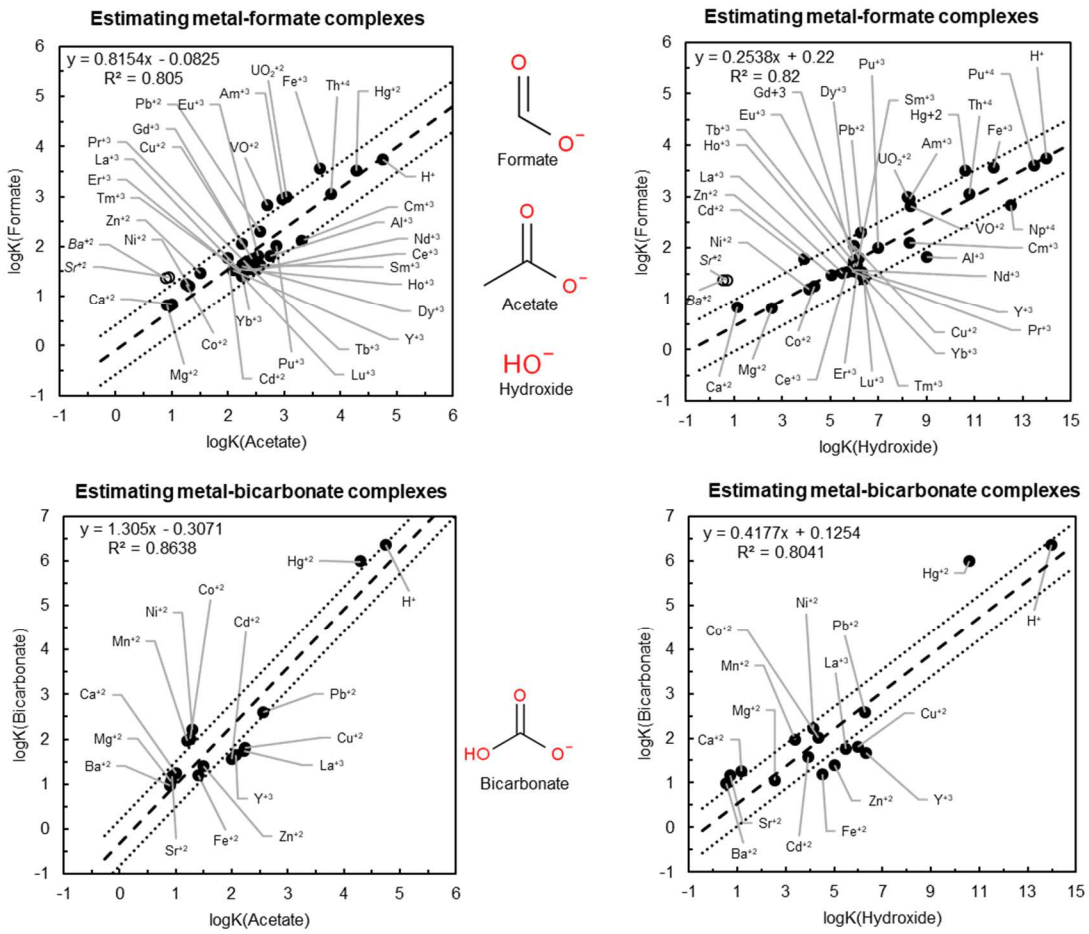

Fig 6. Both acetate and hydroxide LFERs seem equally applicable for two monovalent oxygen ligands with the carboxylate group but without C-C bond. The hollow circles are experimental measurements that were rejected upon critical evaluation from the literature.

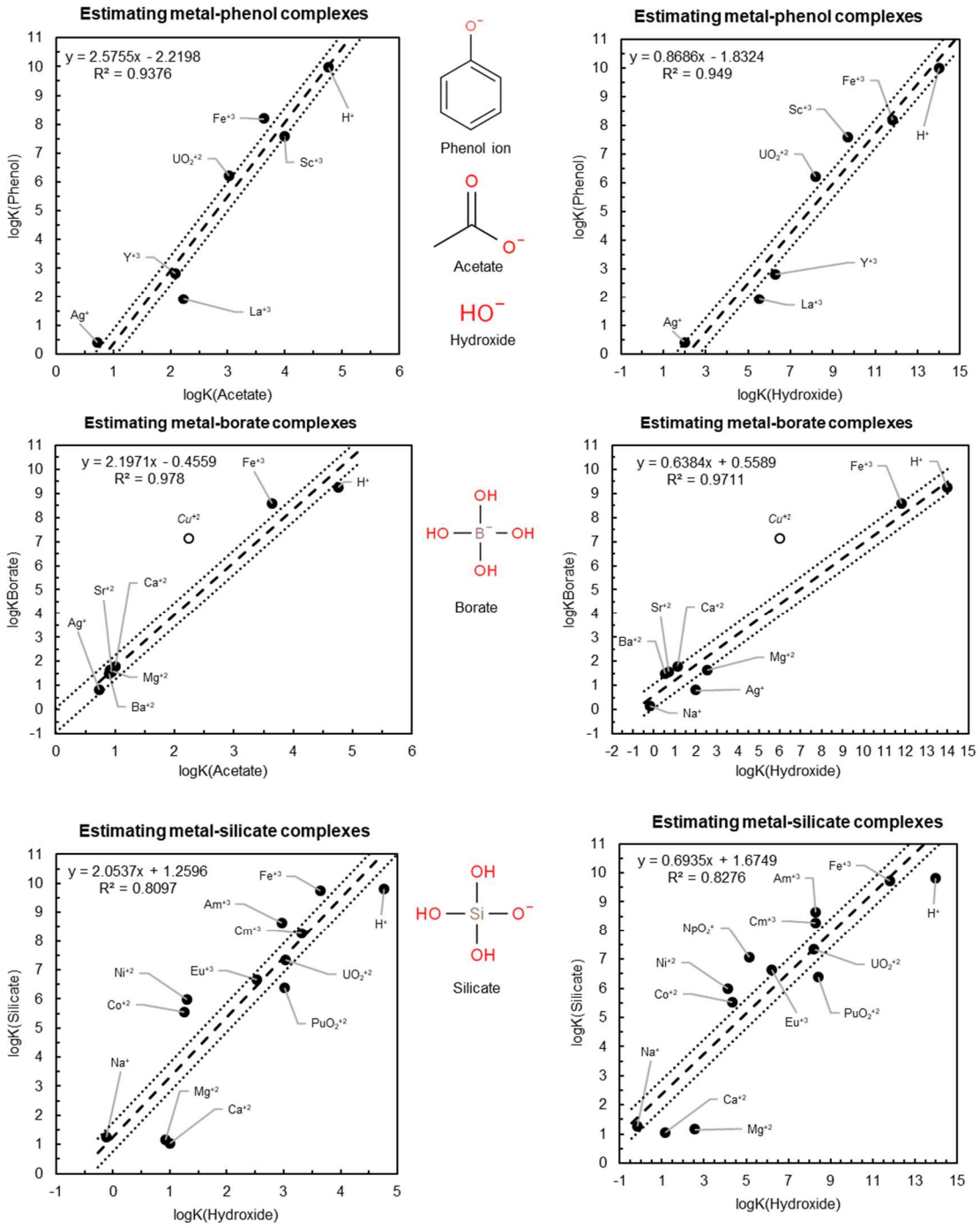

Fig 7. Hydroxide LFERs better than acetate LFERs for these monovalent oxygen ligands with high pK_a and no carboxylate group. The hollow circles are experimental measurements that were rejected upon critical evaluation from the literature.

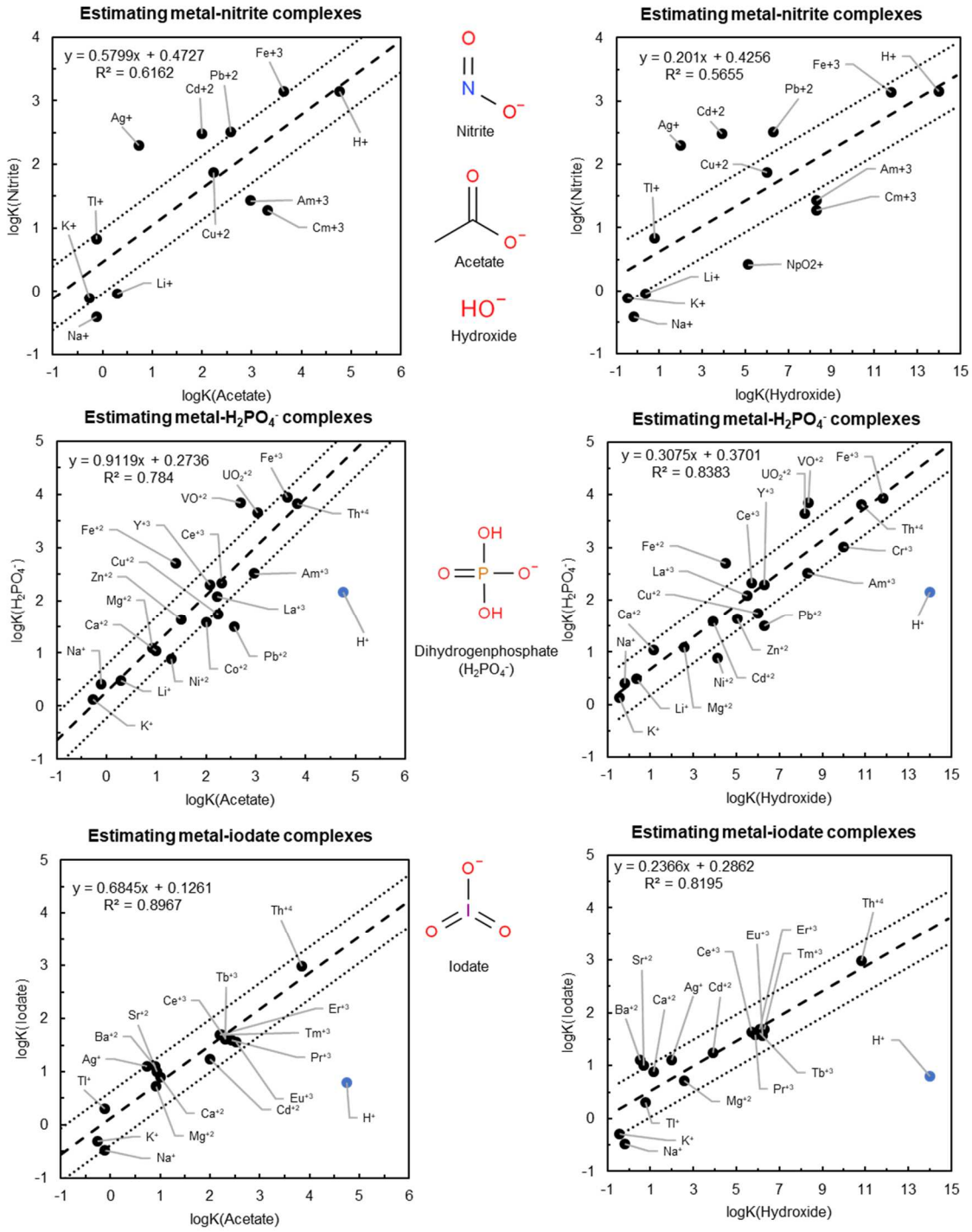

Fig 8. LFERs for some diverse inorganic monovalent ligands. The higher $\log K_{ML}$ (black) for dihydrogenphosphate and iodate is perhaps due to higher denticity. pK_a values (blue) have been correspondingly plotted separately.

obtaining slopes from 1-prameter fits that largely governed by the ligand pK_a. As a test of the usefulness of these correlations, we compared estimates from 1-parameter fits with those from 2-parameter fits for two ligands for which a moderate amount of $logK_{ML}$ data were available: 3-chloropropanoate and phenoxyacetate as shown in Fig. 9. The acetate correlations can be compared in Fig. 9(a) while the hydroxide correlations can be compared in Fig. 9(b). As seen in both cases, the 1-parameter correlations can be fit to all available stability constant data within ±0.5 log units. These correlations gave us confidence to set up similar correlations for a host of ligands with four or less $logK_{ML}$ values, some of which are shown in Fig. 10, in which Fig. 10(a) shows acetate correlations and Fig. 10(b) depicts hydroxide correlations. The resulting 1-parameter slopes were used to estimate stability constants for 2625 additional metal-ligand complexes comprising of 75 metal ions and 35 monovalent oxygen-bearing ligands. While the acetate correlations were given preference for carboxylates, the hydroxide correlations were used to estimate metal-phenol stability constants.

2.4.3 Ligands with no $logK_{ML}$ data

While there are no $logK_{ML}$ measurements for most of the ligands in our compilation (157), we found pK_a values for all of them. Ligand pK_a values were used to estimate slopes by setting the intercepts to zero, and the resulting slope values are depicted in Figs. 11 & 12. Since acetate correlations offered higher accuracy over the hydroxide correlations, a separate acetate correlation was made using only the data available from carboxylates (Fig. 11). Correlation between ligand pK_a and 1-parameter hydroxide correlations are shown in Fig. 12(a) while those for 1-parameter acetate correlations are shown in Fig. 12(b). Ligands with additional functional groups like

lactate and pyruvate were excluded from this correlation for reasons mentioned in the previous sections and such ligands were excluded from the estimation inventory. While Fig. 11 was adopted for carboxylates, Fig. 12(a) was used for the metal ions for which $\log K_{M\text{-acetate}}$ measurements are unavailable. Conversely, Fig. 12(a) was employed for phenols and aldehydes while Fig. 12(b) was used to for the metal ions without $\log K_{M\text{-hydroxide}}$ measurements. These correlations were used to make an additional 11,775 $\log K_{ML}$ estimates.

2.5 Estimating entropies of association at 25°C & 1 bar

The strategy we developed to estimate metal-ligand complexation entropies is analogous to that for metal-ligand stability constants: use the closest proxy ligand with the most data. As with stability constants, entropy of association correlations for monovalent oxygen ligands can be broadly divided into carboxylates, phenols, and inorganic ligands. As the presence of additional coordinating groups can increase the metal-ligand reaction entropy via the 'chelate effect' (Martell & Hancock 1996), we considered ligands comprised of a single coordinating group. Since the standard state enthalpy (ΔH°), entropy (ΔS°) and Gibbs energy (ΔG°) of a reaction are related (ΔG°= ΔH°-T ΔS°), and the stability constant and Gibbs energy of reaction are related (ΔG°=-2.303RTlogK), knowing both the $\log K_{ML}$ and entropy of association yields the enthalpy of the complexation reaction. These three properties can be used to obtain the temperature dependence of log K using the van't Hoff equation in the form

$$logK(T) = \frac{-\Delta_r H^{\circ}_{Tr}}{2.303RT} + \frac{-\Delta_r S^{\circ}_{Tr}}{2.303R} \quad (2)$$

to estimate the temperature dependence of stability constants from 0° to 125°C using the

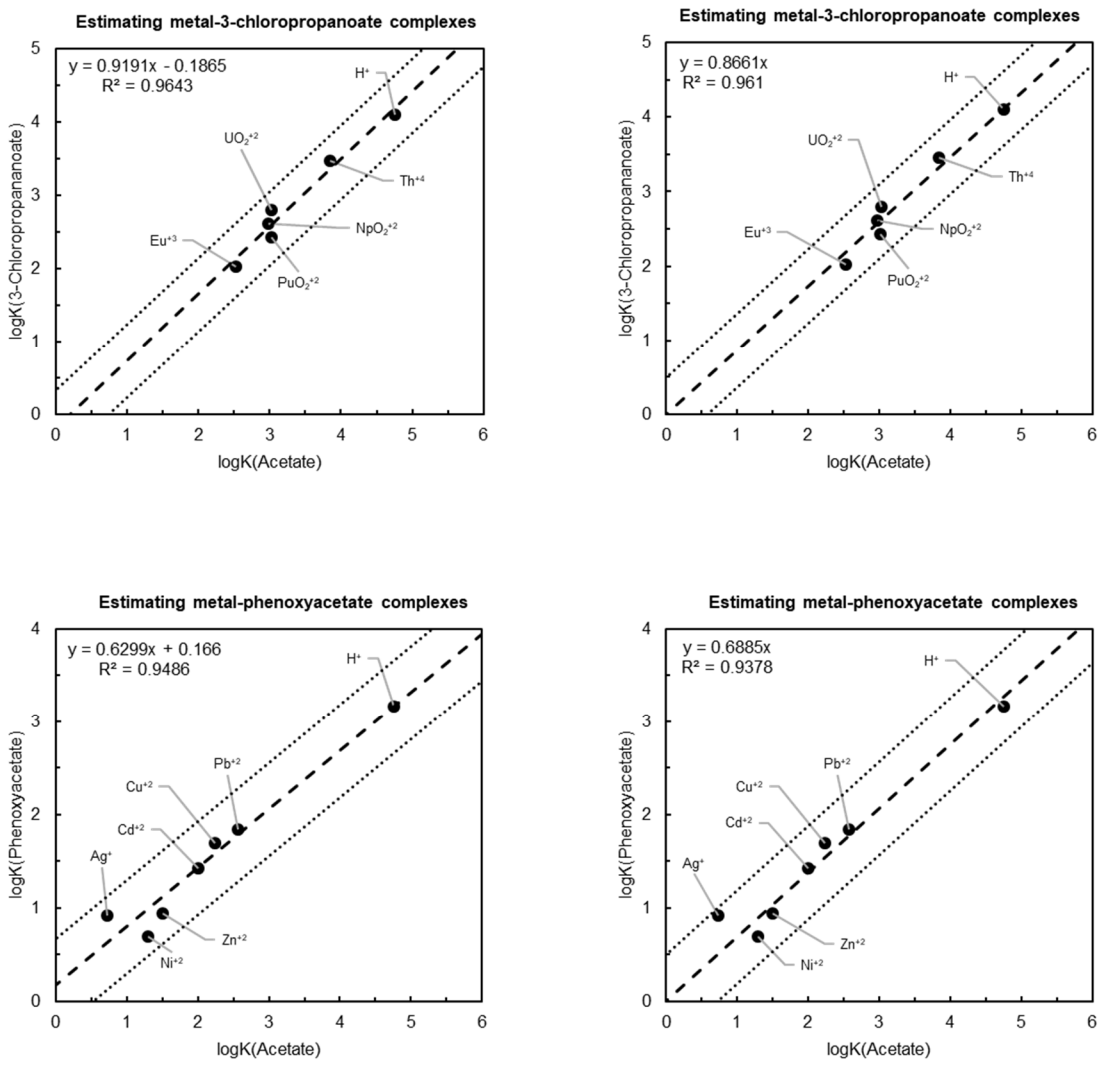

Fig 9(a). Comparison between 2-parameter and 1-parameter acetate LFERs for some monovalent oxygen ligands.

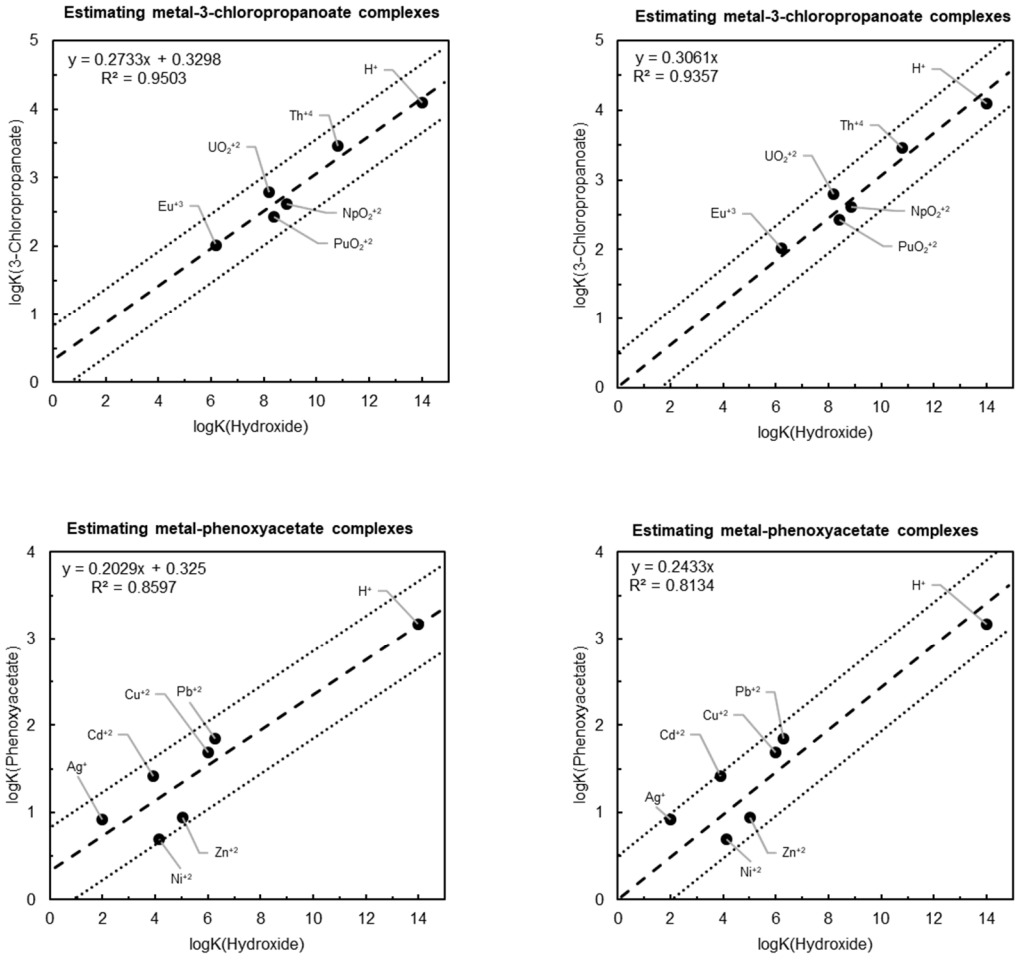

Fig 9(b). Comparison between 2-parameter and 1-parameter hydroxide LFERs for some monovalent oxygen ligands.

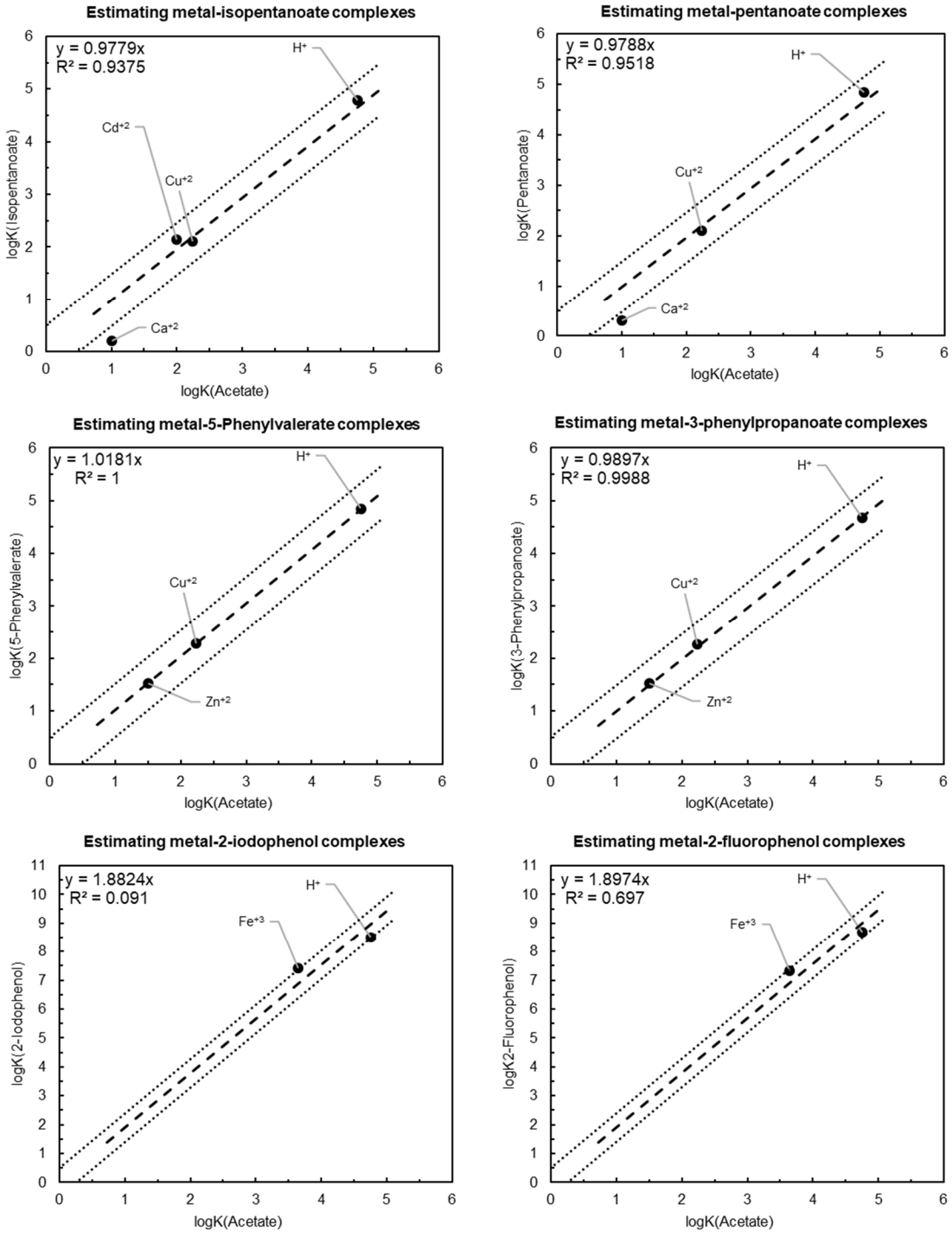

Fig 10(a). 1-parameter acetate LFERs for some monovalent oxygen ligands.

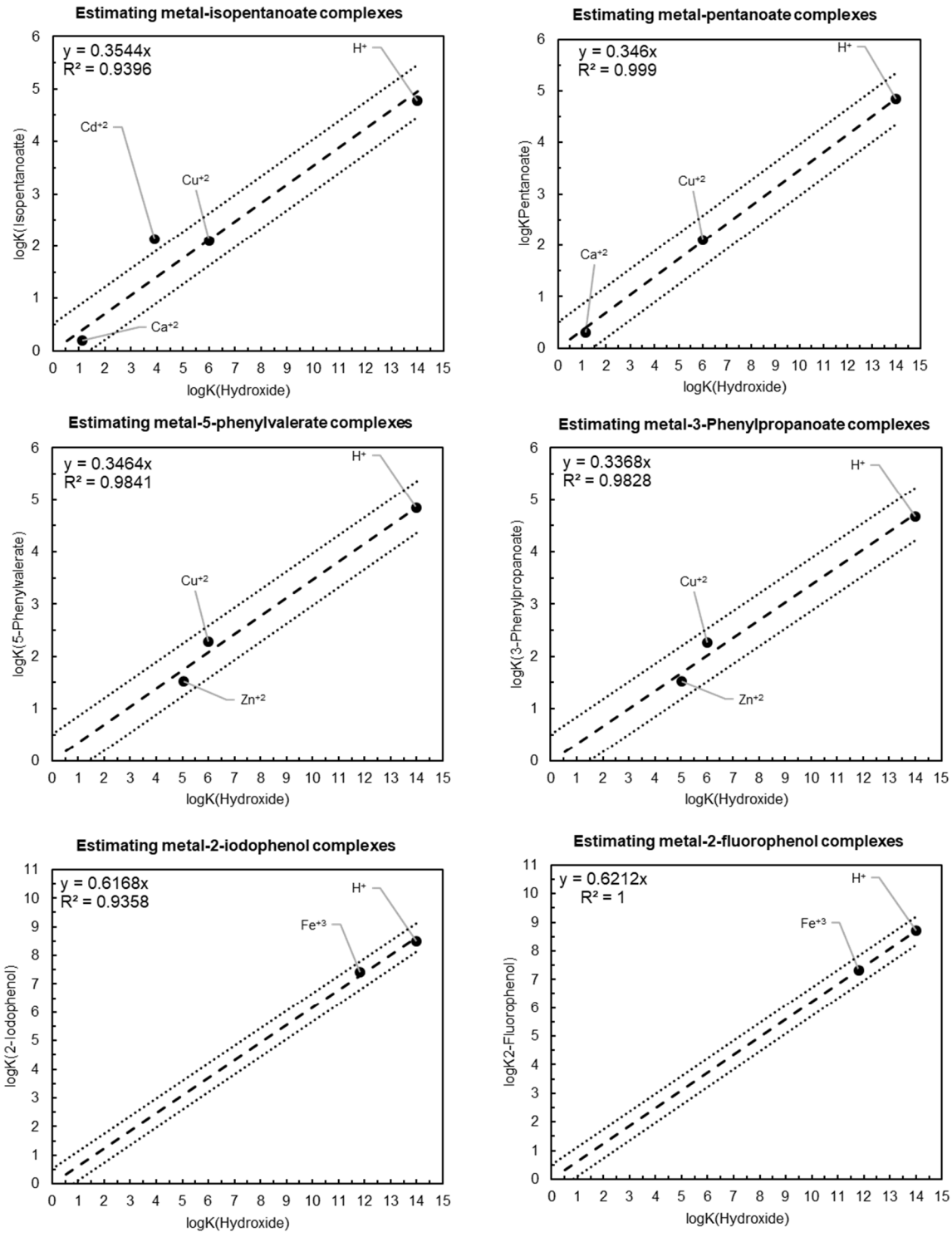

Fig 10(b). 1-parameter hydroxide LFERs for the monovalent oxygen ligands of Fig. 8.

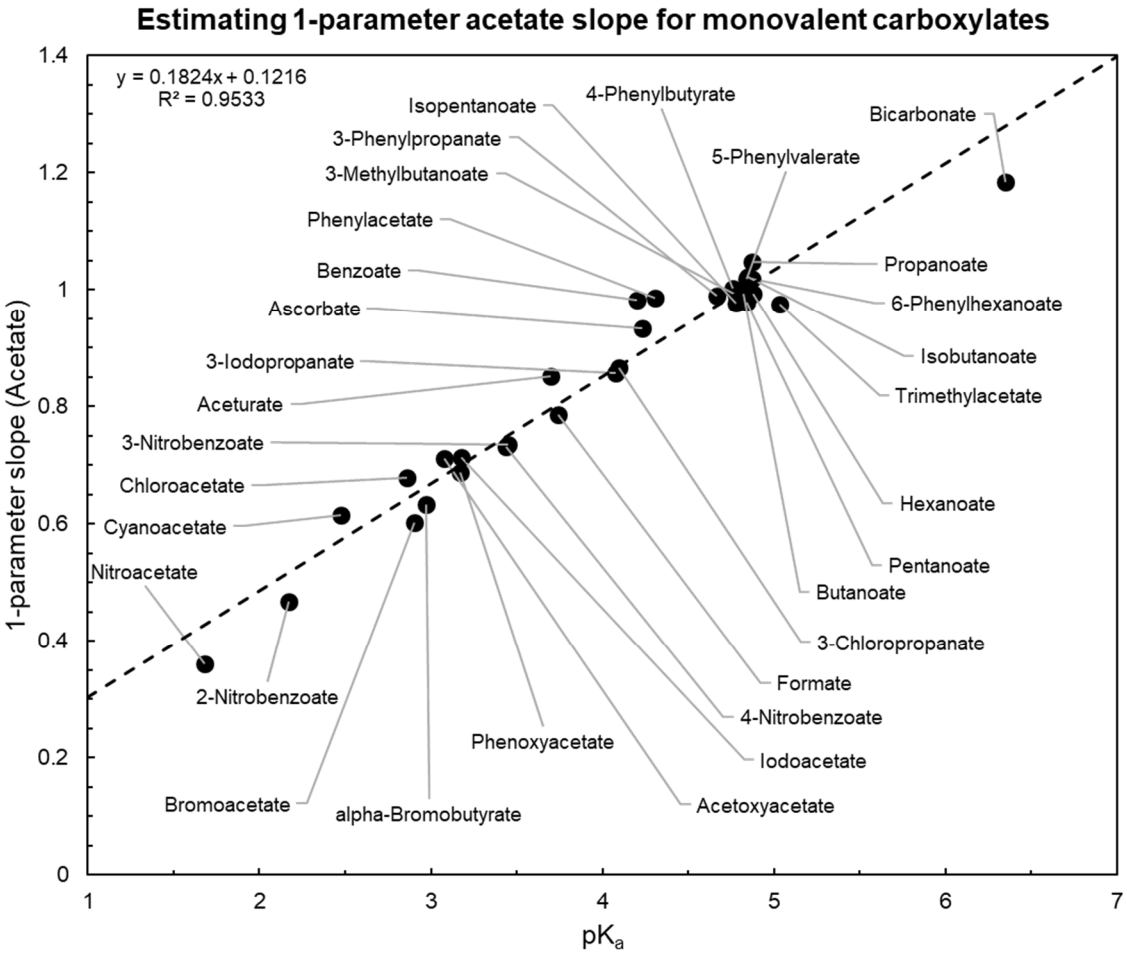

Fig 11. Estimating any metal-carboxylate from its pK_a.

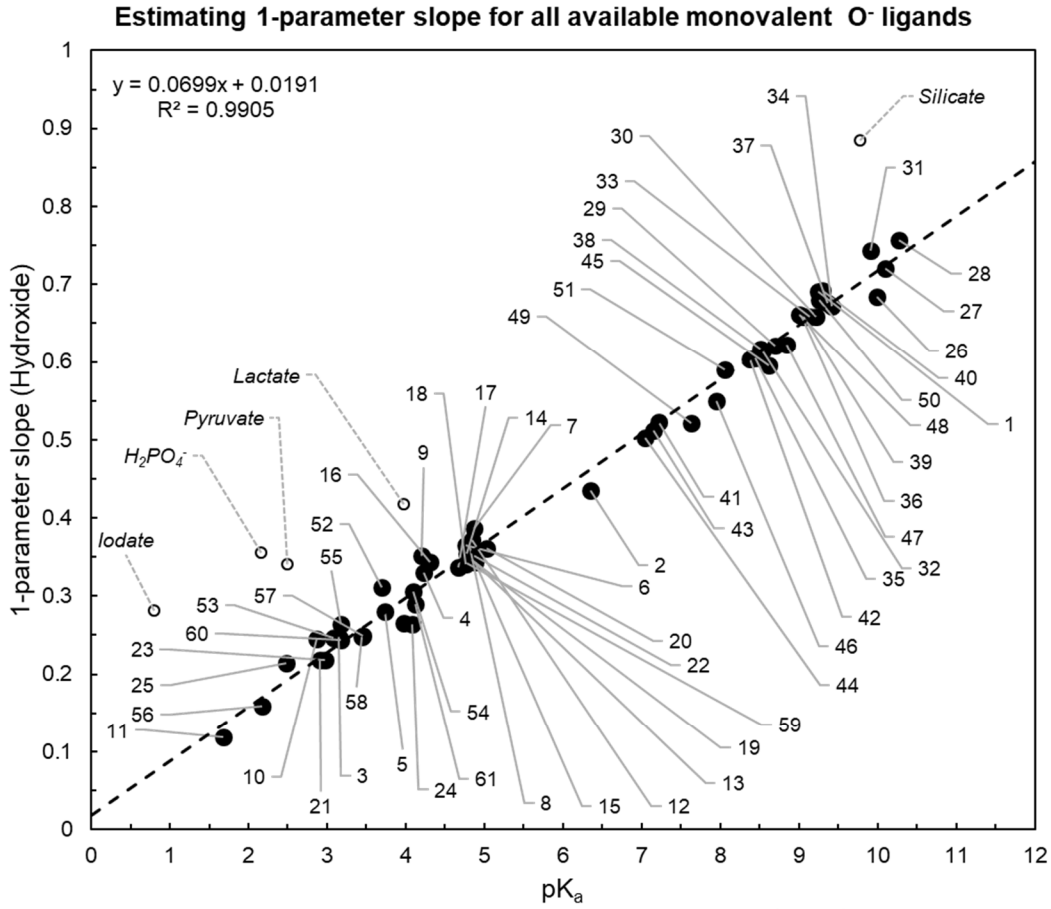

1	Borate
2	Bicarbonate
3	Nitrite
4	Ascorbate
5	Formate
6	Acetate
7	Propanoate
8	Butanoate
9	Benzoate
10	Chloroacetate
11	Nitroacetate
12	Isobutanoate
13	Pentanoate
14	Isopentanoate
15	Hexanoate
16	Phenylacetate
17	3-Phenylpropanate
18	4-Phenylbutyrate
19	5-Phenylvalerate
20	Trimethylacetate

21	Bromoacetate
22	6-Phenylhexanoate
23	α-Bromobutyrate
24	3-Iodopropanate
25	Cyanoacetate
26	Phenol
27	3-methyl phenol
28	4-methyl phenol
29	2-Fluoro phenol
30	3-Fluoro phenol
31	4-Fluoro phenol
32	2-Chloro phenol
33	3-Chloro phenol
34	4-Chloro phenol
35	2-Bromo phenol
36	3-Bromo phenol
37	4-Bromo phenol
38	2-Iodo phenol
39	3-Iodo phenol
40	4-Iodo phenol

41	2-Nitro phenol
42	3-Nitro phenol
43	4-Nitro phenol
44	2-cyanophenol
45	3-cyanophenol
46	4-cyanophenol
47	4-sulfophenol
48	3-Hydroxybenzaldehyde
49	4-Hydroxybenzaldehyde
50	3-Acetylphenol
51	4-Acetylphenol
52	Aceturate
53	Acetoxyacetate
54	3-Chloropropanate
55	Iodoacetate
56	2-Nitrobenzoate
57	3-Nitrobenzoate
58	4-Nitrobenzoate
59	3-Methylbutanoate
60	Phenoxyacetate
61	2,4-Dinitrophenol

Fig 12(a). Estimating $\log K_{ML}$ for any metal-monovalent oxygen ligand (with exceptions) from its pK_a using hydroxide correlations.

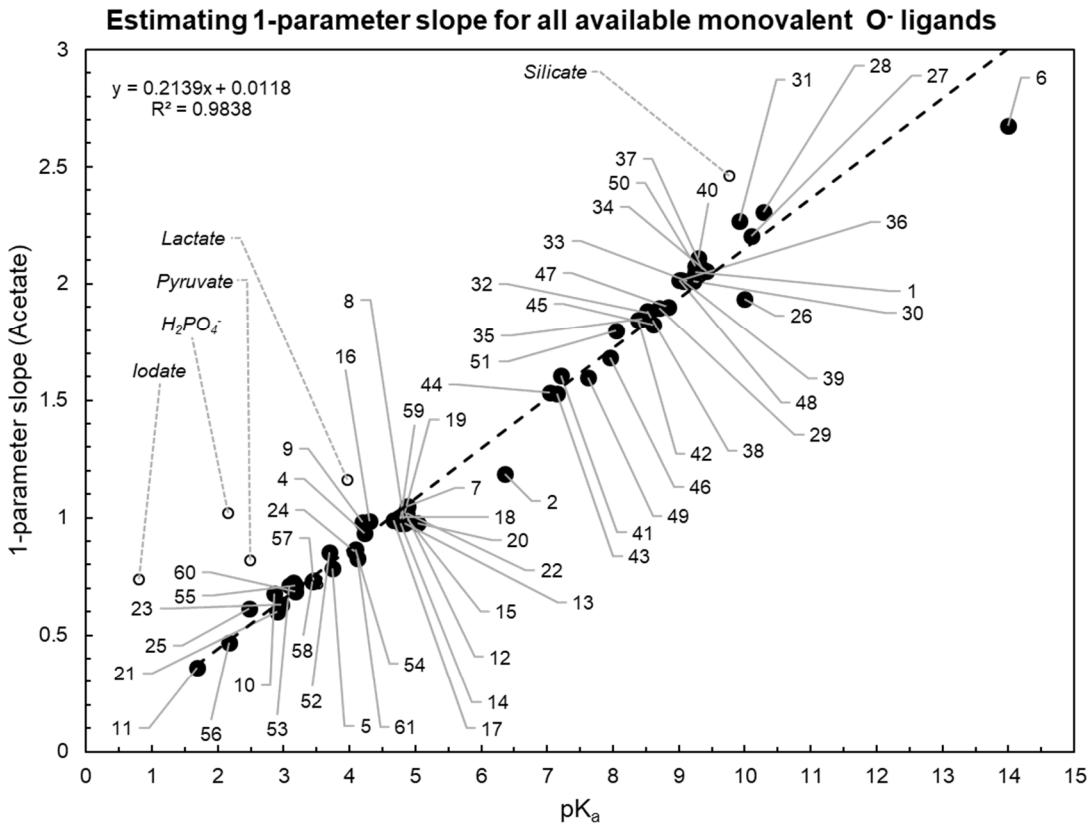

1	Borate
2	Bicarbonate
3	Nitrite
4	Ascorbate
5	Formate
6	Hydroxide
7	Propanoate
8	Butanoate
9	Benzoate
10	Chloroacetate
11	Nitroacetate
12	Isobutanoate
13	Pentanoate
14	Isopentanoate
15	Hexanoate
16	Phenylacetate
17	3-Phenylpropanate
18	4-Phenylbutyrate
19	5-Phenylvalerate
20	Trimethylacetate

21	Bromoacetate
22	6-Phenylhexanoate
23	α-Bromobutyrate
24	3-Iodopropanate
25	Cyanoacetate
26	Phenol
27	3-methyl phenol
28	4-methyl phenol
29	2-Fluoro phenol
30	3-Fluoro phenol
31	4-Fluoro phenol
32	2-Chloro phenol
33	3-Chloro phenol
34	4-Chloro phenol
35	2-Bromo phenol
36	3-Bromo phenol
37	4-Bromo phenol
38	2-Iodo phenol
39	3-Iodo phenol
40	4-Iodo phenol

41	2-Nitro phenol
42	3-Nitro phenol
43	4-Nitro phenol
44	2-cyanophenol
45	3-cyanophenol
46	4-cyanophenol
47	4-sulfophenol
48	3-Hydroxybenzaldehyde
49	4-Hydroxybenzaldehyde
50	3-Acetylphenol
51	4-Acetylphenol
52	Aceturate
53	Acetoxyacetate
54	3-Chloropropanate
55	Iodoacetate
56	2-Nitrobenzoate
57	3-Nitrobenzoate
58	4-Nitrobenzoate
59	3-Methylbutanoate
60	Phenoxyacetate
61	2,4-Dinitrophenol

Fig 12(b). Estimating $\log K_{ML}$ for any metal-monovalent oxygen ligand (with exceptions) from its pK_a using acetate correlations.

standard enthalpy and entropy of association at the reference temperature (Tr = 298.15K) and pressure (Pr = 1 bar). Holding the standard enthalpy and entropy of association constant implies that the heat capacity of association can be approximated by zero. While generally not suitable at temperatures higher than ~125°C, this relationship allows estimates at lower temperatures where change in heat capacity of association are minimal (Shock and Koretsky, 1995; Prapaipong et al., 1999; Prapaipong & Shock, 2001). Resulting estimates of the temperature dependence of log K_{ML} cover the known temperature range of microbial life, an allow predictions of metal speciation throughout the temperature range of the known biosphere.

2.5.1 Metal-carboxylate entropy of association

Investigation of the literature revealed only ten monovalent O-bearing ligands with entropy of association measurements for two or more metal ions: hydroxide, acetate, propanoate, butanoate, isobutanoate, chloroacetate, 3-chloropropanoate, formate, benzoate and phenylacetate. Analogous to the case of stability constants, hydroxide and acetate were the ligands with the most $\Delta S°_{ML}$ measurements (26 and 31 respectively) and hence, correlations were made using the respective sets of data. A lack of correlation between metal-hydroxide and metal-carboxylate entropies (not shown) suggested that hydroxide is a poor proxy ligand for carboxylate ligands. Instead, all carboxylates were observed to correlate closely with acetate even if a one-parameter relationship was used. These relations are illustrated in Fig. 13, which includes two-parameter and one-parameters fits side-by side for the eight organic-ligand entropies of association plotted against those for acetate. Due to the limited availability of experimental values, using the 1-parameter correlations allows greater variety and number of estimates and precludes

skewness of data. Despite the slight loss of accuracy, the one-parameter fit accommodates an induced uncertainty envelop of ± 2 cal mol^{-1} K^{-1}, which minimizes the resulting uncertainty in the calculated temperature dependence of log K. Additionally, the one-parameter slopes exhibit a correlation with the ligand protonation entropy as shown in Fig. 14. The resulting correlation permits estimates of hypothetical slopes for one-parameter fits of $\Delta S°_{ML}$ against the corresponding property of acetate complexes for a plethora of ligands for which only the protonation entropy (ΔS_a) is known.

In addition to a relationship between ΔS_a and the 1-parameter entropy slopes, we also found a correlation between ΔS_a and pK_a for carboxylate ligands as shown in Fig. 15. While the correlation includes a variety of ligands, we excluded substituted benzoates as they deviated considerably from the correlation. We suspect that the presence of additional resonance structures may contribute to this observation. However, it should be noted that many of these ΔS_a values are based on single studies, which could be benefit from additional experimental verification. Nonetheless, this correlation provides protonation entropy and 1-parameter slopes (from Fig. 14) for 67 additional carboxylate ligands for which only pK_a is known. These correlations help us estimate an additional 2077 $\Delta S°_{ML}$ values.

While $\Delta S°_{ML}$ measurements are rare for carboxylates, this information was even sparser for metal-phenol complexes with experimental values existing for only a few ferric-phenol complexes. However, the correlation shown in Fig 16 between these values and the protonation entropy suggests that metal-phenol $\Delta S°_{ML}$ values can be estimated in a manner analogous to metal-carboxylate complexation entropies. Additionally, we found a close relationship between ΔS_a and pK_a values for phenols as shown in Fig. 17

analogous to that for carboxylates albeit with different slope and intercept, as demonstrated in Fig. 18. This relationship helped us estimate ΔS_a values for 34 additional phenols for which only pK_a values were available, and Fig. 16 was used to obtain the corresponding ferric-phenol complexation entropies. As hydroxide was the closer proxy ligand for phenol in $\log K_{ML}$ estimation, we used metal-hydroxide complexation entropies to estimate corresponding metal-phenol $\Delta S°_{ML}$ values. Support for this approach is offered by the correlation for metal-silicate complexes shown in Fig. 19. While this correlation does not yield estimates of $\Delta S°_{ML}$ within ±2 cal mol^{-1} K^{-1}, it does yield estimates within ±5 cal mol^{-1} K^{-1}. Metal-hydroxide complexation entropies were also used to estimate metal-nitrite $\Delta S°_{ML}$ values as the correlation was based on three experimental values in comparison to the two values for acetate complexes as shown in Fig 20.

2.5.2 Predicting metal-ligand association throughout the known biosphere

$\Delta S°_{ML}$ values for eight geobiologically relevant metal ions (Al^{+3}, Na^{+}, Fe^{+3}, Fe^{+2}, Zn^{+2}, Ba^{+2}, La^{+3} and Th^{+4}), either obtained from the literature or estimated from Fig. 13 from experimental $\Delta S°_{M\text{-}Acetate}$ values, together with experimental or estimated $\log K_{ML}$ values, were used to obtain the van't Hoff plots shown in Fig. 21 (details in Supplementary Tables). Since no experimental measurement for the ferric-acetate complexation entropy was found, a value of 29.2 cal·mol^{-1}·K^{-1} was estimated using the benzoate correlation in Fig. 13 and the experimental $\Delta S°_{M\text{-}Benzoate}$ of 29.63 cal·mol^{-1}·K^{-1} reported by Basaran et al. (1994). We have not included such second-order estimates in the Supplementary Tables as they might have higher uncertainty, but provisional values can be obtained when no experimental data exists. For most metal ions, stability

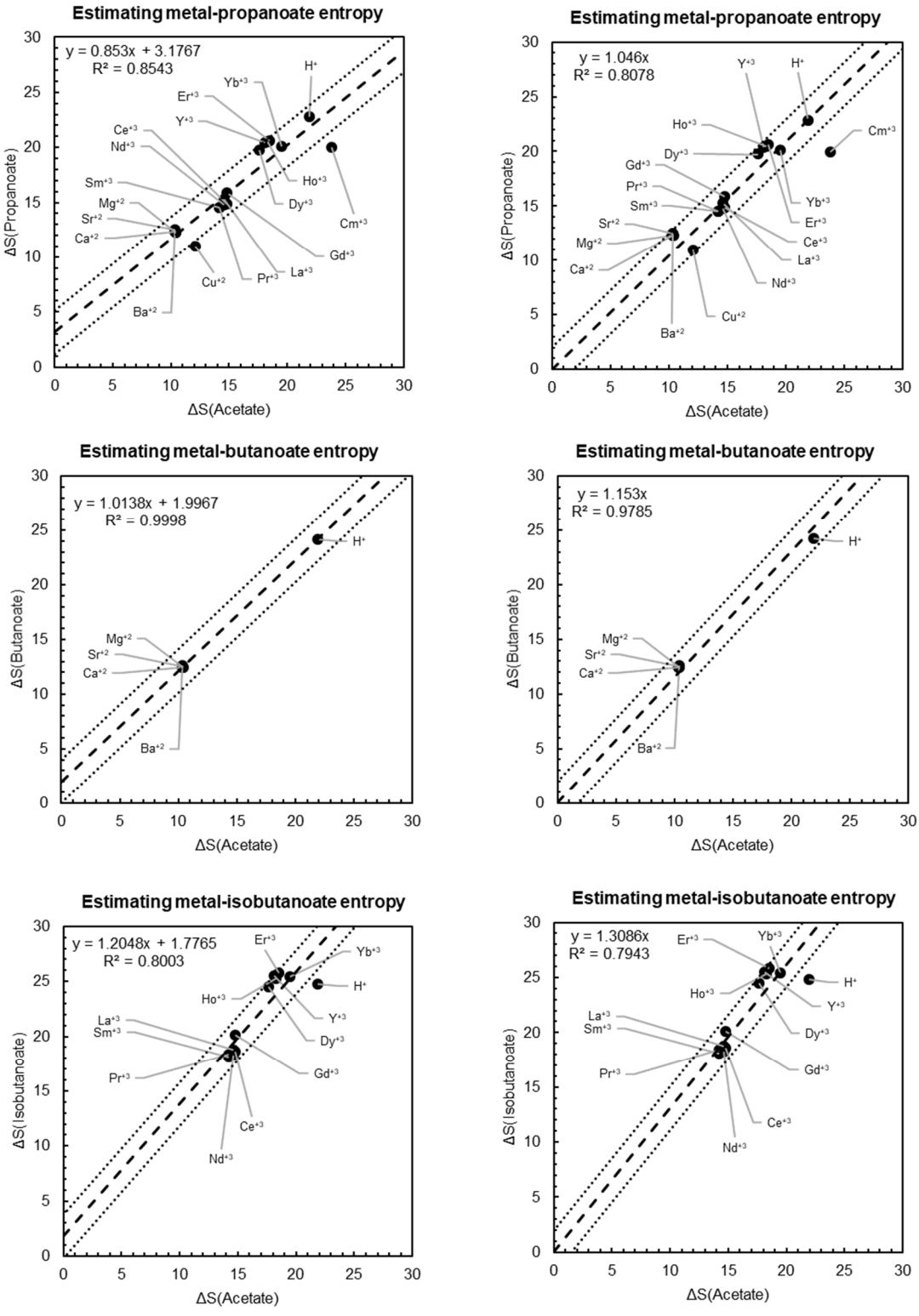

Fig 13. Entropy estimates for metal-carboxylates with available data (contd.)

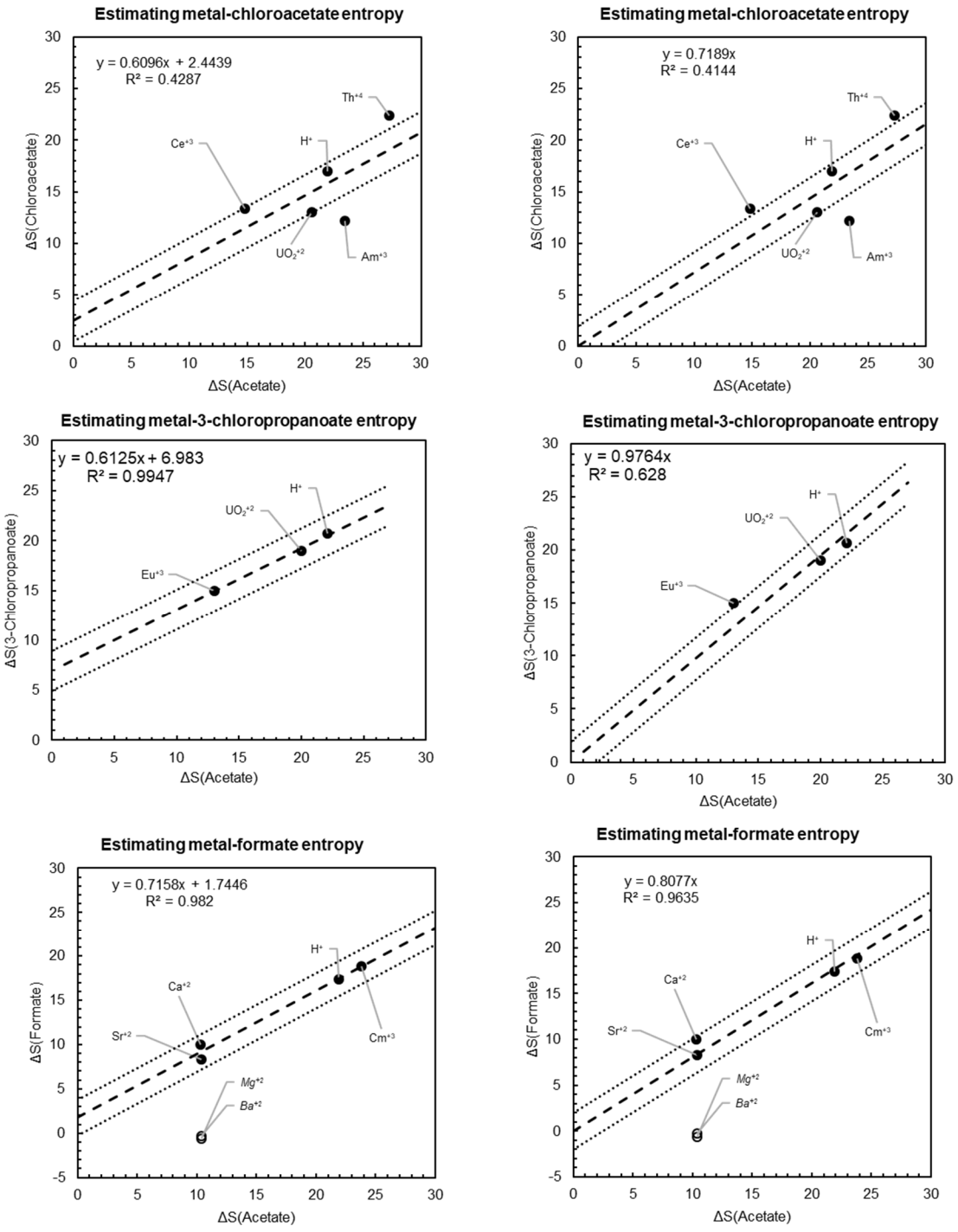

Fig 13. (contd.) Entropy estimates for metal-carboxylates with available data.

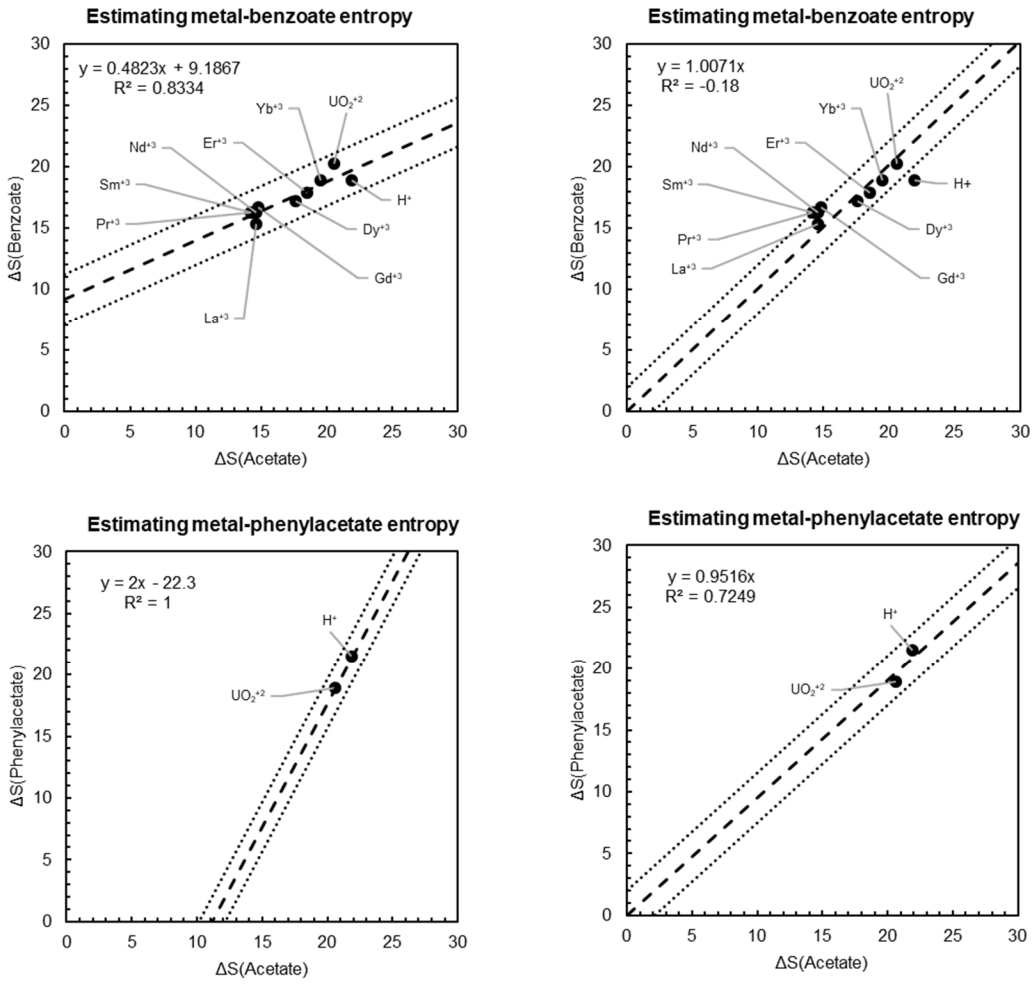

Fig 13. (contd.) Entropy estimates for metal-carboxylates with available data.

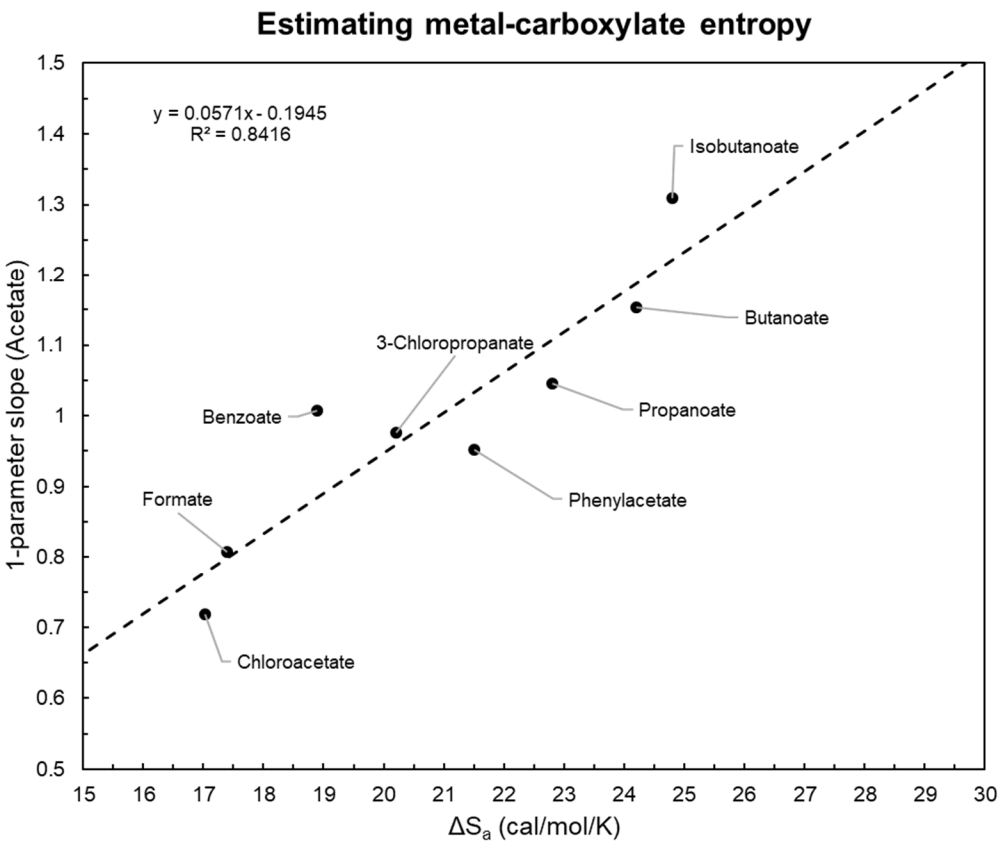

Fig 14. Estimating 1-parameter slopes (acetate) from protonation entropy of the ligand. This correlation provides reasonable estimates of metal-carboxylate entropy when only protonation entropy is known.

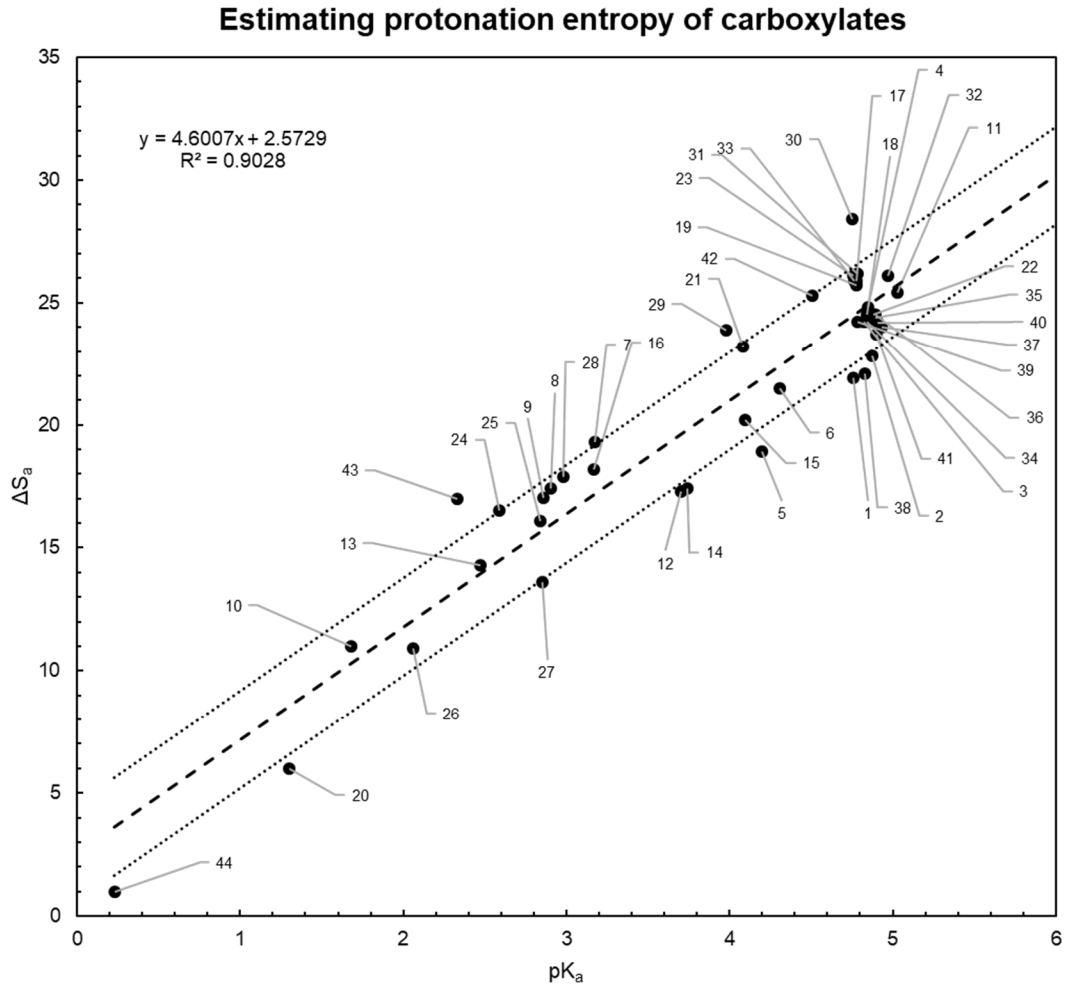

1	Acetate	16	Phenoxyacetate	31	2-Methylpentanoate
2	Propanoate	17	Isopentanoate	32	2,2-Dimethylpentanoate
3	Butanoate	18	Pentanoate	33	3-Methylpentanoate
4	Isobutanoate	19	3-Methylbutanoate	34	4-Methylpentanoate
5	Benzoate)	20	Dichloroacetate	35	Heptanoate
6	Phenylacetate	21	3-Iodopropanate	36	Octanoate
7	Iodoacetate	22	Hexanoate	37	2,2-Dimethylbutanoate
8	Bromoacetate	23	2-Methylbutanoate	38	Cyclopropanecarboxylate
9	Chloroacetate	24	Fluoroacetate	39	Cyclobutanecarboxylate
10	Nitroacetate	25	2-Chloropropanoate	40	Cyclopentanecarboxylate
11	Pivalate	26	2,2-Dichloropropanoate	41	Cyclohexanecarboxylate
12	Aceturate	27	2,3-Dichloropropanoate	42	Cyclohexylcarboxylate
13	Cyanoacetate	28	2-Bromopropanoate	43	2,3-dibromopropanoate
14	Formate	29	3-Bromopropanoate	44	Trifluoroacetate
15	3-Chloropropanoate	30	2-Ethylbutanoate		

Fig 15. Correlation between protonation entropy and protonation stability constant for carboxylates.

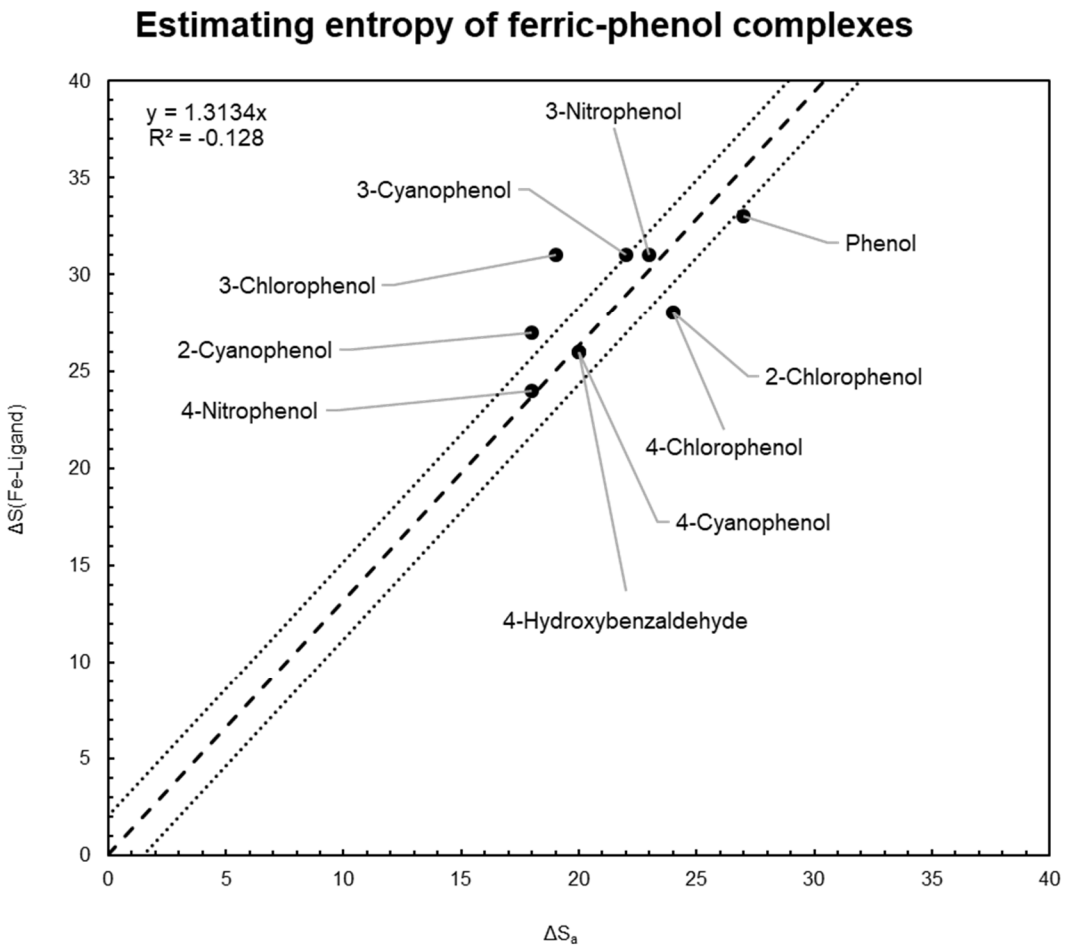

Fig 16. 1-Parameter correlation between ferric-phenolate complexation entropy with phenol protonation entropy.

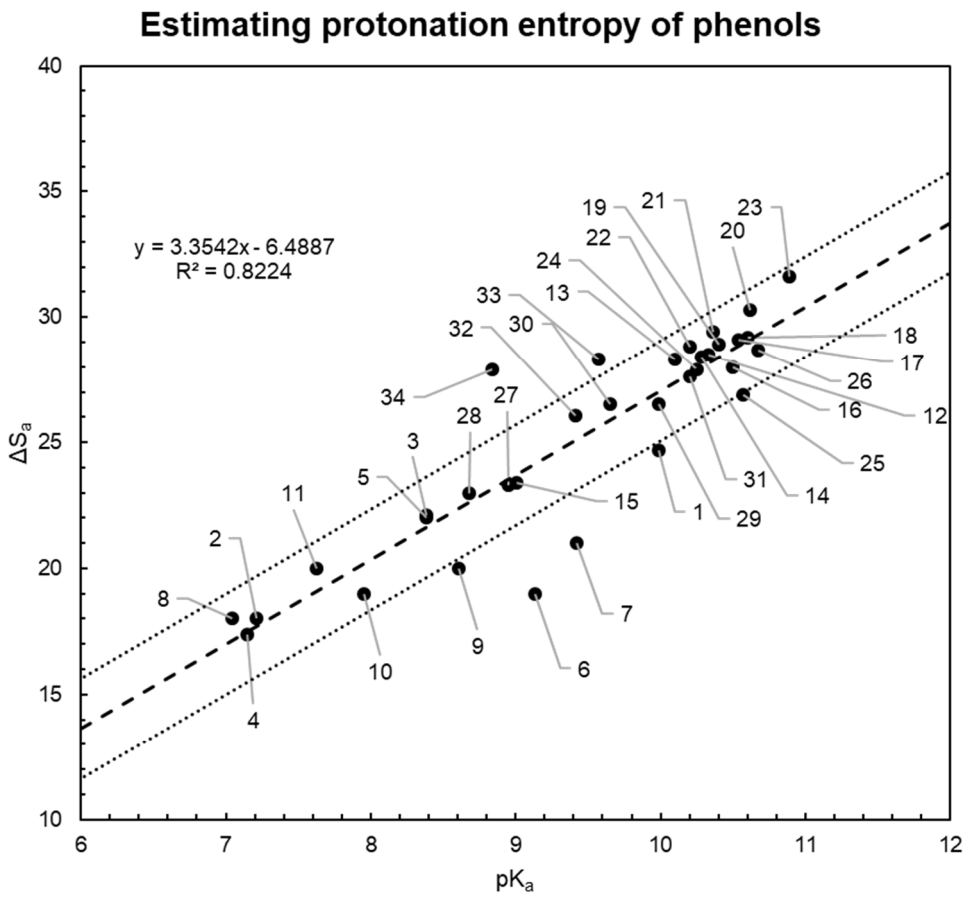

1	Phenol
2	2-Nitrophenol
3	3-Nitrophenol
4	4-Nitrophenol
5	2-Chlorophenol
6	3-Chlorophenol
7	4-Chlorophenol
8	2-Cyanophenol
9	3-Cyanophenol
10	4-Cyanophenol
11	4-Hydroxybenzaldehyde
12	2-Methylphenol
13	3-Methylphenol
14	4-Methylphenol
15	3-Hydroxybenzaldehyde
16	2-Propylphenol
17	2,3-Xylenol

18	2,4-Xylenol
19	2,5-Xylenol
20	2,6-Xylenol
21	3,4-Xylenol
22	3,5-Xylenol
23	2,4,6-Xylenol
24	3,4,5-Trimethylphenol
25	2,4,5-Trimethylphenol
26	2,3,5-Trimethylphenol
27	3-Trifluoromethylphenol
28	4-Trifluoromethylphenol
29	2-Methoxyphenol
30	3-Methoxyphenol
31	4-Methoxyphenol
32	1-Naphthol
33	2-Naphthol
34	4-Sulfophenol

Fig 17. Correlation between protonation entropy and protonation stability constant for phenols.

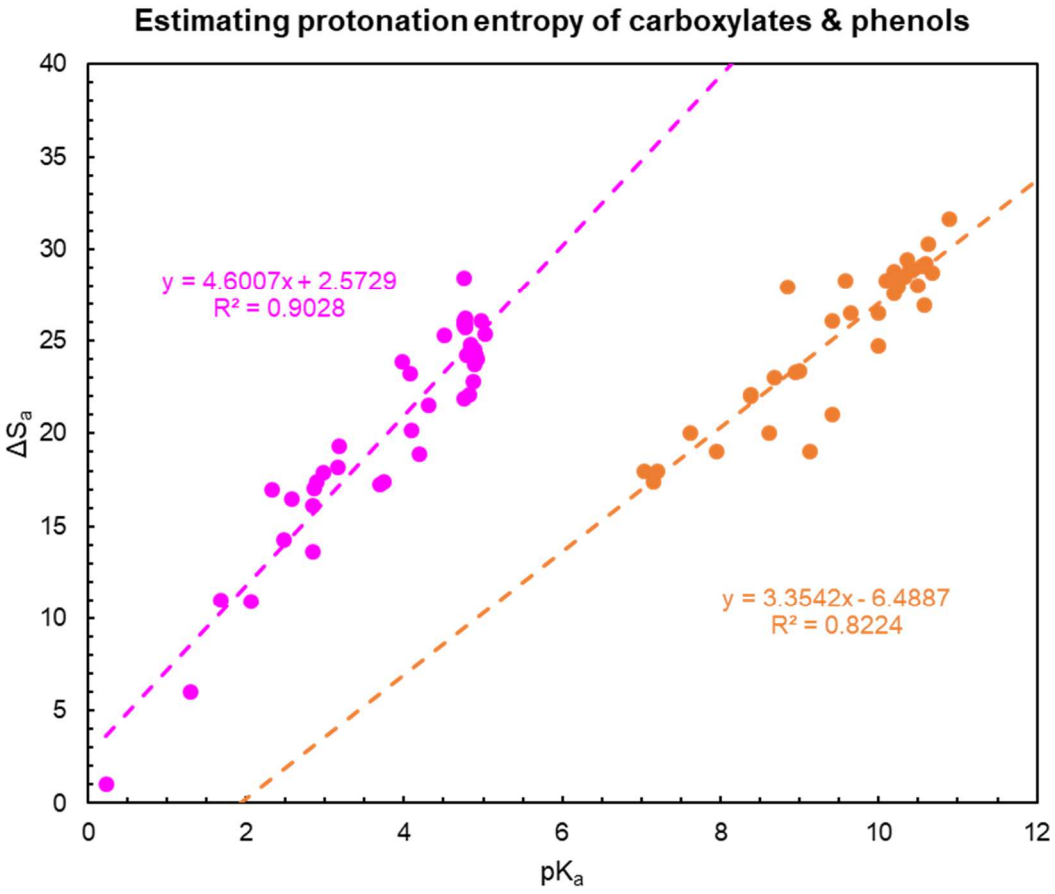

Fig 18. Correlation between protonation entropy and protonation stability constant for carboxylates and phenols. As can be seen from the slopes and intercepts, the relationship is different for the two categories of monovalent O^- ligands.

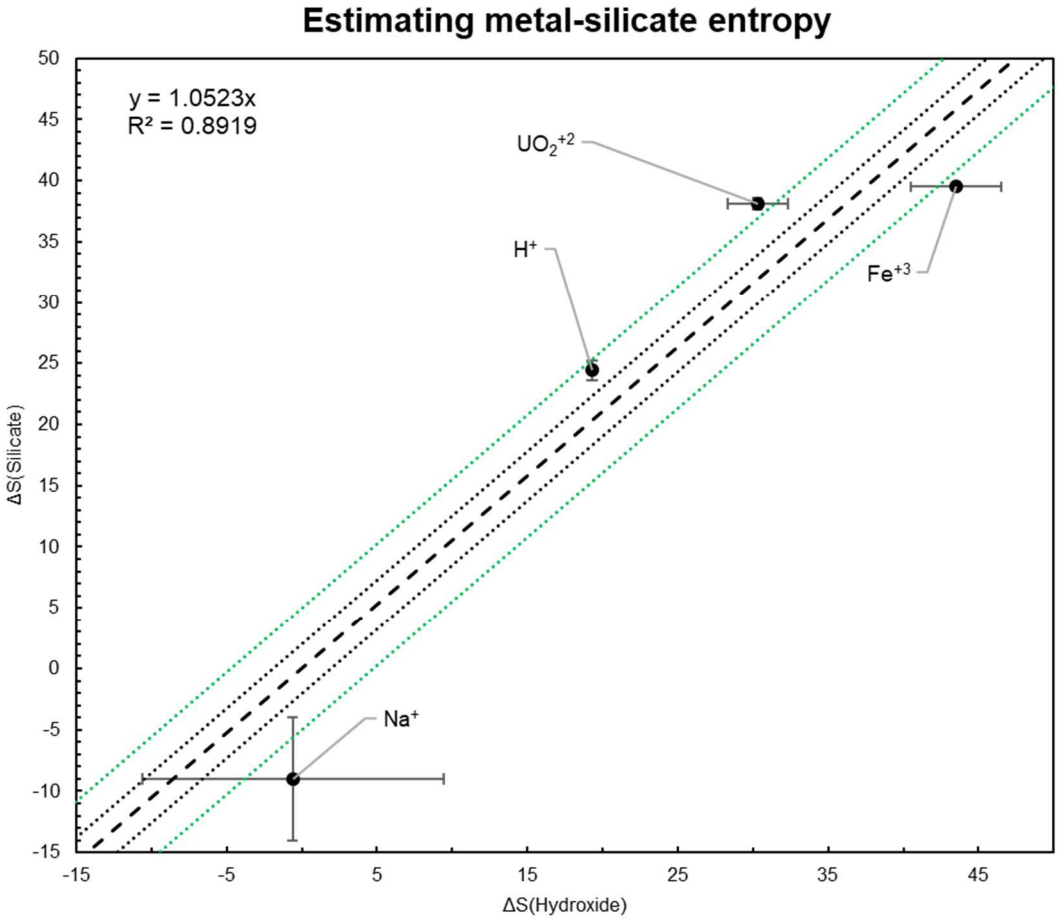

Fig 19. 1-Parameter estimation for metal-silicate entropy with available data. Error bars refer to experimental uncertainty reported in original papers. Dashed line represents the best fit line. Black dotted line represents uncertainty envelope of ±2 cal.mol^{-1}.K^{-1}. Green dotted line represents uncertainty envelope of ±5 cal.mol^{-1}.K^{-1}.

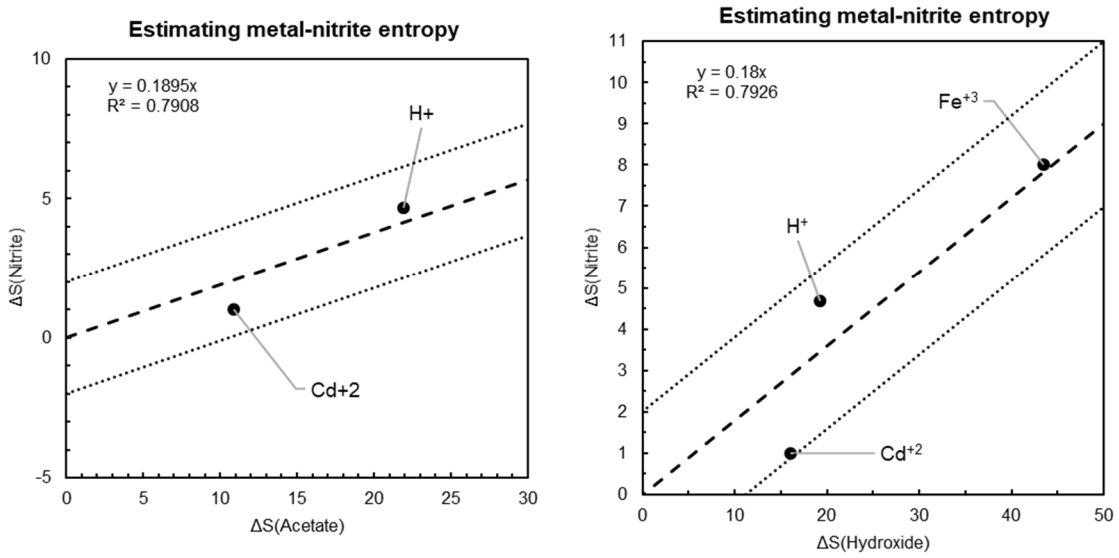

Fig 20. 1-Parameter estimation for metal-nitrite entropy with available data using acetate or hydroxide correlation. Black dotted line represents uncertainty envelope of ±2 cal.mol^{-1}.K^{-1}.

constants increase with temperature while for very few metals like Fe^{+2}, $\log K_{ML}$ decreases with temperature. This arises from the low $\Delta S°_{ML}$ value for ferrous-acetate, which results in a negative enthalpy of association in comparison to the endothermic values for other complexes. Using this same argument, we predict that the K^{+}-carboxylate complexes will have a trend similar to that of the ferrous complexes. It is perhaps worth noting that ligands with disparate 1-parameter slopes like isobutanoate and chloroacetate (see Fig. 14) exhibit contrasting temperature dependences, whereas those with similar 1-parameter slopes such as propanoate and phenylacetate have similar predicted log K_{ML} trends. It is perhaps also worth noting here that these van't Hoff plots include metal-ligand complexes for which both logK and $\Delta S°_{ML}$ values were experimentally obtained (for example Ba^{+2} & La^{+3}-propanoates) and those for which both of these values were estimated (for example Ba^{+2} & La^{+3}-phenylacetates).

Consequences of estimating the temperature dependence of log K_{ML} for diverse carboxylates are illustrated in Fig. 22, which shows predictions for zinc and ferrous complexes of three carboxylates for which only the protonation entropies are known. These ligands were selected because they offer a wide range of $\Delta S°_{a}$ values that correspondingly yield disparate 1-parameter slopes based on the relationship in Fig. 14. Zinc and ferrous ions were selected for this comparison as they have similar $\log K_{ML}$ values at 25°C and 1 bar. As can be seen in Fig 22, the predicted temperature dependences of the association constants for the zinc complexes (solid curves) differ starkly for the three ligands: $\log K_{ML}$ increases with temperature for zinc-2,2-dimethylpropanoate and chloroacetate complexes, but decreases for zinc-trifluoroacetate complexes. This range of differences is a direct consequence of the greater protonation

entropy of 2,2-dimethylpropanoate compared to the lesser protonation entropy of trifluoroacetate. Note that this disparate temperature dependence is not exhibited by predictions for the ferrous complexes, which is a direct consequence of the low entropy of the ferrous-acetate complex.

There are many monovalent O-bearing ligands for which minimal experimental data exist yet their capacity to form complexes with metals may influence geochemical or biological processes. As examples, we focus here on two biologically relevant carboxylates for which no experimental entropy of association data exist: ascorbate, better known as vitamin C, which is an essential biological nutrient, and valproate, which is a prominent epilepsy drug. Predicted association constants for these ligands and the metals used in Fig 21 are shown in Fig 23. Stability constants for ascorbate were estimated using the LFER shown in Fig. 5 while those for valproate were estimated using the 1-parameter slope predictor from Fig. 11. The corresponding $\Delta S°_{ML}$ values were estimated from experimental pK_a values using correlations developed in Figs. 15 and 14. As can be seen in Fig 23, $logK_{ML}$ increases with increasing temperature for almost all metal ions except the ferrous ion similar to most carboxylates shown in Fig. 21. This is a consequence of the fact that the pK_a values for these ligands are similar to the ligands considered in the construction of Fig. 21. In addition to the two ligands considered here, such plots can be obtained for 68 additional ligands.

Similar plots can be generated for metal-phenol complexes. Those for ferric-phenol complexes shown in Fig. 24 were generated using the experimentally obtained logK and $\Delta S°_{ML}$ values available in the literature. Note that even though the $\Delta S°_{ML}$ values for ferric-phenols are similar to those of the carboxylates, the temperature

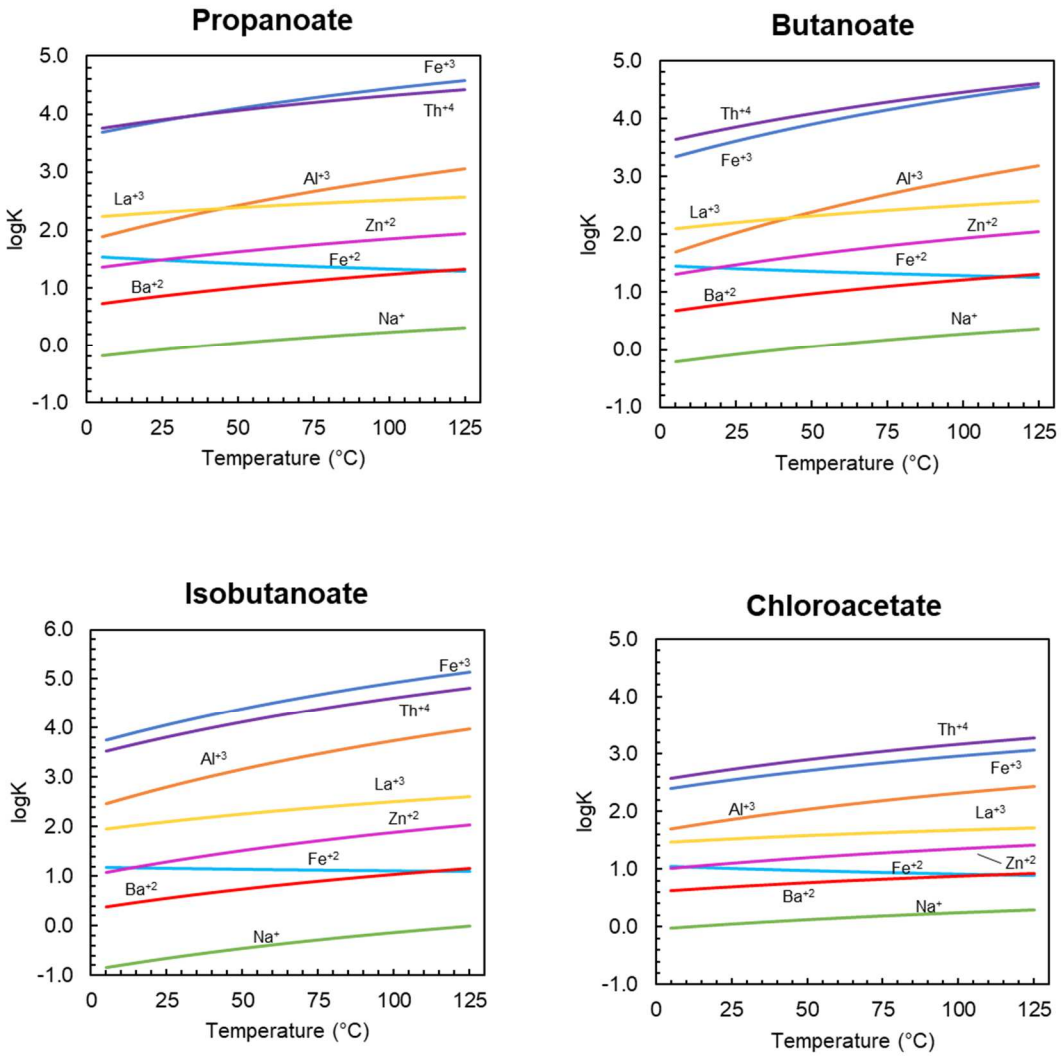

Fig 21. Van't Hoff plots displaying temperature dependence of metal-ligand stability constants using 1-parameter entropy estimates from Fig. 13 (contd.)

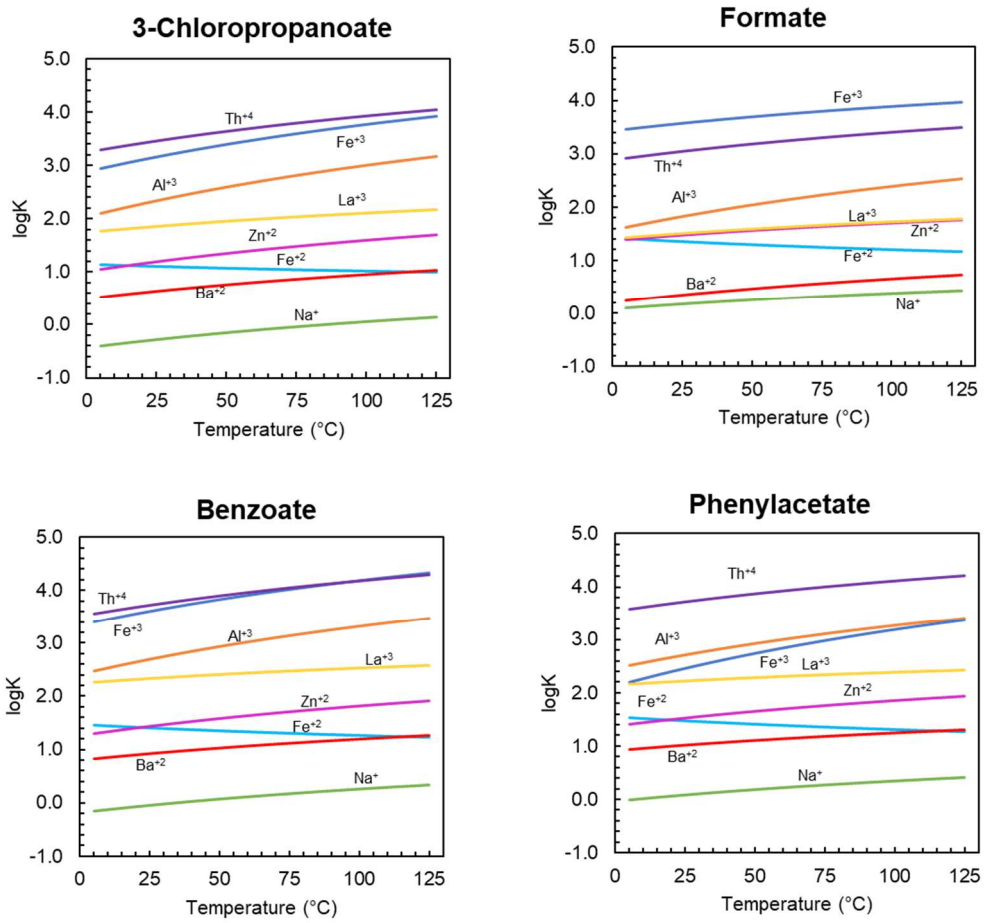

Fig 21. (contd.) Van't Hoff plots displaying temperature dependence of metal-ligand stability constants using 1-parameter entropy estimates from Fig. 13.

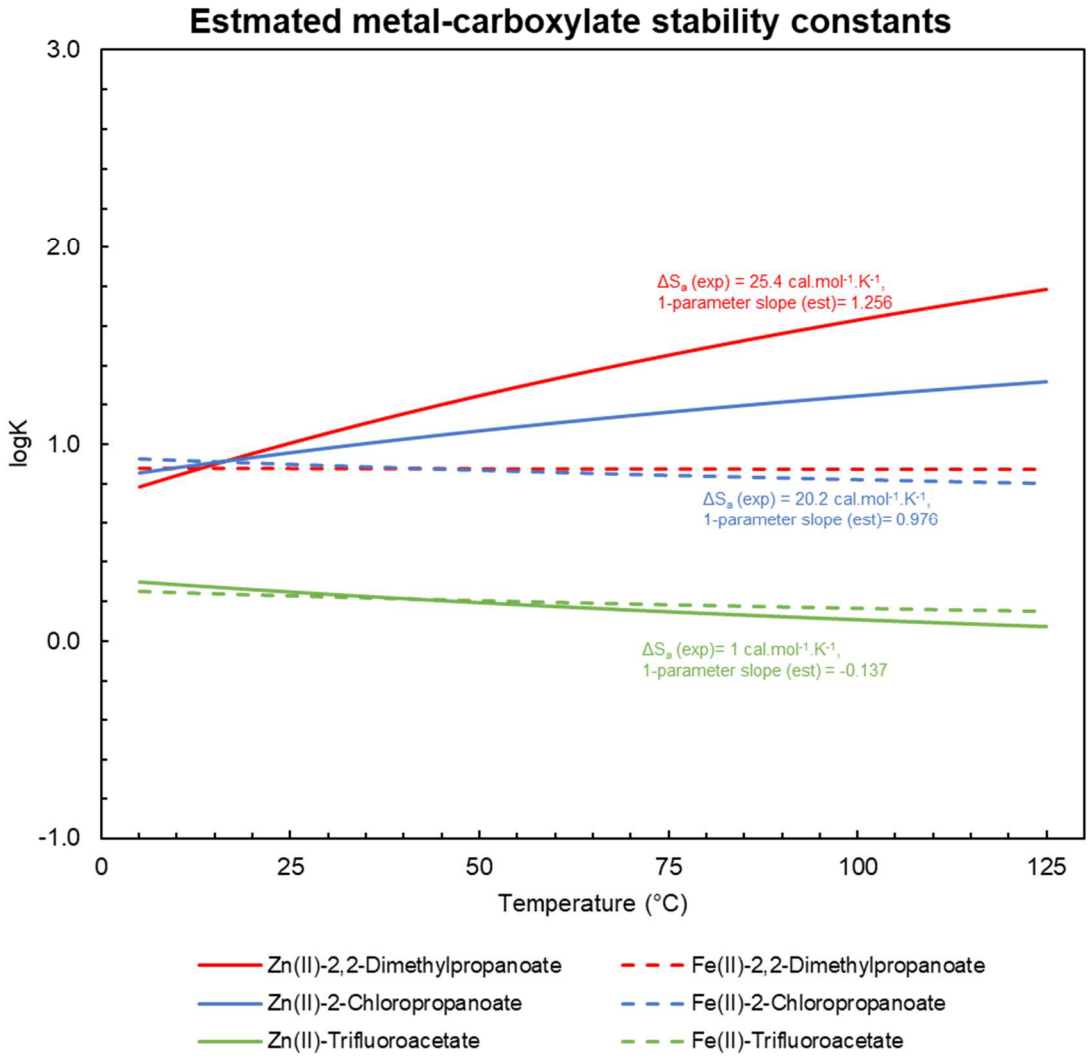

Fig 22. Van't Hoff plots created using only the ligand protonation entropy from relationship obtained in Fig. 14.

dependence of the stability constants gently decreases rather than increasing, which is due to a difference in the sign in the corresponding enthalpies of association. Analogous curves were generated for ferric complexes of six other phenols for which only pK_a and $\Delta S°_a$ are known, as shown in Fig. 25. In these cases we estimated $\log K_{Fe(III)-L}$ using the correlation shown in Fig. 12(a) and $\Delta S°_{Fe(III)-L}$ with the correlation in Fig. 16. As in the case of the curves shown in Fig. 24, stability constants for most ferric-phenol complexes in this figure decrease somewhat with increasing temperature. The rather constant nature of stability constants in the case of 2,4,6-trimethylphenol is consistent with it having the least negative enthalpy of association of this set of predicted values.

As mentioned above, experimentally determined entropies of association for metal-phenol complexes are scarce. Nevertheless, it is possible to make estimates using methods outlined above even in cases where only pK_a values are known. Examples are shown in Fig. 26 for association of the metal ions 2,4,6-trinitrophenol and 2-methoxy-4-methylphenol, which were selected as they have the lowest and the highest pK_a values, respectively, for this category of ligands. Additionally, 2,4,6-trinitrophenol can enter the environment through human activities owing to its use as an explosive and antiseptic agent. As in the case of the estimates shown in Fig. 24, these stability constant predictions were obtained using the correlation shown in Fig. 12(a), and a combination of the correlations shown in Figs. 16 and 17 to obtain the corresponding $\Delta S°_{Fe(III)-L}$ values. The remaining $\Delta S°_{ML}$ values were obtained by multiplying metal-hydroxide entropy of association with corresponding $\Delta S°_{Fe(III)-L}/ \Delta S°_{Fe(III)-Hydroxide}$ values. As can be seen from Fig. 26, we predict a drastic change in the temperature dependence of 2,4,6-trinitrophenol

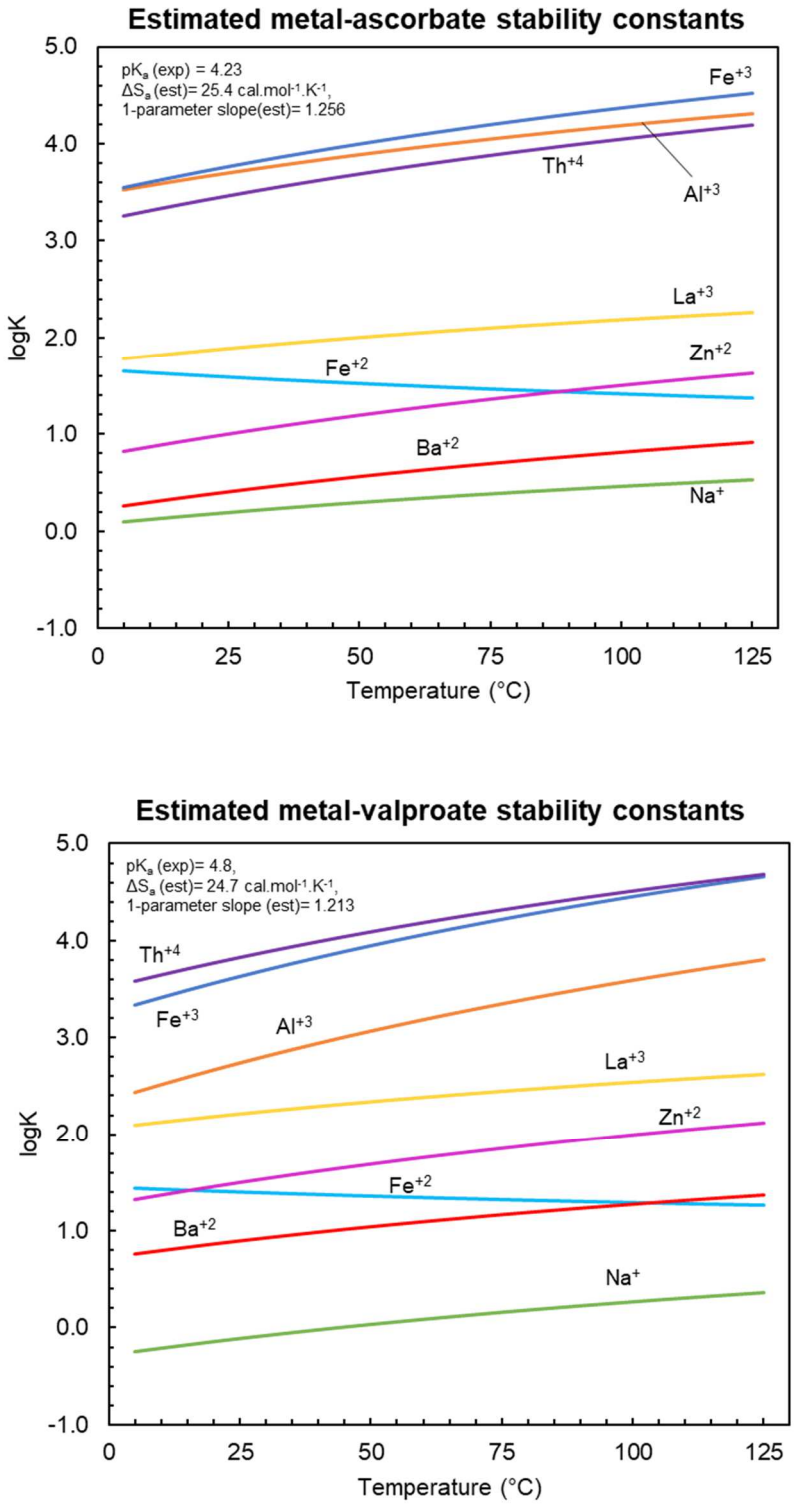

Fig 23. Van't Hoff plots created using only the ligand protonation constant from relationship obtained in Fig.15 & Fig.14.

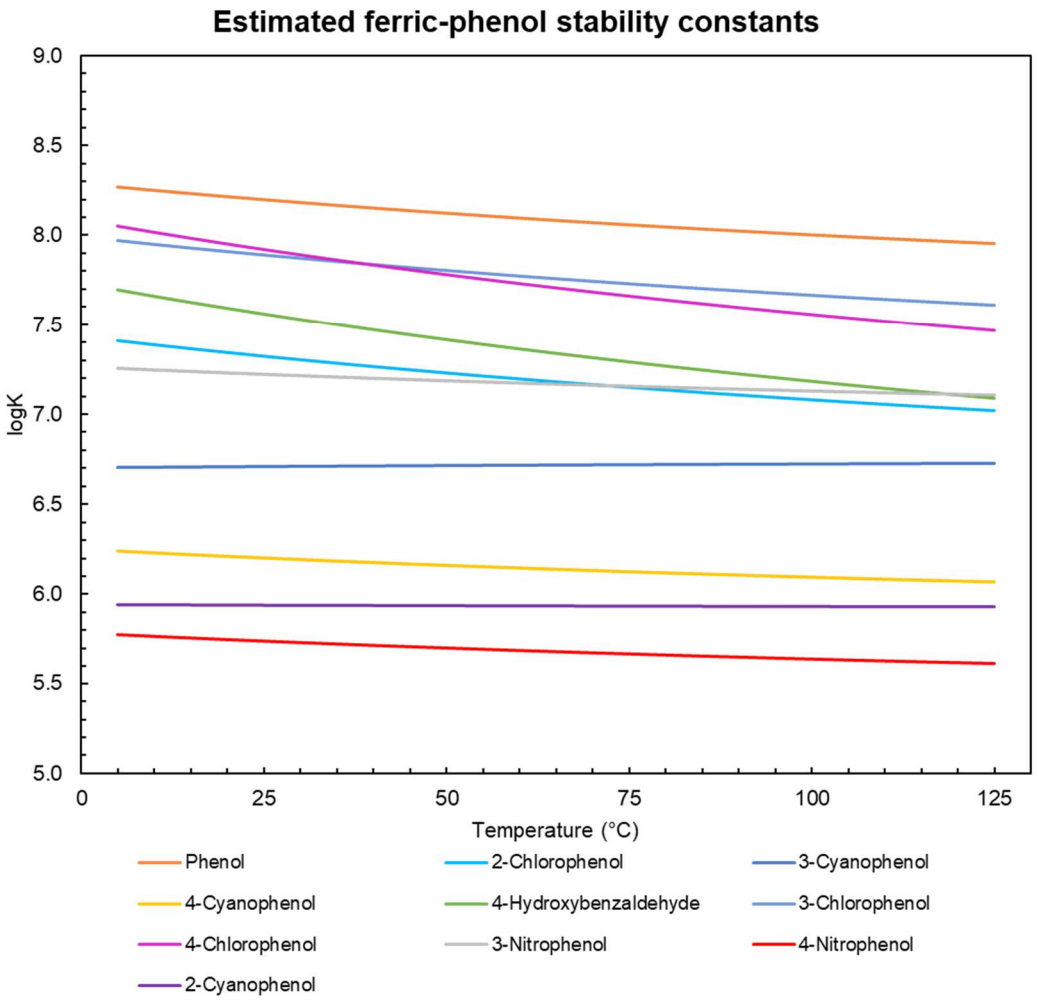

Fig 24. Van't Hoff plots created using experimental data plotted in Fig.16.

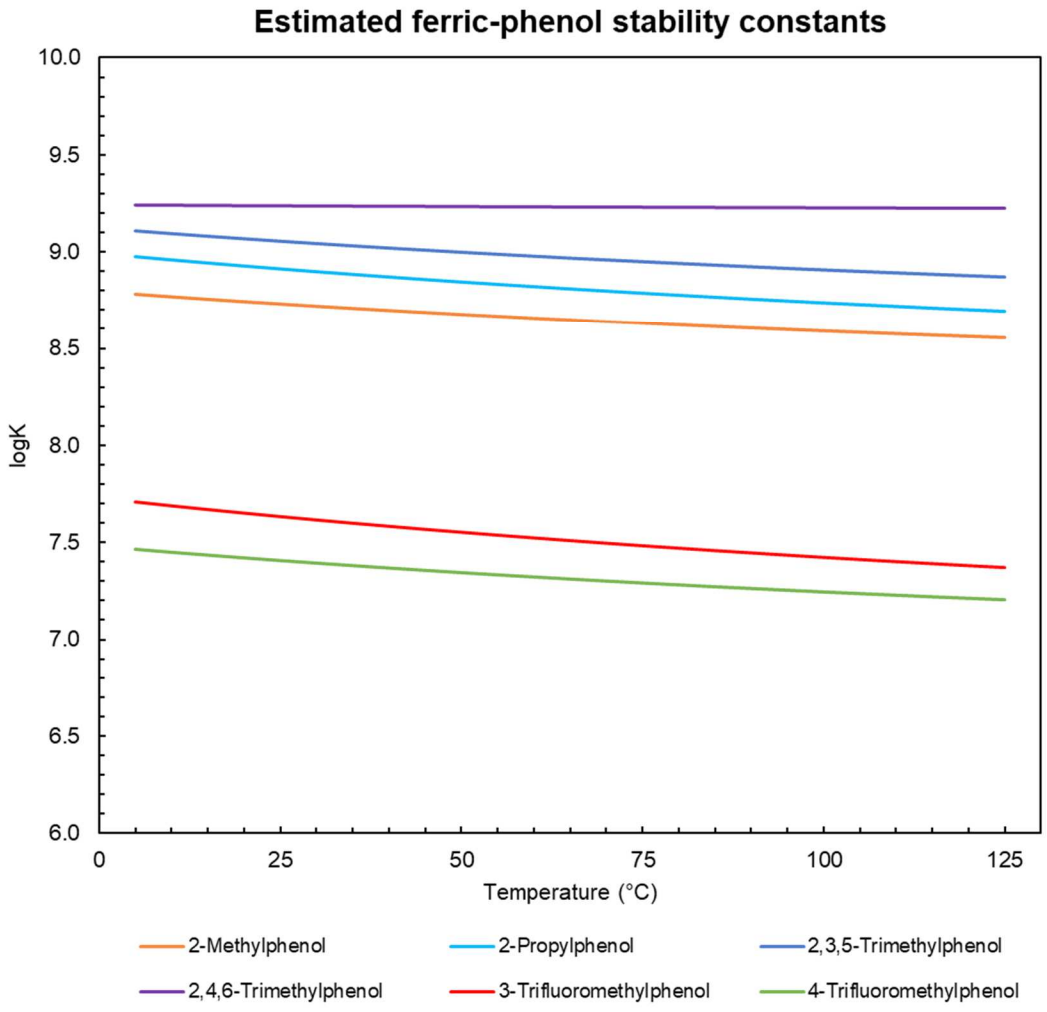

Fig 25. Van't Hoff plots created using only protonation thermodynamics of phenols. Stability constants were estimated from Fig.12(a) and entropy was estimated using correlation in Fig.16.

and 2-methoxy-4-methylphenol complexes owing to the ~ 10 orders in magnitude of difference in the protonation constants.

Analogous plots of predicted association constants for silicate and nitrite complexes obtained in a similar manner are shown in Fig. 27. In the case of silicate, the $\log K_{ML}$ values at the reference conditions are from the literature or estimated using the hydroxide correlation in Fig. 7 and $\Delta S°_{ML}$ values were obtained using the correlation shown in Fig. 19 if experimental values were unavailable. Note that the van't Hoff plots for metal-silicate complexes mirror those of the metal-phenol complexes when experimental $\log K_{ML}$ and $\Delta S°_{ML}$ values exist (as with Fe^{+3} and Na^{+}), which lends support to our estimates. Similarly, $\log K_{ML}$ values for all metal ions except Fe^{+3} were estimated using the correlation shown in Fig. 8 while $\Delta S°_{ML}$ values were obtained using the hydroxide correlation from Fig. 20. The decrease in stability constants with temperature is due to the negative enthalpies of association values for these reactions that arise from the low values of $\log K_{ML}$ and $\Delta S°_{ML}$.

Additional predictions shown in Fig 28 were made for two inorganic ligands-iodate and $H_2PO_4^-$, for which only $\Delta S°_a$ values are available. While $\log K_{ML}$ values were obtained from the correlations shown in Fig. 8, $\Delta S°_{ML}$ values were obtained by multiplying metal-hydroxide entropy of association with corresponding $\Delta S°_{a,L}$/ $\Delta S°_{a,Hydroxide}$ values. The positive temperature dependence of the predicted association constants stems from the large positive values of $\Delta S°_{ML}$ predicted from the $\Delta S°_a$ values for these ligands.

2.6 Concluding Remarks

We live in a world of ever-increasing production of diverse metals used in computers, high-tech devices, plumbing, wiring and automobiles (Gordon et al., 2006; Tansel, 2017), accompanied by a constant rise in novel pharmaceuticals, designer chemicals and green organic molecules (Dieleman et al., 2016; Sheldon, 2018; Shledon & Woodley, 2018). It is predictable that metal-ligand complexes are going to be a ubiquitous presence in our environment in the coming future. Speciation of both metals and ligands will be crucial in monitoring and controlling their abundance in our surroundings. At the same time, metal-ligand complexes have benefits with recent advances including metal-based anti-cancer and antidiabetic drugs (Levina et al., 2017; Kiss et al., 2017). Since metal-ligand speciation depends directly on metal-ligand thermodynamics, methods to estimate these properties, especially the stability constants, are increasingly in demand. Rigorous analytical measurement of these properties requires time and investment, leading to an inevitable inability to keep up with the rising diversity of metals and ligands. As a step toward addressing this problem, we have developed estimation strategies to estimate metal-ligand association constants over the biologically relevant temperature range of 0 to 125°C for a large class of metals and ligands.

In addition to estimating stability constants that fill gaps in the available experimental data for well- and lesser-studied monovalent oxygen ligands, our methods allow estimating $\log K_{ML}$ values for ligands with no thermodynamic data except for the ligand pK_a. The total number of estimated metal-ligand stability constants at 25°C and 1 bar amounts to 16,629 covering 69 metal ions and 241 ligands. This increases the currently available experimentally measured $\log K_{ML}$ values (417) by almost factor of 40. We predict that most of these stability constants are accurate within ±0.5 log units and

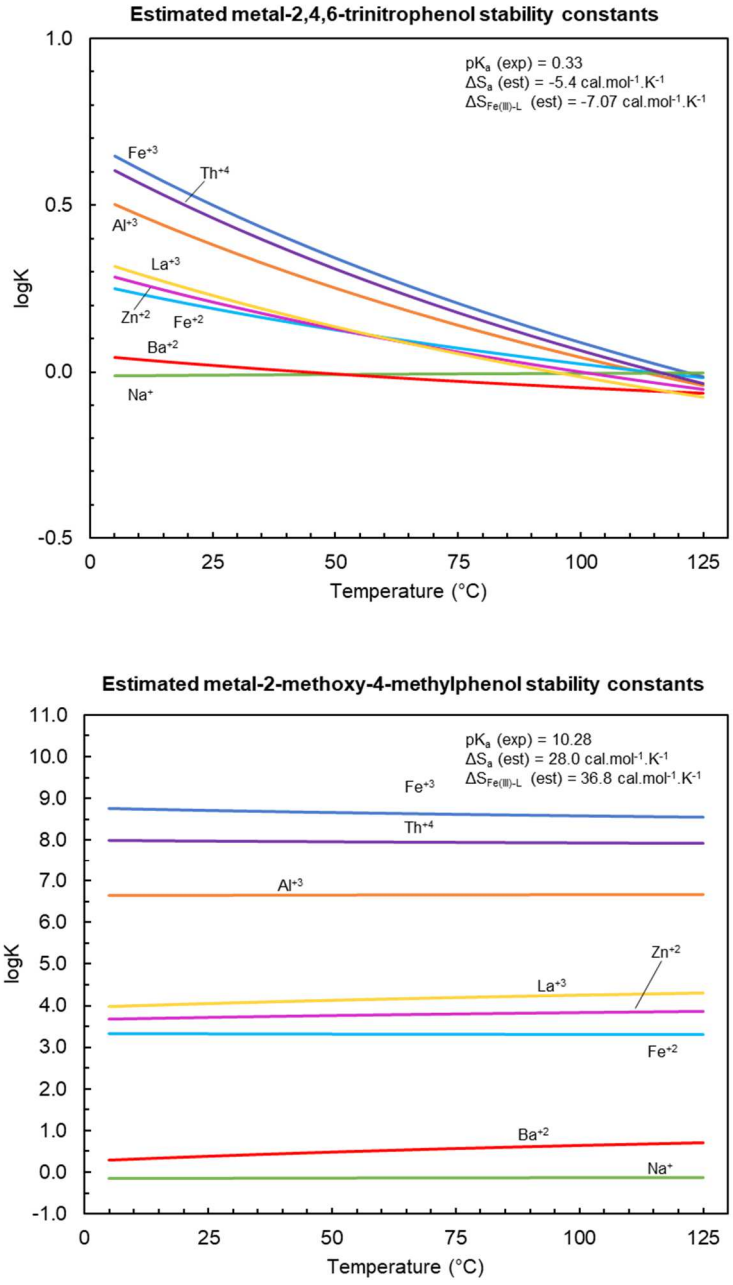

Fig 26. Van't Hoff plots created using only the ligand protonation constant from relationship obtained in Fig.17, Fig.16. and slopes from Supplementary Table 1. Stability constants were estimated from Fig. 12(a).

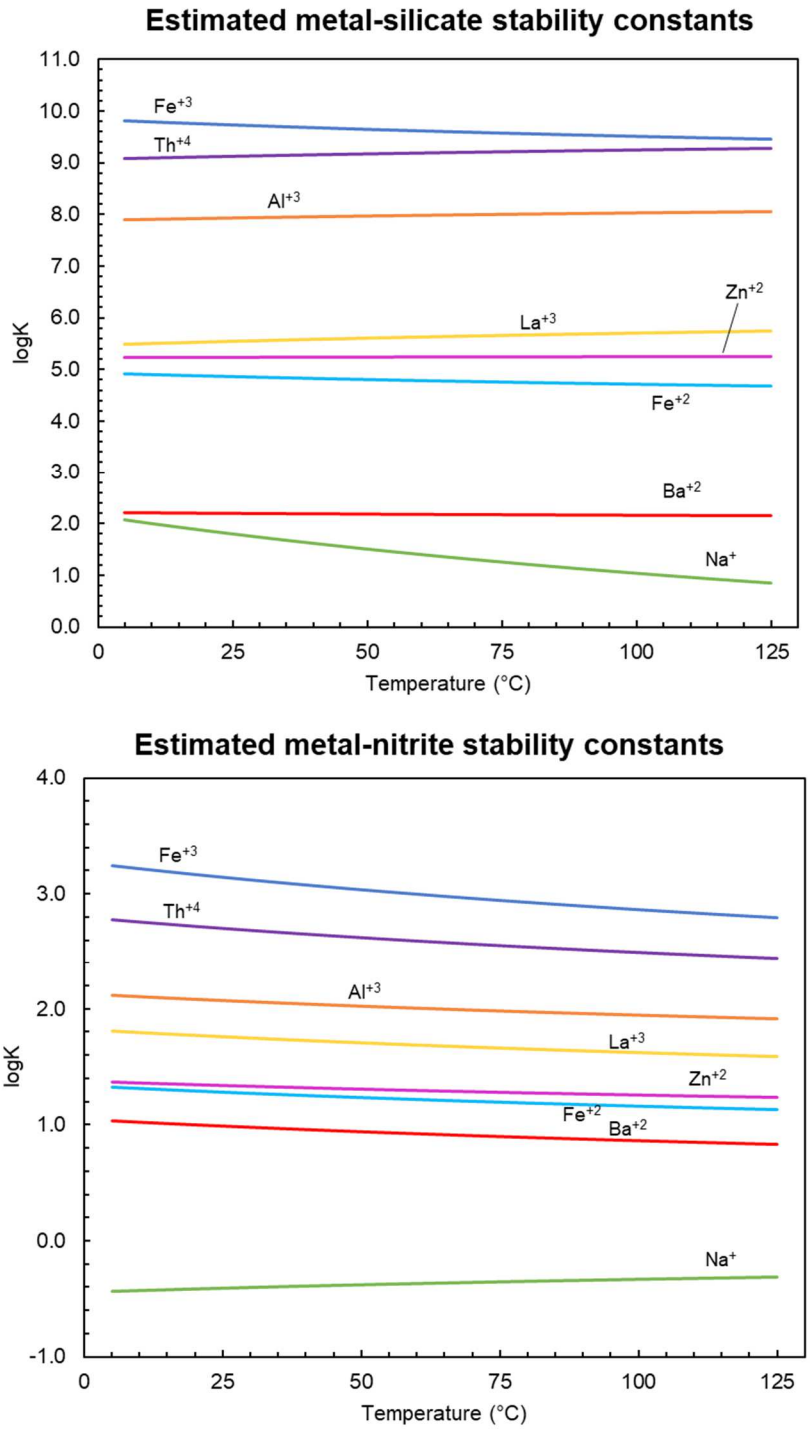

Fig 27. Van't Hoff plots for inorganic ligands from hydroxide entropy data. Stability constants were estimated using Fig. 7 & 8 while complexation entropy was estimated using Fig. 19 & 20.

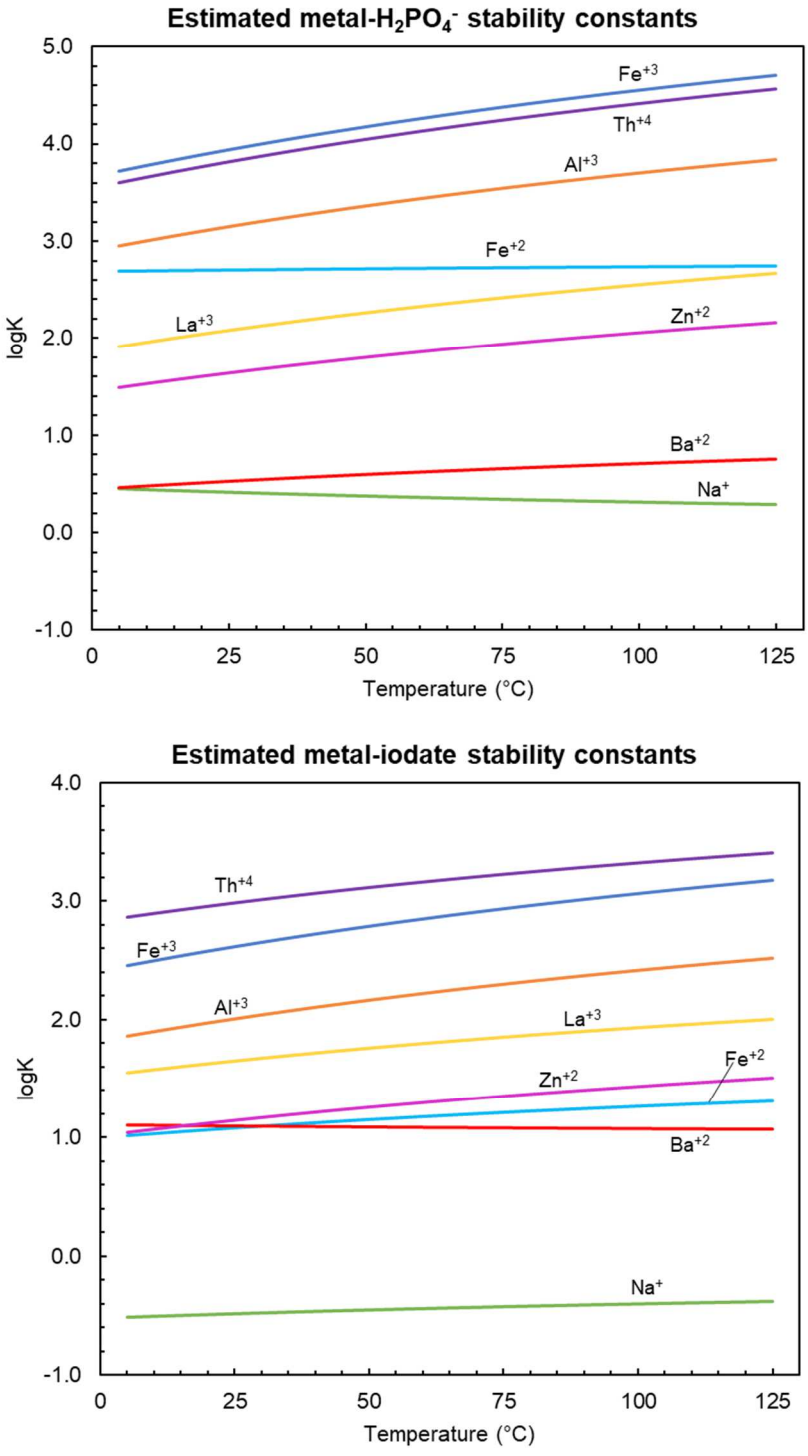

Fig 28. Van't Hoff plots created for inorganic ligands with for which no metal-ligand entropy values were available.

thus are unlikely to affect speciation calculations adversely. Since metal-ligand complexation entropy measurements are scarcer, the total number of $\Delta_r S°_{ML}$ values estimated are much fewer: 1848 metal complexes for 66 phenols with 28 metal ions and 4992 complexes of 156 carboxylic acids with 32 metal ions. We predict that these estimates at 25°C and 1 bar are accurate within ±2 cal $mol^{-1}K^{-1}$, which keeps predictions of log K_{ML} over the range of 0 to 125°C within ±0.5 log units. However, as these values are low in magnitude, they are not likely to affect van't Hoff extrapolations of the corresponding stability constants substantially.

Such estimation exercises are challenged by two potentially contradictory goals: high accuracy and extensive applicability. In this study we assembled an extensive database of experimentally obtained thermodynamic values, which permitted a search for the closest proxy ligands for building correlations. As a consequence, we believe we have achieved these goals simultaneously. Multiple correlations among structurally related ligands suggest that these patterns reflect properties of the ligand molecular structures and provide a foundation for further extention of methods to predict metal-ligand thermodynamics.

CHAPTER 3

ESTIMATING STABILITY CONSTANTS AND ENTROPY FOR METAL-LIGAND ASSOCIATION IN BLOOD PLASMA AND MICROBIAL GROWTH MEDIA

3.1 Introduction

From a chemical perspective, living organisms are complex aqueous systems composed of inorganic components like metal ions and organic components like amino acids. For example, a human adult's body mass is approximately 72% water, 21% organics and 7% inorganic components in which metals constitute one-third of the inorganic mass-fraction (Lentner 1981). As organic molecules have high reactivity towards many metal ions and outnumber them stoichiometrically, they end up dominating the metal distribution in most biological systems- for example, the serum protein transferrin alone complexes almost all of the Fe(III) in the blood plasma of a healthy human adult. Inorganic ions prevalent in biological systems like phosphate may also influence the distribution of several metals. Any significant disruption in the state of metallic distribution in any biological system can lead to disastrous results as evidenced by cases of iron-overloading and heavy-metal toxicity. On the other hand, the knowledge of biological metal distribution is also crucial to exploit the positive effects of metals as in the case of zinc-based antidiabetics and gallium-based anticancer drugs. Moreover, there is now substantial evidence that metal-ligand complexes cross the cell membrane via ion channels and essential metal transport proteins (Levina et al. 2017). Thus, it is becoming increasingly vital to study the distribution of metals and ligands in biological systems.

Accurate determination of elemental distribution in a complex system at low concentration has proved to be extremely difficult via analytical techniques (Kiss et al. 2017). Alternatively, this information can be obtained using computer programs that obtain the equilibrium distribution of these elements using equilibrium constants (or stability constants) of the associated reactions in the system. As these programs assume a state of equilibrium, they are appropriate to study metal-ligand distribution as metal-ligand complexation reactions have low kinetic barriers and reach equilibrium within seconds. This approach is also desirable as many of these programs (like EQ3/6) are freely available and perform these calculations in the order of milliseconds. However, these programs are also limited as the thermodynamic data for several of these reactions is not available. To ameliorate this problem, we estimated metal-ligand stability constants for all ligands present at micromolar concentration in blood plasma and those routinely used in microbial growth media.

Our estimation strategy can be best summed up as: 'create linear free energy relationships between the ligand of interest and the best proxy ligand with the most data'. Linear free energy relationships (LFER) have been used for several decades to estimate metal-ligand thermodynamic properties (Irving & Rossotti 1956, Shock & Koretsky 1993, Shock & Koretsky 1995, Martell & Hancock 1996, Sverjensky et al. 1997, Carbonaro & Di Toro 2007, Carbonaro et al. 2011, Atalay et al. 2013). These LFERs are created by correlating one set of metal-ligand thermodynamic properties with another set of thermodynamic properties such as correlating stability constants for one metal and a set of ligands with the pK_a of the respective ligands. As summarized by Martell &

Hancock 1996, multiple variants of LFER have been used over the years. However, many of them can be misleading if the nature of metal-ligand interaction is not properly considered (Hancock 1995). Thus, metal-ligand stability constants warrant careful consideration as error of only a few log units may significantly alter the predicted metal distribution. We have employed a similar approach to estimate stability constants for metal complexes of monovalent oxygen ligands (Prasad & Shock 2019a). In this work, we have extended this approach to include metal complexes of amino acids, peptides, proteins, dicarboxylic acids and vitamins.

In addition to making estimates of stability constants, we have found that the above-mentioned strategy also works for estimating metal-ligand entropy of association. This is particularly useful as both estimates in conjunction can be used to estimate the metal-ligand stability constant reasonably accurately over the biologically relevant range of 0-120°C where no experimental data exists. This is made possible using the van't Hoff relationship (Eq. 2) which is routinely used in thermodynamics to get the temperature dependence of stability constants from 0 to 125°C using enthalpy and entropy at reference temperature (298K).

Our present and previous work (Prasad & Shock 2019a) demonstrates that such estimation strategies can be used to estimate the thermodynamic properties of a wide variety of ligands in addition to the ones we have considered. The "compound libraries" in the Developmental Therapeutics Program of the United States National Cancer Institute consist of over 600,000 synthetic and natural molecules (Ng 2015). Moreover, modern "virtual libraries" of pharmaceutical companies amount to ~10^{18} chemical

compounds (Hoffman & Gastreich 2019). Given the astronomical number and diversity of ligands, it is practically impossible to experimentally obtain stability constants for all metal-ligand complexes due to cost and time constraints. Alternatively, estimation strategies like ours can provide thermodynamic data for countless molecules belonging to these gigantic datasets, especially the ones with carboxylic, amino, sulfhydryl and imidazole groups. We have utilized these estimates to obtain metal-ligand distribution in biological growth media and blood (Prasad & Shock 2019c, Prasad & Shock 2019d) that enable a better understanding of metal bioavailability and uptake.

In addition to estimating metal-ligand stability constants and entropy for a variety of complex ligands based on the nature of chemical interaction, we have also found the converse to be true- i.e., these correlations can be used to obtain the metal-interacting regions of ligands with multiple functional groups. In this way, thermodynamic data can be used to obtain the nature of metal-ligand coordination. This approach can help decipher the functional groups of pharmaceutical drugs that may interact with metal ions and help locate 'metal-binding sites' on proteins.

The purpose of this paper is to provide the most accurate estimates of stability constants from 0 to 125°C for some of the most biologically relevant metal-ligand complexes. Our inventory of complexes includes approximately 3000 metal-ligand complexes for ~60 metal ions and ~50 ligands ranging from vitamins to proteins. Since all our correlations include the protonation reaction and many of them have intercepts close to zero, they suggest that metal-ligand thermodynamic properties can be obtained with sufficient accuracy using only the ligand protonation property. This implies that

such 1-parameter (slope) correlations can be used to derive stability constants for possibly unlimited metal-ligand complexes that belong to the respective categories of proxy ligands. We have carefully noted the cases where the intercepts deviate substantially from zero that can be explained by the concepts of denticity and chelate-ring size. While most of our stability constant estimations can be predicted within ±0.5 log units, most of our entropy estimates are within ±2 cal/mol/K which mirrors the order of experimental uncertainty. These estimates have been generated from correlations of critically evaluated experimental measurements of more than 900 metal-ligand complexes performed over the past 90 years. The grounding of these correlations in coordination chemistry adds to their rigor and has been explained in more detail in the subsequent sections.

3.2 Definitions and data evaluation

In this work, we have only considered the first step in the reaction between a metal ion and a ligand. So, the stability constant and entropy values correspond to the following general reaction:

$$M^{y+} + L^{z-} = ML^{y-z} \qquad (1)$$

where M refers to a metal ion of charge y and L refers to a ligand of charge -z. The stability constant of such a reaction (same as the equilibrium constant) is designated as K while the entropy of association for this reaction has been designated as $\Delta S°$. Since stability constants are mostly described in their logarithmic forms, the term 'logK' has been used to refer to metal-ligand stability constants described in this work.

While the standard state equilibrium constant of a reaction only depends on the temperature and pressure of the system, it is mostly measured as the stoichiometric constant (K'), that is also dependent on ionic strength. The relationship between K and K' for Reaction (1) is:

$$K = K' * \frac{\gamma_{ML}}{\gamma_M * \gamma_L} \quad (2)$$

where γ represents ionic strength dependent activity coefficient of the chemical species involved in the chemical reaction. The activity coefficient of a chemical species can be closely approximated using the B-dot equation for experiments performed at low ionic strength (Helgeson, 1969). We have used this equation to convert the reported stoichiometric constants from the literature measured at variable ionic strengths into standard state equilibrium constants that correspond to an ionic strength of zero. In addition to the need to standardize stability constants, the B-dot equation was used so that these extrapolated values could be directly used in equilibrium speciation software like EQ3/6 (Wolery 2010) that also employ this equation. Thus, no extrapolation errors would be made upon using the modified equilibrium constant at the original ionic strength in this program. Most of the stability constants considered in this work refer to measurements reported at 25°C and 1 bar. Careful consideration was spent on selecting the most accurate stability constant values which are outlined in the Supplementary Tables.

Chemical speciation is defined as the distribution of a system component in different chemical species. For example, ~45% of the total calcium in blood plasma is

bound to serum proteins (mainly albumin), ~45% is free Ca^{+2} and the remaining 10% is complexed to low molecular mass molecules like bicarbonate and citrate (Peters 1996). This concept can also be extended to ligands like carbonate that exist predominantly as CO_3^{-2} at high pH, HCO_3^- between pH 6.3 to 10.3 and as carbonic acid at low pH. Chemical speciation of a system can be obtained by including equilibrium constants of all reactions that may occur between each chemical species of a chemical system along with the total analytical concentration of the chemical components and solving the system of equations obtained upon observing the law of mass action and the law of mass balance. While this process can be performed by hand, computer programs like EQ3/6 and PHREEQC (Parkhurst 2013) can perform such calculations in a more expedient manner.

3.3 Estimation strategy

Decades of scientific investigation on metal-ligand coordination has revealed that the associated thermodynamic properties are dependent on the following chemical attributes- metal ionic radius, metal coordination number, charge of the metal ion, charge of the ligand, type of ligand electron-donor atom, ligand denticity, chelate ring size, ligand preorganization, steric effects and inductive effects (Martell & Hancock 1996). As the ligand chemical attributes like denticity and electron-donor atom are more variable, we found that ligand-specific LFERs are more rigorous than cation-specific LFERs. Thus, our strategy for the estimation of metal-ligand stability constants can be best described as : pick the best proxy ligand with the most data. The strategy of choosing the 'best proxy ligand' has been described in our previous work (Prasad & Shock 2019a). Briefly, the best proxy ligand has the same metal coordination sphere as that of the ligand

of concern. A correlation between such ligands produces a slope ~1 and an intercept ~0 as in the case of α-alaninate and glycinate in Fig. 29. This is because both α-alaninate and glycinate coordinate with metal ions in a bidentate manner with the same electron-donor atoms (a primary amino group and a carboxylate group) making 5-membered chelate rings. The slight deviation from unit slope and null intercept occurs due to the difference in the 'side-groups' (-H for glycinate and $-CH_3$ for α-alaninate) that impart minor inductive and steric effects. The existence of experimental stability constants for almost 50 metal ions suggested glycinate is a good choice to approximate stability constants for amino acids.

However, the correlation between histidine and glycinate stability constants was found to be quite weak (not shown). Instead, histidine and bipyridine (BIPY) complexes correlated very well, thereby suggesting that the imidazole sidechain of histidine is involved in the metal coordination. The significantly higher intercept (~1.72) suggests that metal-histidine complexes are of a higher denticity than metal-BIPY complexes. Other correlations of ligands in Fig. 29 demonstrate that different proxy ligands are needed to estimate metal-complexation properties of chemically different ligands based on the nature of electron donor atom (sulfhydryl groups in glutathione vs. cysteine and carboxylate groups in succinate vs. diglycolate), charge (trivalent in PO_4^{-3} and citrate) while accounting for denticity (inosine vs. imidazole and HPO_4^{-2} vs. hydroxide) . It must be noted that we have precluded the weak correlations with inappropriate proxy ligands to save readers' time and effort. For more details on how these correlations were made,

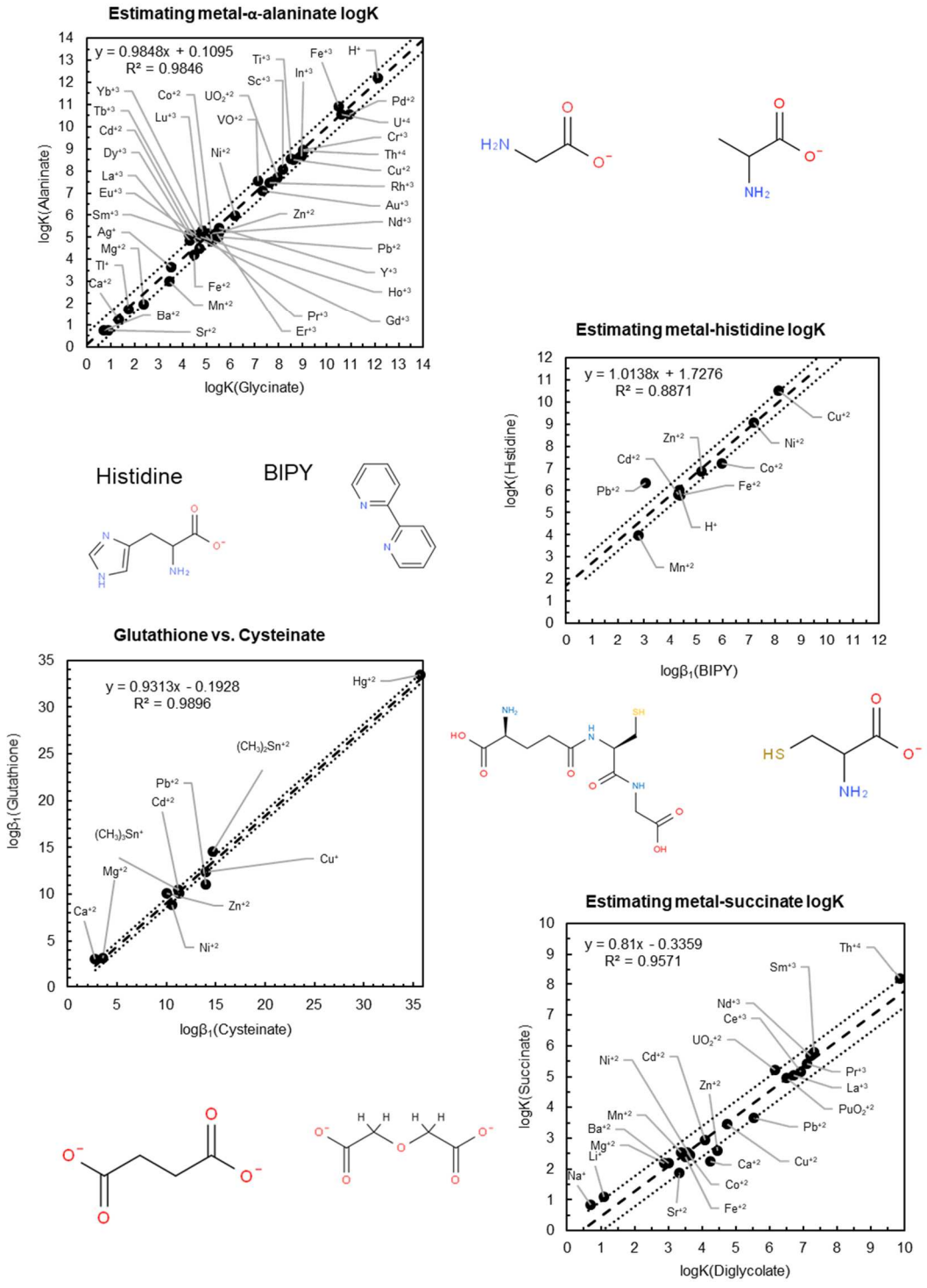

Fig 29. Different estimation strategies to estimate different types of ligands (contd.)

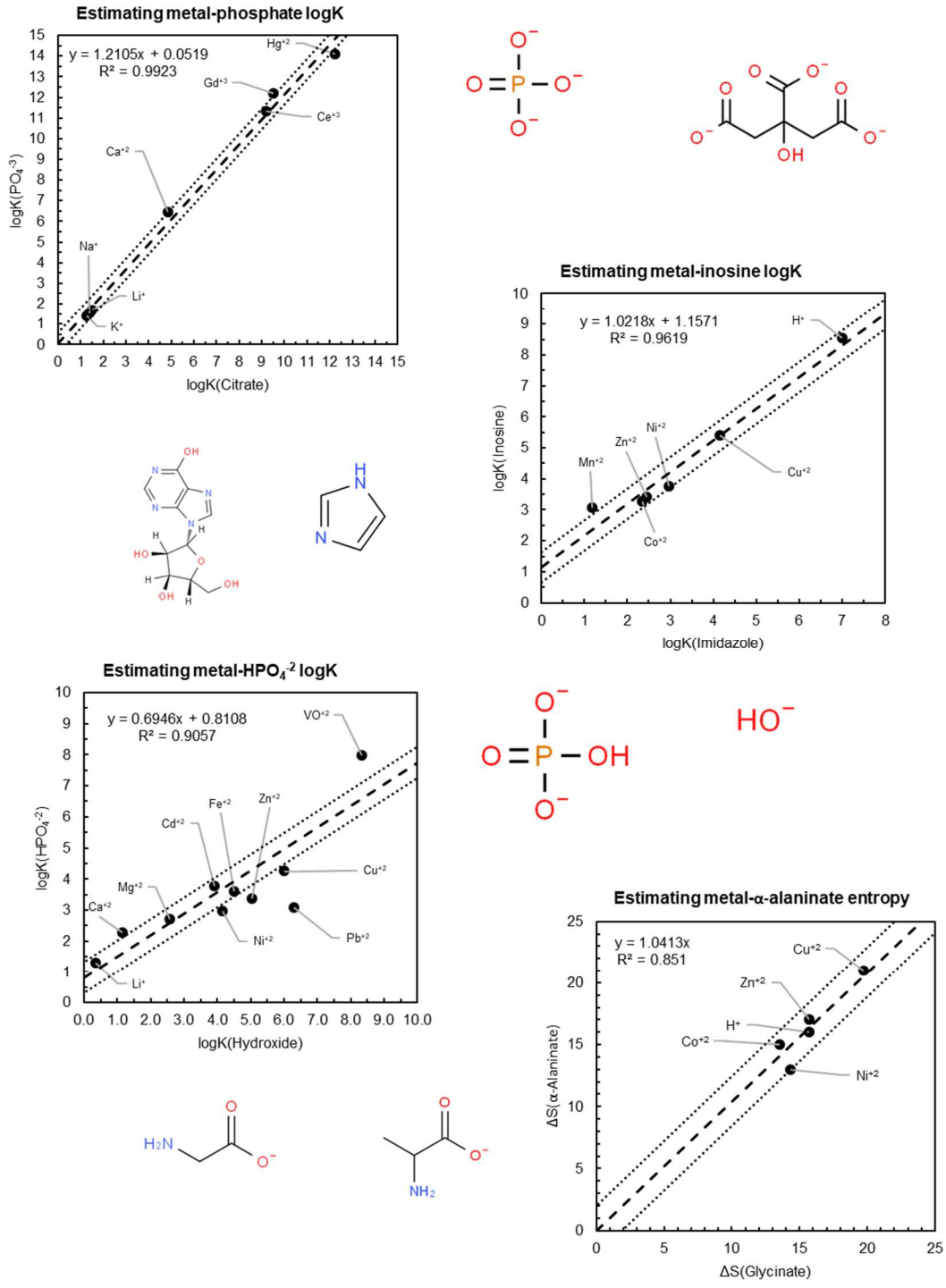

(contd) Fig 29. Different estimation strategies to estimate different types of ligands.

the readers are requested to refer to the corresponding sections of amino acids, dicarboxylic acids, peptides, proteins and vitamins.

The strategy of using 'the best proxy ligand with most data' was also used to estimate metal-ligand entropy of association as displayed in the correlation between $\Delta_r S$ values of α-alaninate and glycinate complexes in Fig. 29. Due to the limited reports of this thermodynamic property in the literature, the intercepts of our entropy correlations have been set to zero to avoid estimation errors due to skewing of data. While this practice reduces the correlation coefficient, it is perhaps a better predictive approach for multiple types of ligands.

3.4 Estimating stability constants at 25°C and 1 bar

3 .4.1 Amino acids

Amino acids amount to almost 3 millimolar concentration in blood plasma and are routinely employed in chemically defined microbial growth media or as peptones and meat extract in chemically undefined media (Lentner 1981; DSMZ, Leibniz 2019). Besides serving as the building blocks of proteins, they are also involved in cell-signaling, gene expression, protein phosphorylation cascade and hormone syntheses (Wu 2009). While they are crucial for these biological processes, elevated levels of amino acids cause neurological disorders and oxidative stress (Wu 2009). Thus, knowledge of amino acid speciation can be very useful in tracking the distribution and bioavailability of these molecules in biological systems. Here, we present techniques to estimate metal-amino acid stability constants that can help facilitate these calculations.

The success of α-alaninate vs. glycinate correlation of Fig. 29 suggested that similar correlations should be made for other amino acids with alkyl sidechains. Expectedly, correlations with glycinate for these amino acids like valinate, leucinate and isoleucinate resulted in highly rigorous correlations with slope close to unity, intercept close to zero and all experimental values ranging within ±0.5 log units (Fig. 30). A similar result was obtained for 2-aminopentanoate and 2-aminohexanoate that is shown in Fig.A1 of Appendix A. The "H^+" on these correlations is the sum of the pK_a values of amino and carboxylic groups. The slightly negative intercepts on these correlations can be explained by higher steric effects of these alkyl side-groups in comparison with -H group of glycinate.

While the glycinate correlations were expected to work for amino acids with alkyl sidechains, it was interesting to note that these correlations also worked for amino acids with polar side chains (Fig. 31). These amino acids include side chains with polar oxygen (serine), polar sulfur (methionine), polar nitrogen (asparagine and glutamine) and even ionizable side chains like phenyl (tyrosine) and guanidine (arginine). The slope and intercept of these correlations are again close to 1 & 0 respectively and all experimental values lie within ±0.5 units of the correlation line with minor exceptions that suggests that these amino acids are complexing metal ions in a "glycinate like" manner-i.e. a bidentate 5-membered chelate ring with amino and carboxylic groups. Perhaps an exception to this is the Hg(II)-methioninate complex that has additional strength due to the "soft" interaction between Hg & S based on the Pearson classification (Pearson 1963).

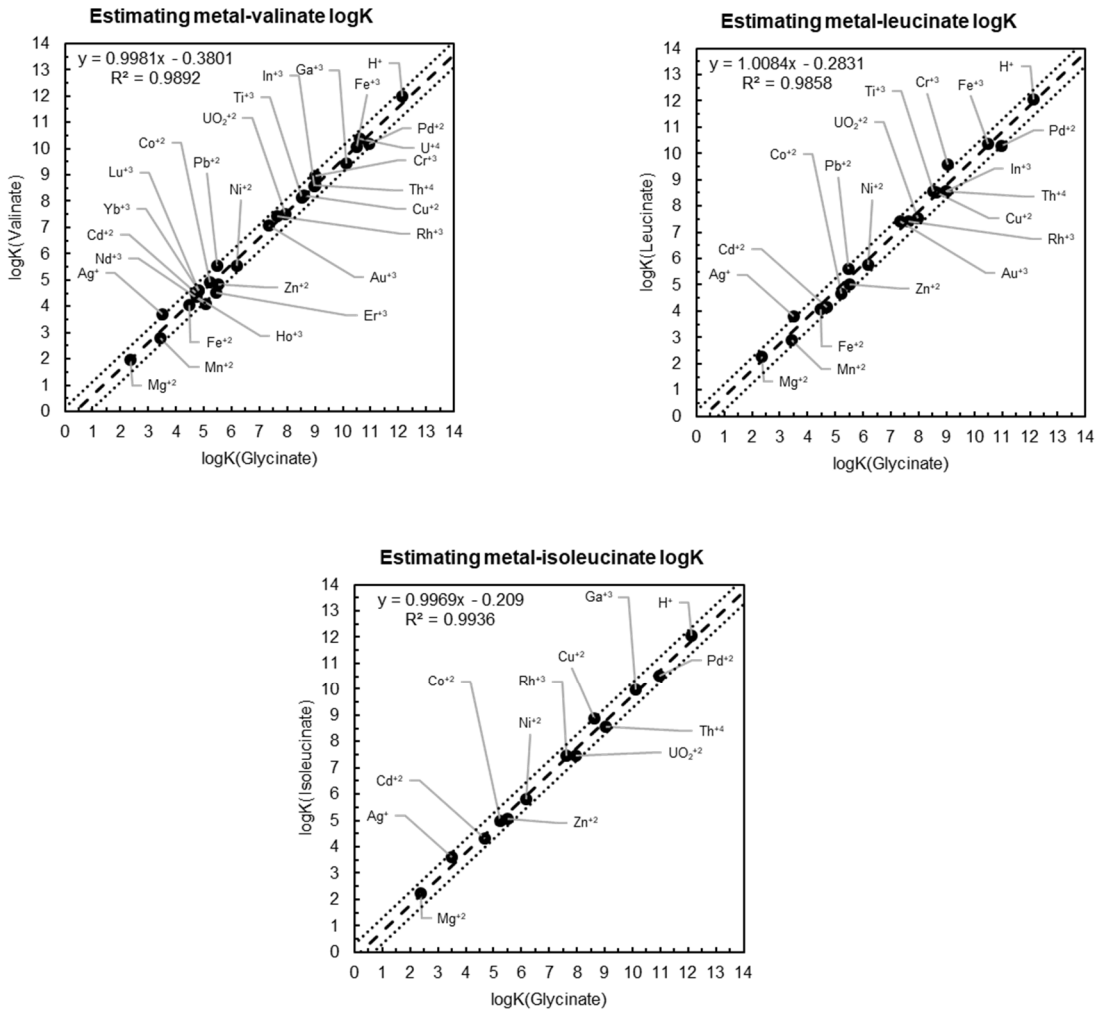

Fig 30. Expected “glycinate-like” LFERs for amino acids with alkyl side groups (contd.)

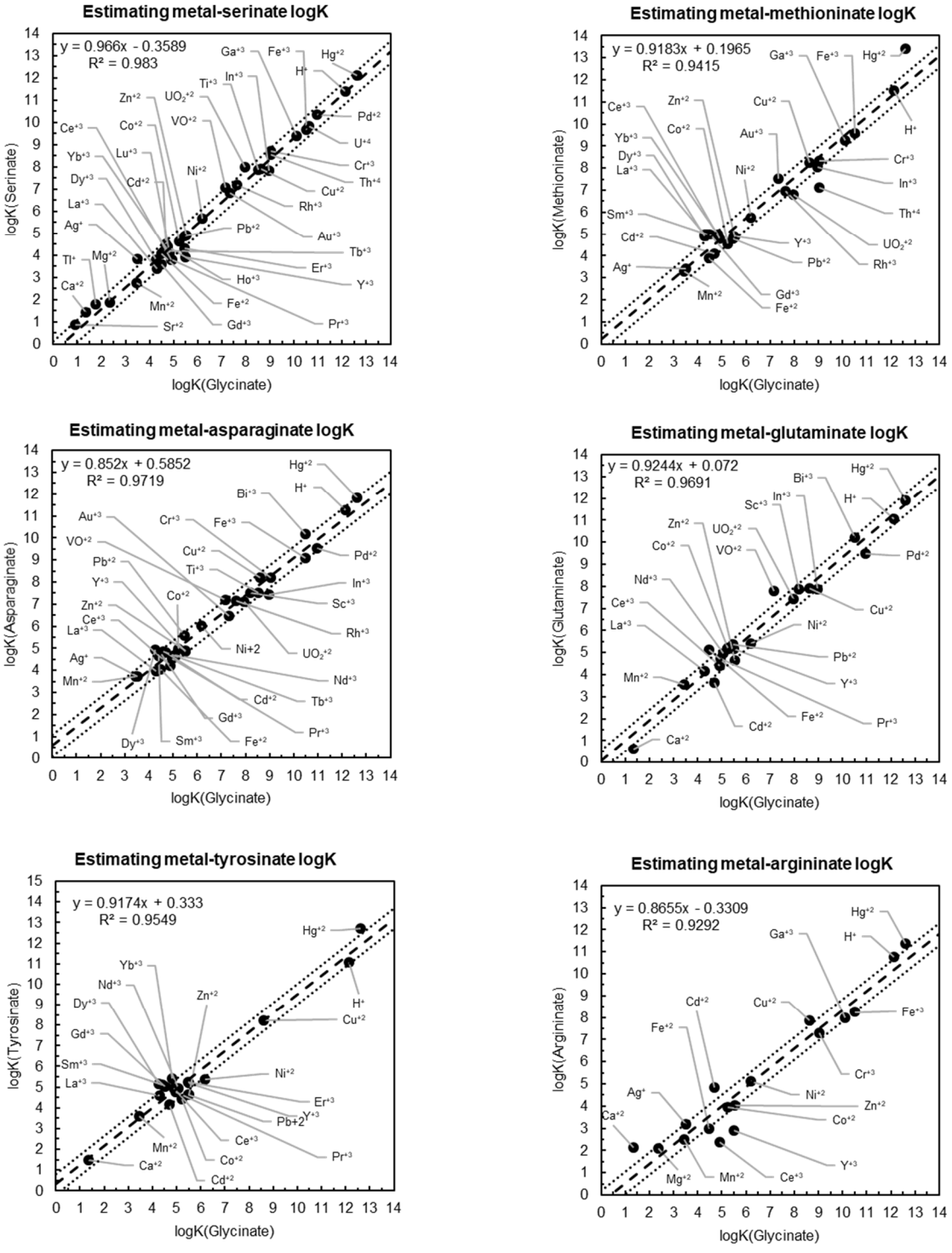

Fig 31. Unexpected “glycinate-like” LFERs for amino acids with polar side groups

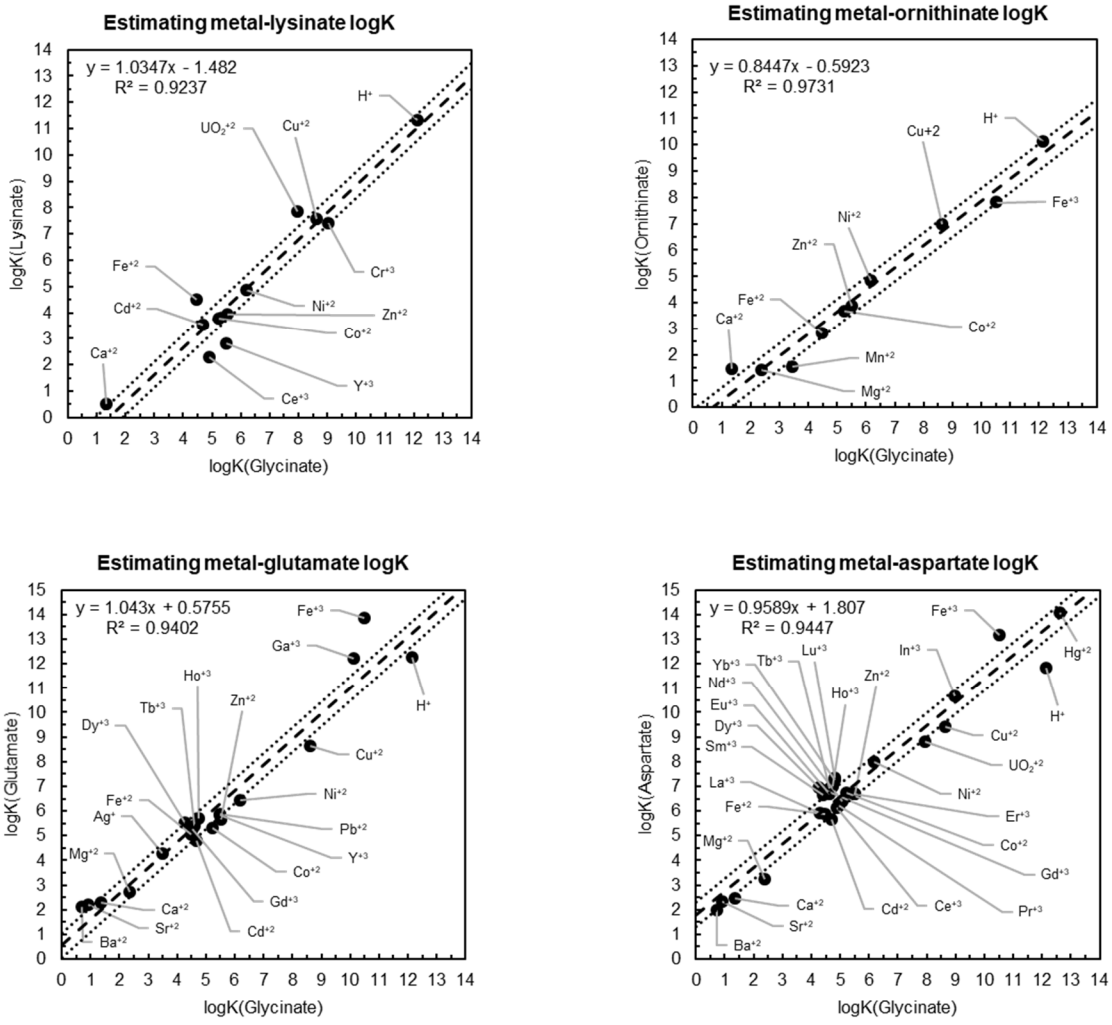

Fig 32. Effect on LFER intercept for amino acids with ionizable side groups

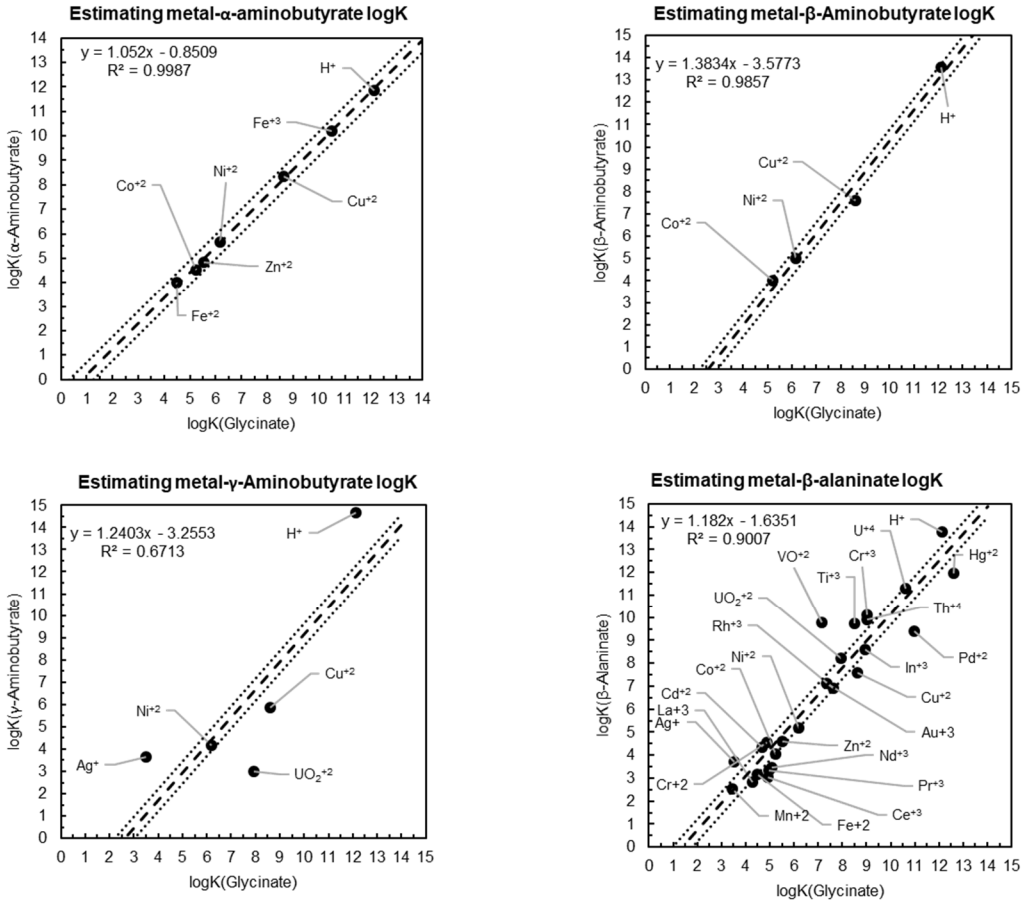

Fig 33. Effect on LFER intercept for amino acids with different chelate-ring size.

This systemic behavior of unit slope and null intercept for glycinate correlations reaches a breaking point when such correlations are made for other amino acids with ionizable sidechains like lysinate, onithinate, glutamate and aspartate (Fig. 32). The intercepts for all these correlations are outside the acceptable uncertainty of ±0.5 units. It is interesting however to note that these intercepts are positive for the positively charged side chains of (lysinate & ornithinate) and negative for the negatively charged side chains (glutamate and aspartate), perhaps reflecting an electrostatic interaction with the positively charged metal ions. Additionally, the significantly higher intercept of aspartate in comparison to glutamate can perhaps be explained by the closer proximity of the carboxylate sidechain (β for aspartate, γ for glutamate) that enables a stronger interaction with the metal ion for the aspartate molecule.

The effect of chelate-ring size on LFER can be observed in the trend of negative intercepts in Fig. 33. While α-aminobutyrate makes 5-membered chelate-rings, β-aminobutyrate and γ-aminobutyrate make chelate-rings of size 6 and 7 respectively. This seems to have an impact on the metal-ligand stability as the intercept value decreases from ~ -0.85 to ~ -3.58 for α-aminobutyrate and β-aminobutyrate respectively. A low correlation coefficient for the γ-aminobutyrate LFER suggests that glycinate may not be the right proxy ligand for this ligand. A similar phenomenon is observed in the glycinate correlations of α-alaninate (Fig. 29) and β-alaninate (Fig.33) where the intercept value decreases from +0.11 to -1.63. The effect of chelate-ring size on metal-ligand logK has been observed before and is explained in more detail in Martell & Hancock 1996.

3.4.2 Peptides & proteins

Like amino acids, peptides and proteins also amount to millimolar concentration in blood plasma as is reflected by the abundance of glutathione, serum albumin, cystine and transferrin. Besides high concentration, proteins like transferrin have 'metal-binding sites' with high chelating tendency. This makes proteins and peptides enormous reservoirs of metal distribution in biological fluids. However, these molecules are generally absent from the database of most speciation programs possibly due to the lack of necessary data (Kiss et al. 2017). Thus, we created customized LFERs for these molecules to obtain the required metal-ligand stability constants that may be used to obtain metal speciation in biological fluids like blood plasma and cerebrospinal fluid.

Of all the molecules mentioned above, transferrin is the best studied metal-chelator, perhaps largely due to the high stability constants with trivalent cations. It has two 'metal-binding site' located in each of the two domains of the ~80kDa molecule. Each site is composed of two tyrosine, one aspartate, one histidine and a carbonate molecule that acts as a "synergistic anion" (Harris 2012). Owing to the presence of the carbonate ion, the metal complexation reaction is a ternary reaction comprising of the metal ion, the transferrin molecule and the bicarbonate ion (Aasa et al. 1963; Aisen et al. 1978). The stoichiometry of the two complexation reactions at the respective sites can be given as:

$$M^{y+} + Transferrin^{z-} + HCO_3^- = (M.Transferrin.CO_3)^{y-z-2} + nH^+ \quad (3)$$

$$M^{y+} + (M.Transferrin.CO_3)^{y-z-2} + HCO_3^- = (M_2.Transferrin.(CO_3)_2)^{2(y-z-2)} + 2nH^+ \quad (4)$$

where M^{y+} refers to the metal ion, z- refers to the charge on transferrin and n refers to the number of protons released per reaction. The transferrin LFERs in Fig. 34 correspond to

the above ternary reactions that accounts for the negative intercepts. Due to the presence of numerous O^- groups at the transferrin 'metal-binding site', hydroxide has been considered as the appropriate 'proxy ligand' (Sun et al. 1997). However, the correlation with the first hydroxide complexation resulted in a very high slope (not shown) that leads to high estimation uncertainty. Instead, we resolved to create a correlation with the second hydroxide complexation that yields a slope ~1, thereby significantly decreasing the errors associated with stability constant predictions. The transferrin stability constants were obtained by regressing the reported measurements summarized in Supplementary Table 2 using EQ3/6. As the regressions were performed with the metal-complexation written as the actual ternary reaction (Reactions 3 & 4), they slightly differ from the original studies that report the values as a binary reaction. Additionally, as our regressions incorporated the transferrin protonation reactions that were reported subsequent to the metal-complexation studies, they do not suffer from pH dependence as is generally observed in reports on metal-protein association. It is worth noting that the values reported by these studies are extremely sensitive to the stability constants of the associated 'competing ligands'. Thus, acute caution needs to be observed while measuring and analyzing metal-protein stability constants.

Albumin has four predominant metal-complexation sites- the Multi-Metal Binding Site (MBS), the N-Terminal Site (NTS), Site B and Cys34 (Bal et al. 2013). Due to the limited measurements performed for NTS, Site B and Cys34, it is hard to create functional correlations to estimate corresponding metal-albumin stability constants. However, perhaps this is not a cause of concern as NTS has a high specificity for copper

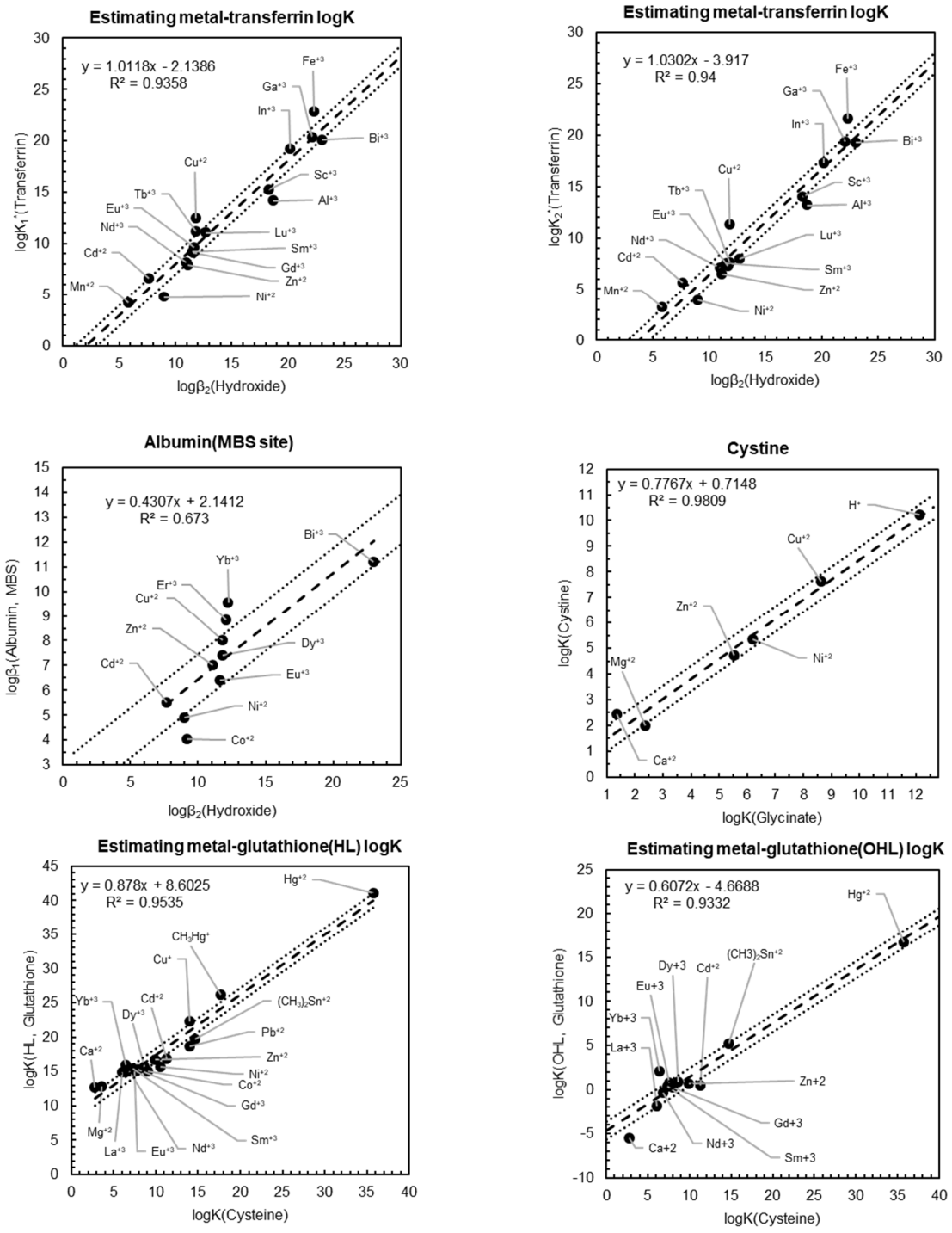

Fig 34. LFERs for peptides and proteins prevalent in blood plasma.

(due to multiple N-based groups) and Cys34 only feebly interacts with 'soft metal ions' as it comprises of a single thiol group. Additionally, the reported stability constants for a metal ion at Site B are lower than those reported for MBS which makes MBS the predominant metal-complexation site on albumin. Thus, several estimation techniques were employed to robustly predict metal stability constants at the MBS site. The presence of two O-bearing groups and an equal number of N-bearing groups at the site suggested that a proxy ligand with both oxygen and nitrogen based functional groups might yield the most secure correlation. However, the LFER with hydroxide was found to be the best predictive technique (Fig. 34) in comparison with other proxy ligands like glycinate and imidazole (not shown). This suggests that aspartate and asparagine are more strongly involved in metal coordination as compared to the histidine residues at the MBS site.

As cystine is a cysteine dimer connected via the disulfide bridge, metal-cystine stability constants correlated rather poorly with metal-cysteine stability constants. Instead, the cystinate-glycinate correlation was far more rigorous (Fig. 34), suggesting that metal ions are interacting with the amino and carboxylic groups of cystine without much involvement from the sulfur groups which concurs with the results of Paul et al. 2012. The cartesian ordinate of H^+ on the correlation corresponds to the sum of two functional groups out of the four protonation sites on cystine (the higher amino and carboxylic pK_a values), that further buttresses our coordination inference. Thus, metal-ligand LFERs can be used to obtain metal-ligand coordination for ligands with multiple functional groups.

In addition to creating LFERs for the completely deprotonated form of glutathione, we extended this approach to the singly protonated and hydroxylated forms of the tripeptide. Making these estimates could be crucial for metal distribution in blood plasma given the high concentration of glutathione (~1 mM) and the sparse dataset. Like the correlation for the completely deprotonated glutathione (Fig. 29), we made cysteine based LFERs for these forms that are shown in Fig. 34. Corresponding correlations with respective protonated and hydroxylated complexes of cysteine were not possible as the data was very limited. These well constrained correlations suggest that the metal-thiol interaction dominates for these forms of glutathione and can serve as a general framework to estimate similar variants of ligands.

3.4.3 Dianionic carboxylic acids

Divalent carboxylic acids are naturally present in human bodily fluids at micromolar concentration and are routinely employed in microbial growth media. Owing to the presence of two carboxylic groups, they make good metal-chelators as is reflected in the stability constant values of metal-oxalate complexes. Others like salicylate are used in bismuth-based antacids that are popular over-the-counter drugs. We had laid out a general framework to estimate stability constants of metal complexes with monocarboxylates in Prasad & Shock 2019a. Here, we present estimation techniques to predict stability constants of metal-dicarboxylates.

Following our general strategy of "best proxy ligand with most data", we had used diglycolate as the ligand of choice for dicarboxylates as it consists of two carboxylic groups and has been extensively studied with stability constant measurements for over 40

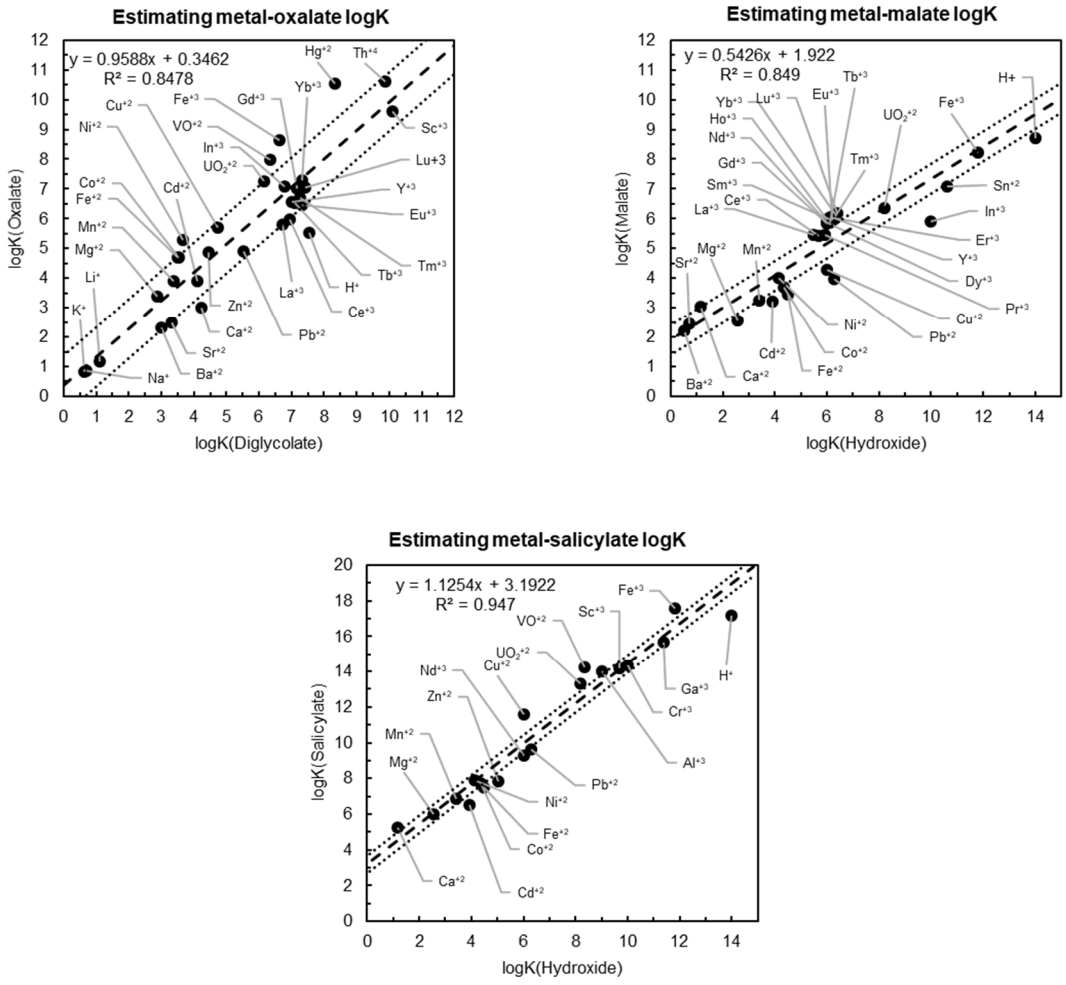

Fig 35. LFERs for dicarboxylates prevalent in blood plasma.

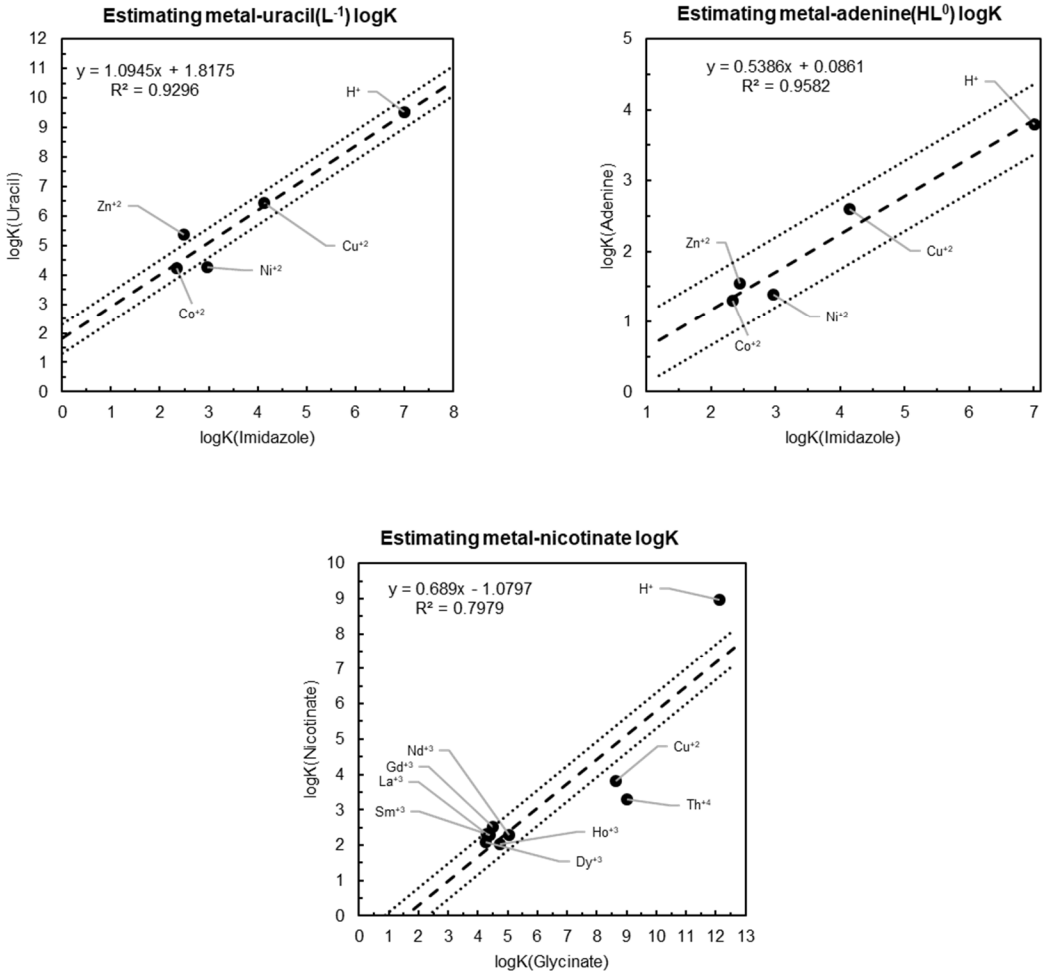

Fig 36. LFERs for vitamins and nutrients used in growth media

metal ions. This strategy had been effective in the estimation of metal-succinate complexes as demonstrated in Fig. 29. It yet again proved useful in estimating metal-oxalate stability constants as can be observed in Fig. 35 from a slope ~1 and an intercept ~0. While metal-diglycolate stability constants correlated well with malate and salicylate complexes (not shown), the correlation-coefficient was much higher for the hydroxide correlation. While the intercept for the malate-hydroxide correlation is close to the theoretical prediction (Martell & Hancock 1996), the unusually high intercept for the salicylate correlation is perhaps due to a higher degree of ligand preorganization that is generally observed for aromatic groups.

3.4.4 Vitamins & growth factors

Since vitamins and growth factors amount to a low abundance in most microbial growth media, they are expected to play a minimal role in metal speciation. Instead, their distribution can be expected to be dictated by Group I & II metals like Na^{+} and Ca^{+2} that are employed in high concentration in growth media. In Fig. 36, we have extended our estimation strategy to molecules like uracil, adenine and nicotinate (vitamin B_3). While imidazole provided the best correlations with uracil and adenine, glycinate proved to be the 'best proxy ligand' owing to structural similarities in the respective cases. As can be seen from the figure, despite the limited stability constant dataset, the correlations obtained are quite robust with high correlation coefficient. The relatively low accuracy of the nicotinate-glycinate correlation may be addressed to the limited reports of metal-nicotinate stability constants (only three). We suspect that further investigation of this dataset will yield better correlations.

3.5 Estimating entropy of association at 25°C and 1 bar

Since our strategy for estimating stability constants was rooted in a fundamental understanding of the metal-ligand chemical structure, it was evident that the same could be extended to estimating metal-ligand entropy of association (ΔS°). As glycinate and diglycolate were the best studied ligands of their respective categories, they were chosen as the proxy ligands to estimate ΔS° for amino acids and dicarboxylates, respectively. However, as the ΔS° dataset was still very limited for these "best proxy ligands" (only 22 values for glycinate and 28 for diglycolate), a different estimation strategy needed to be employed to obtain metal-glycinate and metal-diglycolate entropy of association. Thus, we used the strategy employed by Prapaipong et al. (Prapaipong et al. 1998 and Prapaipong & Shock 2001) where entropy of association was correlated with the third law entropy of metal ions for over 30 ligands (obtained from Shock et al. 1997). These correlations are shown in Fig. 37 along with the associated uncertainty in the logK calculated using the van't Hoff equation. As can be seen from Fig. 37(a), the glycinate correlation is quite weak in comparison to the diglycolate correlation. However, almost all the experimental ΔS° values fall within the correlation uncertainty of ±5 cal/mol/K for both ligands. This only leads to a maximum error of ±0.5 log units in stability constant calculations (Fig. 37(b)) that is well within the uncertainty associated with our logK correlations. Thus, these correlations may be used estimate metal-glycinate and metal-diglycolate ΔS° values when no such measurements may be present. These estimations have been made using the third law entropy for over 60 cations in Supplementary Table 2.

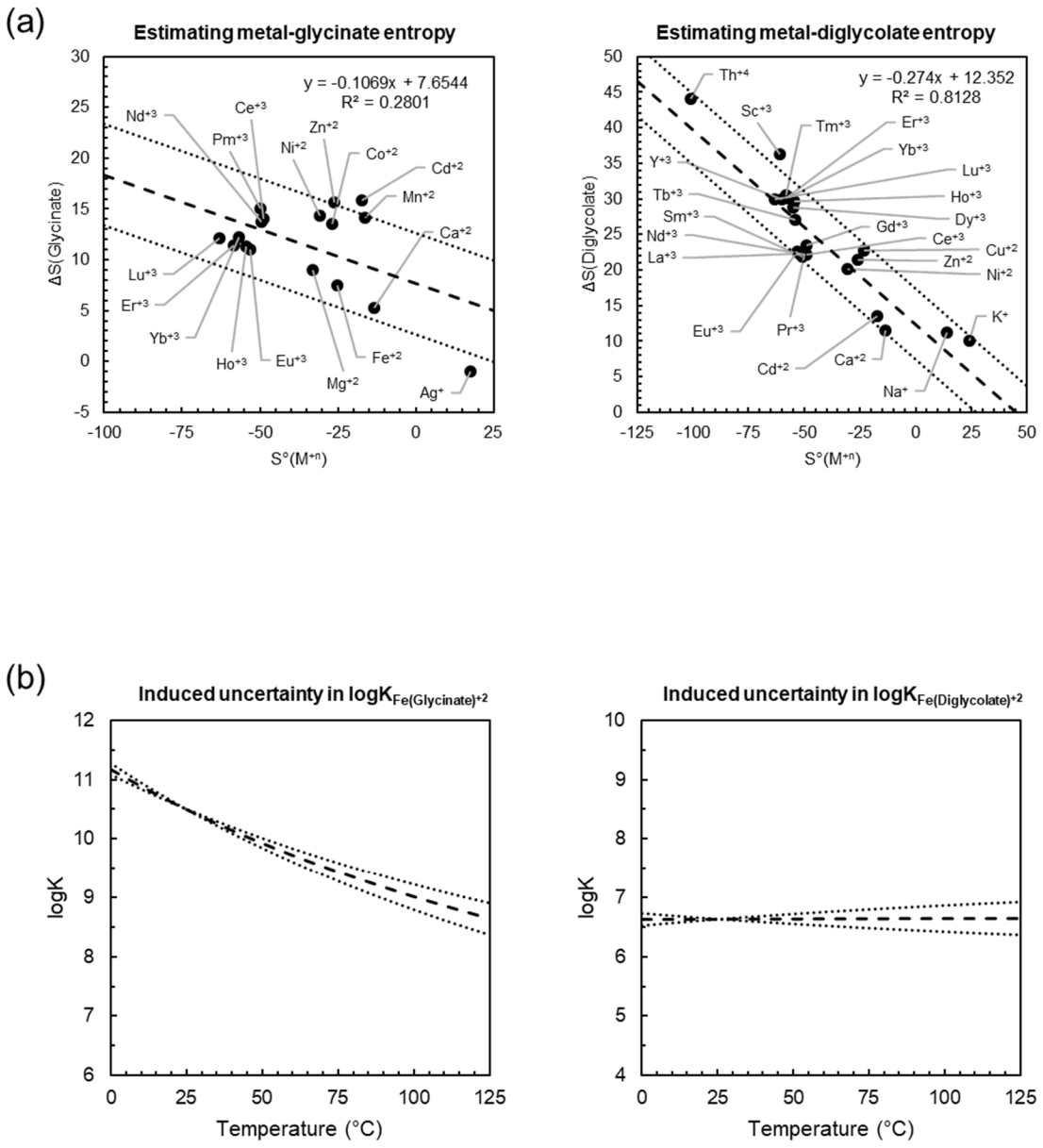

Fig 37. Estimating metal-ligand complexation entropy for the proxy ligands glycinate and diglycolate.

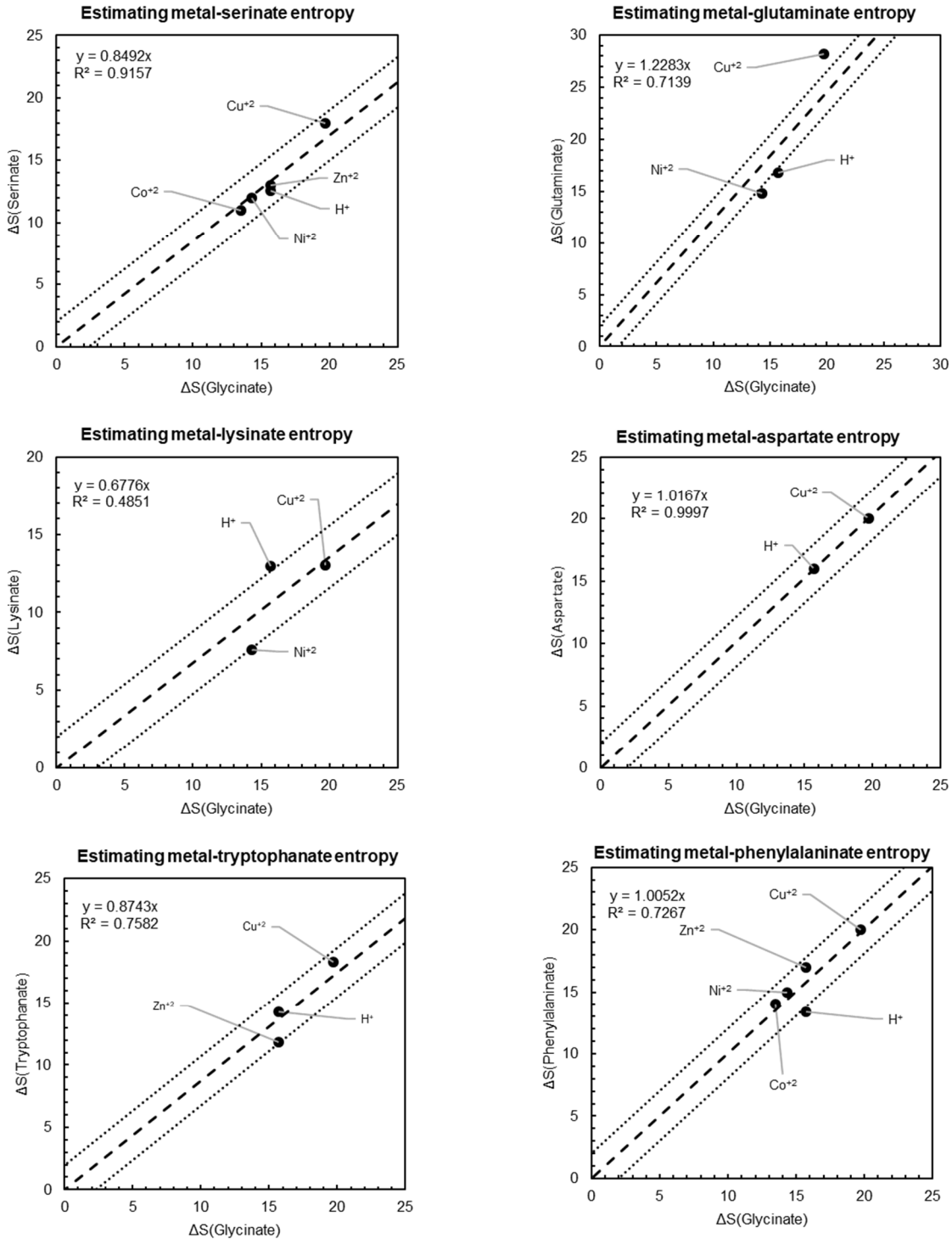

Fig 38. Estimating metal-ligand complexation entropy for amino acids.

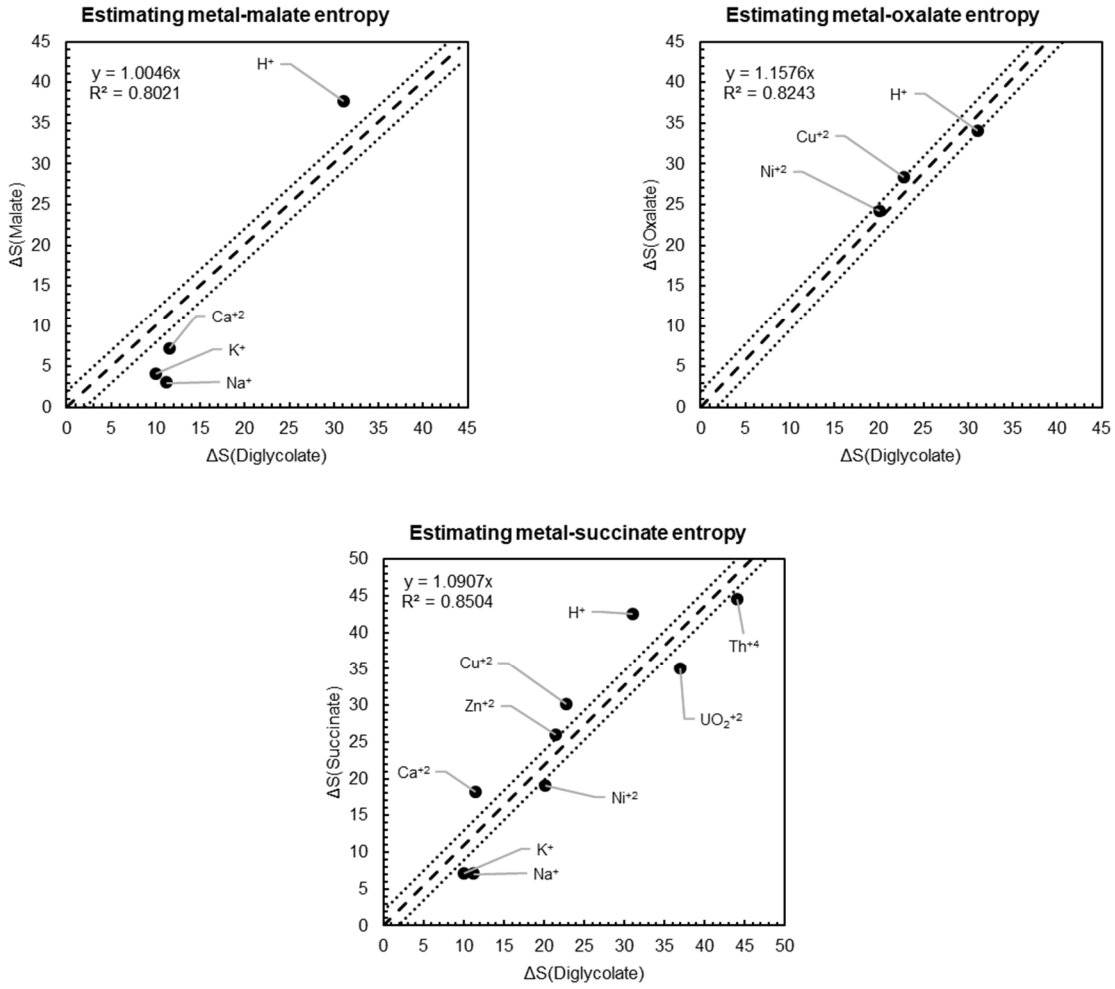

Fig 39. Estimating metal-ligand complexation entropy for dicarboxylates.

Like their logK analogues, the glycinate entropy correlations worked for all amino acids with different functional groups (Fig. 38). This included amino acids with neutral polar groups (serinate and glutaminate), amino acids with ionizable side chains (lysine and aspartate) and amino acids with aromatic side groups (tryptophanate and phenylalaninate). Similar correlations for 16 other amino acids are given in Fig. A2 of Appendix A. The "H^+" on these correlations is the sum of the protonation entropy of only the core amino and carboxylic groups. Creation of 2-parameter correlations (variable slope and intercept) led to estimation equations with unreasonably high or low slopes and intercepts due to the limited number of ΔS° measurements. We thus resorted to creating 1-parameter correlations (intercept set to zero) to avoid errors resulting from skewing of data. While this decreased the correlation coefficient slightly, the experimental values were still constrained within an error of ±2 cal/mol/K. The high accuracy of these correlations predicts stability constants within ±0.2 log units over the biologically relevant range of 0-120°C. Similar strategy was employed in estimating dicarboxylate entropy of association for malate, oxalate and succinate (Fig. 39).

3.6 van't Hoff plots

The Van't Hoff equation (Eqn. 5) is routinely used in thermodynamics to get the temperature dependence of stability constants from 0 to 125°C using enthalpy and entropy at reference temperature (298K)

$$logK(T) = \frac{-\Delta H^{\circ}_{298}}{2.303RT} + \frac{-\Delta S^{\circ}_{298}}{2.303R} \quad (5)$$

While not suitable at higher temperature, this relationship holds true from 0 to 125°C as the effects on enthalpy and entropy due to heat capacity are minimal in this temperature range. Since enthalpy (ΔH°), entropy (ΔS°) and Gibbs energy (ΔG°) of a reaction are related (ΔG°= ΔH°-T ΔS°), and the stability constant and Gibbs energy of reaction are related (ΔG°=-2.303RTlogK), knowing both the logK and entropy of reaction yields the enthalpy of the complexation reaction. These three properties were used to obtain the temperature dependence of logK for amino acids and dicarboxylates using the van't Hoff equation in Fig. 40 and 41 respectively.

While such logK extrapolations may be performed for over 45 cations (listed in Supplementary Table 2), we have chosen 8 diverse and biologically relevant metal ions to illustrate the temperature dependence of stability constants- Th^{+4}, Fe^{+3}, Cu^{+2}, Lu^{+3}, La^{+3}, Zn^{+2}, Fe^{+2} and Ca^{+2}. These calculations include cases where both logK & ΔS° were obtained from the literature (solid curves), logK was obtained from the literature and ΔS° obtained from our correlations (dashed curves) and both logK and ΔS° were obtained from our correlations (dotted curves). The uncertainty in the solid curves corresponds to the experimental uncertainty (~ ±0.2 log units), while those of the dashed and dotted curves corresponds to ±0.5 log units and ±1.0 log units respectively.

Fig. 40 presents the temperature dependence of metal stability constants for 9 select amino acids with diverse functional groups. Similar figures have been created for 18 other amino acids in Fig. A3 of Appendix A. The overall decreasing trend of these stability constants suggests that metal-amino acid bonding gets weaker as temperature raises from 0 to 125°C.

Additionally, the trend for the dashed and dotted lines matches the trend for the solid lines, thereby indicating that our logK and ΔS° estimations are quite sensible. Moreover, the trend is similar for different amino acid complexes of the same metal ion (except Ca^{+2}). Clearly, stability constants decrease more significantly for some metal ions (like Fe^{+3}) and to a lesser degree for other metal ions. It is also worth noting that the range of logK for the 8 metal ions of interest ranges from approximately 0 to 7 for nicotinate and approximately 2 to 14 for aspartate.

Similar plots have been made for four dicarboxylates- diglycolate, malate, oxalate and succinate (Fig. 41). The overall trend for these ligands is quite different from that of the amino acids. Here, stability constants mostly remain constant over the temperature range of 0 to 125°C with slight increase or decrease. Here again, the dashed and dotted curves closely resemble the solid curves adding to the validity of our logK and ΔS° estimates. The logK coverage of all ligands seem to fall within the range of approximately 2 to 10. It is likely that metal stability constants for other dicarboxylates will fall within this range.

3.7 Conclusion

Using a very simple chemical approach, we have estimated metal-ligand stability constants for 41 diverse and biologically relevant chelators including amino acids,

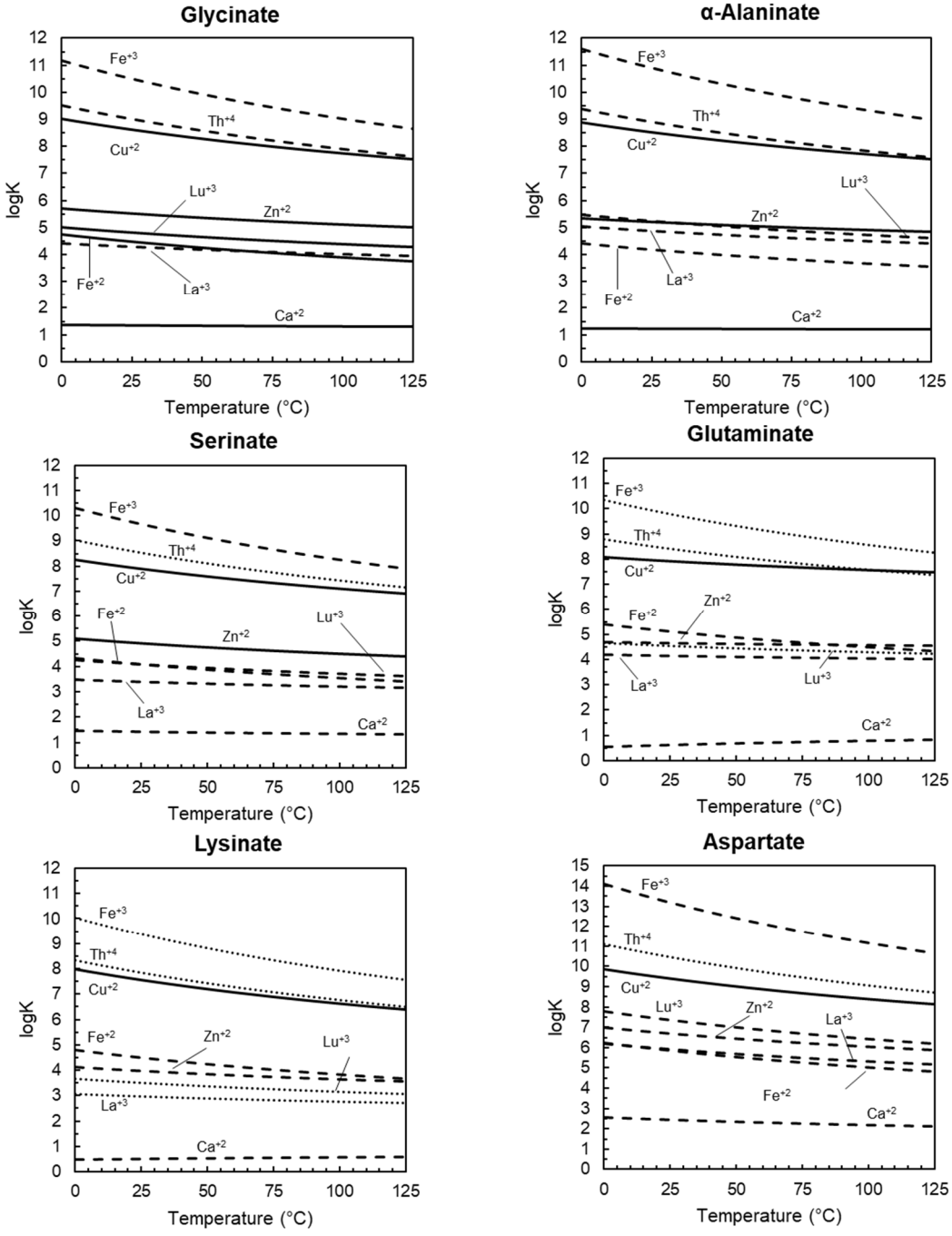

Fig 40. van't Hoff plots for metal-ligand complexes over biologically relevant temperature range using experimental values obtained from the literature or obtained from glycinate correlations. Solid curves represent van't Hoff calculations generated from experimental logK & ΔS, dashed curves represent van't Hoff calculations from experimental logK and estimated ΔS while dotted curves represent van't Hoff calculations from estimated logK & ΔS. (contd.)

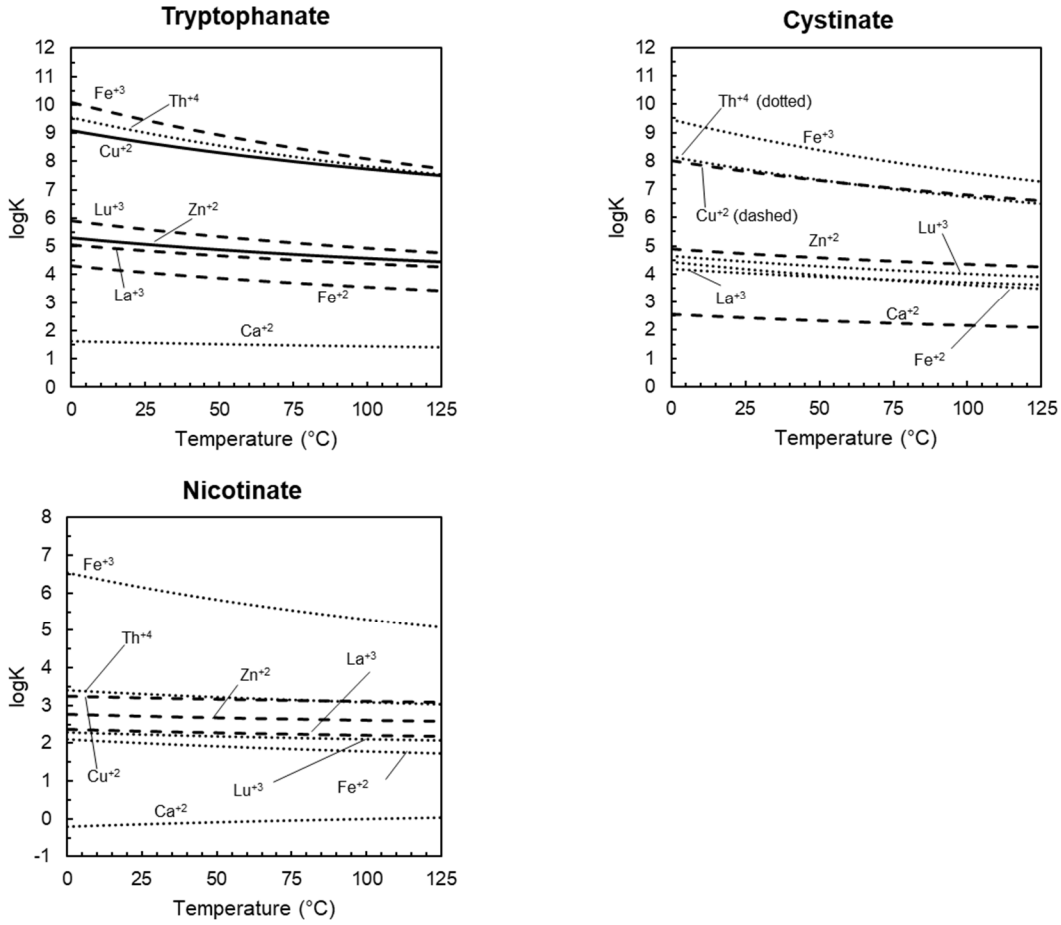

(contd.) Fig 40. van't Hoff plots for metal-ligand complexes over biologically relevant temperature range using experimental values obtained from the literature or obtained from glycinate correlations. Solid curves represent van't Hoff calculations generated from experimental logK & ΔS, dashed curves represent van't Hoff calculations from experimental logK and estimated ΔS while dotted curves represent van't Hoff calculations from estimated logK & ΔS.

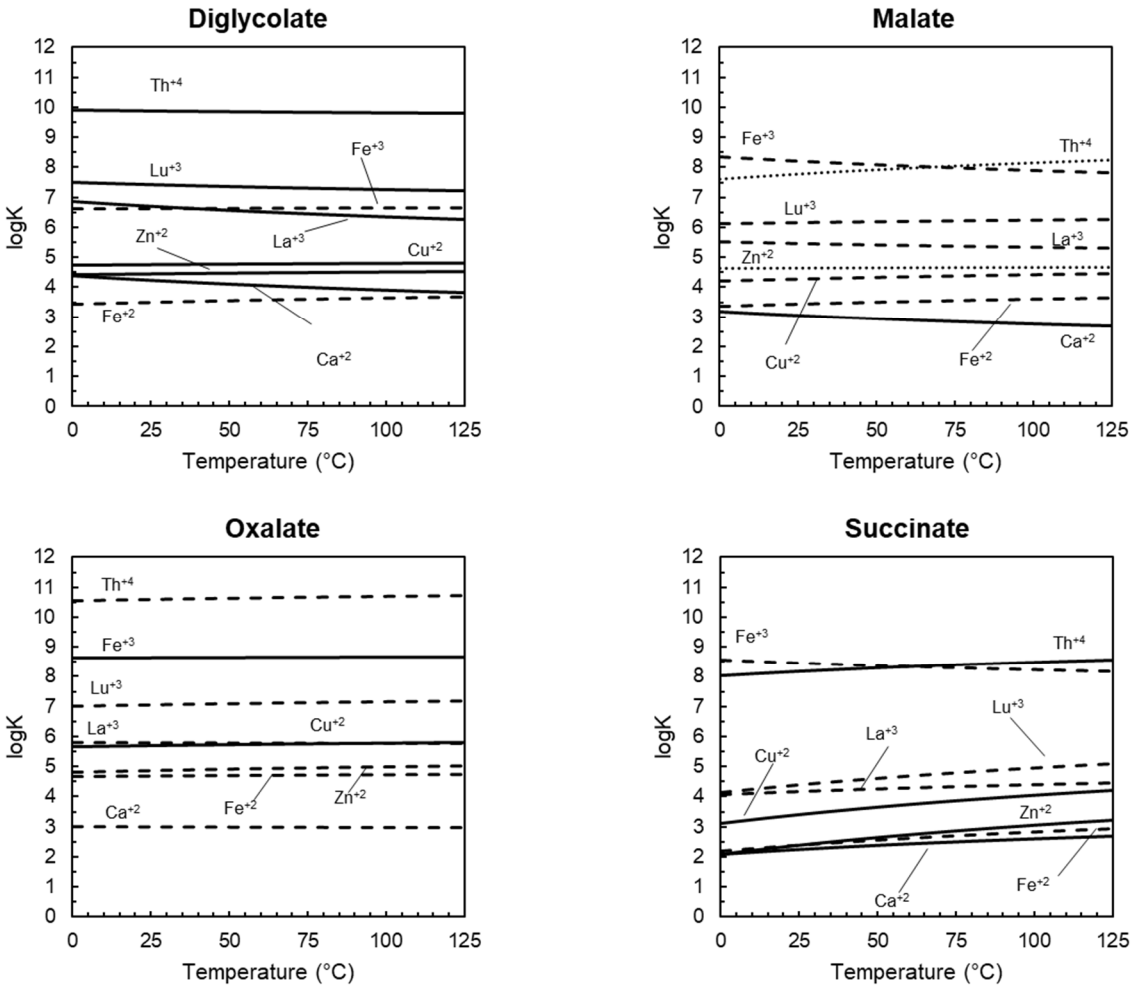

Fig 41. van't Hoff plots for metal-ligand complexes over biologically relevant temperature range using experimental values obtained from the literature or obtained from diglycolate and hydroxide correlations. Solid curves represent van't Hoff calculations generated from experimental logK & ΔS, dashed curves represent van't Hoff calculations from experimental logK and estimated ΔS while dotted curves represent van't Hoff calculations from estimated logK & ΔS.

dicarboxylic acids, proteins and inorganic molecules. From a collection of 853 critically evaluated stability constants published over the past century, we have expanded the dataset to 1878 logK values. Additionally, we have estimated entropy of association of 1456 metal-ligand complexes for 32 chelators using 165 experimental measurements, thereby increasing current knowledge over 8-fold. These estimates facilitate logK calculation over the entire biologically relevant temperature range and can help drive metal-related research across the biosphere from human bodily fluids to hot-spring microbiology. We have utilized these estimates to speciate blood (Prasad & Shock 2019d) and correlate metal-speciation with microbial bioavailability (Prasad & Shock 2019c). We hope these estimates and strategies prove to be useful to other scientists performing research in the related disciplines.

While these theoretical predictions are indeed useful, there is still considerable scope to fill in the gaps in the experimental literature. In particular, further experimental measurements of metal-albumin stability constants can be extremely valuable to metal speciation research. As mentioned in the previous section, our regression of metal-protein stability constants has revealed that these values are exceptionally dependent on the stability constants of the 'competing ligands' like NTA and EDTA. The logK reports for these metal-complexes are known to vary by 2-3 units that can significantly affect the accuracy of metal-protein stability constants. Moreover, additional forms of these metal-ligand complexes (protonated or hydroxylated) may dominate the metal speciation and need to be accounted for. Besides, many reports of metal-protein stability constants are devoid of ionic strength measurements that severely diminishes their validity. Thus,

careful consideration needs to be given to the measurement of metal-protein stability constants.

In the contemporary world of metal-based research, metals are being investigated both for therapeutic purposes as gallium-based anticancer drugs (Enyedy et al. 2015) but also for neurological damage in Alzheimer's Disease (Adlard & Bush 2018). This is clearly an exciting time for metal-speciation research and given its past success with iron-overloading and chelation therapy (Templeton 2015), it is likely to reap enormous rewards if pursued further. As this research is deeply rooted in the laws of thermodynamics, it is a great tool to bridge the gap between in the inanimate world of metal-ligand chemistry to the animate world of biological fluids. We hope this work proves to be a step in that direction.

CHAPTER 4

METAL SPECIATION AND BIOAVAILABILITY IN MICROBIAL GROWTH MEDIA

4.1 Introduction

Ever since the seminal works of Sunda & Guillard 1976, it has been known that all chemical forms of a metal are not bioavailable. This knowledge is of key importance as many metals like iron and copper are essential at low concentration but toxic at higher abundance. Some of the earlier research on this topic suggested that perhaps only the free metal ion is taken up by life which gave birth to the free ion activity model (FIAM) (Morel et al. 1978). However, numerous exceptions to this model have emerged over the years (Poldoski et al. 1979, Pärt & Wikmark 1984 and Daly et al. 1990). The present scientific consensus is that in addition to the free metal ion, metal-ligand complexes are also taken up by living cells (Levina et al. 2017).

Owing to their strong interaction, metal-ligand complexes have been a topic of scientific interest for over a hundred years (Werner & Guber 1901). Many ligands like EDTA (ethylene diamine tetraacetate) and NTA (nitrilotriacetate) are regularly used as 'chelators' to control the bioavailability of metals in microbial growth media. Additionally, microbes have evolved to synthesize proteins called siderophores and chalkophores that selectively chelate metal ions that are essential to their biological function. The predominance of ligands in the metal distribution in these biological systems can be attributed to the high equilibrium constant for the association reaction (stability constant) between metal ions and the afore-mentioned ligands. However, this

predominance is not likely to uphold for all ligands, especially at low concentration. For example, the aqueous distribution of trivalent cations like gallium and bismuth is heavily dominated by hydroxide complexes even in the presence of metal-chelators (Harris & Pecoraro 1983 and Sun et al. 2001). The metal distribution in a system is a complex function of all possible reactions with the metal ion and the associated stability constant and concentration.

In lieu of the complicated nature of metal-ligand interaction and metal-bioavailability, it is crucial to obtain accurate chemical distribution of metals (metal speciation) in biological systems to assess their toxicity and requirement. Direct measurement of metal speciation via analytical techniques in systems of low metal concentration with multiple ligands has not proved to be reliable (Kiss et al. 2017). Alternatively, metal speciation may be obtained theoretically under the equilibrium assumption using law of mass action and law of mass-balance. As metal-ligand complexation is quite rapid (reaching equilibrium within seconds), this is a reasonable assumption to make. These laws have been incorporated in several equilibrium speciation programs like EQ3/6 (Wolery 2010) that are routinely used to obtain elemental speciation in geochemical systems. However, these theoretical alternatives generally suffer from a lack of thermodynamic data (Kiss et al. 2017). Recently, considerable progress has been made in supplementing experimental measurements of metal-ligand thermodynamic properties with estimates of stability constant and entropy (Prasad & Shock 2019a and Prasad & Shock 2019b). This database and the estimation techniques therein permit metal speciation calculations for a large set of metal-ligand complexes from 0°C to 125°C.

In this work, we have performed metal-speciation calculations for ligands in bacterial and algal growth media and made correlations with published research on metal bioavailability. In the following section, we have defined the terms 'metal speciation' and 'metal bioavailability' with examples and briefly explained their relationship. In the subsequent section, we have performed speciation calculations for a metal-toxicity study on an algal strain that did not report any speciation measurements or calculations. A similar enterprise was performed on another bioavailability study reporting copper toxicity for a marine amphipod that made erroneous assumptions regarding copper speciation. In the succeeding section, we have performed speciation calculations for a bacterial medium used to make food products that reported different requirements for manganese and zinc. Lastly, we have reported speciation calculations for all defined/mineral growth media listed on the DSMZ website and how minor alterations in these media affects metal speciation.

4.2 Metal speciation and metal bioavailability: definitions and relationship

Metal speciation is defined as the chemical distribution of the total metal in different chemical forms. For example, if 1 millimole salt $ZnCl_2$(cr) is dissolved in 1 liter of pure water at 25°C and 1 bar, its speciation is given as 99.65% Zn^{+2}(aq) while the remaining 0.35 % of the total zinc is as $Zn(OH)^{+}$(aq), $Zn(OH)_2$, $ZnCl^{+}$ and $ZnCl_2$(aq). Comparatively, in a 1mM aqueous solution of $Zn(Oxine)_2$, 98.92% of the total zinc is as $Zn(Oxine)_2$(aq), 1.06% as $Zn(Oxine)^{+}$ and the remaining as the afore-mentioned species. Thus, metal speciation is heavily dependent on the ligands present in the system.

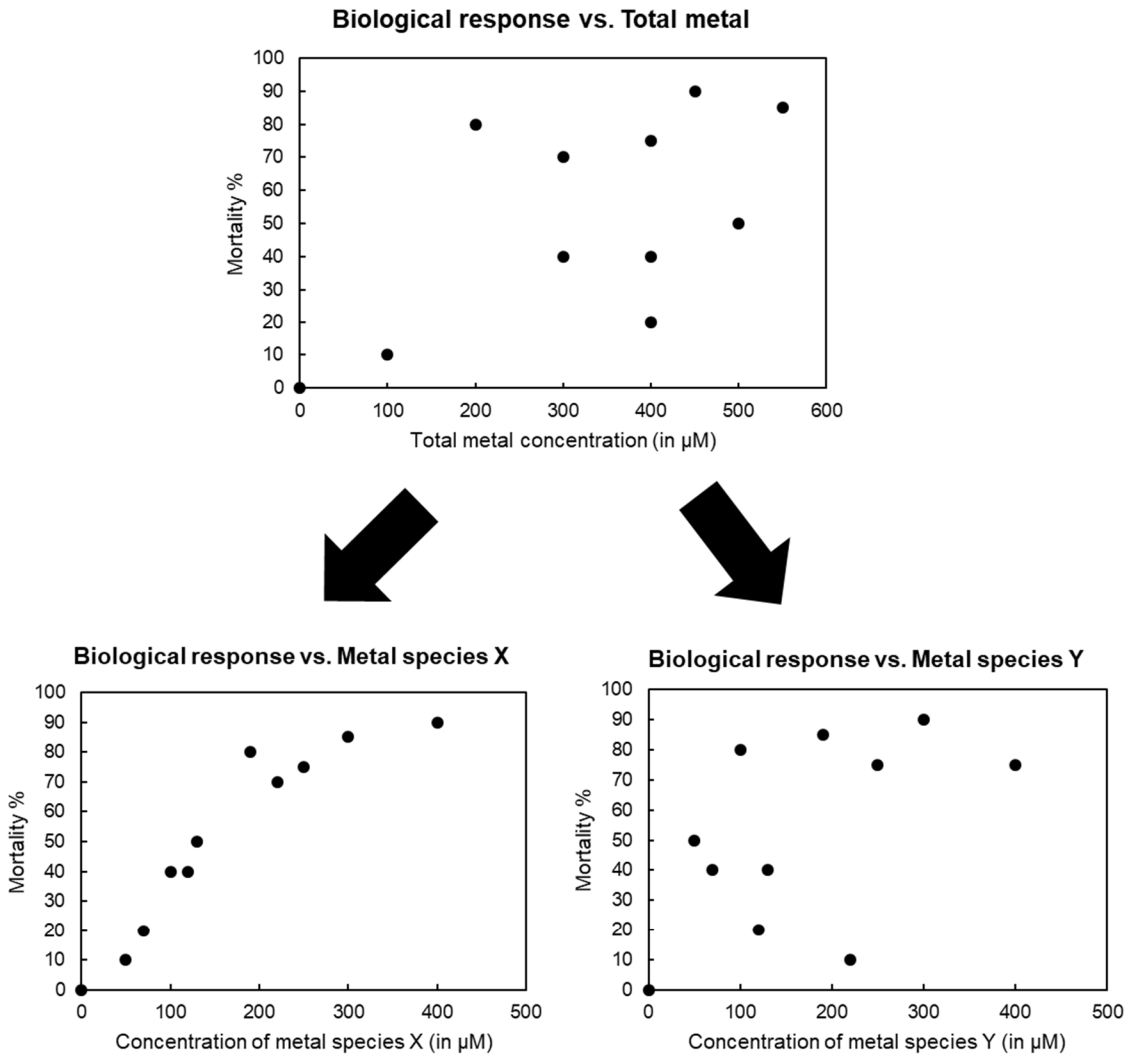

Fig 42. Schematic of relationship between speciation and bioavailability.

Metal bioavailability is a much more loosely defined concept. This term is generally used to describe the metal species that can be transported across the lipid bilayer from the bulk solution via any transport pathway. Its usage may be contradictory- for example, metal precipitates are not considered to be bioavailable while small insoluble metal complexes are (Schwarzenbach et al. 2003 vis a vis Levina et al. 2017). Additionally, some metal-ligand complexes like EDTA are not considered bioavailable (Campbell 1995) while others like oxine complexes are (Ahsanullah & Florence 1984).

The relationship between metal speciation and bioavailability has now been observed for a diverse set of organisms like prokaryotic microorganisms (Sunda & Gillespie 1979, Sunda & Ferguson 1983 and Morton et al. 2000), eukaryotic microorganisms (Sunda & Guillard 1976, Anderson & Morel 1978, Sunda & Huntsman 1986, Sunda & Huntsman 1992 and Canterford & Canterford 1980), animals (Sunda et al. 1978 and Daly et al. 1990) and human cell cultures (Zhu et al. 2006, Scheers et al. 2014, Peng et al. 2014, Pereira et al. 2014, Nday et al. 2012 and Hart et al. 2015). While all these studies report a qualitative difference in biological response to changes in metal speciation, very few have attempted to establish quantitative relationships between metal speciation and bioavailability. Most of these studies (like Sunda & Guillard 1976 and Engel et al. 1981) report a trend like the schematic demonstrated in Fig. 42 where the biological response (like metal-toxicity) has no correlation with total metal concentration but mimics a smooth mathematical function when plotted against the concentration of the perceived bioavailable species. Such a mathematical relationship is quite desirable as not only is it founded in theory (Morel et al. 1979), it may also inform which metal species

may be bioavailable and which species are unlikely bioavailable candidates. An established quantitative model of metal speciation and bioavailability can simulate experiments and predict the conditions where the presence or absence of metals has significant biological impact. While it is understood that this relationship is likely to get more complicated in more complex systems (multiple bioavailable species and multiple transport pathways), efforts are nevertheless warranted owing to the enormous power that such correlations might bring. We have tried to make these correlations in the following sections after replicating some of the well-received studies on metal speciation and bioavailability (Appendix B).

4.3 Simulation of a bioavailability study without speciation analysis

In 1980, Laube et al. published a study of metal toxicity on the blue-green alga (Cyanobacterium) *Anabaena*, strain 7120. In the study, Laube et al. examined the differences in the growth of the alga (with optical density measurements) over a wide range of cadmium, copper and lead concentrations (10^{-8} to 10^{-3} M) with and without equimolar concentrations of NTA in a defined growth medium over 15-20 days. Quite remarkably, Laube et al. 1980 reported that NTA 'did not reduce, and in some cases increased, metal toxicity to *Anabaena* 7120' and suggested that 'these metals do not act on this alga only in the ionic form', thereby against the free ion activity model. However, no speciation calculations were reported, nor any attempts made subsequently by studies citing the paper. One study deemed it 'problematic' and suggested that increased toxicity with high NTA concentrations might still be caused by appreciable concentrations of the

free ions due to competition with metals like Fe or due to volumetric errors (Campbell, 1995).

To obtain a clearer understanding of this study, we performed speciation calculations for the growth media used by Laube et al. 1980 using critically evaluated thermodynamic data from the literature and estimates of metal-ligand stability constants for the unmeasured complexes (Prasad & Shock 2019a and Prasad & Shock 2019b). The calculations were performed using the software EQ3/6 (Wolery 2010) at 25°C and 1 bar as that was similar to the experimental conditions reported in the paper (20°C and supposedly 1 atm) and happen to be the conditions where most experimental thermodynamic data is reported. To investigate whether these experiments were indeed in disagreement with the free ion activity model, we obtained the activity (molality*activity coefficient) of the free metal ion for both set of experiments- with and without chelator. The calculated logarithm of the free cadmium activity (log $a_{Cd^{+2}}$) is given next to the respective experiments in Fig. 43a. As may be seen from the figure, log $a_{Cd^{+2}}$ is almost identical for both set of experiments (with and without NTA) for the sub-micromolar experiments and the millimolar experiments (i.e 10^{-3}M, 10^{-6} M, 10^{-7} M and 10^{-8}M total cadmium). The similarity of the growth curves for these set of experiments along with our calculated activity of the free metal suggests that the algal growth agreed with the free ion activity model, in stark contrast to the conclusions reached by the authors of the original study. The higher growth for the experiments done without NTA at 10^{-5}M Cd_T in comparison to 10^{-6}M Cd_T belies explanation and perhaps is due to volumetric errors as suggested by Campbell 1995. The negligible growth for experiments performed at 10^{-4}

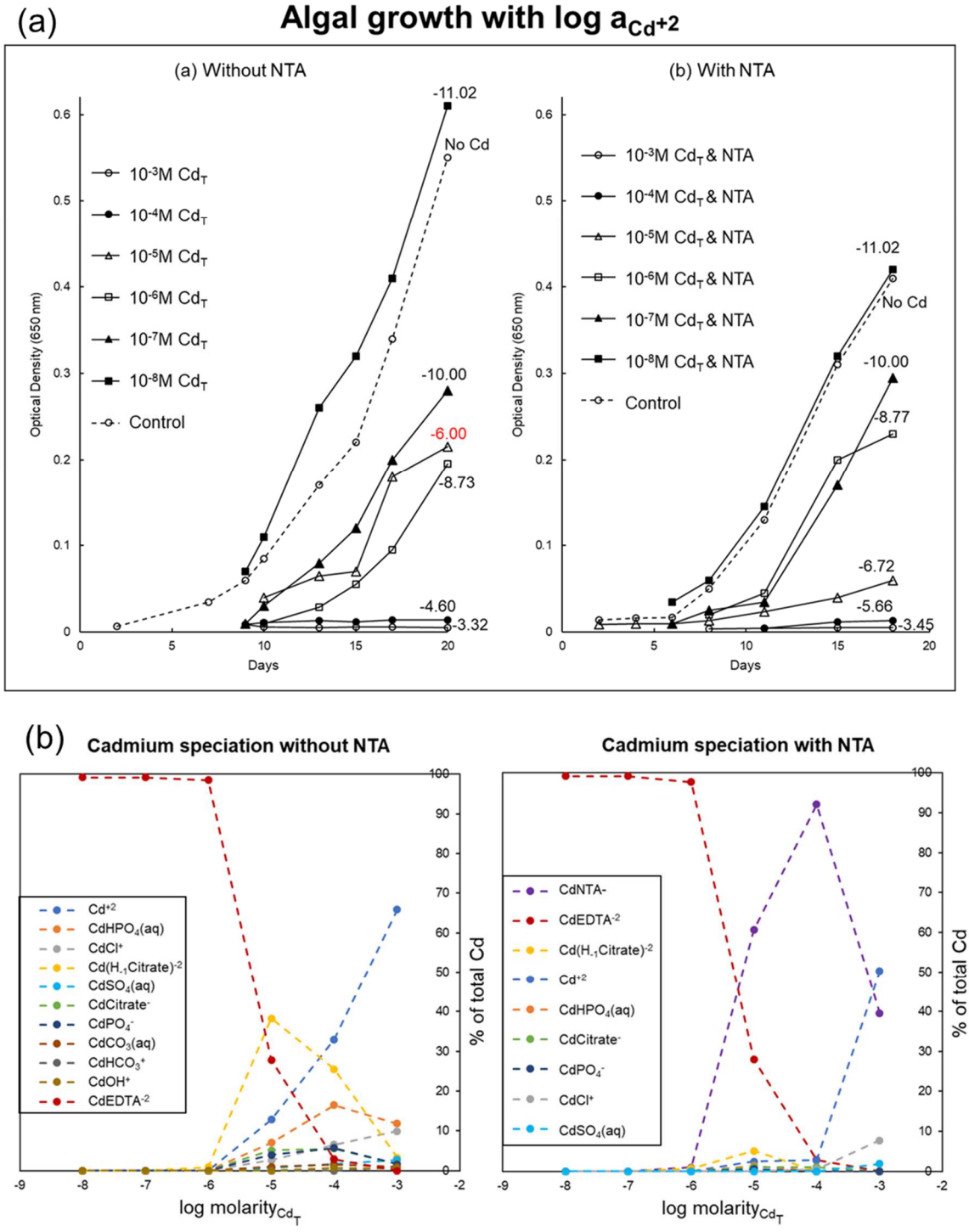

Fig 43 (a-c). Cadmium speciation in Laube et al. 1980. (contd.)

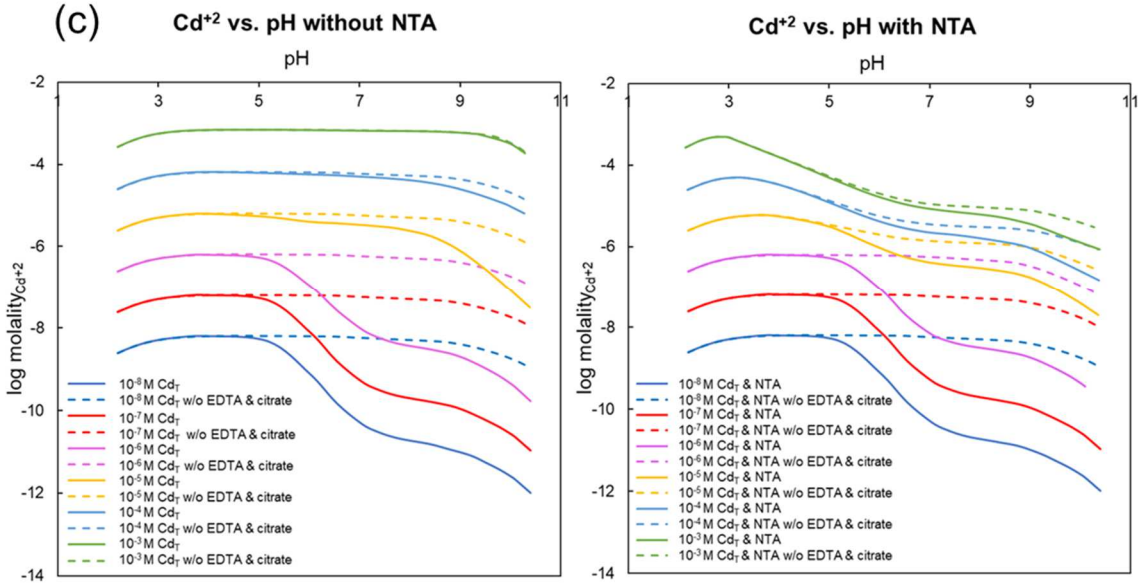

(contd.) Fig 43 (a-c). Cadmium speciation in Laube et al. 1980.

Cd_T may be explained by the excessively high levels of free cadmium for both set of experiments (corresponding to high micromolar values) and thus is still not in disagreement with the free ion activity model. This example clearly illustrates how erroneous conclusions about metal bioavailability may be reached without the knowledge of metal speciation.

Perhaps the reason for the conclusions reached by Laube et al. stems from the common assumption that a chelator always dominates the metal speciation in all conditions for all metals. Our speciation calculations for cadmium (Fig. 43b) demonstrate that this is clearly not the case in these experiments. Our calculations show that for experiments with NTA, the Cd-NTA complex only dominates the speciation for the experiments carried out at 10^{-4} Cd_T and 10^{-5} Cd_T. This is because cadmium speciation at sub-micromolar cadmium concentration (10^{-6}M, 10^{-7}M and 10^{-8}M Cd_T) is dominated by EDTA that is present in the default growth medium. As EDTA has octahedral coordination and is known to completely envelope the metal ion, the metal ion cannot interact with membrane proteins and cross the cell membrane.

While the addition of NTA in the manner of original administration does not seem to affect the free cadmium concentration, we found that this is liable to change at higher pH (Fig. 43c). For the super-micromolar concentrations of cadmium (10^{-5}M, 10^{-4}M and 10^{-3}M Cd_T), the free cadmium concentration decreased by 1-3 orders of magnitude from pH 7-9. We predict that under these conditions, the addition of NTA is likely to cause a change in cadmium toxicity under the default assumption of free ion activity model. Additionally, we have presented the free cadmium concentration if these experiments are

carried out in the absence of the other chelators including EDTA and citrate. As can be seen from the figure, these curves closely mimic the original curves with the chelators without being identical. In this way, speciation calculations can be used to predict bioavailability and choose the right set of conditions to verify such predictions with experiments.

Similar explanations can be given for the lead toxicity experiments made in the study. The growth curves were largely similar for experiments performed with or without NTA. However, these experiments were marred by precipitation and no account was reported of the lead lost in these precipitates. Thus, speciation calculations could not be made for these experiments to verify the compliance with the free ion activity model.

While addition of NTA did not largely affect growth for cadmium and lead experiments, it certainly decreased algal growth in the case of copper. Expectedly, the free copper activity ($a_{Cu^{+2}}$) could not explain the growth curves. Nevertheless, we also found that these growth curves could not be explained with the combination of (a_{Cu}^{+2}) and ($a_{Cu\text{-}NTA}$) as suggested by Laube et al (data not shown). Thus, we could not prove that Cu-NTA complexes were bioavailable as no qualitative or quantitative relationship could be established between Cu-NTA abundance and algal growth. We believe that this may be due to a different uptake mechanism of copper as also suggested in the original study. Thus, these experiments warrant further investigation to lend a better understanding of metal bioavailability.

4.4 Simulation of a bioavailability study with erroneous speciation calculations

As the cell membrane is largely hydrophobic in nature, molecules with hydrophobic moieties like benzyl groups have a high tendency to cross the lipid bilayer via passive diffusion. This ability to cross the lipid bilayer could perhaps also be extended to metal complexes of ligands like oxine that have two electron-bearing groups (phenol and pyridine) attached to a benzene ring. To investigate this, Ahsanullah & Florence (Ahsanullah & Florence 1984) conducted a toxicity study in artificial seawater on a marine amphipod *Allorchestes compressa*, in which they analyzed copper-induced mortality with and without oxine.

Copper toxicity without oxine was carried out over a wide range of total copper concentration (black circles in Fig. 44a) in organic-free seawater (organics destroyed by ultraviolet radiation) over 96 hours. Copper toxicity experiments with oxine were carried out in the same medium with 0.5 μM, 1 μM and 2 μM oxine (black squares in Fig. 44a). Comparing the two sets of experiments, Ahsanullah and Florence concluded that copper-oxine complexes (the assumed bioavailable metal species in experiments with oxine) were more toxic than free copper ion (the assumed bioavailable metal specimen in experiments without oxine) as lesser copper elicited the same or higher mortality with the addition of oxine.

However, the authors of the original study did not directly compare the mortality curves with the free copper and copper-oxine abundance as they had not performed speciation measurements or calculations for experiments performed without oxine. While they correctly obtained copper speciation for experiments with 2 μM oxine, they wrongly assumed that this speciation would hold for experiments performed at lower oxine

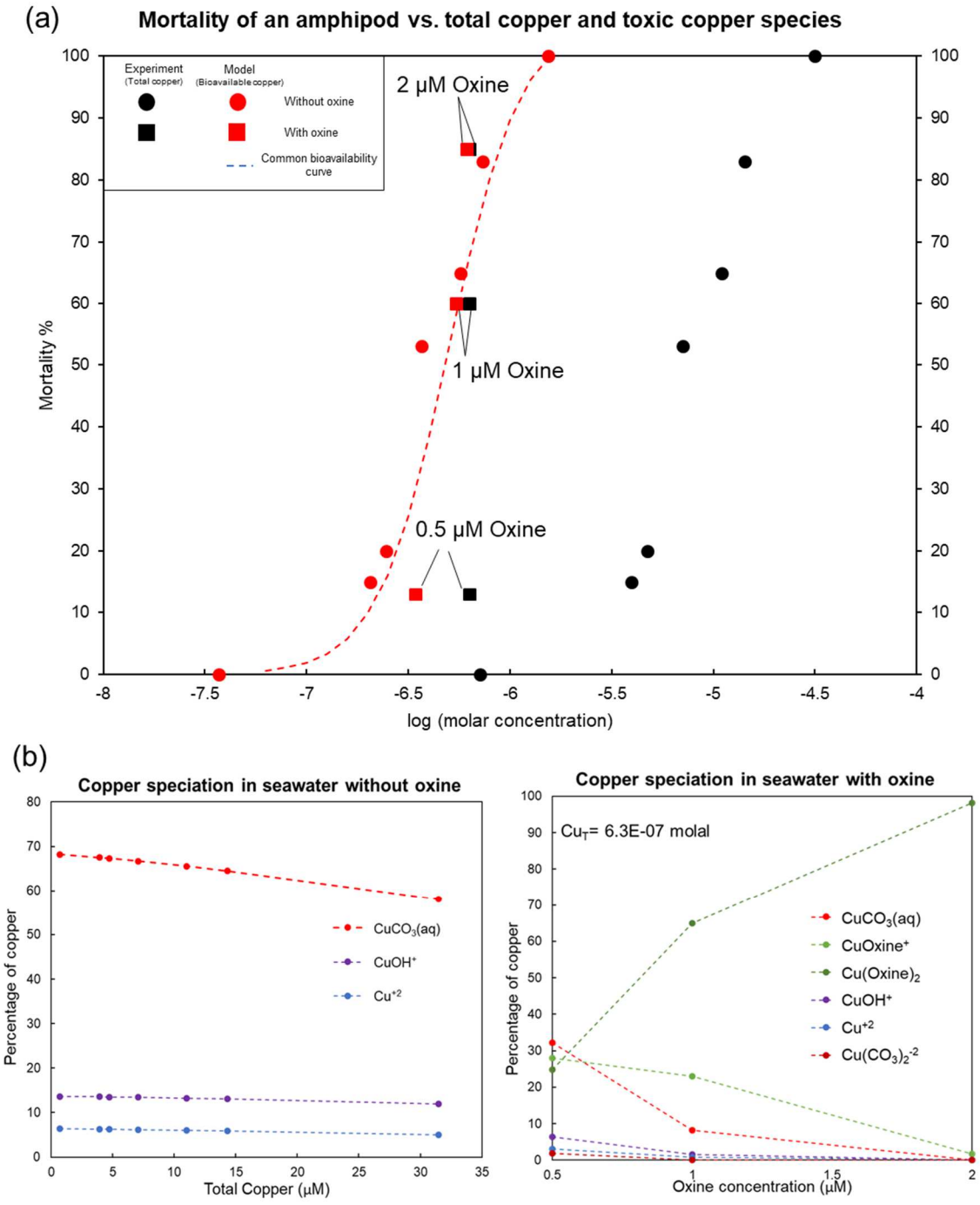

Fig 44(a-c). Speciaton calculations of Ahsanullah & Florence 1984. (contd.)

(c)

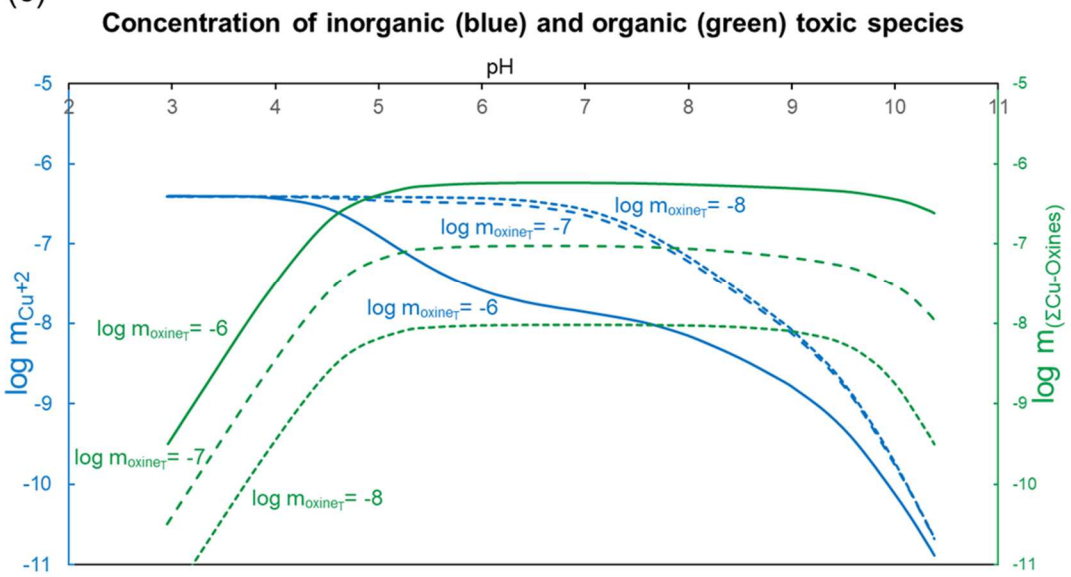

(contd.) Fig 44(a-c). Speciaton calculations of Ahsanullah & Florence 1984.

concentration (Fig. 43b). We performed the speciation calculations for all experiments using critically evaluated metal-ligand stability constant data from the literature or using analogous estimates obtained via linear free energy relationships (Prasad & Shock 2019a and Prasad & Shock 2019b). We subsequently compared the copper-induced mortality to the abundance of actual bioavailable species- free copper ion for experiments without oxine (red circles) vs. both free copper ion and copper-oxine complexes for experiments with oxine (red squares). This assessment revealed that the biological response for free copper ion is very similar to that of copper-oxine species, in clear disagreement with the conclusion reached by the authors of the original study. Even more glaringly, free copper ion elicits a higher mortality at lower concentrations in comparison to the 0.5 μM oxine experiment.

The reason for the difference between the free copper (Cu^{+2}) concentration and the total metal concentration can be seen in Fig. 44b. Only about 5-7% of the total copper is as Cu^{+2}, which is perhaps why Cu^{+2} (red circles) and Cu_T (black circles) are separated by about 1.5 log units in Fig. 44a. Also, while our speciation calculations of copper with 2 μM oxine (Fig. 44b) matched those of Ahsanullah & Florence 1984, we found that the speciation was different at other oxine concentrations, particularly in 0.5 μM oxine where $CuCO_3$ (aq) is the predominant copper species.

To predict copper toxicity in diverse environments, we performed speciation calculations in different conditions and found that copper speciation was extremely sensitive to pH (Fig. 44c). While copper-oxine complexes (green) dominate at high pH, free copper dominates the copper speciation at pH lower than 4.8 even at micromolar

concentration of oxine. This may be due to the complete protonation of oxine as the pK_a values associated with the two ionizable groups of oxine are 9.82 and 4.92.

4.5 Speciation in a bacterial growth media with contrasting transition metal requirements

Leuconostoc mesenteroides is a fermentative bacterium employed in several foods like kimchi and sauerkraut. In 2012, a study was published presenting an optimal growth medium for the strain ATCC8293 using the single omission technique (Kim et al. 2012). In this technique, growth is monitored as single nutrients are systematically removed from the medium. If the growth rate with the removal of a nutrient is less than 50% of the maximum growth rate, the nutrient is classified as 'essential'. The nutrient was termed 'stimulatory' if the omission led to a growth rate between 50-90% and 'non-essential' if the growth rate was greater than 90%. Along with amino acids and vitamins, the impact of transition metals on growth was also assessed and manganese was found to stimulate growth unlike iron (II), zinc, cobalt and copper.

This led us to speculate if metal speciation could be playing a role in the differential bioavailability of transition metals. We obtained equilibrium constants from the literature or made estimates (Prasad & Shock 2019a and Prasad & Shock 2019b) for all protonation and metal-complexation reactions that could take place in the medium. Equilibrium speciation calculations were made using EQ3/6 for the composition and conditions given in the study. As manganese was a 'stimulatory' nutrient, it was included in the composition as a sulfate salt while the other transition metals were not part of the chemically defined minimal medium. We performed speciation calculations for the

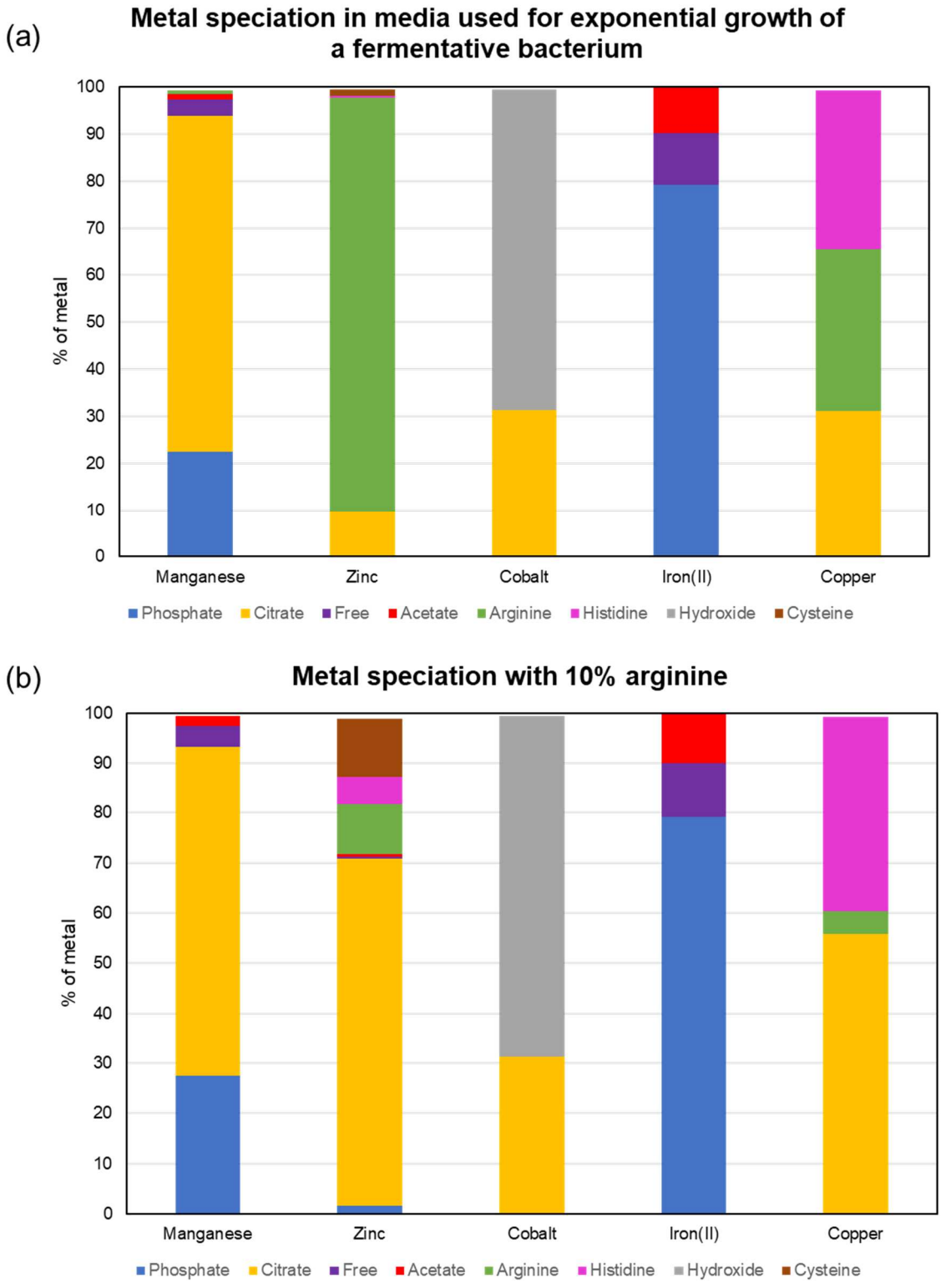

Fig 45(a-c). Manganese speciation in media employed by Kim et al. 2012.

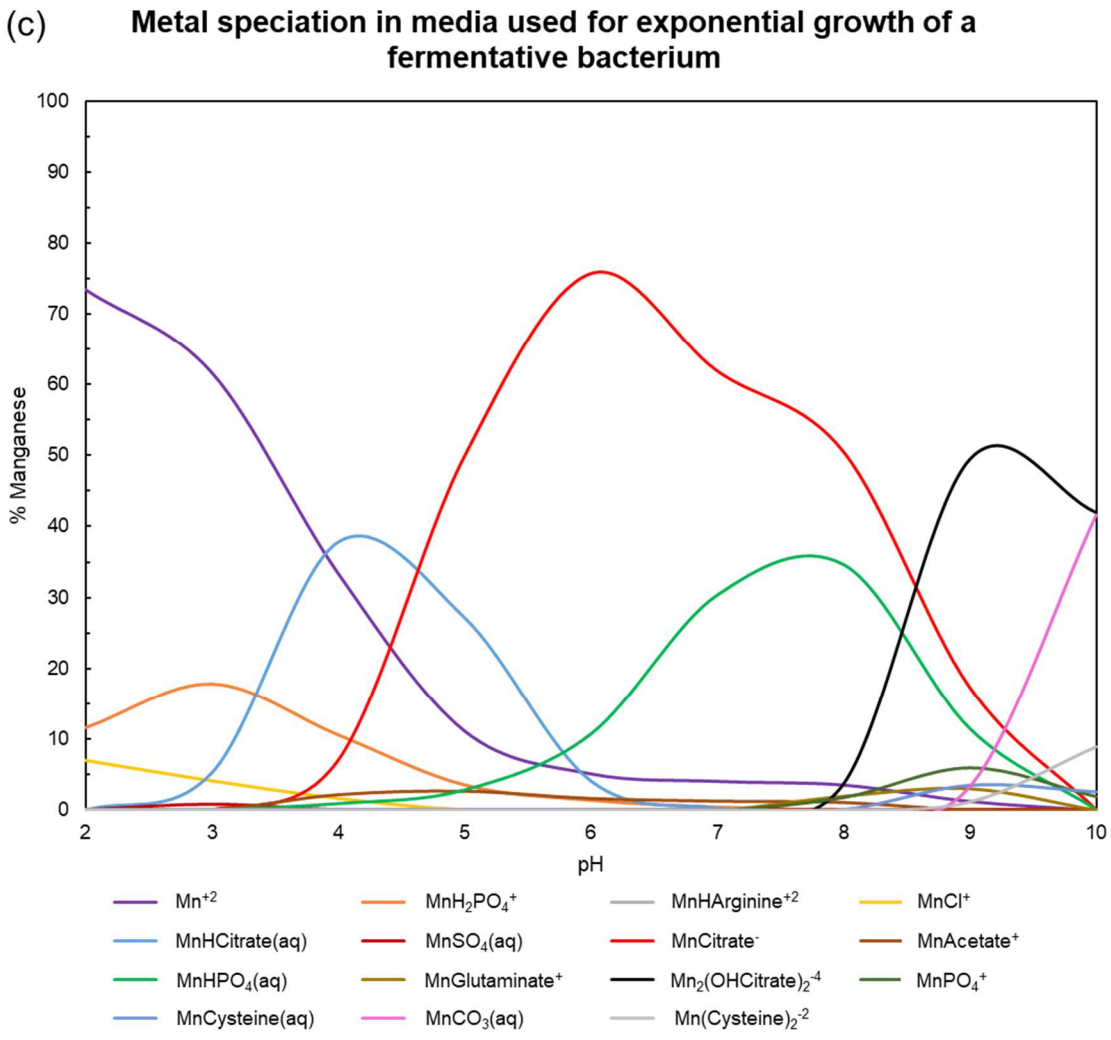

Fig 45(a-c). Manganese speciation in media employed by Kim et al. 2012.

composition reported in the study and exchanged manganese with the other transition metals to simulate the respective omission experiments.

The speciation for all ligands was governed by their respective pK_a values as their concentration was much higher than the transition metal concentration. The speciation of the divalent transition metals in the respective omission experiment simulations was found to be case dependent. While manganese speciation was dominated by citrate, zinc and copper speciation was dominated by arginine while cobalt and iron (II) speciation was dominated by phosphate and hydroxide respectively (Fig. 45a). More specifically, manganese speciation was dominated by $Mn(Citrate)^{-}$, zinc speciation by $Zn(Arginine)^{+2}$, copper speciation by $Cu(Arginine)^{+2}$, cobalt speciation by $Co_2(OH)_3^{+}$ while iron (II) speciation was dominated by aqueous $FeHPO_4^{0}$. As small molecule transport across the cell membrane is heavily dependent on charge, it is perhaps worth deliberation if the unique requirement of manganese in the medium is because it is predominantly distributed as a negatively charged species. We additionally found that decreasing the arginine concentration by a factor of 10 substantially increased the predominance of citrate complexes for most metals. As a substantial fraction of all these metals (except iron) is present as the negatively charged citrate complex, perhaps they would have similar bioavailability. Further experimental investigation on this topic can shed more light on the speciation-bioavailability relationship and on transport of small molecules across biological membranes.

To illustrate the effect of pH on the 'stimulatory' nutrient manganese, we performed speciation calculations from pH of 2 to 10 (Fig. 45c). Greater than 1% of

manganese was found to be distributed across 15 species. Expectedly, free manganese and protonated citrate complexes dominated the speciation at low pH while carbonate and hydroxylated citrate complexes dominated at higher pH. The diversity of species suggests that manganese bioavailability is likely to be heavily influenced by pH. We hope such calculations are performed in conjunction of experiments and can help guide and optimize the creation of chemically defined media in the future.

4.6 Metal speciation of defined growth media listed on the DSMZ website

The German Collection of Microorganisms and Cell Cultures (generally referred as DSMZ for their German name- Deutsche Sammlung von Mikroorganismen und Zellkulturen) is one of the most comprehensive resources for microbiology. They acquire and maintain a large collection of cell lines of all taxonomical variety and their website (https://www.dsmz.de/) contains a large list of standardized growth media that are often used to grow microorganisms (Zhang et al. 2018, Zhu et al. 2018, Ghavipanjeh et al. 2018, Haddad et al. 2014). As a service to future scientists that may be interested in the impact of metals in microbial growth, we performed speciation calculations in all chemically defined growth media listed on the DSMZ website. Since the exact chemical compositions of growth media with tryptone, beef extract and yeast extract are not known, speciation calculations could not be performed for these cases.

Out of the 1703 media listed on the DSMZ website, we only found 26 that had exact chemical compositions (chemically defined media). Many of these were variants of a common set of chemicals with minor variations. We obtained metal speciation for six representative media using experimental equilibrium constants reported in the literature

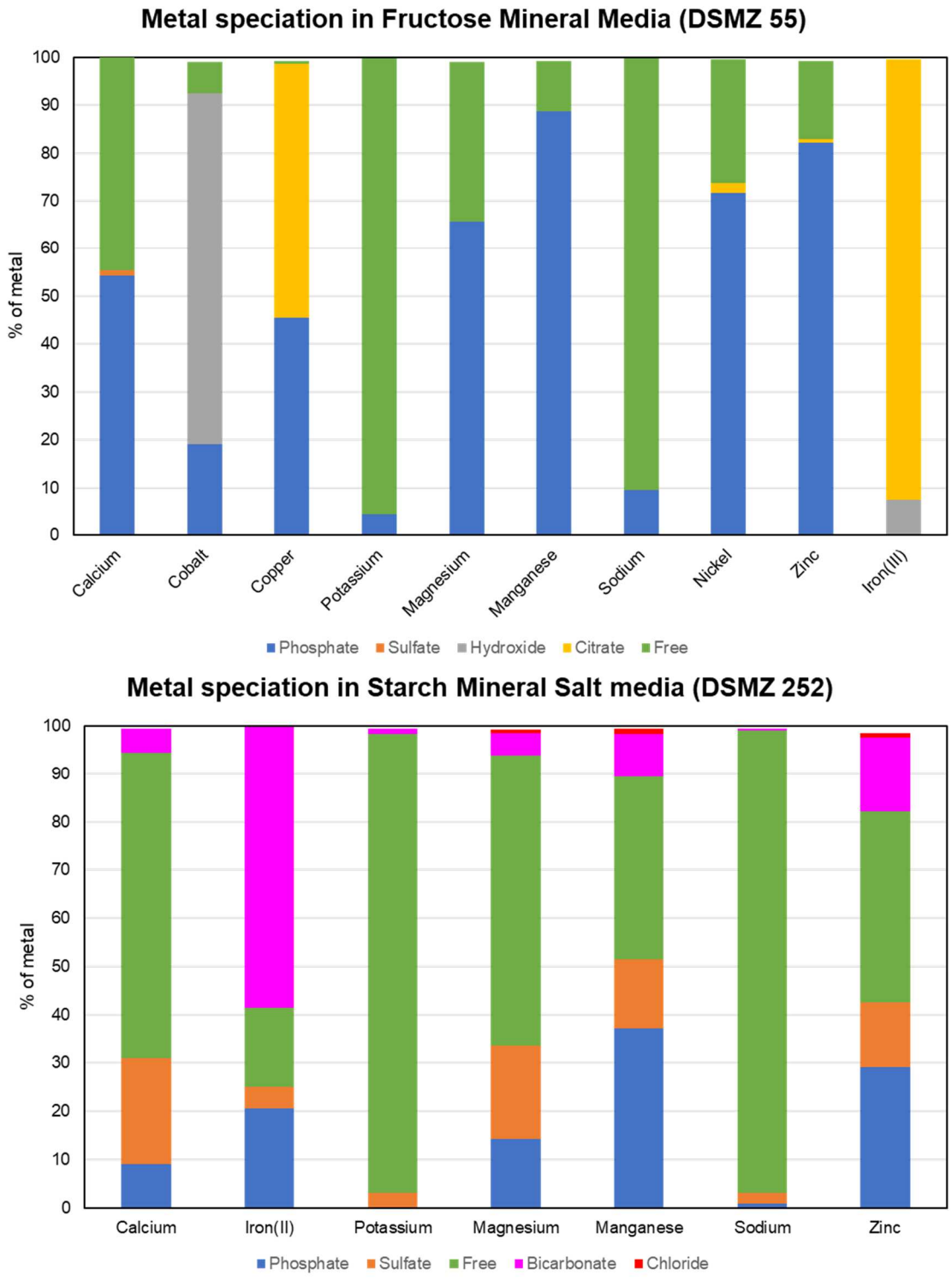

Fig 46a. Metal speciaton of defined growth media at DSMZ website.

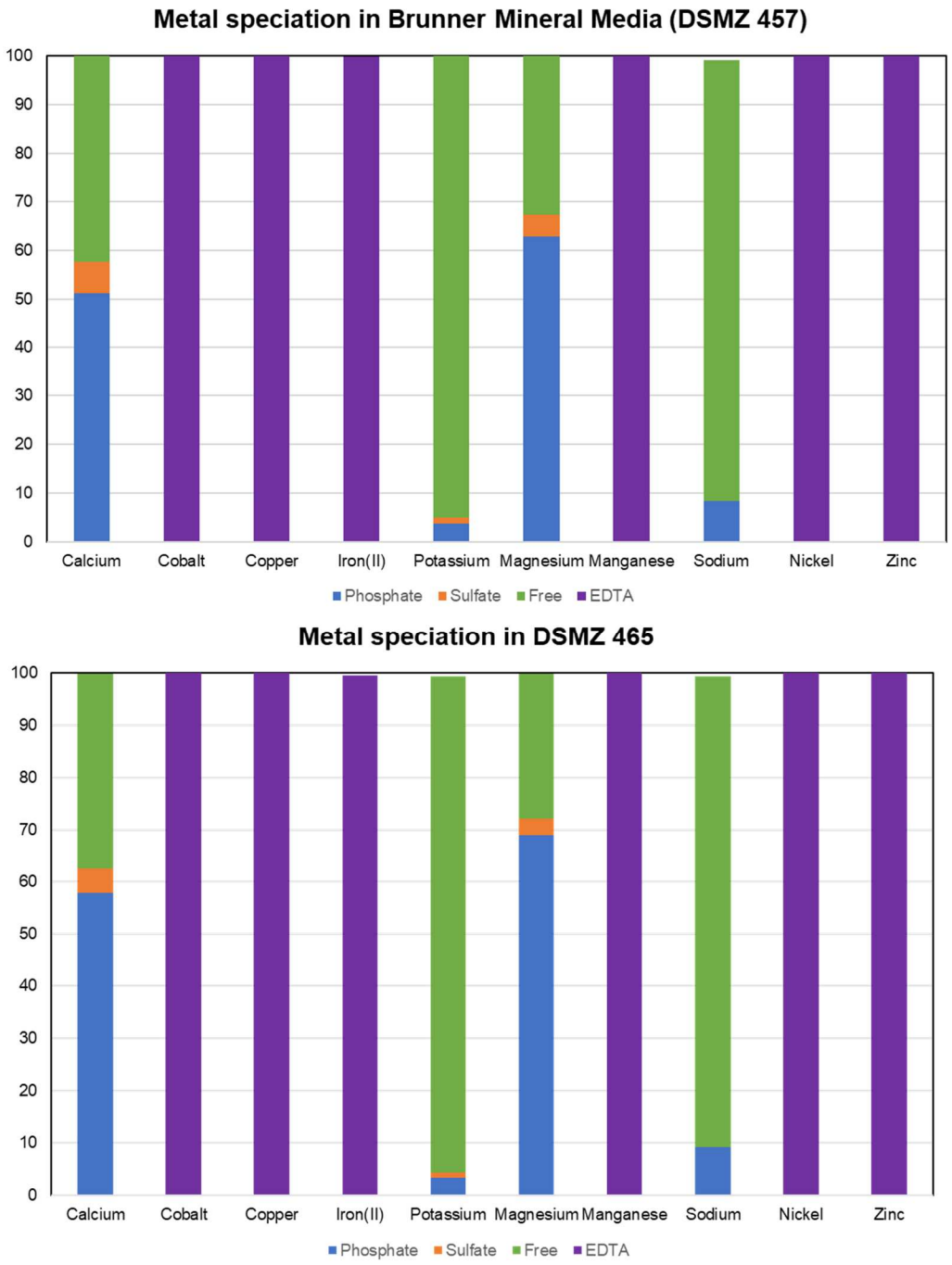

(contd.) Fig 46a. Metal speciaton of defined growth media at DSMZ website.(contd.)

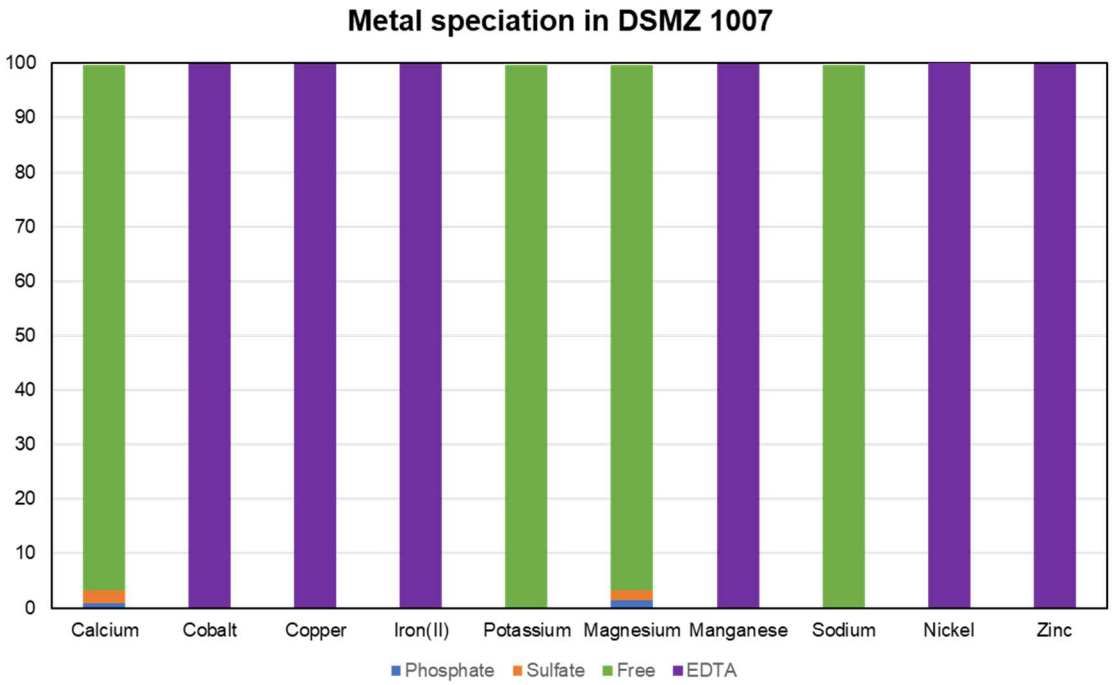

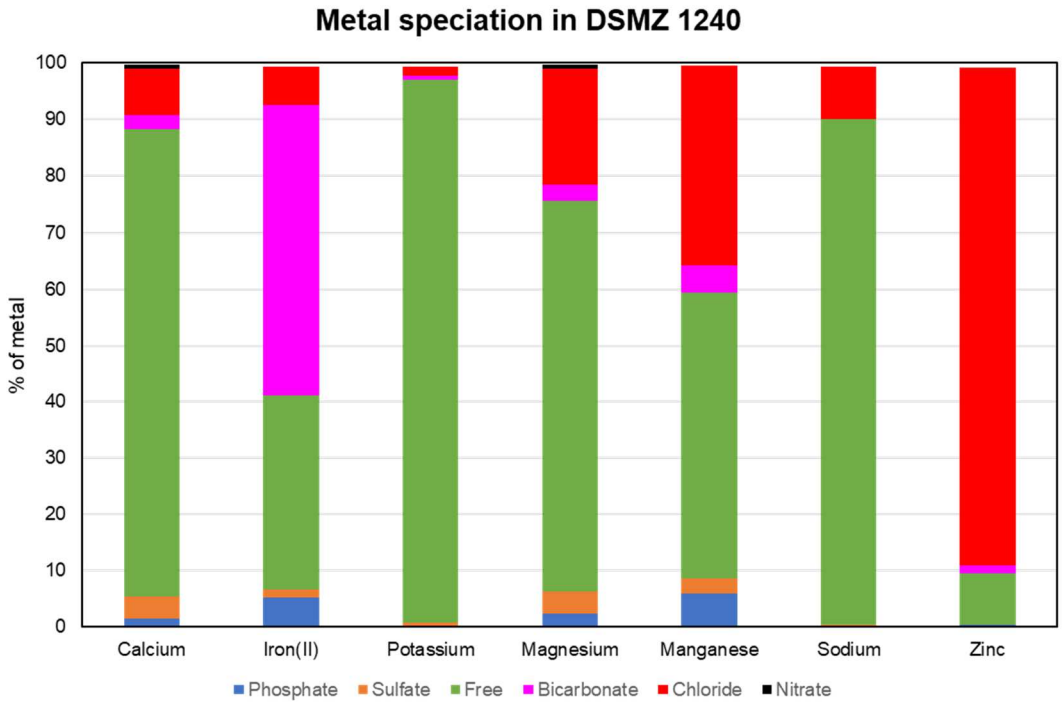

(contd.) Fig 46a. Metal speciaton of defined growth media at DSMZ website.

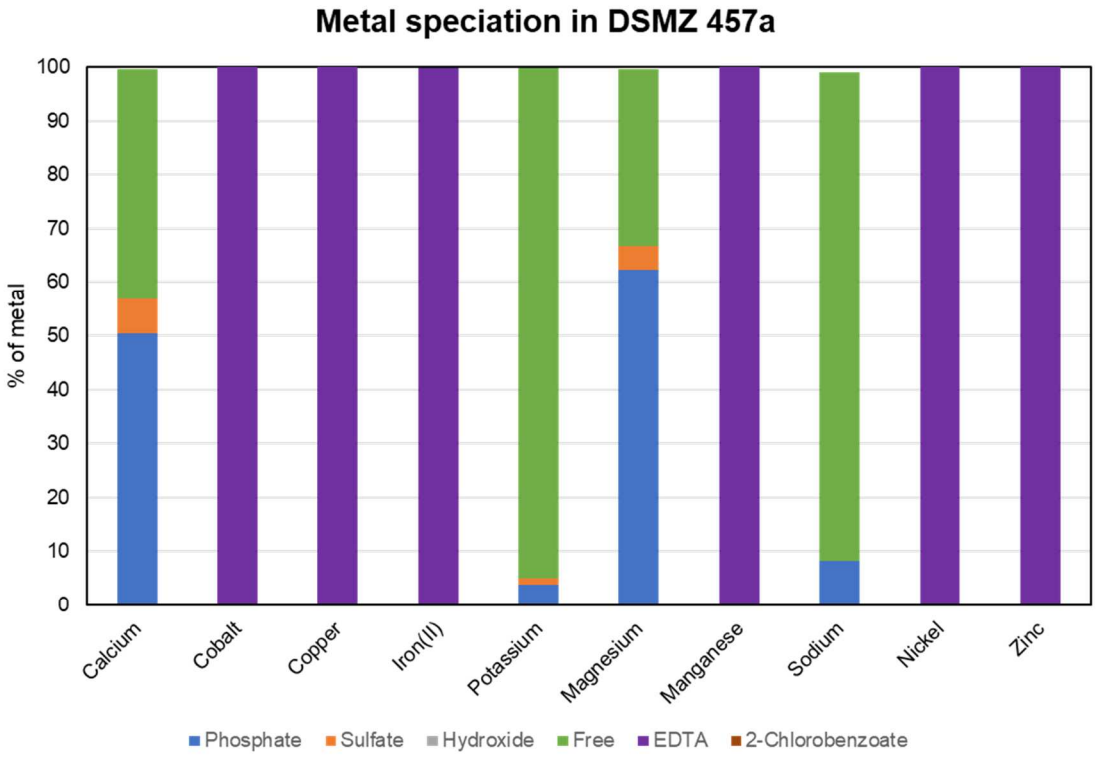

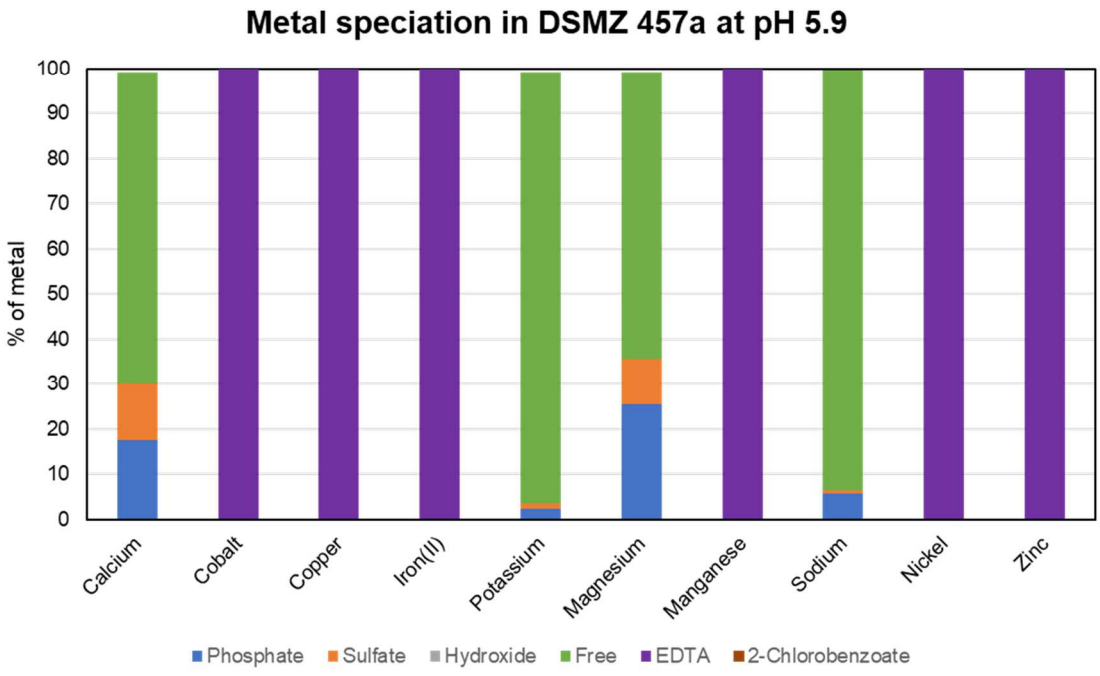

Fig 46b. Metal speciaton in DSMZ 457a with minor variations in composition (contd.)

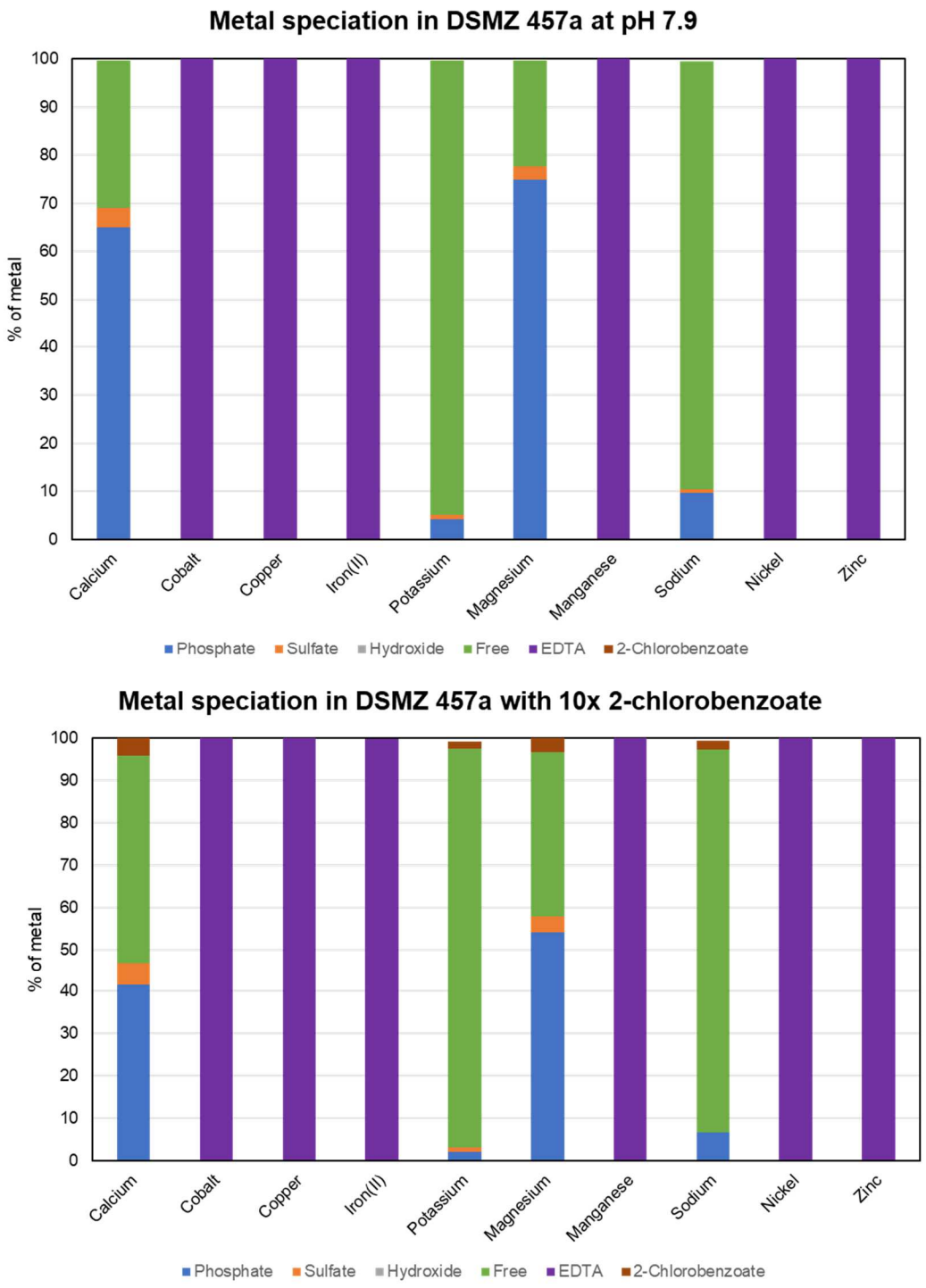

Fig 46b. Metal speciaton in DSMZ 457a with minor variations in composition (contd.)

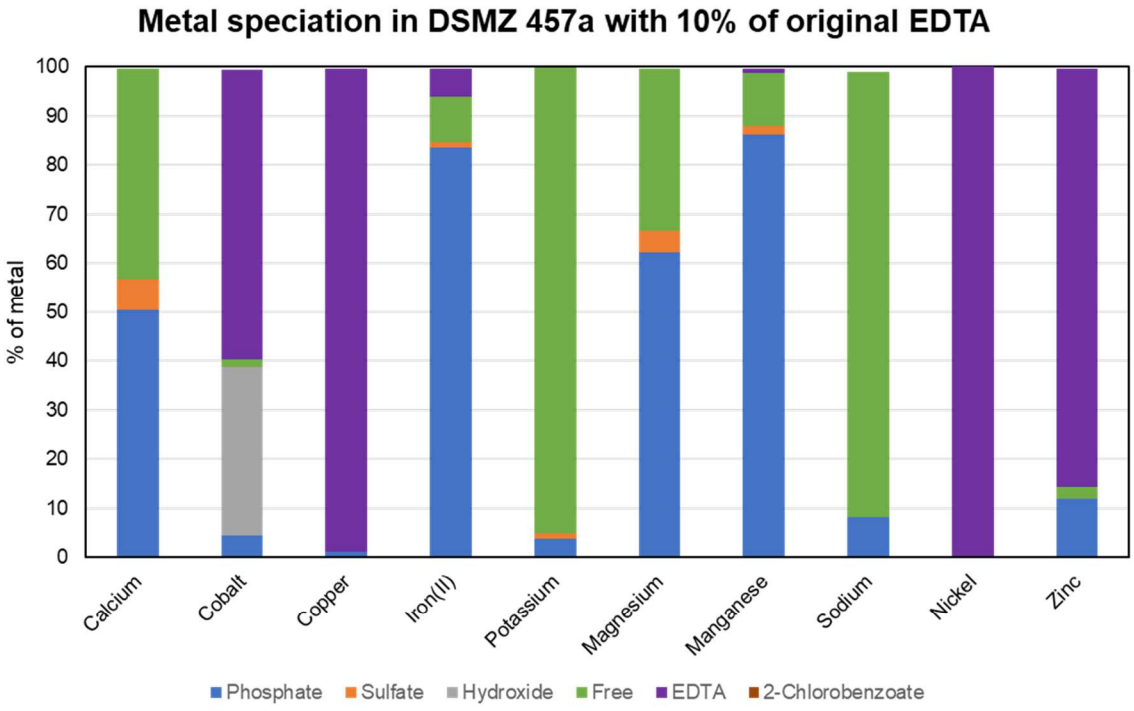

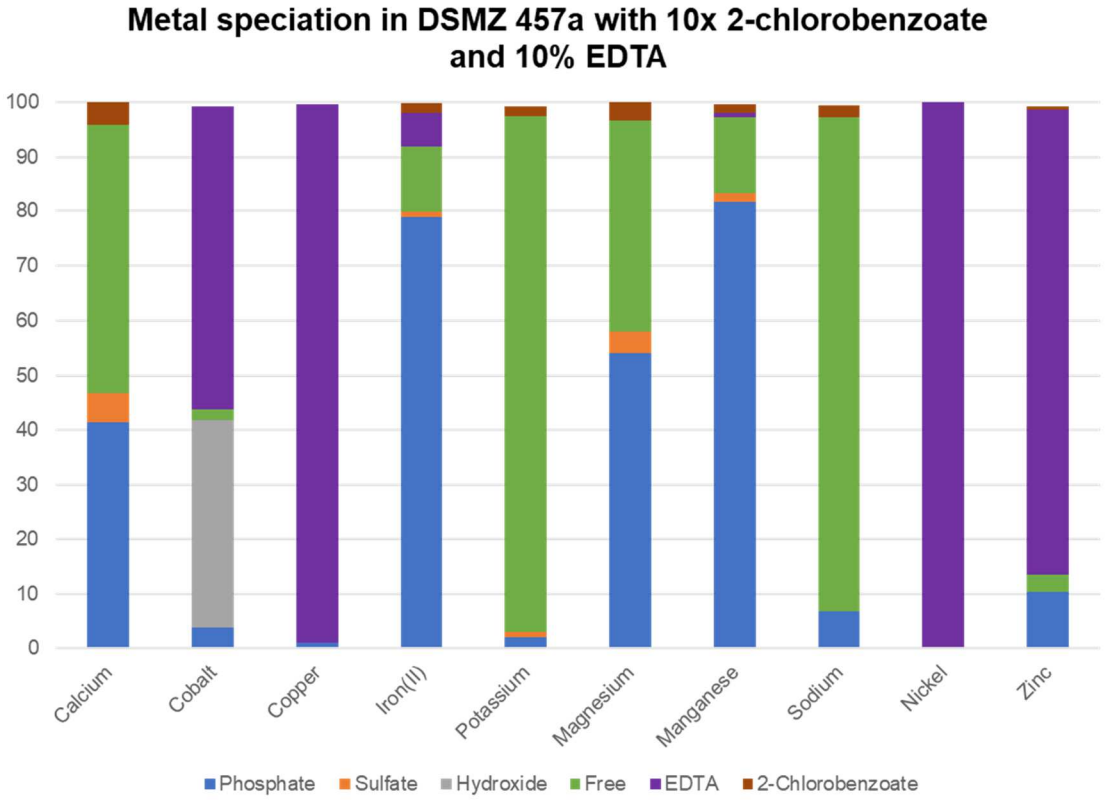

Fig 46b. Metal speciaton in DSMZ 457a with minor variations in composition (contd.)

or estimated metal-ligand stability constants (Prasad & Shock 2019a, Prasad & Shock 2019b). Speciation for all metals present in these media is shown in Fig. 46a.

As may be seen from the figure, speciation may be similar or drastically different for metals in the same media. As an illustration, nickel and zinc have similar distribution in the fructose mineral media while cobalt and copper are speciated completely differently. It may be worth noting that all the metals above are divalent transition metals. Other speciation observations of significance are that EDTA dominates the transition metal speciation in DSMZ 457, 465 & 1007 unlike other transition metals and that chloride dominates zinc speciation in DSMZ 1240.

Many of the above chemically defined media like DSMZ 457 and 465, have variants with minor additions to the original composition. For example, DSMZ 457a can be synthesized by adding ~5mM 2-chlorobenzoate that may be used as a sole carbon and energy source. As 2- chlorobenzoate has a metallophilic carboxylate group, we suspected if this ligand would disrupt the metal speciation in the medium. To theoretically test this, we performed metal speciation in DSMZ 457a using stability constants for metal complexes of 2- chlorobenzoate estimated by Prasad & Shock 2019a. These estimations were made using numerous linear free energy relationships as no stability constant measurements were available for any metal ion. As may be seen from Fig. 46b, the metal speciation in DSMZ 457a is almost identical to DSMZ 457. To investigate the impact of composition on the metal speciation in the medium, we performed these calculations with minor modifications. The metal speciation was largely similar when pH was decreased and increased by 1 unit. Raising the concentration of 2-chlorobenzoate by 10 times

changed the speciation of calcium, potassium, magnesium and sodium by a few percent but no change was made to the transition metal speciation. However, reducing EDTA concentration by a factor of 10 significantly changed the speciation of the transition metals iron (II) and manganese. These metals were predominantly distributed as phosphate complexes (mainly HPO_4^{-2}) in this composition with EDTA complexes accounting for less than 6% of the total metal. Speciation for cobalt and zinc was minorly affected as more than 60% of these metals were distributed as their EDTA complexes. On the other hand, copper and nickel distribution was completely unaffected with EDTA chelates predominating the respective speciation. This speciation was largely preserved when the concentration of 2-chlorobenzoate was additionally increased by a factor of 10. Thus, decreasing micromolar EDTA concentration has a bigger impact on metal speciation than increasing millimolar 2-chlorobenzoate concentration. Similar calculations can be performed for many chemically defined growth media using stability constant values estimated in Prasad & Shock 2019a and Prasad & Shock 2019b.

4.7 Conclusion

We have obtained metal speciation in some commonly used microbial growth media employing an updated thermodynamic database. We have evaluated how metal speciation changes with variations in medium composition. Our results suggest that the slightest modifications in pH and chelator concentration can significantly alter metal speciation. Such calculations are only limited by the availability of metal-ligand stability constants. When experimental values for such stability constants were not present in the literature, estimation methods were utilized to fulfill this requirement. We have

additionally made correlations of metal speciation with experimental measurements of biological response. These correlations informed us about the metal species taken up by different life forms and the associated uptake mechanisms. We evaluated the applicability of the free ion activity model in two case-studies and critiqued the findings of the original authors.

While a relationship between metal speciation and metal bioavailability was first proposed over 40 years ago, there is still a lot to learn on this topic. A deep understanding of this subject is needed to assess the degree of metal-requirement and the dangers of metal-toxicity to microbes and human cells alike. We hope future microbial growth experiments are performed in conjunction with these speciation calculations that are free of cost and easy to obtain.

CHAPTER 5

METAL SPECIATION IN BLOOD PLASMA

5.1 Introduction

Metals are indispensable to life. They serve as cofactors in numerous enzymatic reactions, help stabilize protein conformations, and may also be used as sources of energy via redox transformations. Different metals are present at multiple levels of abundance- while potassium is needed in millimolar concentration in an organism, nickel may be present only at nanomolar levels. Evidently, metal requirements are essential for human life too, iron in hemoglobin of red blood cells being a common example. Over the past 40 years, a mountain of evidence has emerged demonstrating that not all forms of metal are bioavailable (Sunda & Guillard 1976, Anderson & Morel 1978, Sunda & Gillespie 1979, Daly et al. 1990, Canterford & Canterford 1992, Morton et al. 2000, Zhu et al. 2006, Scheers et al. 2014, Peng et al. 2014, Pereira et al. 2014, Nday et al. 2012 and Hart et al. 2015). The organisms investigated in these studies comprise prokaryotes and eukaryotes including human beings. Therefore, quantifying metal distribution (or metal speciation) in a living system can be of enormous benefit, as evidenced by the application of iron speciation in the treatment of iron-overloading (Temraz et al. 2014 and Templeton 2015). However, obtaining metal speciation in complex aqueous systems like human bodily fluids presents extreme experimental difficulties (Levina et al. 2017). Theoretical modeling offers a promising alternative but is generally limited by lack of thermodynamic data (Wilke et al. 2017 and Kiss et al. 2017). Existing models of metal speciation suffer from exclusion of large molecules like albumin and rarely include

comparisons with experimental measurements, which inhibits their applicability (May et al. 1976 and Konigsberger et al. 2015).

In this work, our aim is to overcome such limitations by creating models of metal speciation, including proteins and peptides, and comparing our calculations with metal speciation measurements in simple systems. Our thermodynamic model was created using critically evaluated experimental stability constant data measured over the past 100 years and includes stability constant estimates made using linear free energy relationships (Prasad & Shock 2019a and Prasad & Shock 2019b). In previous work, we obtained metal speciation in microbial growth media and made correlations with biological response to evaluate metal bioavailability (Prasad & Shock 2019c). Here, we predict metal speciation in blood plasma for several naturally occurring metals and those that may be present as therapeutic agents (metal-based antacid, anti-diabetes and anticancer drugs) or as toxic agents (copper and manganese toxicity). As the medium that transports nutrients and waste products across most human cells, blood plasma is arguably the most crucial biofluid in the human body. Our model replicates the speciation of metals for which elemental distribution in blood plasma is well known and provides metal speciation for cases with extremely limited information on biologically relevant metal-ligand systems. We encourage future experimentalists to test the theoretical predictions made in this work and hope this endeavor furthers research on metal-ligand thermodynamics and metal bioavailability in the human body.

5.2 Calculating speciation

Elemental speciation in any system at equilibrium can be obtained by solving the law of mass-action for all reactions that may happen in the system. So, for the chemical reaction: bB + cC = dD + eE, the law of mass-action is given as:

$$K = \frac{a_D^d \cdot a_E^e}{a_B^b \cdot a_C^c} \quad (1)$$

where 'K' is the equilibrium constant of the reaction; 'B', 'C', 'D' & 'E' are the chemical entities involved in the reaction; 'a' is the activity of these entities (also known as 'corrected concentration') and 'b', 'c', 'd' & 'e' are the stoichiometric constants. As most metal-ligand reactions are complexation reactions, 'd' or 'e' is 0 and the equilibrium constants are referred to as stability constants. As metal-ligand complexation reactions do not have large kinetic barriers (completing on the order of seconds), the assumption of equilibrium is valid. If the analytical composition (or total composition) of a system is additionally known, the law of mass action can be combined with mass-balance and charge-balance constraints to obtain the chemical distribution of elements occurring in different forms (like calcium as Ca^{+2} or $CaOH^{+}$, $CaCl^{+}$, etc.).

Such speciation calculations can be performed using numerous programs like PHREEQC (Parkhurst 2013) and JESS (May 2015). We have used the software EQ3/6 (Wolery 2010) as it is freely available, and the thermodynamic databases can be easily modified. The composition of blood was obtained from the compilation in the Geigy Tables (Lentner 1981). This composition represents the average blood plasma composition of a healthy human adult and is given in Table 1. As ligand abundance plays a major role in determining metal speciation, we did not include ligands present at

Ligand Component	Concentration (mM)
Chloride	104
Carbonate	25
Lactate	1.8
Phosphate	1.6
Glutathione	1.09
Serum Albumin	0.72
Glutaminate	0.52
Alanate	0.37
Glycinate	0.24
Valinate	0.23
Prolinate	0.21
Sulphate	0.21
Lysinate	0.18
Threoninate	0.15
Silicate	0.14
Leucinate	0.12
Serinate	0.12
Citrate	0.11
Arginine	0.095
Pyruvate	0.095
Histidinate	0.085
Isoleucinate	0.065
Phenylalanate	0.064
Ornithinate	0.058
Tyrosinate	0.058
Asparaginate	0.055
Glutamate	0.048
Ascorbate	0.043
Succinate	0.042
Cystinate	0.04
Malate	0.035
Methionate	0.029
Citrullinate	0.027
Transferrin	0.025
Aminobutyrate	0.024
Ammonia	0.024
Cysteinate	0.023
Thiocynate	0.014
Oxalate	0.012
Tryptophanate	0.01
α2 Microglobulin (α2M)	0.006
Hydroxyprolinate	0.007
Aspartate	0.005
Salicylate	0.005
Ceruloplasmin	0.0038
OH-	0.0012

Metal Component	Concentration (mM)
Sodium	142
Potassium	4.03
Calcium	2.50
Magnesium	0.74
Iron	0.018
Copper	0.015
Zinc	0.014

Table 1. Default composition of blood plasma used in this study.

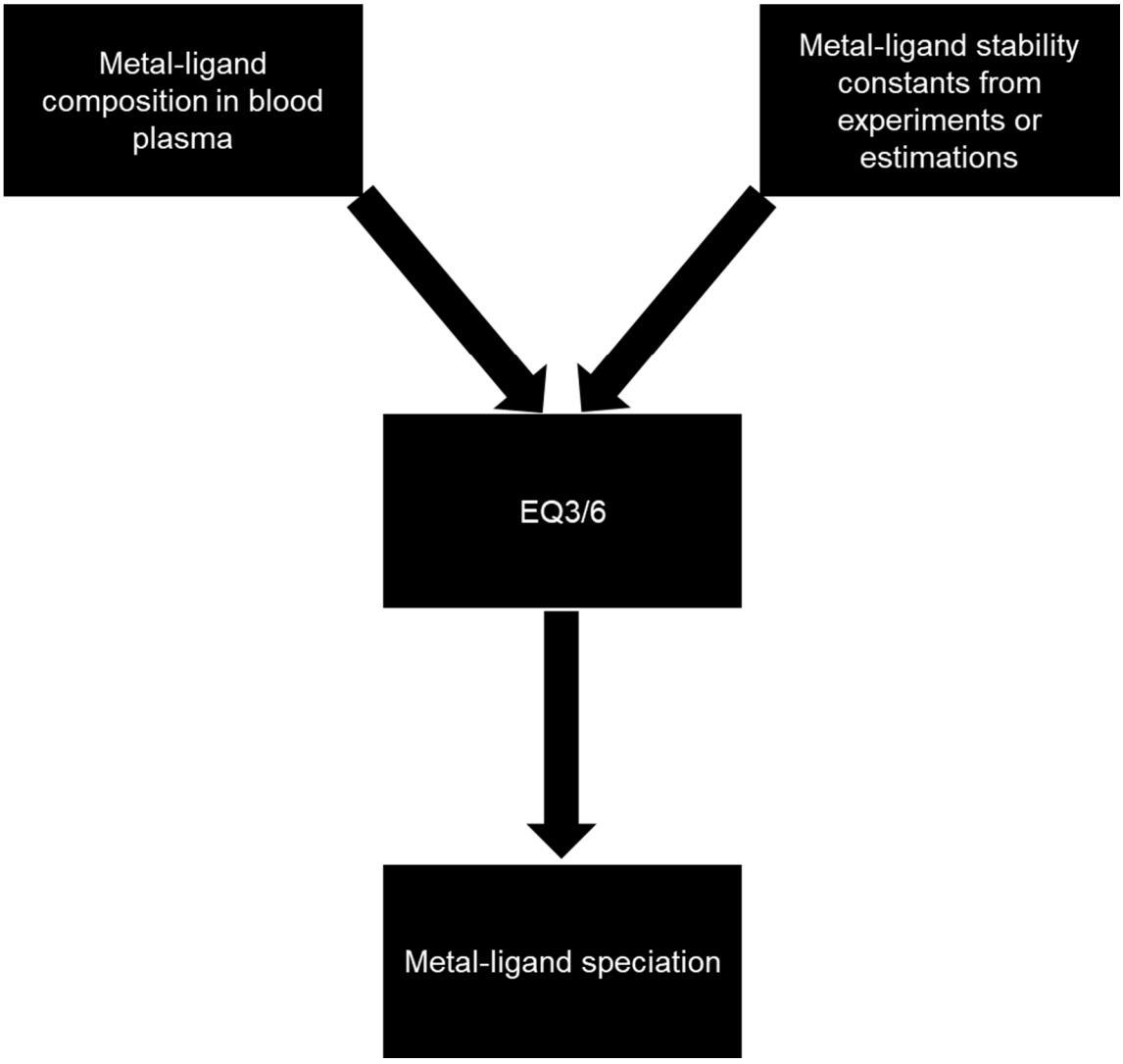

Fig 47. Flowchart for obtaining metal-speciation.

concentration < 1μM. The metal-ligand complexes for which experimental equilibrium constants were absent in the literature, were estimated using linear free energy relationships (Prasad & Shock 2019a and Prasad & Shock 2019b). These include metal complexes of albumin, transferrin, glutathione, several amino acids, lactate and ascorbate. A schematic for the flow of information in the procurement of metal-ligand speciation is presented in Fig. 47.

5.3 Speciation of predominant metals in default blood plasma composition

As documented in Table 1, potassium, sodium, calcium and magnesium in an average, healthy human are present at millimolar concentrations while iron, copper and zinc are present at micromolar levels. Owing to their high abundance, the predominant forms of these metals are well established; potassium and sodium are mostly present as free cations, 45% of calcium and magnesium is bound to serum proteins (Peters 1996), almost all of the iron is bound to transferrin (Levina et al. 2017), copper is mostly bound to ceruloplasmin (Hellman & Gitlin 2002) and the majority of zinc is bound to albumin (Kiss et al. 2009). Our speciation calculations reproduce these results and additionally, provide the distribution of these metals in the lesser dominant forms. The speciations for metals present at millimolar and micromolar concentrations are given in Fig. 48a and Fig. 48b, respectively.

Among these seven dominant metals, potassium and sodium are the only ones unaffected by protein complexation. This is understandable due to their low charge and high ionic radii that limit coordination at ‘metal-binding sites’ of proteins. There have been multiple contradictory reports of calcium-albumin stability constants in the literature

(McLean & Hastings 1935, Pedersen 1971, Fogh-Andersen 1977 and Kragh-Hansen & Vorum 1993). We found that stability constant values ($K=10^{2.7}$) and number of binding sites (5) reported by Vorum et al. (1995) gave results consistent with the established calcium partitioning in albumin of ~45 % (Peters 1996). While the albumin-fraction obtained using the thermodynamic data provided by some studies (Pedersen 1971, Fogh-Andersen 1977 and Kragh-Hansen & Vorum 1993) was slightly lower (by 10-20%), it was extremely low with the data provided by McLean & Hastings 1935 (by ~40%). Among the remaining calcium, 41% is distributed as the free ion and ~9% is complexed with bicarbonate, phosphate and citrate, all of which agrees with the overall speciation of calcium (Peters 1996). As magnesium is known to share calcium-binding sites (Peters 1996), we used an identical set of thermodynamic information (same sites and same stability constant values as Ca-albumin) for the magnesium-albumin interaction that produced the accepted magnesium distribution in blood plasma (Peters 1996). These results illustrate how speciation calculations may be used to critically evaluate ambiguous or limited thermodynamic data.

As can be seen from Fig. 48(b), transferrin dominates iron speciation in blood plasma. Iron(III)-transferrin interaction has been well-studied and the stoichiometric constants (reaction quotient expressed with concentration) reported by Aisen et al. (1978) are frequently used in the literature. However, these values vary with pH and do not qualify as thermodynamic equilibrium constants (reaction quotient expressed with activity). Additionally, the investigation precluded acid association constants (pK_a) of amino acids at the metal-binding site. Subsequent research (Sun et al. 2004) shows that

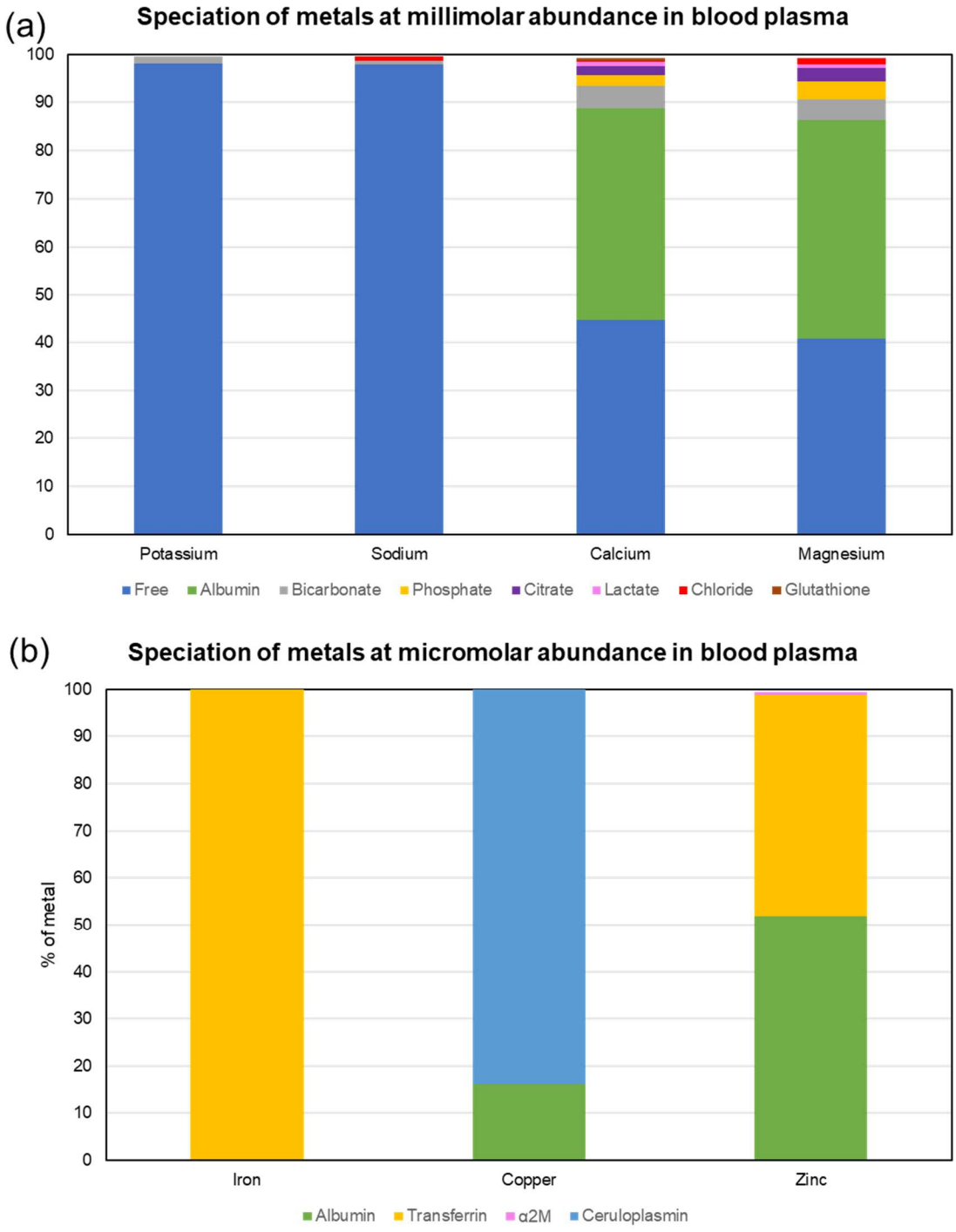

Fig 48(a-b). Speciation of metals present at an abundance of (a) 1mM or higher (b) 1µM or higher.

the pK_a of one tyrosine at the site (Tyr188) is considerably lower (7.2) than the pK_a of the free tyrosine sidechain (10.2). The pK_a of the histidine at the site (His249) was found to be comparable to imidazole pK_a (Woodworth et al. 1987, Valcour & Woodworth 1987 and Kubal et al. 1994) and those of the other amino acids (Tyr95 and Asp63) were assumed to be same as the corresponding sidechain pK_a. As transferrin has two metal-binding sites, the same considerations were made for the other site (Tyr517, His585, Tyr426 and Asp392). These pK_a values were incorporated in our database along with the corresponding thermodynamic data associated with the competitive ligand citrate which allowed us to obtain thermodynamic stability constant values for Fe(III)-transferrin by regression of experimental data reported by Aisen et al. (1978) (see Appendix C). While the use of these thermodynamic stability constants does not change the iron speciation at the pH of blood plasma (Fig. 48b), it has substantial effect on iron speciation at lower pH (see below).

While most investigations into copper speciation agree that the protein ceruloplasmin dominates copper speciation in blood plasma, the fraction of copper as ceruloplasmin ranges from 65% (Linder et al. 1996) to 95% (Hellman & Gitlin 2002). Additionally, the thermodynamic information for metal-ceruloplasmin complexes is very limited. While it is well agreed upon that ceruloplasmin has six primary sites for copper (Hellman & Gitlin 2002), data on stability constants are obscure at best. Speciation calculations with data reported by Zgirski & Frieden (1990) underestimate copper-ceruloplasmin abundance by several orders of magnitude. Subsequent X-ray crystallography investigations revealed a preponderance of cysteine and histidine groups

in the three 'types' of copper sites in the protein (Hellman & Gitlin 2002) suggesting that stability constant values are much larger than the reported values ($K \sim 10^7$). Additionally, as ceruloplasmin dominates copper speciation despite the higher concentration of serum albumin, Cu-ceruloplasmin stability constants should be larger than Cu-albumin stability constants that are known to be ~ 10^{12}-10^{13} for the N-terminus site (NTS). We adopted an average stability constant of 10^{14} for the six Cu-ceruloplasmin sites that results in the speciation shown in Fig. 48(b). Cu-ceruloplasmin constitutes ~84% of the total copper while ~15% is distributed as Cu-albumin. Copper speciation is extremely sensitive to this stability constant value as chancing K from $10^{13.5}$ to $10^{14.5}$ resulted in Cu-ceruloplasmin varying across the established speciation range of 65% to 95%.

Through modeling calculations, it is largely established that almost all zinc in blood plasma (~98%) is bound to the serum proteins albumin, α2-microglobulin (α2M) and transferrin (Kiss et al. 2017). However, the ratio of zinc distribution among these proteins is still ambiguous. To resolve this issue, we simulated zinc speciation measurements associated with these proteins using stability constants reported in the literature while obtaining stability constants by regression. Zn-albumin stability constants reported by Lu et al. (2012) for the Multi-Binding Site and for Site B by Ohyoshi et al. (1999) agree closely with the experimental measurements reported by Bytzek et al. (2009) (see Appendix). Zn-transferrin stability constants were obtained using a procedure similar to the method used to obtain values for Fe(III)-transferrin based on experimental measurements reported by Harris & Stenback (1988) (see Appendix), while stability constants reported by Adham et al. (1977) were used for Zn-α2M

complexes. Using the above set of data and the stability constants for other ligands mentioned previously, we predict that ~95% of zinc in blood plasma is bound to serum proteins (Fig. 48b). While this agrees with the value of Zn-protein fraction established in the literature (Bytzek et al. 2009, Lu et al. 2012 and Kiss et al. 2017), we found that transferrin takes up ~40% of the total zinc, which is much higher than the conventional values (Bytzek et al. 2009). Most papers in the literature report that albumin takes up 70-85% of zinc while α2M constitutes ~10-30% of total zinc (Falchuk et al. 1977, Charlswood 1979, Kiilerich & Christiansen 1986, Boyett & Sullivan 1970, and Foote & Delves 1984). However, these studies were performed before the experiments of Harris & Stenback (1988), which was the first study that carefully evaluated Zn-transferrin association. Additionally, none of these studies evaluated zinc distribution in the presence of all three proteins. Moreover, while the stability constants for Zn-transferrin and Zn-α2M are comparable, transferrin is more abundant than α2M in blood plasma by a factor of 6 (Table 1). For these reasons, we predict that our calculated speciation is closer to the *in vivo* zinc speciation and encourage future researchers to investigate this subject via experimentation. Our fraction of Zn-albumin (~53%) is closer to the values reported by Peters (1996) and Vallee & Falchuk (1993) (65-70%).

While the metals mentioned above are evidently needed, major changes in their abundance and distribution can severely affect human health either profitably or adversely. In the subsequent sections, we describe several cases where metals are investigated for their therapeutic potential or their toxicity. We have predicted the

speciations of these metal-based drugs and explored their dependence on pH, ligand concentration, and metal abundance.

5.4 Metal speciation in therapeutic or toxic scenarios

5.4.1 Gallium-based anticancer drugs

Gallium-based compounds have been a topic of interest in anticancer research for almost 50 years (Hart & Adamson 1971, Foster et al. 1986, Chitambar & Sax 1992, Chen et al. 2007 and Cao et al. 2019). Besides being agents of cytotoxicity, they are also used in cancer research for tumor-imaging owing to the radioactive properties of isotopes ^{67}Ga and ^{68}Ga (Edwards & Hayes 1969, Jackson & Byrne 1996, Shuhmacher et al. 2001, McInnes et al. 2017 and Yaxley et al. 2019). While it is generally accepted that lipophilic complexes of gallium increase its cellular uptake in comparison to inorganic salts (Kiss et al. 2017 and Levina et al. 2017), there is limited work establishing the dependence of gallium bioavailability on its speciation and dosage in bodily fluids. Speciation is of direct relevance because metal-based anticancer drugs are known to produce long-lasting anticancer immune responses (Englinger et al. 2019). Here, we report predicted gallium speciation in blood upon addition as $Ga(Maltol)_3$ and compare our calculations with experimental results and models from the literature.

The antineoplastic effects of $Ga(Maltol)_3$ were first reported in 2000 (Bernstein et al. 2000) and even reached Phase I-II of clinical trials in United States in 2005 (https://clinicaltrials.gov/ct2/show/study/NCT00050687). Even though the results of the clinical trials have not been published, subsequent research on $Ga(Maltol)_3$ cytotoxicity

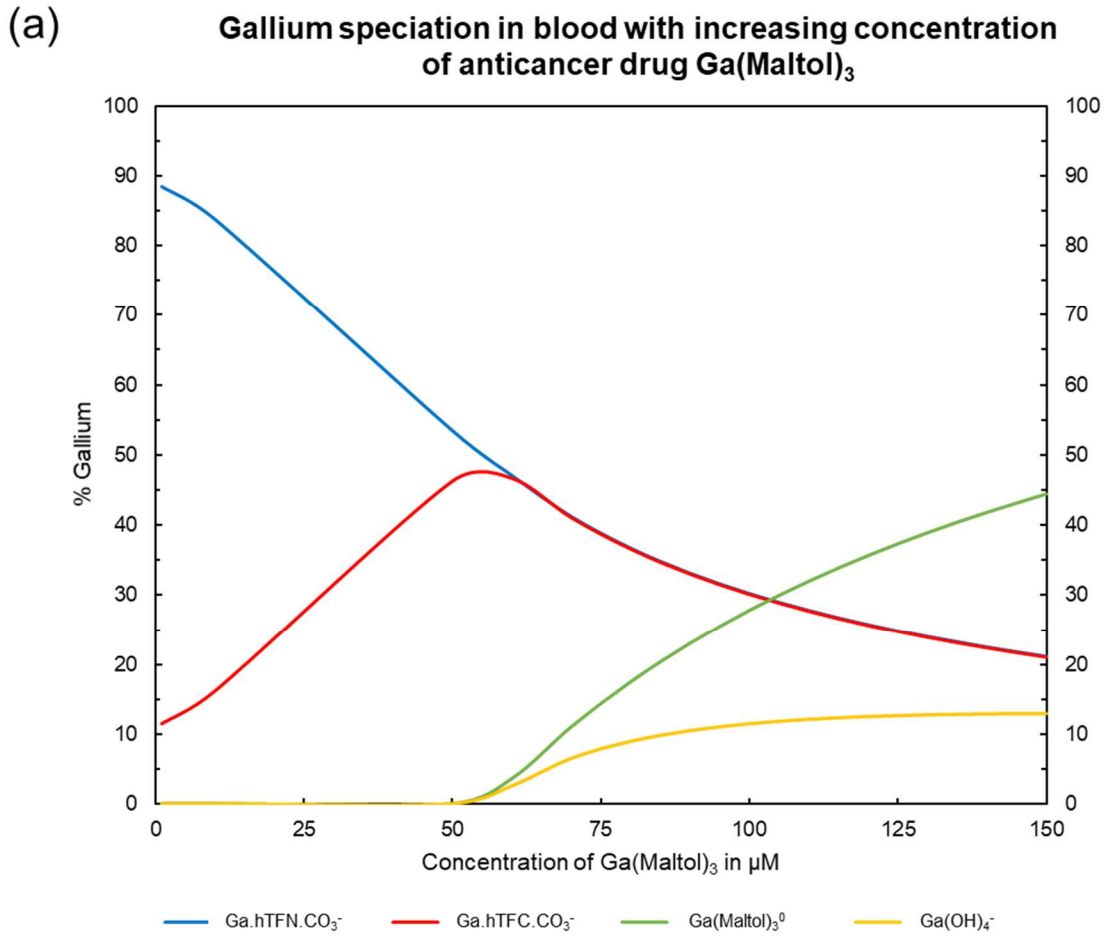

Fig 49(a-b). Speciation and bioavailability of gallium-based anticancer drugs (contd.)

(b)

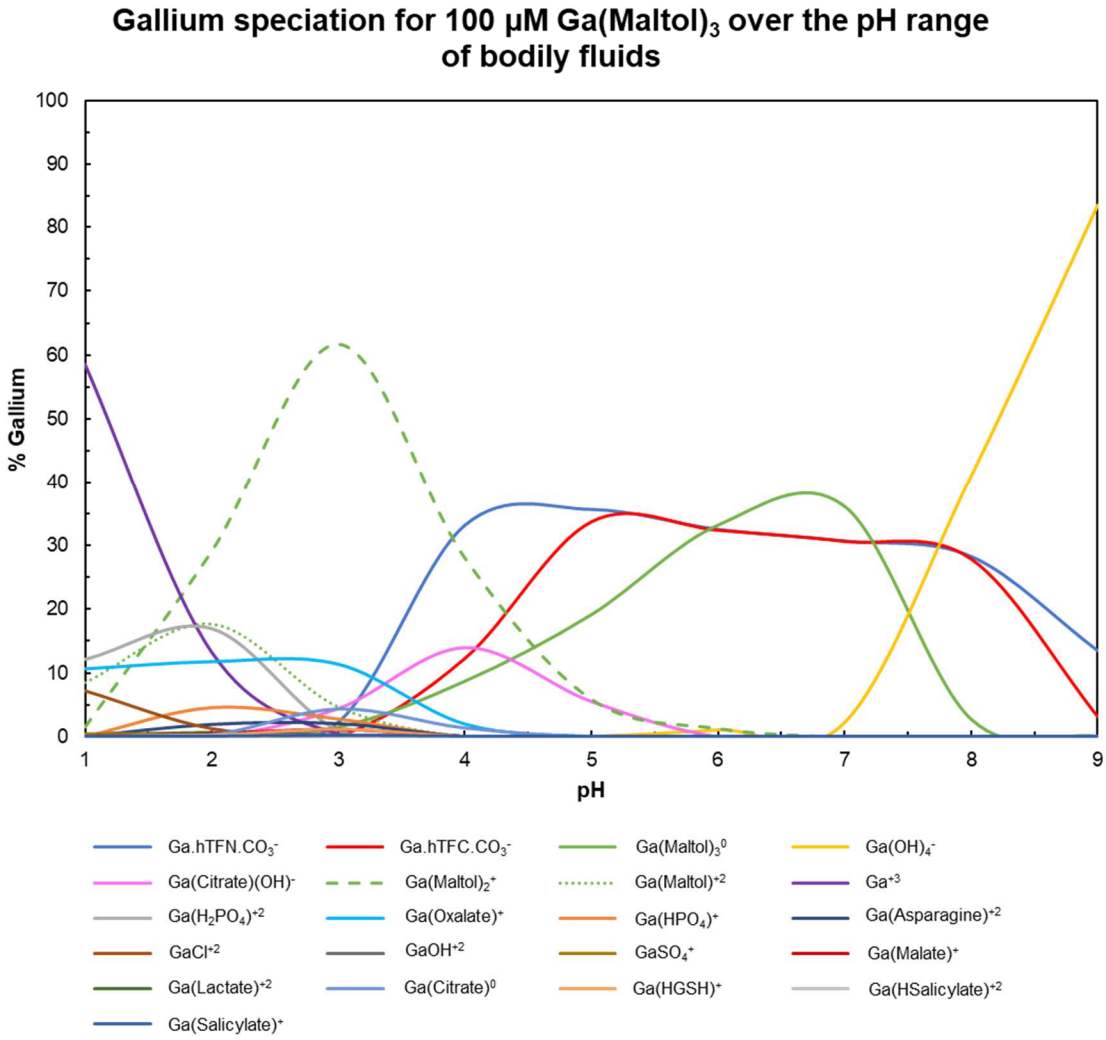

Fig 49(a-b). (contd.) Speciation and bioavailability of gallium-based anticancer drugs.

has generally produced favorable results (Chua et al. 2006, Chitambar et al. 2007, Merli et al. 2018 and Chitambar et al. 2018). Perhaps one of the reasons for the continued interest in $Ga(Maltol)_3$ research is its high oral bioavailability. Due to its relatively high lipophilicity (neutral overall charge and aromatic chelate rings), it has the tendency to cross the lipid barrier via passive diffusion. This phenomenon seems to be ligand dependent as maltol complexes of aluminum and iron are also known to have high bioavailability (Finnegan et al. 1986, Finnegan et al. 1987, Reffitt et al. 2000, Murukami et al. 2006, Pereita et al. 2014 and Stallmach & Buning 2015). The mechanism of action of Ga(III)-based anticancer drugs has largely been attributed to its Fe(III)-like properties. As cancer cells have a high iron dependence, this leads to the disruption of several iron-dependent processes in the cell like iron homeostasis, iron-dependent ribonucleotide reductase activity and the activation of Bax protein that triggers apoptosis through the mitochondrial release of cytochrome c and caspase-3 (McInnes et al. 2017, Chitambar 2017 and Englinger et al. 2019). For these reasons, $Ga(Maltol)_3$ is still a sought-after drug in anticancer research.

Despite the large body of research on $Ga(Maltol)_3$, we found only one study that investigated its speciation. Enyedy et al. (2015) evaluated the interaction between $Ga(Maltol)_3$ and the two predominant serum proteins albumin and transferrin using multiple techniques. They also reported conditional thermodynamic constants for drug-protein binding (Kiss et al. 2009) and computed gallium distribution as a function of $Ga(Maltol)_3$ concentration (Enyedy et al. 2015). However, this distribution was reported for a relatively simple system comprising of only four ligands (maltol, albumin,

transferrin and hydroxide). To investigate if other common ligands in blood like citrate, lactate and amino acids affect gallium distribution, we performed gallium speciation calculations for the default composition of blood reported in Table 1. We found that our results for gallium distribution closely mirrored the speciation reported by Enyedy et al. (2015) as illustrated in Fig. 49a. This suggests that the LMM (low molecular mass) ligands do not significantly impact gallium speciation at the physiological pH of 7.4. However, we found that gallium speciation was completely different at lower pH as shown in Fig. 49b. For example, for 100μM $Ga(Maltol)_3$ at a pH of 4, which is close to the pH of endosomes, only about 45% of gallium is bound to transferrin whereas $Ga(Maltol)_3^0$ takes up only ~9% gallium. The rest of the gallium is predominantly distributed as $Ga(Maltol)_2^+$ and citrate complexes that may have a different biological fate in comparison to the lipophilic $Ga(Maltol)_3^0$ and the transferrin-bound gallium. At pH>7.4, gallium is predominantly distributed as $Ga(OH)_4^-$, which is consistent with results found in the literature (Harris & Pecoraro 1983).

The results discussed above show how thermodynamic models of metal-based drugs can provide useful information on their distribution and bioavailability in the human body. Such models can also be made for the next generation of gallium-based anticancer drugs currently under preclinical trial like corroles, azoles and thiolates (Chitambar 2017). As speciation calculations are rapid and inexpensive, they are an excellent means to selecting metal-based drugs with high bioavailability. Experimental research performed in conjunction with these calculations can constrain dosage levels for these anticancer drugs

that elicit cytotoxic tumor response without causing long-lasting anticancer immune responses.

5.4.2 Copper dysregulation and Wilson Disease

Owing to its redox nature and high crustal abundance, all living cells use copper as a source and acceptor of electrons at the active sites of many enzymes like cytochrome c oxidase and superoxide dismutase. Therefore, copper is an essential trace metal, vitally important for human health and well-being. Copper deficiency (hypocupremia) in humans is known to cause myelopathy that is known to be associated with Vitamin B_{12} deficiency (Kumar et al. 2004, Prodan et al. 2007) while excess of copper (hypercupremia) may lead to cancer (Buchwald & Hudson 1944, Margalioth et al. 1983, Gupte & Mumper 2009). The plasma copper concentration associated with these diseases ranges from 1.5μM in hypocupremia to 50 μM in hypercupremia (Lentner 1981). Our predicted speciation for copper in blood plasma under these conditions is shown in Fig. 50a. Note that the majority of copper is distributed between the proteins ceruloplasmin and albumin (specifically the NTS). As the concentration of albumin (0.63mM) is much higher than that of ceruloplasmin (3μM), the Cu-albumin fraction increases as total copper in blood plasma increases. As the established role of the NTS on albumin is to transfer copper from the intestine to liver (Bal et al. 2013), this may have implications on hepatotoxicity. As albumin is regarded as a primary component of the exchangeable copper in the plasma (Linder & Hazegh-Azam 1996), the high Cu-albumin fraction could explain why copper is toxic despite being completely distributed among plasma proteins.

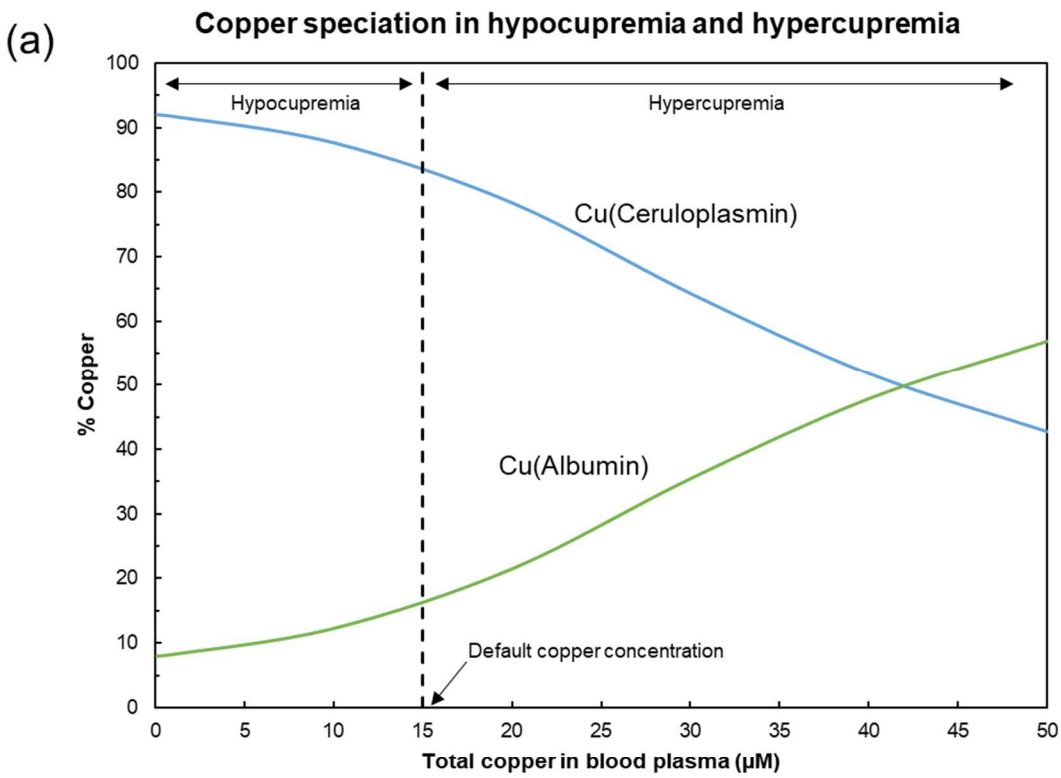

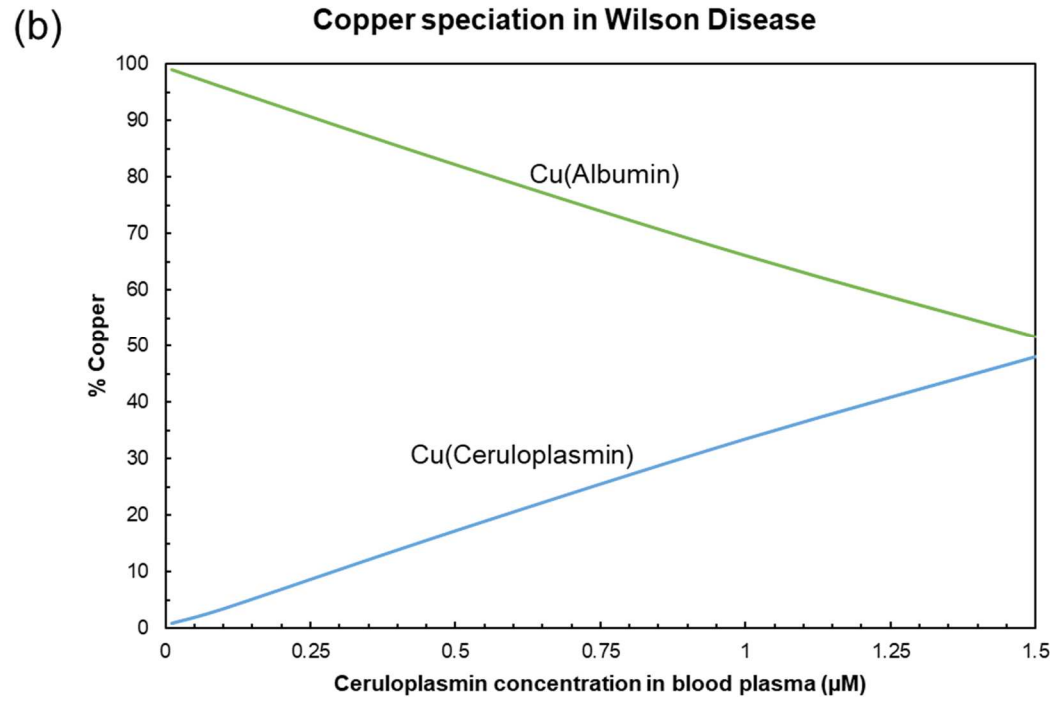

Fig 50(a-c). Copper(II) speciation in blood plasma under different conditions (contd).

(c)

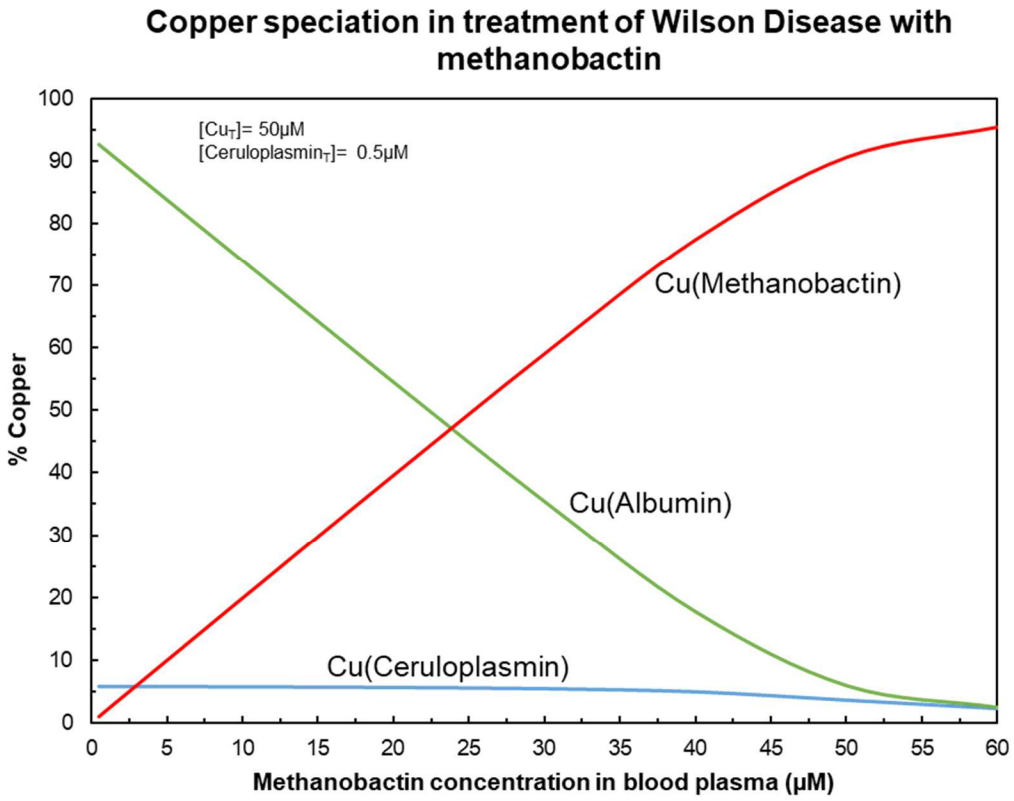

Fig 50(a-c). Copper(II) speciation in blood plasma under different conditions (contd).

Copper dysregulation in humans may also occur due to genetic reasons. Mutations in the gene encoding for the ATP7A protein causes Menkes Disease that leads to impaired copper absorption in the blood (Prohaska 2008). On the other hand, Wilson Disease (or Wilson's Disease) is caused by disabling mutations in both copies of the gene encoding for the ATP7B protein, which leads to copper excess mainly in the liver and brain (Bull et al. 1993, Prohaska 2008). As Wilson Disease is about ten times more prevalent than Menkes Disease (de Bie et al. 2007), we have focused our attention on Wilson Disease in this work.

One of the key characteristics of Wilson Disease (WD) is a deficiency of ceruloplasmin in blood plasma (Scheinberg & Gitlin 1952, Hellman & Gitlin 2002). The low ceruloplasmin concentration in patients suffering with WD is a consequence of the lack of functional ATP7B in hepatocytes, resulting in the secretion of a rapidly degraded apoprotein (Gitlin 2003). Generally, individuals suffering from WD have ceruloplasmin concentration lower than 1.3μM, which is about 30% of normal levels (Gitlin 2003). The predicted dependence of plasma ceruloplasmin abundance on copper speciation is demonstrated in Fig. 50b. Note that throughout this range of ceruloplasmin concentration, the Cu-albumin fraction dominates over the Cu-ceruloplasmin fraction, which may explain the copper toxicity associated with the disease.

There are primarily two treatments for Wilson Disease- chelation therapy and zinc supplementation. For patients who are unresponsive to both treatments, liver transplantation is the only recourse. Zinc supplementation inhibits the absorption of copper in the gastrointestinal mucosa and stimulates metallothionein synthesis in the

enterocytes that have a higher capacity to chelate dietary copper (Patil et al. 2013, Delangle & Mitz 2012, Brewer 2009). While this strategy has limited side-effects, its relative slow response makes it a suitable method of treatment at the presymptomatic stage (Huster 2009, Linn et al. 2009). Chelation therapy is the preferred form of treatment in the clinical stages of Wilson Disease. Several copper-chelators have been investigated as putative WD drugs such as penicillamine, triethylenetetramine and tetrathiomolybdate (Delangle & Mitz 2009). Recently, the naturally produced chalkophore methanobactin was used as a chelator to reverse liver failure in Wilson Disease (Lichtmannegger et al. 2016, Summer et al. 2011). Methanobactin (Mb) is a 1154 Da post-translationally modified peptide produced by the methanotroph *Myethylosinus trichosporium* OB3b to accumulate copper that is essential for the activity of the methane monooxygenase enzymes (Morton et al. 2000, Knapp et al. 2007, Semrau et al. 2010, Kenney & Rosenzweig 2013). It chelates copper with a 1:1 stoichiometry with an extremely large stability constant ($K= 10^{20.8}$, Ghazouani et al. 2011). While other metals like cobalt, nickel and zinc can also be chelated by Mb (Choi et al. 2006), the nitrogen-sulfur N_2S_2 coordination imparts a strong selectivity for copper consistent with its Cu detoxifying ability. The predicted effect of methanobactin on copper speciation in an extreme case of WD is illustrated in Fig. 50c. The values for methanobactin protonation constants (pK_a) were taken from Pesch et al. (2012). Using a total plasma copper concentration of 50 μM and total plasma ceruloplasmin concentration of 0.5 μM, our model predicts that ~ 60 μM (~0.07g) methanobactin can restore the exchangeable copper abundance on albumin to normal levels. Similar models can be made for specific cases of copper and ceruloplasmin abundance in plasma of WD patients. Evidently, similar models need to be

made for bile, intracellular hepatocyte composition and urine to obtain a deeper understanding of copper distribution in this disease. We hope these results encourage future researchers to conduct further experimental investigations on this topic in conjunction with models of copper speciation.

5.4.3 Zinc-based antidiabetics

The role of zinc in diabetes is a topic of considerable interest in the current scientific community with over 50 studies published in the last year exploring the associated physiology, molecular machinery and genetics (including: Lee et al. 2019, Nazem et al. 2019, Bosma et al. 2019, Jonsdottir et al. 2019, Adulcikas et al. 2019, Sobczak et al. 2019, Patel et al. 2019). While many researchers agree that zinc supplementation has a beneficial effect on diabetes patients (Wang et al. 2019, Nazem et al. 2019), others are more skeptical of the benefits of additional zinc intake (Fernandez-Cao et al. 2019, Perez et al. 2018). Some reports suggest that diabetic physiochemistry is associated with dysregulation of zinc homeostasis rather than total zinc levels (Fukunaka & Fujitani 2018, Chu et al. 2017, Fernandez-Cao et al. 2018). Thus, while there is a general cognizance of the relationship between zinc and diabetes, perhaps understanding may improve by investigating zinc speciation.

Some studies have obtained zinc speciation with multiple putative carrier-ligands that might increase zinc-bioavailability and hence elicit high anti-diabetic activity (Enyedy et al. 2008, 2012, Kiss et al. 2009, 2012, Bytzek et al. 2009). However, these studies were performed in simple aqueous solutions containing of only 5-6 ligands. We realized that obtaining zinc speciation in a composition more reflective of blood plasma

(a)

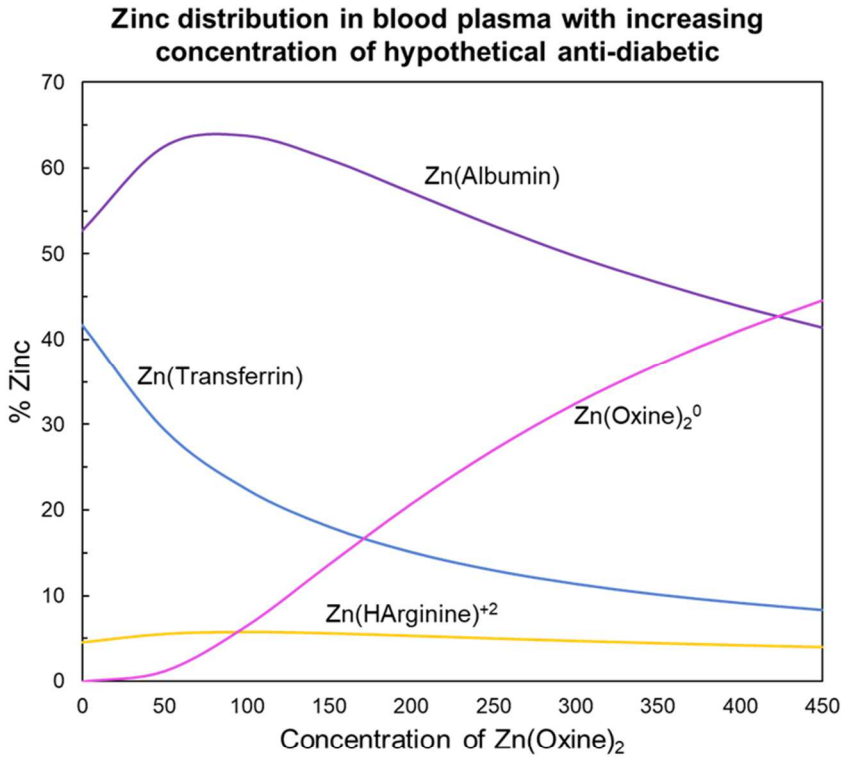

(b)

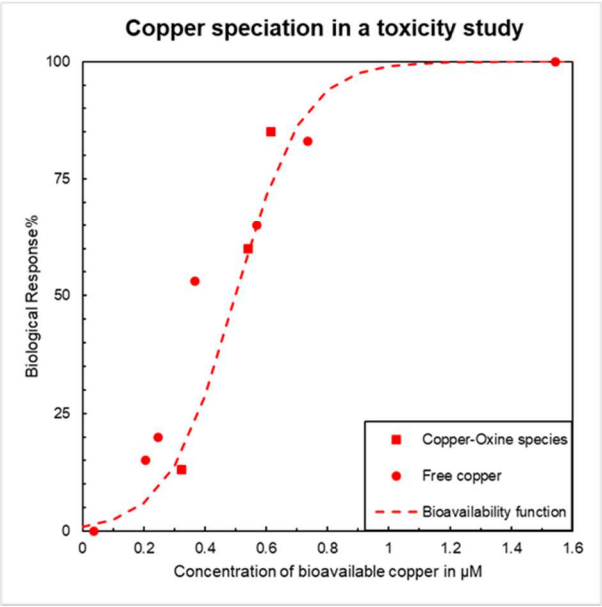

Fig 51(a-b). Speciation and bioavailability of zinc-based antidiabetics.

would enhance the current state of knowledge for prospective zinc-based antidiabetic drugs. Therefore, we predicted zinc-speciation in blood plasma including the ligand oxine, a commonly used carrier-ligand.

Zn-oxine stability constants were taken from Nasanen & Penttinen (1952) and Fresco & Freiser (1964), while the oxine-albumin stability constant was taken from Enyedy et al. (2015). Stability constants for other complexes were taken from the literature or estimated using linear free energy relationships, as summarized by Prasad & Shock (2019b). These stability constants along with the composition described in Table 1 were used to obtain the speciation of zinc as a function of the total $Zn(Oxine)_2$ in blood plasma shown in Fig. 51a. As can be seen in the figure, the abundance of the neutral aqueous complex $Zn(Oxine)_2^0$ changes in a non-linear manner with increasing concentration of total $Zn(Oxine)_2$ in blood plasma. Additionally, note that $Zn(Oxine)_2^0$ dominates zinc speciation above 450μM, which is quite high. Adjudicating a suitable dose for this prospective drug is enabled by investigating the bioavailability of zinc in solutions of $Zn(Oxine)_2$.

The bioavailability of many metal-based drugs depend on the form in which they are administered. For example, iron administered as a maltol complex is known to be highly bioavailable in human cells (Stallmach & Buning 2015, Pereita et al. 2014, Murukami et al. 2006, Reffitt et al. 2000). Choosing ligands like oxine and maltol as carrier-ligands enhances the lipophilic/hydrophobic nature of the molecules. As an example, $Zn(Oxine)_2^0$ consists of a polar nucleus consisting of the zinc ion and polar functional groups of the two oxine molecules (oxygen and nitrogen). The outer regions of

this binary complex are two aromatic rings that have high lipophilicity. This type of structure allows such molecules to pass though the hydrophobic lipid bilayer via passive diffusion. This phenomenon was demonstrated in an amphipod copper toxicity study (Ahsanullah & Florence 1984), for which we obtained the bioavailability curve Fig. 51b consisting of free copper and copper-oxine complexes (Prasad & Shock, 2019c). As can be seen from the figure, the biological response was extremely low when the concentration of the bioavailable metal was 0-0.3 μM but increased considerably thereafter. Given the similar behavior of Cu^{+2} and Zn^{+2}, we propose that a similar response can be expected with the administration of zinc-oxine complexes.

One way of determining the anti-diabetic activity of a drug is by measuring the inhibition of free fatty acid (FFA) release in adipocytes upon addition of epinephrine (Nakai et al. 1995). This property was measured by Sakurai et al. (2002) for a variety of metal ions including Zn^{+2} in the presence of insulin from mice that had been administered zinc-based compounds (3mg per kg of mouse weight) for two weeks. The inhibition of free fatty acid release for Zn^{+2} was measured to be ~23%, that was only slightly lower than the corresponding values for V^{+3} and VO^{+2} compounds that have been antidiabetic candidates for several decades. The zinc-based compounds investigated included $Zn(Maltol)_2$, $Zn(Picolinate)_2$ and $Zn(6\text{-methyl picolinate})_2$, all of which can pass through the lipid bilayer via passive diffusion like $Zn(Oxine)_2$. Given that the lipid bilayer is universal to life, it may be postulated that bioavailability of lipophilic complexes will be similar in amphipods and human cells. Combining this assumption with the information provided by Sakurai et al. (2002), we obtain that 60 μM of total $Zn(Oxine)_2$ in blood

plasma is enough to elicit the maximum possible anti-diabetic zinc activity as it is present at > 1 μM abundance., This dosage is more moderate in comparison to the recommended dose of Nazem et al. (2019).Arriving at a suitable dosage could be attained by combining experiments and speciation calculations across the digestive system to account for the change in $Zn(Oxine)_2$ speciation from the concentration in mouth to the concentration in blood.

5.4.4 Bismuth-based antacids

For over 200 years, bismuth-based compounds have been used worldwide to treat gastrointestinal complaints like dyspepsia and diarrhea (Chambers 1875, Bierer 1990). However, bismuth-based drugs are also known to cause nephrotoxicity with earliest reports dating back to 1802 (Leonard 1926, Gryboski & Gotoff 1961, Czerwinski & Ginn 1964, Cengiz et al. 2005, Liu et al. 2018). Additionally, bismuth compounds are known to cause neurotoxicity and brain encephalopathy as demonstrated by the bismuth epidemic of the 1970s that killed over 100 people in France and Australia (Morrow 1973, Burns et al. 1974, Martin-Bouyer et al. 1981). Despite its toxic history, bismuth compounds continue to attract attention for therapeutic purposes such as eradication of the stomach-infesting bacteria *Heliobacter pylori* (Gisbert 2011, Fallone et al. 2016, Gu et al. 2019), as broad-spectrum inhibitors of antibiotic resistant enzymes like metallo-β-lactamase (Wang et al. 2018), as non-steroidal anti-inflammatory drugs (Hawksworth et al. 2014), and as anticancer agents (Sathekge et al. 2017, Cheng et al. 2018, Ahamed et al. 2019, Chan et al. 2019). Thus, owing to the dual nature of bismuth, regulating its

(a)

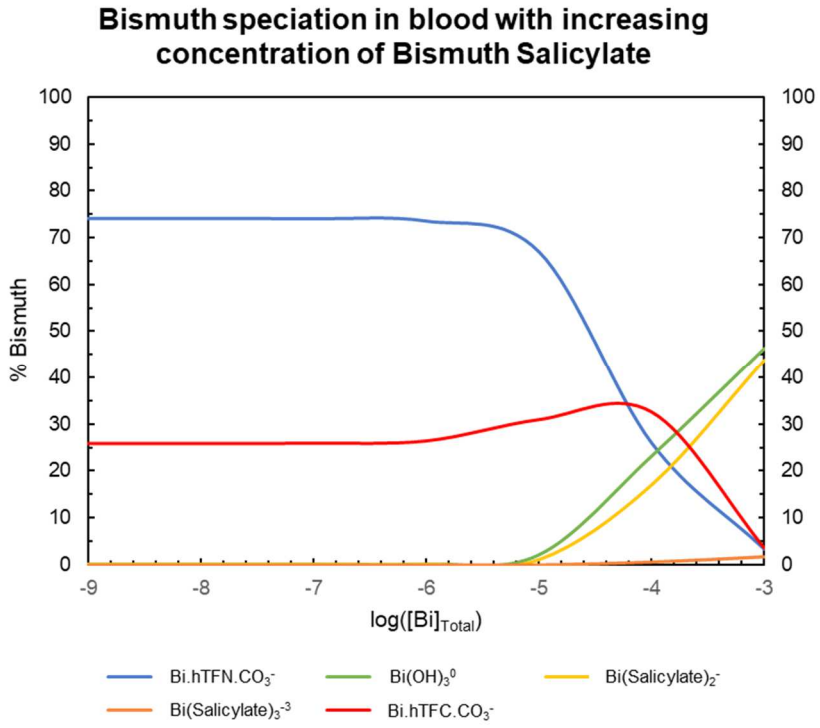

(b)

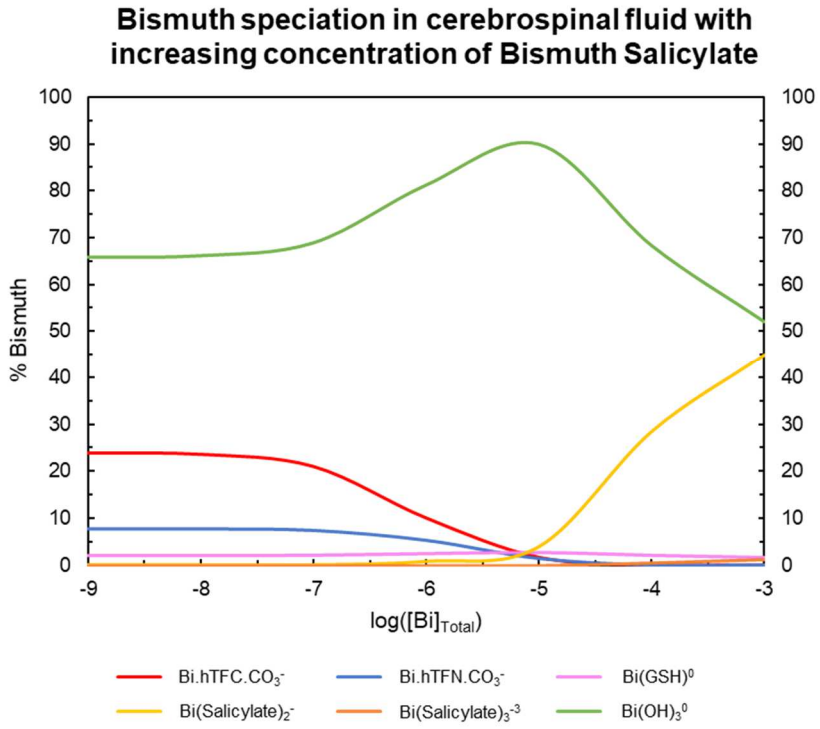

Fig 52(a-e). Speciation and bioavailability of bismuth in human bodily fluids (contd).

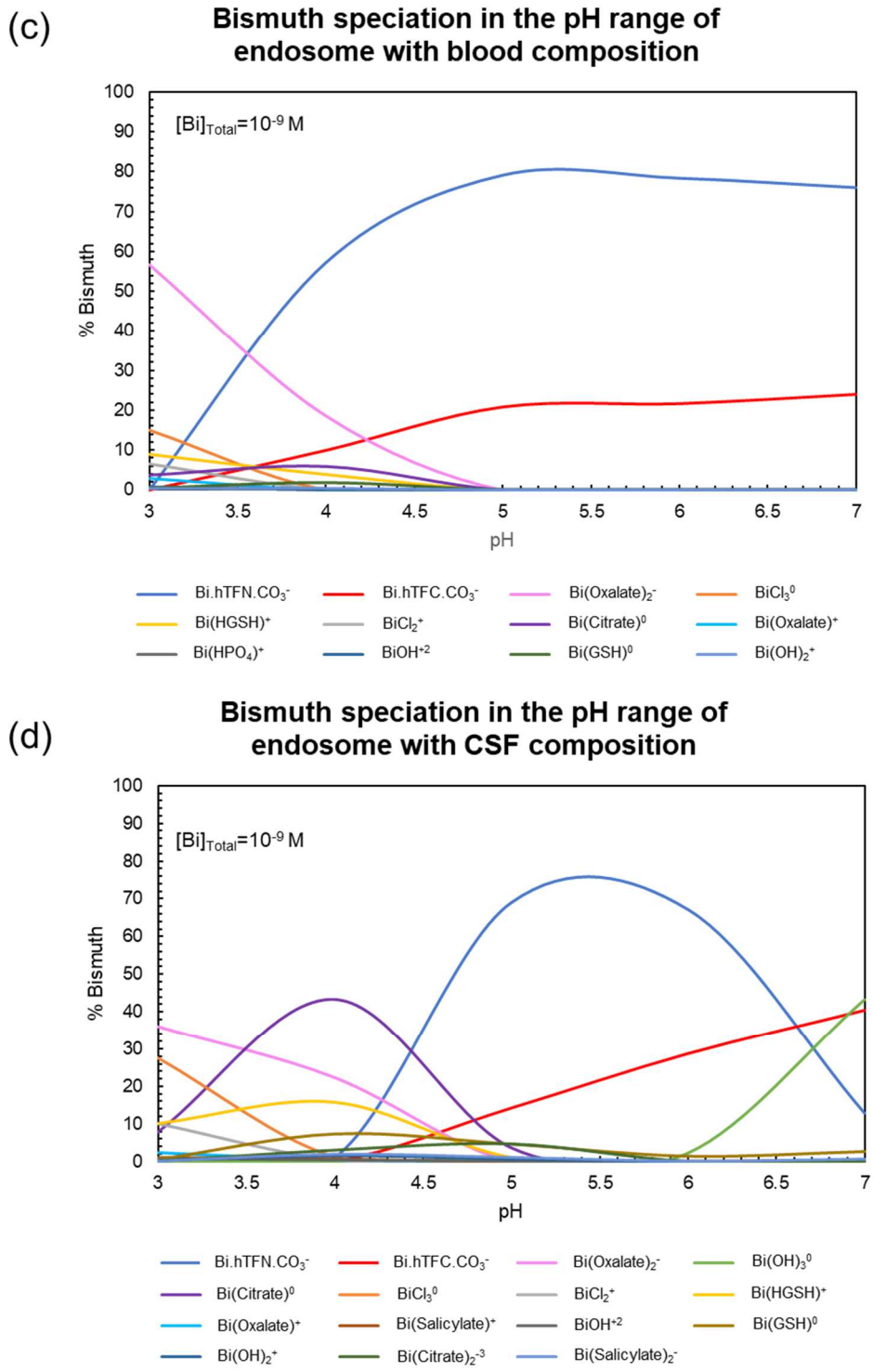

Fig 52(a-e). Speciation and bioavailability of bismuth in human bodily fluids (contd).

(e)

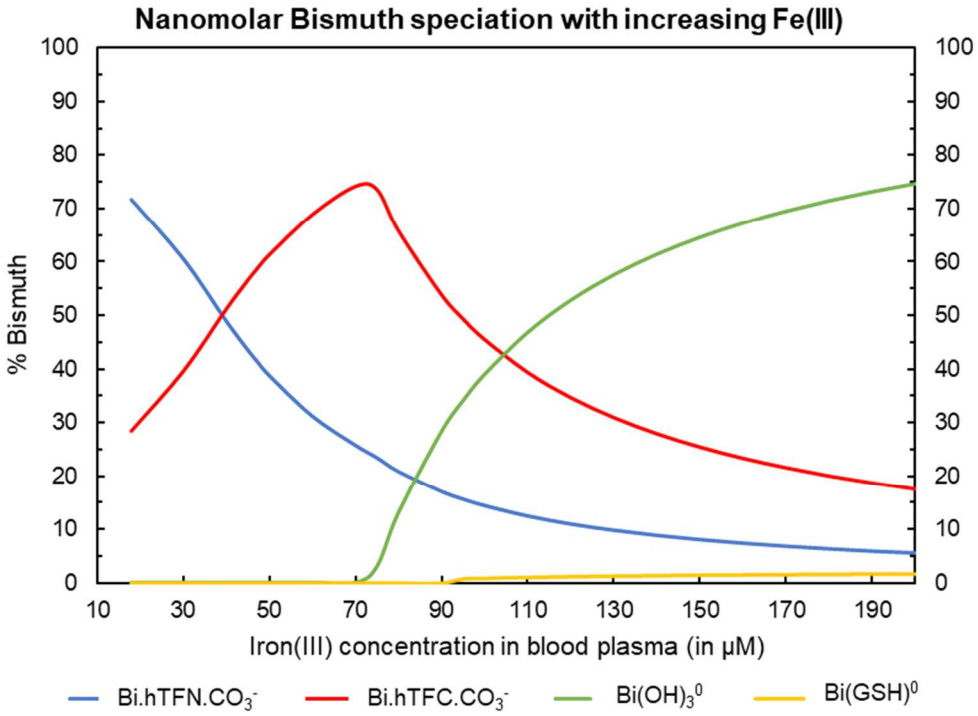

Fig 52(a-e). Speciation and bioavailability of bismuth in human bodily fluids.

dosage should help to maximize the beneficial effects while minimizing the toxic side-effects.

While the bioavailability of bismuth-based compounds has been discussed for many years, limited research exists on bismuth speciation in human bodily fluids (Bierer 1990, Tillman et al. 1996, Michalke et al. 2009). We found only one study in which the investigators demonstrated that transferrin controls bismuth speciation in blood plasma (Montavon et al. 2012). We found no results on bismuth speciation in cerebrospinal fluid (CSF) despite its direct implications to neurotoxicity and brain encephalopathy. In order to bridge this gap, we predicted bismuth speciation in the two bodily fluids and the endosome that transfers bismuth across the blood-brain barrier via receptor-mediated endocytosis. Implications on bismuth bioavailability and neurotoxicity are discussed below.

As six recent studies reported cases of bismuth-induced encephalopathy due to the intake of the commercially available form of bismuth subsalicylate (Reynolds et al. 2012, Masannat et al. 2013, Siram et al. 2017, Ali et al. 2017, Hogan et al. 2018, Borbinha et al. 2019), we performed speciation calculations reflecting increasing concentrations of this drug. Bismuth-transferrin stability constants were obtained by regressing stoichiometric constants reported by Li et al. (1996) in conjunction with subsequently measured transferrin pK_a values (Appendix). Since no measurements for bismuth-salicylate stability constants exist in the literature, these values were estimated using linear free energy relationships reported by Prasad & Shock (2019b) and Shock & Koretsky (1995). Stability constants for other metal-ligand complexes were obtained from compilation or

estimates reported in Prasad & Shock (2019b). It should be noted that for most ligands present in blood plasma, stability constants for bismuth complexes were estimated due to the scarcity of experimental measurements.

Predicted speciations of bismuth from nanomolar to millimolar concentration in blood and cerebrospinal fluid are shown in Fig. 52a and 62b, respectively. Comparison of these plots shows that bismuth speciation is completely different in the two bodily fluids- while transferrin dominates the speciation in blood, $Bi(OH)_3$ is the predominant form of bismuth in cerebrospinal fluid. A major contributing factor is the substantially lower concentration of transferrin in cerebrospinal fluid (~0.17 μM) compared to the corresponding concentration in blood (~ 37 μM). As neutral LMM complexes tend to pass through the lipid bilayer via passive diffusion (Levina et al. 2017), $Bi(OH)_3$ may be more readily bioavailable than other forms of bismuth. Recently, $Bi(OH)_3$ nanoparticles were found to possess high toxicity against malignant cancer cells (Bogusz et al. 2018). It is therefore likely that the corresponding aqueous form is also cytotoxic, which may also help explain the neurological dysfunction associated with this metal. We suggest that additional studies of the influence of $Bi(OH)_3$ are warranted.

As a considerable amount of bismuth is present in blood as the transferrin complex, it is likely to be transported to cells via receptor-mediated endocytosis (Guo et al. 2000, Zhang et al. 2001). As the endosomal pH ranges from 3.5 to 6.5 (Diering & Numata 2014, Hu et al. 2015), bismuth speciation is likely to be considerably different under these conditions than its speciation in blood plasma. Since the chemical composition of the endosome is currently unknown, we performed speciation calculations

with blood and CSF compositions over the known pH range of the endosome. The results are shown in Figs. 52c and 52d, which both illustrate differences in bismuth speciation as functions of pH. At low pH, oxalate complexes constitute a considerable fraction of bismuth in either the blood or the CFS models of the endosome. In the case of CSF, Bi-citrate complexes are also predicted to be relatively abundant at low pH as shown in Fig 52d. In both cases, transferrin complexes dominate the speciation at pH >5, and it is rivaled in abundance by $Bi(OH)_3$ at higher pH in the CSF model. These results are consistent with the reported release of metal (Fe^{+3} and Bi^{+3}) from transferrin at pH 4.5-2.0 (Guo et al. 2000, Zhang et al. 2001) and have direct implications for the bioavailability of bismuth.

In addition to transferrin concentration and pH, we found that bismuth speciation also depends strongly on iron(III) abundance. As iron(III)-transferrin stability constants are larger than the corresponding bismuth stability constants, iron spontaneously displaces transferrin-bound bismuth, thereby increasing the bismuth-LMM fraction. The calculated dependence of total plasma iron(III) concentration on bismuth speciation is shown in Fig. 52e. Note that the transferrin fraction of bismuth maximizes at 74 μM iron(III), which corresponds to the maximum metal-carrying capacity of transferrin. Exceeding this maximum is likely to transpire in cases of genetic iron-overload (hemochromatosis). At a total iron(III) concentration of 80 μM, the non-transferrin bound iron (NTBI) concentration amounts to ~6 μM (Fig. 52f), which is commonly seen in patients suffering from some form of iron-overload (Brissot et al. 2012). At this concentration, our calculations reveal that about 14% of bismuth exists as the neutral

LMM complex $Bi(OH)_3$, which may be bioavailable. Thus, iron-overload conditions may be associated with high bismuth cytotoxicity.

In summary, we find that bismuth speciation depends strongly on transferrin, proton and iron(III) abundance in the biological system of interest. Bismuth speciation is considerably different in blood compared to cerebrospinal fluid, which may help explain the associated neuropathy of the metal. Our calculations of bismuth speciation as a function of pH are consistent with experimental measurements performed in simpler systems. It may be worth reiterating that estimates of stability constants for bismuth complexes with oxalate and salicylate were crucial in obtaining these simulations. We hope these models can drive further investigation on the exciting field of bismuth-based drugs.

5.4.5 Rhodium-based anticancer drugs

Rhodium-based drugs have been of interest to the anticancer community for over six decades (Taylor & Carmichael 1953, Giraldi et al. 1977, Rao et al. 1980, Kopf-Maier 1994, Katsaros & Anagnostopoulou 2002, Junicke et al. 2003, Jungwirth et al. 2011, Domotor & Enyedy 2019). The predominant mode of action of rhodium and other platinum-group metals (like ruthenium, palladium, osmium and iridium) differs from that of gallium-based anticancer drugs. The platinum-based drugs appear to bend DNA by cross-linking adjacent guanines leading to adherence by DNA-binding proteins (Jamieson & Lippard 1999). Rhodium complexes have been found to interfere with oncogenic signaling and cancer-promoting or epigenetic regulatory processes (Leung et al. 2012, Kang et al. 2017). Most rhodium compounds eliciting anticancer activity are octahedral

complexes of polypyridine, polyquinoline and other aromatic chelates. Here we report rhodium speciation in blood plasma with two chelators- maltol and oxine that are known to increase metal bioavailability as discussed above. Additionally, we report rhodium speciation with the first rhodium complex known to have anti-tumor activity- $RhCl_3$ (Taylor & Carmichael 1953).

Perhaps the extremely high cost of rhodium over the last century (Zientek et al. 2017) has contributed to the limited thermodynamic data for rhodium complexes. In lieu of this, stability constants for rhodium complexes can be estimated to obtain rhodium speciation in any biological fluid system of interest. In this study, values were estimated using multiple linear free energy relationships for rhodium complexes of maltol and oxine, as well as the ligands listed in Table 1 including transferrin and albumin (MBS site) (Prasad & Shock 2019b). Additional stability constants for rhodium-chloride complexes were taken from Cozzi & Pantani (1958) while the solubility product of $Rh(OH)_3(s)$ was taken from Forrester & Ayres (1959).

Predicted changes in the speciation of rhodium in blood with increasing concentration of $RhCl_3$ is depicted in Fig. 53a. It can be seen that almost all of the rhodium is bound to the proteins transferrin and albumin. Transferrin dominates the speciation at low rhodium abundance as it has a higher stability constant but gets saturated at about 60 μM rhodium as its carrying capacity is reached. At this point, the albumin fraction of rhodium begins to increase with increasing total $RhCl_3$ concentration and dominates the speciation at ≥ 120 μM rhodium. Note that at ~70 μM rhodium, $Rh(OH)_3(s)$ reaches saturation.

(a)

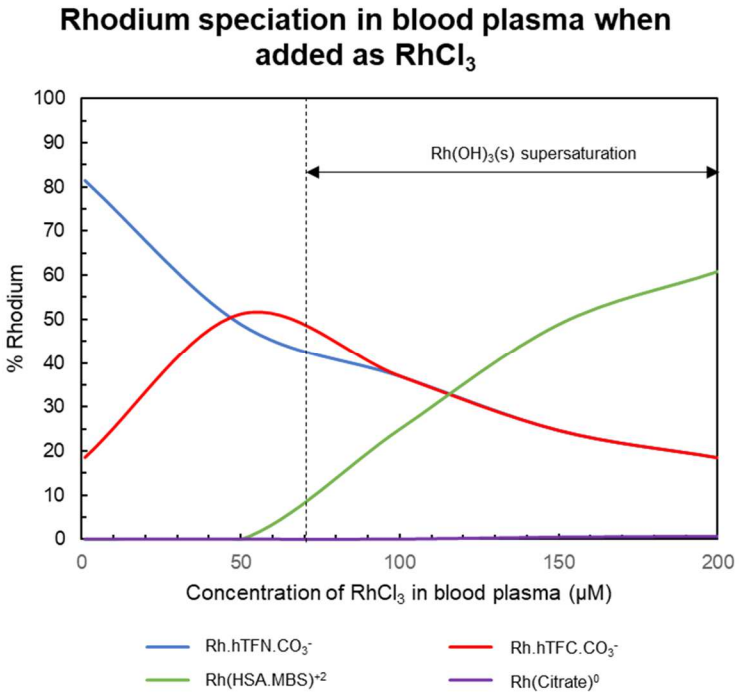

(b)

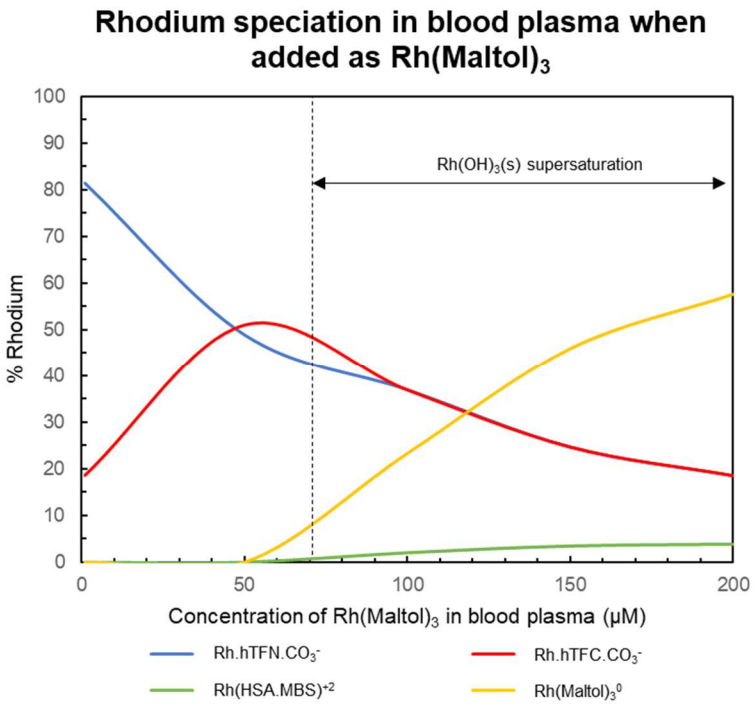

Fig 53(a-c). Rhodium speciation in blood plasma. (contd)

(c)

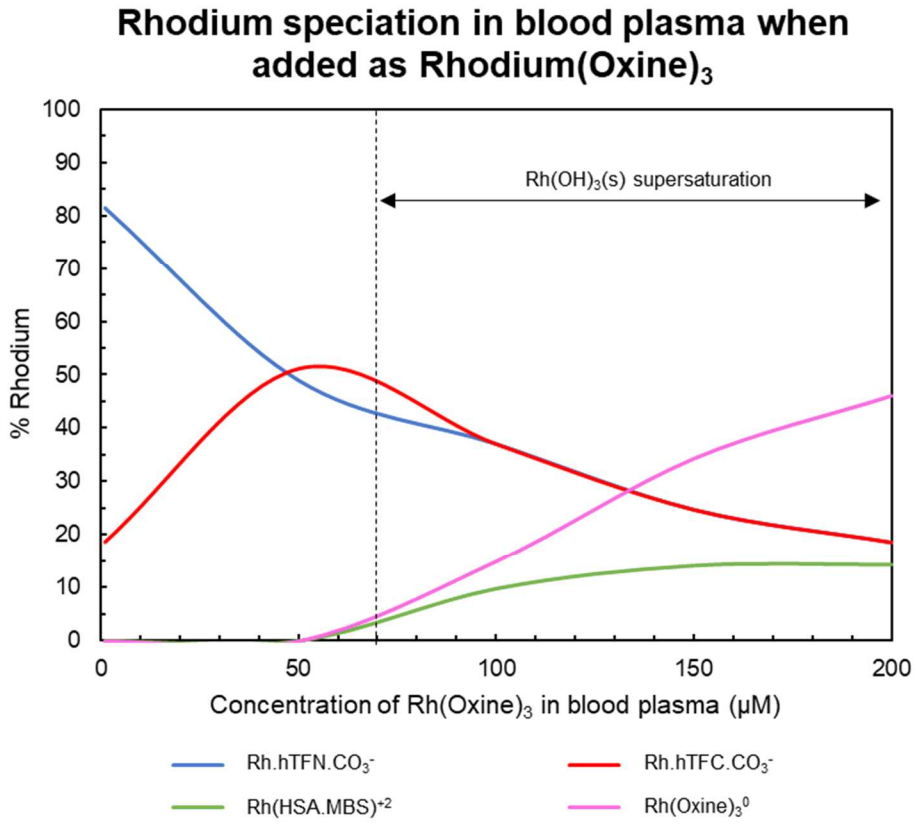

Fig 53(a-c). Rhodium speciation in blood plasma.

Similar calculations with $Rh(Maltol)_3$ and $Rh(Oxine)_3$ are displayed in Fig. 53b and 53c, respectively. While rhodium speciation is virtually identical in both cases up to ~50 μM rhodium, it differs considerably beyond this concentration. At 200 μM of total $Rh(Maltol)_3$, about 58% of the rhodium exists as $Rh(Maltol)_3^0$ while at the corresponding concentration of total $Rh(Oxine)_3$, ~45% of rhodium exists as $Rh(Oxine)_3^0$. However, at 100 μM, the distribution of rhodium as the corresponding tris complexes (1:3 metal-ligand complex) is about the same at ~20%, which corresponds to a considerable bioavailable fraction assuming no losses from precipitation.

We hope these results outline the practical utility of performing speciation calculations for medical applications involving expensive metals like rhodium. Similar calculations can prove to be useful for other organometallic forms of rhodium that are being used for pharmaceutical applications (Öhrström 2006, Domotor et al. 2014, Domotor & Enyedy 2019). As these are mixed-ligand complexes, the strategy for stability constant estimation is likely to differ from methods used in this study. We hope such theoretical endeavors are mutually assisted by progress in stability constant measurements and elucidation of rhodium-associated cytotoxic activity. As rhodium has several other applications including in catalytic converters of automobile exhaust and in the manufacture of nitric oxide that is the raw material for explosives, fertilizers, and nitric acid (Öhrström 2006 and Zientek et al. 2017), it is a relevant metal presently and is likely to stay pertinent in the near future (Jasinski et al. 2018).

5.5 Conclusion

Previously, a shortcoming of metal speciation modeling in biological systems was the limited number of relevant metal complexes, especially involving organic compounds (Kiss et al. 2017, Wilke et al. 2017). We ameliorated this problem by estimating stability constants of over 18,000 metal-organic complexes including proteins, peptides, amino acids, carboxylates and phenols (Prasad & Shock 2019a and Prasad & Shock 2019b). In this work, we used those estimates to conduct metal speciation calculations of 10 metals in blood plasma, a biological system integral to human health. As a foundation, we predicted the speciation of the seven predominant metals in blood. In addition, we calculated the speciation of gallium and rhodium based anticancer drugs, copper in Wilson Disease, zinc-based antidiabetics and bismuth-based antacids. A special emphasis was placed on the implications of our speciation calculations for the bioavailability of these metals and the associated therapeutic or toxic potential.

Our calculations reveal that proteins dominate the speciation of all metals and are therefore crucial for model construction of metal transport and distribution in the human body. Additionally, proteins have distinct functional groups that select for specific metals and mirror the selectivity seen for LMM ligands. Other predominant factors that significantly affect metal speciation are pH, chelator concentration and competition with other metal ions. In addition to blood plasma, we predicted metal speciation for cerebrospinal fluid and for associated vesicles at low pH.

A major part of our focus was to limit errors in speciation models, which allows us to identify areas where improvements can be made. Based on our assessment, care is warranted while determining stability constants for metal-protein complexes. Currently,

these values are obtained via competition experiments with LMM ligands like EDTA and NTA. Consequently, metal-protein log K values are extremely sensitive to the corresponding property associated with the metal complexes of these competitive ligands. Thus, accurate stability constants of these complexes, including all multi-ligand and protonated/hydroxylated forms, are needed to obtain accurate values of metal-protein log K. Additionally, several studies on metal-protein equilibria do not report and may not monitor the ionic strength of the system. Improvements for metal-LMM complexes can also be made, especially for mixed ligands of biological relevance like compounds associated with platinum-based anticancer compounds.

Besides the physiological conditions discussed in this paper, metals are involved in aging (Bredesen 2015), Alzheimer's Disease (Adlard & Bush 2018), manganese toxicity (Michalke et al. 2017), lead toxicity (Yedju et al. 2010) and lithium-based antidepressants (Cipriani et al. 2013). Additionally, metals like gadolinium, cobalt and technetium are used in diagnostic medical imaging as radioisotopes or contrast agents (Jackson & Byrne 1996 and McInnes et al. 2017). In this work, we have tried to bridge the gap between the biotic and abiotic aspects of metal speciation using the foundational theory of thermodynamics. We hope this work helps induce a more symbiotic association between the fields of metal-speciation modeling and metal-based pharmacology. We firmly believe that both fields not only have a lot to offer each other but each can drive innovation in its counterpart.

CHAPTER-6

CONCLUSION

As the laws of thermodynamics are some of the most fundamental laws of nature, they are utilized by scientists everyday to solve a multitude of problems. These laws have been incorporated in geochemical systems to study elemental distribution and transport for over five decades (Garrels et al. 1961 and Sillen 1967). These efforts were soon followed by application of thermodynamic models in simple microbiological systems (Sunda & Guillard 1976 and Morel et al. 1978). However, such attempts have been largely missing from the microbiology literature since, perhaps due to the higher chemical complexity of these systems. Analogous attempts in biological fluids like blood plasma have been made for over 40 years (May et al. 1976) but these models are mostly incomplete- either omitting proteins (May et al. 1976) or excluding low molecular mass ligands (Enyedy et al. 2015). We have tried to ameliorate these issues in the present work and have additionally addressed metal-dependent toxicity, anticancer activity and antidiabetic activity. Indeed, there is a lot more to be investigated on the subject of metal speciation and bioavailability in biological systems. These pointers have been explained in more detail in the individual chapters and are summarized subsequently.

While we have explained the slopes and intercepts of our linear free energy relationships on the basis of simple coordination chemistry concepts, perhaps more quantitative explanations may be given in the future. This would require a considerable amount of additional thermodynamic data from experiments for a spectrum of ligands orderly varying in their denticity, steric hindrance and nature of electron donating

functional groups. Theoretical calculations made using molecular dynamics simulations and density functional theory would indeed be useful in elucidating the intricacies of metal-ligand coordination. While this additional work may not be useful in systems composed of metal-ligand complexes with low stability constant values, it would certainly impact metal speciation calculations in systems composed of metal-ligand complexes with high values of stability constants. Additional emphasis should be given to metal chelators present in biological systems at high concentration like human serum albumin for which limited metal-binding equilibrium constants have been measured.

Further investigation in conducting metal-bioavailability experiments in conjunction with metal-speciation calculations is also encouraged. Given the low cost and precedent of metal-bioavailability work on bacteria and algae, perhaps these living systems can serve as test organisms to drive research on this topic. In the past 15 years, there has been a growing interest in investigating the 'metallome' of organisms, akin to genomes and proteomes (Haraguchi 2017). Intracellular metal-speciation research can prove to be extremely useful in this respect as they could provide the distribution of cells in enzymes, proteins, receptors, chemically labile molecules and other cellular compartments.

Thus, metal-speciation research is a research enterprise with enormous applications and with foundations in one of the most fundamental laws of nature. It therefore serves as a suitable candidate for future investment. We hope this dissertation helps to bridge the gap between the 'inanimate' world of metal-ligand coordination chemistry and the 'animate' world of cellular growth and toxicity.

REFERENCES

Aasa, R., Malmström, B. G., Saltman, P., & Vänngård, T. (1963). The specific binding of iron(III) and copper(II) to transferrin and conalbumin. *BBA - Biochimica et Biophysica Acta*, *75*(C), 203–222.

Adamson, A. W. (1954). A Proposed Approach to the Chelate Effect. *Journal of the American Chemical Society*, *76*(6), 1578–1579.

Adham, N. F., Song, M. K., & Rinderknecht, H. (1977). Binding of zinc to alpha-2-macroglobulin and its role in enzyme binding activity. *BBA - Protein Structure*, *495*(2), 212–219.

Adlard, P. A., & Bush, A. I. (2018). Metals and Alzheimer's Disease: How Far Have We Come in the Clinic? *Journal of Alzheimer's Disease, 62(3),* 1369-1379.

Adulcikas, J., Sonda, S., Norouzi, S., Sohal, S. S., & Myers, S. (2019, February 1). Targeting the zinc transporter ZIP7 in the treatment of insulin resistance and type 2 diabetes. *Nutrients*. MDPI AG.

Ahamed, M., Akhtar, M. J., Khan, M. A. M., Alrokayan, S. A., & Alhadlaq, H. A. (2019). Oxidative stress mediated cytotoxicity and apoptosis response of bismuth oxide (Bi2O3) nanoparticles in human breast cancer (MCF-7) cells. *Chemosphere*, 823–831.

Ahsanullah, M., & Florence, T. M. (1984). Toxicity of copper to the marine amphipod *Allorchestes compressa* in the presence of water-and lipid-soluble ligands. *Marine Biology*, *84*(1), 41–45.

Aisen, P., Leibman, A., & Zweier, J. (1978). Stoichiometric and site characteristics of the binding of iron to human transferrin. *Journal of Biological Chemistry*, *253*(6), 1930–1937.

Ali, F., Murray, J. A., Adams, A. C., & Flanagan, E. P. (2017, July 11). Clinical Reasoning: A 54-year-old woman with dementia, myoclonus, and ataxia. *Neurology*. Lippincott Williams and Wilkins, *89(2)*, e7-e12.

Amend, J. P., Rogers, K. L., Shock, E. L., Gurrieri, S., & Inguaggiato, S. (2003). Energetics of chemolithoautotrophy in the hydrothermal system of Vulcano Island, southern Italy. *Geobiology*, *1*(1), 37–58.

Anderson, D. M., & Morel, F. M. M. (1978). Copper sensitivity of Gonyaulax tamarensis. *Limnology and Oceanography*, *23*(2), 283–295.

Apostoli, P., Cornelis, R., Duffus, J., Hoet, P., Lison, D., & Templeton, D. (2006). Environmental Health Criteria 234 Elemental speciation in human health risk. *World Health Organization*, 1–238.

Atalay, Y. B., Di Toro, D. M., & Carbonaro, R. F. (2013). Estimation of stability constants for metal-ligand complexes containing neutral nitrogen donor atoms with applications to natural organic matter. *Geochimica et Cosmochimica Acta*, *122*, 464–477.

ATSDR. (2012). *Toxicological Profile for Manganese*. *Toxicological Profile* (pp. 1–556).

Bal, W., Sokołowska, M., Kurowska, E., & Faller, P. (2013). Binding of transition metal ions to albumin: Sites, affinities and rates. *Biochimica et Biophysica Acta - General Subjects*, *1830 (12)*, 5444-5455.

Borbinha, C., Serrazina, F., Salavisa, M., & Viana-Baptista, M. (2019). Bismuth encephalopathy- a rare complication of long-standing use of bismuth subsalicylate. *BMC Neurology*, *19*(1).

Başaran, B., Avşar, E., Göçmen, A., & Erim, F. B. (1994). The thermodynamics of benzoate complexes of copper(II) and iron(III) in aqueous solution. *Thermochimica Acta*, *247*(2), 407–413.

Berthon, G. (1995). The stability constants of metal complexes of amino acids with polar side chains. *Pure and Applied Chemistry*, *67*(7), 1117–1240.

Bierer, D. W. (1990). Bismuth subsalicylate: History, chemistry, and safety. *Reviews of Infectious Diseases*, *12*, S3–S8.

Bogusz, K., Tehei, M., Cardillo, D., Lerch, M., Rosenfeld, A., Dou, S. X., … Konstantinov, K. (2018). High toxicity of Bi(OH)3 and α-Bi2O3 nanoparticles towards malignant 9L and MCF-7 cells. *Materials Science and Engineering C*, *93*, 958–967.

Bosma, K. J., Syring, K. E., Oeser, J. K., Lee, J. D., Benninger, R. K. P., Pamenter, M. E., & O'Brien, R. M. (2019). Evidence that Evolution of the Diabetes Susceptibility Gene SLC30A8 that Encodes the Zinc Transporter ZnT8 Drives Variations in Pancreatic Islet Zinc Content in Multiple Species. *Journal of Molecular Evolution*. Springer New York LLC.

Boyett, J. D., & Sullivan, J. F. (1970). Distribution of protein-bound zinc in normal and cirrhotic serum. *Metabolism*, *19*(2), 148–157.

Bredesen, D. E. (2015). Metabolic profiling distinguishes three subtypes of Alzheimer's disease. *Aging*, *7*(8), 595–600.

Brewer, G. J. (2009). Drug development for orphan diseases in the context of personalized medicine. *Translational Research*. Mosby Inc, *154(6)*, 314-322.

Brissot, P., Ropert, M., Le Lan, C., & Loréal, O. (2012, March). Non-transferrin bound iron: A key role in iron overload and iron toxicity. *Biochimica et Biophysica Acta - General Subjects, 1820(3)*, 403-410.

Burns, R., Thomas, D. W., & Barron, V. J. (1974). Reversible encephalopathy possibly associated with bismuth subgallate ingestion. *British Medical Journal*, *1*(5901), 220–223.

Bytzek, A. K., Enyedy, É. A., Kiss, T., Keppler, B. K., & Hartinger, C. G. (2009). Biodistribution of anti-diabetic Zn(II) complexes in human serum and in vitro protein-binding studies by means of CZE-ICP-MS. In *Electrophoresis* (Vol. 30, pp. 4075–4082).

Campbell, P.G. (1995). Interaction between trace metals and aquatic organisms: a critique of the free-ion activity model. Tessier, André, (editor.) & Turner, D. R. (David R.), (editor.) *Metal speciation and bioavailability in aquatic systems*. J. Wiley, Chichester ; New York

Canterford, G. S., & Canterford, D. R. (1980). Toxicity of heavy metals to the marine diatom ditylum brightwellii (west) grunow: Correlation between toxicity and metal speciation. *Journal of the Marine Biological Association of the United Kingdom*, *60*(1), 227–242.

Cao, W., Qi, J., Qian, K., Tian, L., Cheng, Z., & Wang, Y. (2019). Structure−activity relationships of 2-quinolinecarboxaldehyde thiosemicarbazone gallium(III) complexes with potent and selective anticancer activity. *Journal of Inorganic Biochemistry*, *191*, 174–182.

Carbonaro, R. F., & Di Toro, D. M. (2007). Linear free energy relationships for metal-ligand complexation: Monodentate binding to negatively-charged oxygen donor atoms. *Geochimica et Cosmochimica Acta*, *71*(16), 3958–3968.

Carbonaro, R. F., Atalay, Y. B., & Di Toro, D. M. (2011). Linear free energy relationships for metal-ligand complexation: Bidentate binding to negatively-charged oxygen donor atoms. *Geochimica et Cosmochimica Acta*, *75*(9), 2499–2511.

Cengiz, N., Uslu, Y., Gök, F., & Anarat, A. (2005). Acute renal failure after overdose of colloidal bismuth subcitrate. *Pediatric Nephrology*, *20*(9), 1355–1358.

Chambers, T. K., Practical Lectures On The Management Of The Digestion In Disease (1857), The Lancet, *70 (1767),* 25-27.

Chan, S., Wang, R., Man, K., Nicholls, J., Li, H., Sun, H., & Chan, G. C. F. (2019). A Novel Synthetic Compound, Bismuth Zinc Citrate, Could Potentially Reduce Cisplatin-Induced Toxicity Without Compromising the Anticancer Effect Through Enhanced Expression of Antioxidant Protein. *Translational Oncology*, *12*(5), 788–799.

Charlwood, P. A. (1979). The relative affinity of transferrin and albumin for zinc. *BBA - Protein Structure*, *581*(2), 260–265.

Chen, D., Frezza, M., Shakya, R., Cui, Q. C., Milacic, V., Verani, C. N., & Dou, Q. P. (2007). Inhibition of the proteasome activity by gallium(III) complexes contributes to their anti-prostate tumor effects. *Cancer Research*, *67*(19), 9258–9265.

Cheng, Y., Chang, Y., Feng, Y., Jian, H., Tang, Z., & Zhang, H. (2018). Deep-Level Defect Enhanced Photothermal Performance of Bismuth Sulfide–Gold Heterojunction Nanorods for Photothermal Therapy of Cancer Guided by Computed Tomography Imaging. *Angewandte Chemie - International Edition*, *57*(1), 246–251.

Chitambar, C. R. (2017, January 1). The therapeutic potential of iron-targeting gallium compounds in human disease: From basic research to clinical application. *Pharmacological Research*. Academic Press, *115*, 56-64.

Chitambar, C. R., Al-Gizawiy, M. M., Alhajala, H. S., Pechman, K. R., Wereley, J. P., Wujek, R., … Schmainda, K. M. (2018). Gallium maltolate disrupts tumor iron metabolism and retards the growth of glioblastoma by inhibiting mitochondrial function and ribonucleotide reductase. *Molecular Cancer Therapeutics*, *17*(6), 1240–1250.

Chitambar, C. R., Purpi, D. P., Woodliff, J., Yang, M., & Wereley, J. P. (2007). Development of gallium compounds for treatment of lymphoma: Gallium maltolate, a novel hydroxypyrone gallium compound, induces apoptosis and circumvents lymphoma cell resistance to gallium nitrate. *Journal of Pharmacology and Experimental Therapeutics*, *322*(3), 1228–1236.

Chitambar, C. R., & Sax, D. (1992). Regulatory effects of gallium on transferrin-independent iron uptake by human leukemic HL60 cells. *Blood*, *80*(2), 505–511.

Choi, D. W., Zea, C. J., Do, Y. S., Semrau, J. D., Antholine, W. E., Hargrove, M. S., … DiSpirito, A. A. (2006). Spectral, kinetic, and thermodynamic properties of Cu(I) and Cu(II) binding by methanobactin from methylosinus trichosporium OB3b. *Biochemistry*, *45*(5), 1442–1453.

Chua, M. S., Bernstein, L. R., Li, R., & So, S. K. S. (2006). Gallium maltolate is a promising chemotherapeutic agent for the treatment of hepatocellular carcinoma. *Anticancer Research*, *26*(3 A), 1739–1743.

Chu, A., Foster, M., Hancock, D., Petocz, P., & Samman, S. (2017). Interrelationships among mediators of cellular zinc homeostasis in healthy and type 2 diabetes mellitus populations. *Molecular Nutrition and Food Research*, *61*(4).

Cipriani, A., Hawton, K., Stockton, S., & Geddes, J. R. (2013). Lithium in the prevention of suicide in mood disorders: Updated systematic review and meta-analysis. *BMJ (Online)*, *347*(7916).

Cobble, J. W. (1953a). Empirical considerations of entropy. I. The entropies of the oxy-anions and related species. *The Journal of Chemical Physics*, *21*(9), 1443–1445.

Cobble, J. W. (1953b). Empirical considerations of entropy. II. The entropies of inorganic complex ions. *The Journal of Chemical Physics*, *21*(9), 1446–1450.

Cozzi, D., & Pantani, F. (1958). The polarographic behaviour of rhodium(III) chlorocomplexes. *Journal of Inorganic and Nuclear Chemistry*, *8*(C), 385–398.

Czerwinski, A. W., & Ginn, H. E. (1964). Bismuth nephrotoxicity. *The American Journal of Medicine*, *37*(6), 969–975.

Daly, H. R., Campbell, I. C., & Hart, B. T. (1990). Copper toxicity to Paratya australiensis: I. Influence of nitrilotriacetic acid and glycine. *Environmental Toxicology and Chemistry*, *9*(8), 997–1006.

Davies, C. W. (1951). 280. The electrolytic dissociation of metal hydroxides. *Journal of the Chemical Society (Resumed)*, 1256–1258.

De Bie, P., Muller, P., Wijmenga, C., & Klomp, L. W. J. (2007, November). Molecular pathogenesis of Wilson and Menkes disease: Correlation of mutations with molecular defects and disease phenotypes. *Journal of Medical Genetics*, *44(11)*, 673-688.

Delangle, P., & Mintz, E. (2012, June 7). Chelation therapy in Wilson's disease: From d-penicillamine to the design of selective bioinspired intracellular Cu(i) chelators. *Dalton Transactions*, *41(21),* 6359- 6370.

Delile, H., Blichert-Toft, J., Goiran, J. P., Keay, S., & Albarède, F. (2014). Lead in ancient Rome's city waters. *Proceedings of the National Academy of Sciences of the United States of America*, *111*(18), 6594–6599.

Delile, H., Keenan-Jones, D., Blichert-Toft, J., Goiran, J. P., Arnaud-Godet, F., & Albarède, F. (2017). Rome's urban history inferred from Pb-contaminated waters trapped in its ancient harbor basins. *Proceedings of the National Academy of Sciences of the United States of America*, *114*(38), 10059–10064.

Dieleman, J. L., Baral, R., Birger, M., Bui, A. L., Bulchis, A., Chapin, A., … Murray, C. J. L. (2016). US spending on personal health care and public health, 1996-2013. *JAMA - Journal of the American Medical Association*, *316*(24), 2627–2646.

Diering, G. H., & Numata, M. (2014). Endosomal pH in neuronal signaling and synaptic transmission: Role of Na+/H+ exchanger NHE5. *Frontiers in Physiology*.

Dömötör, O., Aicher, S., Schmidlehner, M., Novak, M. S., Roller, A., Jakupec, M. A., … Enyedy, É. A. (2014). Antitumor pentamethylcyclopentadienyl rhodium complexes of maltol and allomaltol: Synthesis, solution speciation and bioactivity. *Journal of Inorganic Biochemistry*, *134*, 57–65.

Dömötör, O., & Enyedy, É. A. (2019). Binding mechanisms of half-sandwich Rh(III) and Ru(II) arene complexes on human serum albumin: a comparative study. *JBIC Journal of Biological Inorganic Chemistry*, *24*(5), 703–719.

DSMZ website, www.dsmz.de. Accessed 1 October, 2019.

Edwards, C. L., & Hayes, R. L. (1984). Tumor scanning with67Ga citrate. *Journal of Nuclear Medicine*, *25*(6), 724–726.

El Ghazouani, A., Baslé, A., Firbank, S. J., Knapp, C. W., Gray, J., Graham, D. W., & Dennison, C. (2011). Copper-binding properties and structures of methanobactins from methylosinus trichosporium OB3b. *Inorganic Chemistry*, *50*(4), 1378–1391.

Englinger, B., Pirker, C., Heffeter, P., Terenzi, A., Kowol, C. R., Keppler, B. K., & Berger, W. (2019, January 23). Metal drugs and the anticancer immune response. *Chemical Reviews*. American Chemical Society, *119(2)*, 1519-1624.

Enyedy, É. A., Dömötör, O., Bali, K., Hetényi, A., Tuccinardi, T., & Keppler, B. K. (2015). Interaction of the anticancer gallium(III) complexes of 8-hydroxyquinoline and maltol with human serum proteins. *Journal of Biological Inorganic Chemistry*, *20*(1), 77–88.

Enyedy, É. A., Dömötör, O., Varga, E., Kiss, T., Trondl, R., Hartinger, C. G., & Keppler, B. K. (2012). Comparative solution equilibrium studies of anticancer gallium(III) complexes of 8-hydroxyquinoline and hydroxy(thio)pyrone ligands. *Journal of Inorganic Biochemistry*, *117*, 189–197.

Enyedy, É. A., Lakatos, A., Horváth, L., & Kiss, T. (2008). Interactions of insulin-mimetic zinc(II) complexes with cell constituents: Glutathione and ATP. *Journal of Inorganic Biochemistry*, *102*(7), 1473–1485.

Falchuk, K. H., Mathews, J. M., & Doloff, C. (1977). Effect of Acute Disease and ACTH on Serum Zinc Proteins. *New England Journal of Medicine*, *296*(20), 1129–1134.

Fallone, C. A., Chiba, N., van Zanten, S. V., Fischbach, L., Gisbert, J. P., Hunt, R. H., … Marshall, J. K. (2016). The Toronto Consensus for the Treatment of Helicobacter pylori Infection in Adults. *Gastroenterology*, *151*(1), 51-69.e14.

Fernández-Cao, J. C., Warthon-Medina, M., Hall Moran, V., Arija, V., Doepking, C., & Lowe, N. M. (2018, September 1). Dietary zinc intake and whole blood zinc concentration in subjects with type 2 diabetes versus healthy subjects: A systematic review, meta-analysis and meta-regression. *Journal of Trace Elements in Medicine and Biology*. Elsevier GmbH.

Fernández-Cao, J. C., Warthon-Medina, M., Moran, V. H., Arija, V., Doepking, C., Serra-Majem, L., & Lowe, N. M. (2019, May 1). Zinc intake and status and risk of type 2 diabetes mellitus: A systematic review and meta-analysis. *Nutrients*. MDPI AG.

Finnegan, M. M., Rettig, S. J., & Orvig, C. (1986). A Neutral Water-Soluble Aluminum Complex of Neurological Interest. *Journal of the American Chemical Society*, *108*(16), 5033–5035.

Finnegan, M. M., Lutz, T. G., Nelson, W. O., Smith, A., & Orvig, C. (1987). Neutral Water-Soluble Post-Transition-Metal Chelate Complexes of Medical Interest: Aluminum and Gallium Tris(3-hydroxy-4-pyronates). *Inorganic Chemistry*, *26*(13), 2171–2176.

Fogh-Andersen, N. (1977). Albumin/calcium association at different pH, as determined by potentiometry. *Clinical Chemistry*, *23*(11), 2122–2126.

Foote, J. W., & Delves, H. T. (1984). Albumin bound and α2-macroglobulin bound zinc concentrations in the sera of healthy adults. *Journal of Clinical Pathology*, *37*(9), 1050–1054.

Foster, B. J., Clagett-Carr, K., Hoth, D., & Leyland-Jones, B. (1986). Gallium nitrate: The second metal with clinical activity. *Cancer Treatment Reports*, *70(11)*, 1311-1319.

Fresco, J., & Freiser, H. (1964). Solubilities of Certain Divalent Metal Complexes of 8-Quinolinol and Substituted 8-Quinolinols in Aqueous Media. *Analytical Chemistry*, *36*(2), 372–375.

Fukunaka, A., & Fujitani, Y. (2018, February 6). Role of zinc homeostasis in the pathogenesis of diabetes and obesity. *International Journal of Molecular Sciences*. MDPI AG.

Ghavipanjeh, F., Ziaei Rad, Z., & Pazouki, M. (2018). Devulcanization of Ground Tires by Different Strains of Bacteria: Optimization of Culture Condition by Taguchi Method. *Journal of Polymers and the Environment*, *26*(8), 3168–3175.

Giraldi, T., Sava, G., Bertoli, G., Mestroni, G., & Zassinovich, G. (1977). Antitumor Action of Two Rhodium and Ruthenium Complexes in Comparison with cis-Diamminedichloroplatinum(ll). *Cancer Research*, *37*, 2662–2666.

Gisbert, J. P. (2011). Helicobacter pylori eradication: A new, single-capsule bismuth-containing quadruple therapy. *Nature Reviews Gastroenterology and Hepatology*, *8*(6), 307–309.

Gitlin, J. D. (2003). Wilson Disease. *Gastroenterology*, *125*(6), 1868–1877.

Gordon, R. B., Bertram, M., & Graedel, T. E. (2006). Metal stocks and sustainability. *Proceedings of the National Academy of Sciences of the United States of America*, *103*(5), 1209–1214.

Gryboski, J. D., & Gotoff, S. P. (1961). Bismuth Nephrotoxicity. *New England Journal of Medicine*, *265*(26), 1289–1291.

Gu, L., Li, S., He, Y., Chen, Y., Jiang, Y., Peng, Y., … Yang, H. (2019). Bismuth, rabeprazole, amoxicillin, and doxycycline as first-line Helicobacter pylori therapy in clinical practice: A pilot study. *Helicobacter*, *24*(4).

Guo, M., Sun, H., McArdle, H. J., Gambling, L., & Sadler, P. J. (2000). Ti IV uptake and release by human serum transferrin and recognition of Ti IV-transferrin by cancer

cells: Understanding the mechanism of action of the anticancer drug titanocene dichloride. *Biochemistry*, *39*(33), 10023–10033.

Gupte, A., & Mumper, R. J. (2009, February). Elevated copper and oxidative stress in cancer cells as a target for cancer treatment. *Cancer Treatment Reviews*, *35(1)*, 32-46.

Haddad, M., Vali, H., Paquette, J., & Guiot, S. R. (2014). The role of Carboxydothermus hydrogenoformans in the conversion of calcium phosphate from amorphous to crystalline state. *PLoS ONE*, *9*(2).

Hancock, R. D. (1997). Approaches to predicting stability constants. A critical review. *Analyst*, *122*, (51R-58R)

Hancock, R. D., & Marsicano, F. (1976). The chelate effect: A simple quantitative approach. *Journal of the Chemical Society, Dalton Transactions*, (12), 1096–1098.

Hancock, R. D., & Marsicano, F. (1978). Parametric Correlation of Formation Constants in Aqueous Solution. 1. Ligands with Small Donor Atoms. *Inorganic Chemistry*, *17*(3), 560–564.

Hanna-Attisha, M., LaChance, J., Sadler, R. C., & Schnepp, A. C. (2016). Elevated blood lead levels in children associated with the flint drinking water crisis: A spatial analysis of risk and public health response. *American Journal of Public Health*, *106*(2), 283–290.

Harris, W. R. (2012, March). Anion binding properties of the transferrins. Implications for function. *Biochimica et Biophysica Acta - General Subjects, 1820(3),* 348-361.

Harris, W. R., & Pecoraro, V. L. (1983). Thermodynamic Binding Constants for Gallium Transferrin. *Biochemistry*, *22*(2), 292–299.

Harris, W. R., & Stenback, J. Z. (1988). The bicarbonate-dependence of zinc(II)-transferrin binding. *Journal of Inorganic Biochemistry*, *33*(3), 211–223.

Hart, M. M., & Adamson, R. H. (1971). Antitumor activity and toxicity of salts of inorganic group 3a metals: aluminum, gallium, indium, and thallium. *Proceedings of the National Academy of Sciences of the United States of America*, *68*(7), 1623–1626.

Hart, J. J., Tako, E., Kochian, L. V., & Glahn, R. P. (2015). Identification of Black Bean (Phaseolus vulgaris L.) Polyphenols That Inhibit and Promote Iron Uptake by Caco-2 Cells. *Journal of Agricultural and Food Chemistry*, *63*(25), 5950–5956.

Hawksworth, E. L., Andrews, P. C., Lie, W., Lai, B., & Dillon, C. T. (2014). Biological evaluation of bismuth non-steroidal anti-inflammatory drugs (BiNSAIDs): Stability, toxicity and uptake in HCT-8 colon cancer cells. *Journal of Inorganic Biochemistry*, *135*, 28–39.

Helgeson, H. C. (1969). Thermodynamics of hydrothermal systems at elevated temperatures and pressures. *American Journal of Science*, *267*(7), 729–804.

Hellman, N. E., & Gitlin, J. D. (2002). Ceruloplasmin Metabolism and Function. *Annual Review of Neuroscience*, *22*(1), 439–458.

Hinchey, R. J., & Cobble, J. W. (1970). Standard-State Entropies for the Aqueous Trivalent Lanthanide and Yttrium Ions1,2. *Inorganic Chemistry*, *9*(4), 917–921.

Hoffmann, T., & Gastreich, M. (2019, May 1). The next level in chemical space navigation: going far beyond enumerable compound libraries. *Drug Discovery Today*. Elsevier Ltd, *24(5)*, 1148-1156.

Hogan, D. B., Harbidge, C., & Duncan, A. (2018). Bismuth toxicity presenting as declining mobility and falls. *Canadian Geriatrics Journal*, *21*(4), 307–309.

Hu, Y. B., Dammer, E. B., Ren, R. J., & Wang, G. (2015, September 30). The endosomal-lysosomal system: From acidification and cargo sorting to neurodegeneration. *Translational Neurodegeneration*. BioMed Central Ltd.

Huster, D. (2018). Wilson disease. *Gastroenterologe*, *13*(3), 199–214.

Irving H & Rossotti, H. (1956). Some relationships among the stabilities of metal complexes. *Recueil Des Travaux Chimiques Des Pays□Bas*, *10*, 72–93.

Jackson, G. E., & Byrne, M. J. (1996). Metal ion speciation in blood plasma: Gallium-67-citrate and MRI contrast agents. *Journal of Nuclear Medicine*, *37*(2), 379–386.

Jamieson, E. R., & Lippard, S. J. (1999). Structure, recognition, and processing of cisplatin-DNA adducts. *Chemical Reviews*, *99*(9), 2467–2498.

Jasiński, D., Meredith, J., & Kirwan, K. (2018). The life cycle impact for platinum group metals and lithium to 2070 via surplus cost potential. *International Journal of Life Cycle Assessment*, *23*(4), 773–786.

Jonsdottir, B., Jönsson, I., & Lantz, M. (2019). Prevalence of diabetes and presence of autoantibodies against zinc transporter 8 and glutamic decarboxylase at diagnosis and at follow up of Graves' disease. *Endocrine*, *64*(1), 48–54.

Jungwirth, U., Kowol, C. R., Keppler, B. K., Hartinger, C. G., Berger, W., & Heffeter, P. (2011, August 15). Anticancer activity of metal complexes: Involvement of redox processes. *Antioxidants and Redox Signaling*.

Junicke, H., Hart, J. R., Kisko, J., Glebov, O., Kirsch, I. R., & Barton, J. K. (2003). A rhodium(III) complex for high-affinity DNA base-pair mismatch recognition. *Proceedings of the National Academy of Sciences of the United States of America*, *100*(7), 3737–3742.

Kang, T. S., Wang, W., Zhong, H. J., Liang, J. X., Ko, C. N., Lu, J. J., … Leung, C. H. (2017). A rhodium(III)-based inhibitor of autotaxin with antiproliferative activity. *Biochimica et Biophysica Acta - General Subjects*, *1861*(2), 256–263.

Katsaros, N., & Anagnostopoulou, A. (2002). Rhodium and its compounds as potential agents in cancer treatment. *Critical Reviews in Oncology/Hematology*.

Kenney, G. E., & Rosenzweig, A. C. (2013). Genome mining for methanobactins. *BMC Biology*, *11*.

Kiilerich, S., & Christiansen, C. (1986). Distribution of serum zinc between albumin and α2-macroglobulin in patients with different zinc metabolic disorders. *Clinica Chimica Acta*, *154*(1), 1–6.

Kim, Y. J., Eom, H. J., Seo, E. Y., Lee, D. Y., Kim, J. H., & Han, N. S. (2012). Development of a chemically defined minimal medium for the exponential growth of Leuconostoc mesenteroides ATCC8293. *Journal of Microbiology and Biotechnology*, *22*(11), 1518–1522.

Kiss, T., Jakusch, T., Gyurcsik, B., Lakatos, A., Enyedy, E. A., & Sija, E. (2012, January). Application of modeling calculations in the description of metal ion distribution of bioactive compounds in biological systems. *Coordination Chemistry Reviews*, *256(1-2)*, 125-132.

Kiss, T., Jakusch, T., Hollender, D., Enyedy, É. A., & Horváth, L. (2009). Comparative studies on the biospeciation of antidiabetic VO(IV) and Zn(II) complexes. *Journal of Inorganic Biochemistry*, *103*(4), 527–535.

Kiss, T., Enyedy, É. A., & Jakusch, T. (2017, December 1). Development of the application of speciation in chemistry. *Coordination Chemistry Reviews*. Elsevier B.V.

Knapp, C. W., Fowle, D. A., Kulczycki, E., Roberts, J. A., & Graham, D. W. (2007). Methane monooxygenase gene expression mediated by methanobactin in the

presence of mineral copper sources. *Proceedings of the National Academy of Sciences of the United States of America*, *104*(29), 12040–12045.

Köpf-Maier, P. (1994). Complexes of metals other than platinum as antitumour agents. *European Journal of Clinical Pharmacology*, *47*(1), 1–16.

Kragh-Hansen, U., & Vorum, H. (1993). Quantitative analyses of the interaction between calcium ions and human serum albumin. *Clinical Chemistry*, *39*(2), 202–208.

Kubal, G., Sadler, P. J., & Tucker, A. (1994). pH□induced structural changes in human serum apotransferrin pKa values of histidine residues and N□terminal amino group determined by 1H□NMR spectroscopy. *European Journal of Biochemistry*, *220*(3), 781–787.

Kumar, N., Ahlskog, J. E., & Gross, J. B. (2004). Acquired hypocupremia after gastric surgery. *Clinical Gastroenterology and Hepatology*, *2*(12), 1074–1079.

Laube, V. M., McKenzie, C. N., & Kushner, D. J. (1980). Strategies of response to copper, cadmium, and lead by a blue-green and a green alga. *Canadian Journal of Microbiology*, *26*(11), 1300–1311.

Lehninger, A. L., Nelson, D. L., & Cox, M. M. (2004). *Lehninger principles of biochemistry*. New York: Worth Publishers.

Lentner, C., & CIBA-GEIGY Limited. (1981). *Geigy scientific tables*. Basle, Switzerland: Ciba-Geigy.

Leonard, C., S., (1926). Studies in the pharmacology of bismuth salts ii. Toxicity and urinary elimination of soluble bismuth salts. *Journal of Pharmacology and Experimental Therapeutics, 28(1)*, 89-108.

Leung, C. H., Yang, H., Ma, V. P. Y., Chan, D. S. H., Zhong, H. J., Li, Y. W., … Ma, D. L. (2012). Inhibition of Janus kinase 2 by cyclometalated rhodium complexes. *MedChemComm*, *3*(6), 696–698.

Levina, A., Crans, D. C., & Lay, P. A. (2017, December 1). Speciation of metal drugs, supplements and toxins in media and bodily fluids controls in vitro activities. *Coordination Chemistry Reviews*. Elsevier B.V, *352*, 473-498.

Li, H., Sadler, P. J., & Sun, H. (1996). Unexpectedly strong binding of a large metal ion (Bi^{3+}) to human serum transferrin. *Journal of Biological Chemistry*, *271*(16), 9483–9489.

Lichtmannegger, J., Leitzinger, C., Wimmer, R., Schmitt, S., Schulz, S., Kabiri, Y., … Zischka, H. (2016). Methanobactin reverses acute liver failure in a rat model of Wilson disease. *Journal of Clinical Investigation*, *126*(7), 2721–2735.

Linder, M. C., & Hazegh-Azam, M. (1996, May). Copper biochemistry and molecular biology. *American Journal of Clinical Nutrition*.

Linn, F. H. H., Houwen, R. H. J., Van Hattum, J., Van Der Kleij, S., & Van Erpecum, K. J. (2009). Long-term exclusive zinc monotherapy in symptomatic Wilson disease: Experience in 17 patients. *Hepatology*, *50*(5), 1442–1452.

Liu, Y., Shen, C., Zhang, X., Yu, H., Wang, F., Wang, Y., & Zhang, L. W. (2018, March 1). Exposure and nephrotoxicity concern of bismuth with the occurrence of autophagy. *Toxicology and Industrial Health*. SAGE Publications Ltd.

Lu, J., Stewart, A. J., Sleep, D., Sadler, P. J., Pinheiro, T. J. T., & Blindauer, C. A. (2012). A molecular mechanism for modulating plasma Zn speciation by fatty acids. *Journal of the American Chemical Society*, *134*(3), 1454–1457.

Margalioth, E. J., Schenker, J. G., & Chevion, M. (1983). Copper and Zinc levels in normal and malignant tissues. *Cancer*, *52*(5), 868–872.

Martell, A. E., & Smith, R. M. (1974). *Critical stability constants: Volume 1*. New York: Plenum Press.

Martell, A. E., & Smith, R. M. (1977). *Critical stability constants: Other organic ligands*.

Martell, A. E., Hancock, R. D., Martell, A. E., & Hancock, R. D. (1996). Chelating Ligands. In *Metal Complexes in Aqueous Solutions*. Springer US.

Martin-Bouyer, G., Foulon, G., Guerbois, H., & Barin, C. (1981). Epidemiological study of encephalopathies following bismuth administration per os. Characteristics of intoxicated subjects: Comparison with a control group. *Clinical Toxicology*, *18*(11), 1277–1283.

Masannat, Y., & Nazer, E. (2013). Pepto bismuth associated neurotoxicity: A rare side effect of a commonly used medication. *The West Virginia Medical Journal*, *109*(3), 32–34.

Masten, S. J., Davies, S. H., & McElmurry, S. P. (2016). Flint water crisis: What happened and why? *Journal - American Water Works Association*, *108*(12), 22–34.

May, P. M., Linder, P. W., & Williams, D. R. (1976). Ambivalent effect of protein binding on computed distributions of metal ions complexed by ligands in blood plasma. *Experientia*, *32*(12), 1492–1494.

May, P. M., Linder, P. W., & Williams, D. R. (1977). Computer simulation of metal-ion equilibria in biofluids: Models for the low-molecular-weight complex distribution of calcium(II), magnesium(II), manganese(II), iron(III), copper(II), zinc(II), and lead(II) ions in human blood plasma. *Journal of the Chemical Society, Dalton Transactions*, (6), 588–595.

McInnes, L. E., Rudd, S. E., & Donnelly, P. S. (2017, December 1). Copper, gallium and zirconium positron emission tomography imaging agents: The importance of metal ion speciation. *Coordination Chemistry Reviews*. Elsevier B.V, *352*, 499-516.

Mclean, F. C., & Hastings, A. B. (1935). Clinical estimation and significance of calcium-ion concentrations in the blood. *The American Journal Of The Medical Sciences*, *189*(5), 21–612.

Merli, D., Profumo, A., Bloise, N., Risi, G., Momentè, S., Cucca, L., & Visai, L. (2018). Indium/Gallium Maltolate Effects on Human Breast Carcinoma Cells: In Vitro Investigation on Cytotoxicity and Synergism with Mitoxantrone. *ACS Omega*, *3*(4), 4631–4640.

Michalke, B. (2016, September 1). Review about the manganese speciation project related to neurodegeneration: An analytical chemistry approach to increase the knowledge about manganese related parkinsonian symptoms. *Journal of Trace Elements in Medicine and Biology* , *37*, 50–61.

Michalke, B., Halbach, S., & Nischwitz, V. (2009). JEM Spotlight: Metal speciation related to neurotoxicity in humans. *Journal of Environmental Monitoring, 11(5)*, 939-954.

Montavon, G., Le Du, A., Champion, J., Rabung, T., & Morgenstern, A. (2012). DTPA complexation of bismuth in human blood serum. *Dalton Transactions*, *41*(28), 8615–8623.

Morel, F. M. M., Rueter, J. G., Anderson, D. M., & Guillard, R. R. L. (1979). AQUIL: A chemically defined phytoplankton culture medium for trace metal studies. *Journal of Phycology*, *15*(2), 135–141.

Morrow AW. (1979) Request for reports: adverse reactions with bismuth subgallate. *Medical Journal of Australia, 1(18),* 912-912.

Morton, J. D., Hayes, K. F., & Semrau, J. D. (2000). Effect of copper speciation on whole-cell soluble methane monooxygenase activity in Methylosinus trichosporium OB3B. *Applied and Environmental Microbiology*, *66*(4), 1730–1733.

Murakami, K., Ishida, K., Watakabe, K., Tsubouchi, R., Naruse, M., & Yoshino, M. (2006). Maltol/iron-mediated apoptosis in HL60 cells: Participation of reactive oxygen species. *Toxicology Letters*, *161*(2), 102–107.

Nakai, M., Watanabe, H., Fujiwara, C., Sakurai, H., Kakegawa, H., Satoh, T., … Matsushita, R. (1995). Mechanism On Insulin-Like Action of Vanadyl Sulfate: Studies On Interaction Between Rat Adipocytes and Vanadium Compounds. *Biological and Pharmaceutical Bulletin*, *18*(5), 719–725.

Nancollas, G. H. (1956). Thermodynamics of ion association. Part II.Alkaline earth acetates and formates. *Journal of the Chemical Society (Resumed)*, 735–743.

Näsänen, R., Penttinen, U., Tiselius, A., Plíva, J., Sörensen, J. S., & Sörensen, N. A. (1952). Potentiometric and Spectrophotometric Studies on 8-Quinolinol and Its Derivatives. IV. 8-Quinolinol Chelates of Cadmium, Zinc and Copper in Aqueous Solutions. *Acta Chemica Scandinavica*, *6*, 837–843.

Nday, C. M., Malollari, G., Petanidis, S., & Salifoglou, A. (2012). In vitro neurotoxic Fe(III) and Fe(III)-chelator activities in rat hippocampal cultures. from neurotoxicity to neuroprotection prospects. In *Journal of Inorganic Biochemistry* (Vol. 117, pp. 342–350).

Nevin, R. (2000). How lead exposure relates to temporal changes in IQ, violent crime, and unwed pregnancy. *Environmental Research*, *83*(1), 1–22.

Ng, R. (2015). *Drugs: From discovery to approval*.

Öhrström, L. (2016, January 1). Rhodium roles. *Nature Chemistry*. Nature Publishing Group.

Ohyoshi, E., Hamada, Y., Nakata, K., & Kohata, S. (1999). The interaction between human and bovine serum albumin and zinc studied by a competitive spectrophotometry. *Journal of Inorganic Biochemistry*, *75*(3), 213–218.

Parkhurst, David L., (2013). Description of input and examples for PHREEQC version 3--a computer program for speciation, batch-reaction, one-dimensional transport, and inverse geochemical calculations. *Reston, Virginia :U.S. Department of the Interior, U.S. Geological Survey*.

Pärt, P., & Wikmark, G. (1984). The influence of some complexing agents (EDTA and citrate) on the uptake of cadmium in perfused rainbow trout gills. *Aquatic Toxicology*, *5*(4), 277–289.

Patel, K. A., Weedon, M. N., Shields, B. M., Pearson, E. R., Hattersley, A. T., & McDonald, T. J. (2019, February 1). Zinc transporter 8 autoantibodies (ZnT8A) and a type 1 diabetes genetic risk score can exclude individuals with type 1 diabetes from inappropriate genetic testing for monogenic diabetes. *Diabetes Care*. American Diabetes Association Inc., *42(2)*, E16-E17.

Patil, M., Sheth, K. A., Krishnamurthy, A. C., & Devarbhavi, H. (2013, December). A review and current perspective on wilson disease. *Journal of Clinical and Experimental Hepatology*, *3(4),* 321-336.

Paul, L. E. H., Therrien, B., & Furrer, J. (2012). Interaction of a ruthenium hexacationic prism with amino acids and biological ligands: ESI mass spectrometry and NMR characterisation of the reaction products. In *Journal of Biological Inorganic Chemistry* (Vol. 17, pp. 1053–1062).

Pearson, R. G. (1963). Hard and Soft Acids and Bases. *Journal of the American Chemical Society*, *85*(22), 3533–3539.

Pedersen, K. O. (1971). Binding of calcium to serum albumin I. Stoichiometry and intrinsic association constant at physiological ph, ionic strength, and temperature. *Scandinavian Journal of Clinical and Laboratory Investigation*, *28*(4), 459–469.

Peng, Y., Yadava, P., Heikkinen, A. T., Parrott, N., & Railkar, A. (2014). Applications of a 7-day Caco-2 cell model in drug discovery and development. *European Journal of Pharmaceutical Sciences*, *56*(1), 120–130.

Pereira, D. I. A., Bruggraber, S. F. A., Faria, N., Poots, L. K., Tagmount, M. A., Aslam, M. F., … Powell, J. J. (2014). Nanoparticulate iron(III) oxo-hydroxide delivers safe iron that is well absorbed and utilised in humans. *Nanomedicine: Nanotechnology, Biology, and Medicine*, *10*(8), 1877–1886.

Pérez, A., Rojas, P., Carrasco, F., Basfi-fer, K., Pérez-Bravo, F., Codoceo, J., … Ruz, M. (2018). Zinc Supplementation Does Not Affect Glucagon Response to Intravenous Glucose and Insulin Infusion in Patients with Well-Controlled Type 2 Diabetes. *Biological Trace Element Research*, *185*(2), 255–261.

Pesch, M. L., Christl, I., Hoffmann, M., Kraemer, S. M., & Kretzschmar, R. (2012). Copper complexation of methanobactin isolated from Methylosinus trichosporium

OB3b: PH-dependent speciation and modeling. *Journal of Inorganic Biochemistry*, *116*, 55–62.

Peters, T. (1996). *All about albumin: Biochemistry, genetics, and medical applications*. San Diego: Academic Press.

Pettit, L. D. (1984). International union of pure and applied chemistry:Analytical chemistry division commission on equilibrium data critical evaluation of equilibrium constants in solution part a: Stability constants of metal complexes critical survey of formation constants of complexes of histidine, phenylalanine, tyrosine, l-dopa and tryptophan. *Pure and Applied Chemistry*, *56*(2), 247–292.

Poldoski, J. E. (1979). Cadmium Bioaccumuiation Assays. Their Relationship to Various Ionic Equilibria in Lake Superior Water. *Environmental Science and Technology*, *13*(6), 701–706.

Prapaipong, P., Shock, E. L., & Koretsky, C. M. (1999). Metal-organic complexes in geochemical processes: Temperature dependence of the standard thermodynamic properties of aqueous complexes between metal cations and dicarboxylate ligands. *Geochimica et Cosmochimica Acta*, *63*(17), 2547–2577.

Prapaipong, P., & Shock, E. L. (2001). Estimation of standard-state entropies of association for aqueous metal-organic complexes and chelates at 25°C and 1 bar. *Geochimica et Cosmochimica Acta*, *65*(21), 3931–3953.

Prasad, A, & Shock, E.L.. (2019a) Metal-ligand thermodynamics in the biosphere-estimating stability constants and entropies for reactions between aqueous metal ions and monovalent oxygen-bearing ligands (in preparation).

Prasad, A, & Shock, E.L.. (2019b) Estimating stability constant and entropy for metal-ligand association in blood plasma and microbial growth media (in preparation).

Prasad, A, & Shock, E.L.. (2019c) Metal speciation and bioavailability in microbial growth media (in preparation).

Prasad, A, & Shock, E.L.. (2019d) Metal speciation in blood plasma (in preparation).

Prodan, C. I., Bottomley, S. S., Vincent, A. S., Cowan, L. D., Holland, N. R., & Lind, S. E. (2007). Hypocupremia associated with prior vitamin B 12 deficiency. *American Journal of Hematology*, *82*(4), 288–290.

Prohaska, J. R. (2008). Role of copper transporters in copper homeostasis. In *American Journal of Clinical Nutrition* (Vol. 88).

Rao, P. N., Smith, M. L., Pathak, S., Howard, R. A., & Bear, J. L. (1980). Rhodium (II) butyrate: A potential anticancer drug with cell cycle phase-specific effects in hela cells. *Journal of the National Cancer Institute*, *64*(4), 905–912.

Reffitt, D. M., Burden, T. J., Seed, P. T., Wood, J., Thompson, R. P. H., & Powell, J. J. (2000). Assessment of iron absorption from ferric trimaltol. *Annals of Clinical Biochemistry*, *37*(4), 457–466.

Reynolds, P. T., Abalos, K. C., Hopp, J., & Williams, M. E. (2012). Bismuth Toxicity: A Rare Cause of Neurologic Dysfunction. *International Journal of Clinical Medicine*, *03*(01), 46–48.

Rossotti, H. & Irving H (1956). Some relationships among the stabilities of metal complexes. *Recueil Des Travaux Chimiques Des Pays□Bas*, *75*(7), 763–768.

Sakurai, H., Kojima, Y., Yoshikawa, Y., Kawabe, K., & Yasui, H. (2002). Antidiabetic vanadium(IV) and zinc(II) complexes. In *Coordination Chemistry Reviews* (Vol. 226, pp. 187–198).

Sathekge, M., Knoesen, O., Meckel, M., Modiselle, M., Vorster, M., & Marx, S. (2017). 213Bi-PSMA-617 targeted alpha-radionuclide therapy in metastatic castration-resistant prostate cancer. *European Journal of Nuclear Medicine and Molecular Imaging*, *44*(6), 1099–1100.

Scheers, N. M., Almgren, A. B., & Sandberg, A. S. (2014). Proposing a Caco-2/HepG2 cell model for in vitro iron absorption studies. *Journal of Nutritional Biochemistry*, *25*(7), 710–715.

Scheinberg, I. H., & Gitlin, D. (1952). Deficiency of ceruloplasmin in patients with hepatolenticular degeneration (Wilson's disease). *Science*, *116*(3018), 484–485.

Schuhmacher, J., Kaul, S., Klivényi, G., Junkermann, H., Magener, A., Henze, M., … Bastert, G. (2001). Immunoscintigraphy with positron emission tomography: Gallium-68 chelate imaging of breast cancer pretargeted with bispecific anti-MUC1/anti-Ga chelate antibodies. *Cancer Research*, *61*(9), 3712–3717.

Schwarzenbach, R. P., Gschwend, P. M., & Imboden, D. M. (2003). *Environmental organic chemistry*. New York: Wiley.

Semrau, J. D., Dispirito, A. A., & Yoon, S. (2010). Methanotrophs and copper. *FEMS Microbiology Reviews*. Blackwell Publishing Ltd, *34(4)*, 496-531.

Sheldon, R. A. (2018, January 2). Metrics of Green Chemistry and Sustainability: Past, Present, and Future. *ACS Sustainable Chemistry and Engineering*. American Chemical Society, *6*, 32-48.

Sheldon, R. A., & Woodley, J. M. (2018, January 24). Role of Biocatalysis in Sustainable Chemistry. *Chemical Reviews*. American Chemical Society, *118*, 801-838.

Shock, E. L. (1998) Co-transport of metals and organic compounds in geochemical, biochemical and environmental processes. In: (Marini, L. and Ottonello, G., eds), *Proceedings of the Rome Seminar on Environmental Geochemistry*, Pacini Editore, 73-102

Shock, E. L., Sassani, D. C., Willis, M., & Sverjensky, D. A. (1997). Inorganic species in geologic fluids: Correlations among standard molal thermodynamic properties of aqueous ions and hydroxide complexes. *Geochimica et Cosmochimica Acta*, *61*(5), 907–950.

Shock, E.L., & Canovas, P. (2011). The Potential for Abiotic Organic Synthesis and Biosynthesis at Seafloor Hydrothermal Systems. In *Frontiers in Geofluids* (pp. 161–192). Wiley-Blackwell.

Shock, E. L., & Koretsky, C. M. (1993). Metal-organic complexes in geochemical processes: Calculation of standard partial molal thermodynamic properties of aqueous acetate complexes at high pressures and temperatures. *Geochimica et Cosmochimica Acta*, *57*(20), 4899–4922.

Shock, E. L., & Koretsky, C. M. (1995). Metal-organic complexes in geochemical processes: Estimation of standard partial molal thermodynamic properties of aqueous complexes between metal cations and monovalent organic acid ligands at high pressures and temperatures. *Geochimica et Cosmochimica Acta*, *59*(8), 1497–1532.

Sierra, J., Roig, N., Giménez Papiol, G., Pérez-Gallego, E., & Schuhmacher, M. (2017). Prediction of the bioavailability of potentially toxic elements in freshwaters. Comparison between speciation models and passive samplers. *Science of the Total Environment*, *605–606*, 211–218.

Siram, R., Botta, R., Kashikunte, C., Pal, P. K., & Yadav, R. (2017, January 1). Chronic encephalopathy with ataxia, myoclonus, and auditory neuropathy: A case of bismuth poisoning. *Neurology India*. Medknow Publications.

Smith, R. M., & Martell, A. E. (1975). *Critical Stability Constants: Volume 2: Amines*. Boston, MA: Springer US.

Smith, R. M., & Martell, A. E. (1976). *Critical stability constants: Volume 4*. New York: Plenum Press.

Smith, R. M., & Martell, A. E. (1982). *Critical stability constants. Volume 5. First supplement*. New York, N.Y: Plenum.

Smith, R. M., & Martell, A. E. (1989). *Critical stability constants: Volume 6*. New York: Plenum Press.

Sobczak, A. I. S., Stefanowicz, F., Pitt, S. J., Ajjan, R. A., & Stewart, A. J. (2019). Total plasma magnesium, zinc, copper and selenium concentrations in type-I and type-II diabetes. *BioMetals*, *32*(1), 123–138.

Stallmach, A., & Büning, C. (2015). Ferric maltol (ST10): A novel oral iron supplement for the treatment of iron deficiency anemia in inflammatory bowel disease. *Expert Opinion on Pharmacotherapy*, *16*(18), 2859–2867.

Summer, K. H., Lichtmannegger, J., Bandow, N., Choi, D. W., DiSpirito, A. A., & Michalke, B. (2011). The biogenic methanobactin is an effective chelator for copper in a rat model for Wilson disease. *Journal of Trace Elements in Medicine and Biology*, *25*(1), 36–41.

Sun, H., Cox, M. C., Li, H., & Sadler, P. J. (1997). Rationalisation of metal binding to transferrin: Prediction of metal-protein stability constants (pp. 71–102).

Sun, H., Li, H., Mason, A. B., Woodworth, R. C., & Sadler, P. J. (2001). Competitive Binding of Bismuth to Transferrin and Albumin in Aqueous Solution and in Blood Plasma. *Journal of Biological Chemistry*, *276*(12), 8829–8835.

Sun, X., Sun, H., Ge, R., Richter, M., Woodworth, R. C., Mason, A. B., & He, Q. Y. (2004). The low pKa value of iron-binding ligand Tyr188 and its implication in iron release and anion binding of human transferrin. *FEBS Letters*, *573*(1–3), 181–185.

Sunda, W. G., Engel, D. W., & Thuotte, R. M. (1978). Effect of Chemical Speciation on Toxicity of Cadmium to Grass Shrimp, Palaemonetes pugio: Importance of Free Cadmium Ion. *Environmental Science and Technology*, *12*(4), 409–413.

Sunda, W. G., & Ferguson, R. L. (1983). Sensitivity of natural bacterial communities to additions of copper and to cupric ion activity: a bioassay of copper complexation in seawater. In *NATO Conference Series, (Series) 4: Marine Sciences* (Vol. 9, pp. 871–891). Plenum Press.

Sunda, W. G., & Gillespie, P. A. (1979). The response of a marine bacterium to cupric ion and its use to estimate cupric ion activity in seawater. *J. Mar. Res.*, *37*(4), 761–777.

Sunda, W., & Guillard R. R. L. (1976). The relationship between cupric ion activity and the toxicity of copper to phytoplankton. *Journal of Marine Research, 34,* 511-529.

Sunda, W. G., & Huntsman, S. A. (1986). Relationships among growth rate, cellular manganese concentrations and manganese transport kinetics in estuarine and oceanic species of the diatom thalassiodira. *Journal of Phycology*, *22*(3), 259–270.

Sunda, W. G., & Huntsman, S. A. (1992). Feedback interactions between zinc and phytoplankton in seawater. *Limnology and Oceanography*, *37*(1), 25–40.

Sunda, W. G., & Huntsman, S. A. (2000). Effect of Zn, Mn, and Fe on Cd accumulation in phytoplankton: Implications for oceanic Cd cycling. *Limnology and Oceanography*, *45*(7), 1501–1516.

Sunderman, F. W., Dingle, B., Hopfer, S. M., & Swift, T. (1988). Acute nickel toxicity in electroplating workers who accidently ingested a solution of nickel sulfate and nickel chloride. *American Journal of Industrial Medicine*, *14*(3), 257–266.

Sverjensky, D. A., Shock, E. L., & Helgeson, H. C. (1997). Prediction of the thermodynamic properties of aqueous metal complexes to 1000°C and 5 kb. *Geochimica et Cosmochimica Acta*, *61*(7), 1359–1412.

Tansel, B. (2017). From electronic consumer products to e-wastes: Global outlook, waste quantities, recycling challenges. *Environment International*. Elsevier Ltd. *98*, 35-45.

Taylor, A., & Carmichael, Nell. (1953). The effect of metallic chlorides on the growth of tumor and nontumor tissue. *Univ. Texas Publ.*, *No. 5314*(Biochem. Inst. Studies 5, Cancer Studies 2), 36–79.

Templeton, D. M. (2015, April 28). Speciation in metal toxicity and metal-based therapeutics. *Toxics*. MDPI AG.

Temraz, S., Santini, V., Musallam, K., & Taher, A. (2014). Iron overload and chelation therapy in myelodysplastic syndromes. *Critical Reviews in Oncology/Hematology*. Elsevier Ireland Ltd, *91(1)*, 64-73.

Tillman, L. A., Drake, F. M., Dixon, J. S., & Wood, J. R. (1996). Safety of bismuth in the treatment of gastrointestinal diseases. *Alimentary Pharmacology and Therapeutics*. Blackwell Publishing Ltd, *10(4)*, 459-467.

Tipping, E. (2002). *Cation Binding by Humic Substances* (Cambridge Environmental Chemistry Series). Cambridge: Cambridge University Press.

Unsworth, E. R., Warnken, K. W., Zhang, H., Davison, W., Black, F., Buffle, J., … Xue, H. (2006). Model predictions of metal speciation in freshwaters compared to measurements by in situ techniques. *Environmental Science and Technology*, *40*(6), 1942–1949.

Valcour, A. A., & Woodworth, R. C. (1987). Proton Nuclear Magnetic Resonance Spectroscopy of Human Transferrin N-Terminal Half-Molecule: Titration and Hydrogen-Deuterium Exchange. *Biochemistry*, *26*(11), 3120–3125.

Vallee, B. L., & Falchuk, K. H. (1993). The biochemical basis of zinc physiology. *Physiological Reviews*, *73(1)*, 79-118.

Van Uitert, L. G., Fernelius, W. C., & Douglas, B. E. (1953). Studies on Coordination Compounds. V. A Comparison of the Chelating Tendencies of β -Diketones toward Divalent Metals. *Journal of the American Chemical Society*, *75*(11), 2739–2741.

Van't Hoff, M J H. (1884) Etudes De Dynamique Chimique. *Recueil Des Travaux Chimiques Des Pays-Bas.* 3.10, 333-36.

Vorum, H., Fisker, K., Otagiri, M., Pedersen, A. O., & Kragh-Hansen, U. (1995). Calcium ion binding to clinically relevant chemical modifications of human serum albumin. *Clinical Chemistry*, *41*(11), 1654–1661.

Wang, R., Lai, T. P., Gao, P., Zhang, H., Ho, P. L., Woo, P. C. Y., … Sun, H. (2018). Bismuth antimicrobial drugs serve as broad-spectrum metallo-β-lactamase inhibitors. *Nature Communications*, *9*(1).

Wang, X., Wu, W., Zheng, W., Fang, X., Chen, L., Rink, L., … Wang, F. (2019). Zinc supplementation improves glycemic control for diabetes prevention and management: a systematic review and meta-analysis of randomized controlled trials. *American Journal of Clinical Nutrition*, *110*(1), 76–90.

Werner, A., Gubser A. (1901). On the hydrates of chromium chloride. *Berichte der deutschen chemischen Gesellschaft, 34*, 1579-1604.

Wilke, C., Barkleit, A., Stumpf, T., & Ikeda-Ohno, A. (2017). Speciation of the trivalent f-elements Eu(III) and Cm(III) in digestive media. *Journal of Inorganic Biochemistry*, *175*, 248–258.

Willey, L. M., Kharaka, Y. K., Presser, T. S., Rapp, J. B., & Barnes, I. (1975). Short chain aliphatic acid anions in oil field waters and their contribution to the measured alkalinity. *Geochimica et Cosmochimica Acta*, *39*(12), 1707–1711.

Wolery, T. J. (2010, December 13). EQ3/6 A Software Package for Geochemical Modeling (Version 05) [Computer software].

Woodworth, R. C., Butcher, N. D., Brown, S. A., & Brown-Mason, A. (1987). 1H NMR Study of Effects of Synergistic Anion and Metal Ion Binding on pH Titration of the Histidinyl Side-Chain Residues of the Half-Molecules of Ovotransferrin. *Biochemistry*, *26*(11), 3115–3120.

Wu, G. (2009, May). Amino acids: Metabolism, functions, and nutrition. *Amino Acids*, *37(1)*, 1-17.

Yaxley, J. W., Raveenthiran, S., Nouhaud, F. X., Samaratunga, H., Yaxley, W. J., Coughlin, G., … Wong, D. (2019). Risk of metastatic disease on 68gallium-prostate-specific membrane antigen positron emission tomography/computed tomography scan for primary staging of 1253 men at the diagnosis of prostate cancer. *BJU International*.

Yedjou, C. G., Milner, J. N., Howard, C. B., & Tchounwou, P. B. (2010). Basic apoptotic mechanisms of lead toxicity in human leukemia (Hl-60) cells. *International Journal of Environmental Research and Public Health*, *7*(5), 2008–2017.

Zgirski, A., & Frieden, E. (1990). Binding of Cu(II) to non-prosthetic sites in ceruloplasmin and bovine serum albumin. *Journal of Inorganic Biochemistry*, *39*(2), 137–148.

Zhang, L., Ka Yee Szeto, Wai Biu Wong, Tat Tuck Loh, Sadler, P. J., & Sun, H. (2001). Interactions of bismuth with human lactoferrin and recognition of the BiIII - Lactoferrin complex by intestinal cells. *Biochemistry*, *40*(44), 13281–13287.

Zhang, Y., Zhang, Y., Gao, J., Shen, Q., Bai, Z., Zhuang, X., & Zhuang, G. (2018). Optimization of the medium for the growth of Nitrobacter winogradskyi by statistical method. *Letters in Applied Microbiology*, *67*(3), 306–313.

Zhu, H., Fu, B., Lu, S., Liu, H., & Liu, H. (2018). *Clostridium bovifaecis* sp. nov., a novel acetogenic bacterium isolated from cow manure. *International Journal of Systematic and Evolutionary Microbiology*, *68*(9), 2956–2959.

Zhu, L., Glahn, R. P., Chi, K. Y., & Miller, D. D. (2006). Iron uptake by Caco-2 cells from NaFeEDTA and FeSO4: Effects of ascorbic acid, pH, and a Fe(II) chelating agent. *Journal of Agricultural and Food Chemistry*, *54*(20), 7924–7928.

Zientek, M.L., Loferski, P.J., Parks, H.L., Schulte, R.F., and Seal, R.R., II, 2017, Platinum-group elements, chap. N *of* Schulz, K.J., DeYoung, J.H., Jr., Seal, R.R., II, and Bradley, D.C., eds., Critical mineral resources of the United States—Economic and environmental geology and prospects for future supply: U.S. Geological Survey Professional Paper 1802, p. N1–N91

APPENDIX A

ESTIMATED STABILITY CONSTANT AND ENTROPY OF COMPLEXATION FOR ADDITIONAL METAL-AMINO ACID COMPLEXES PREVELANT IN BIOLOGICAL SYSTEMS

Stability constant and entropy of complexation for additional metal-ligand complexes of biological relevance were obtained using methods adopted in Chapter-2 and Chapter 3. These values were used to calculate stability constant values for a diverse set of metal-ligand complexes from 0 to 125°C.

In Fig. A1, estimates of amino acid stability constants were made using glycinate as the proxy ligand. As may be seen from the set of ligands, glycinate was a suitable proxy ligand for amino acids with aliphatic sidechains (2-aminopentanoate and 2-aminohexanoate), polar sidechains (threoninate and citrullinate) and aromatic sidechains (phenylalaninate and tryptophanate). Equivalent estimates were made for entropy of complexation in Fig. A2. These correlations were able to constrain entropy of complexation within ±2 cal/mol/K for almost all ligands with minor variations. While some of these exceptions are likely to be an artifact of data collection from multiple laboratories using multiple techniques, the deviations for others like β-aminobutyrate may be explained by coordination chemistry principles such as different chelate-ring size. The intercept was set to zero to minimize estimation errors due to limited set of data.

The above estimates along with those made in chapter 3 were used to calculate stability constants for additional amino acids inFig. A3- tyrosinate, phenylalaninate, valinate, leucinate, isoleucinate, 2-aminopentanoate, 2-aminohexanoate, β-alaninate, α-aminobutyrate, β-aminobutyrate, γ-aminobutyrate, threoninate, asparaginate, methiononate, glutamate, argininate, citrullinate and ornithinate.

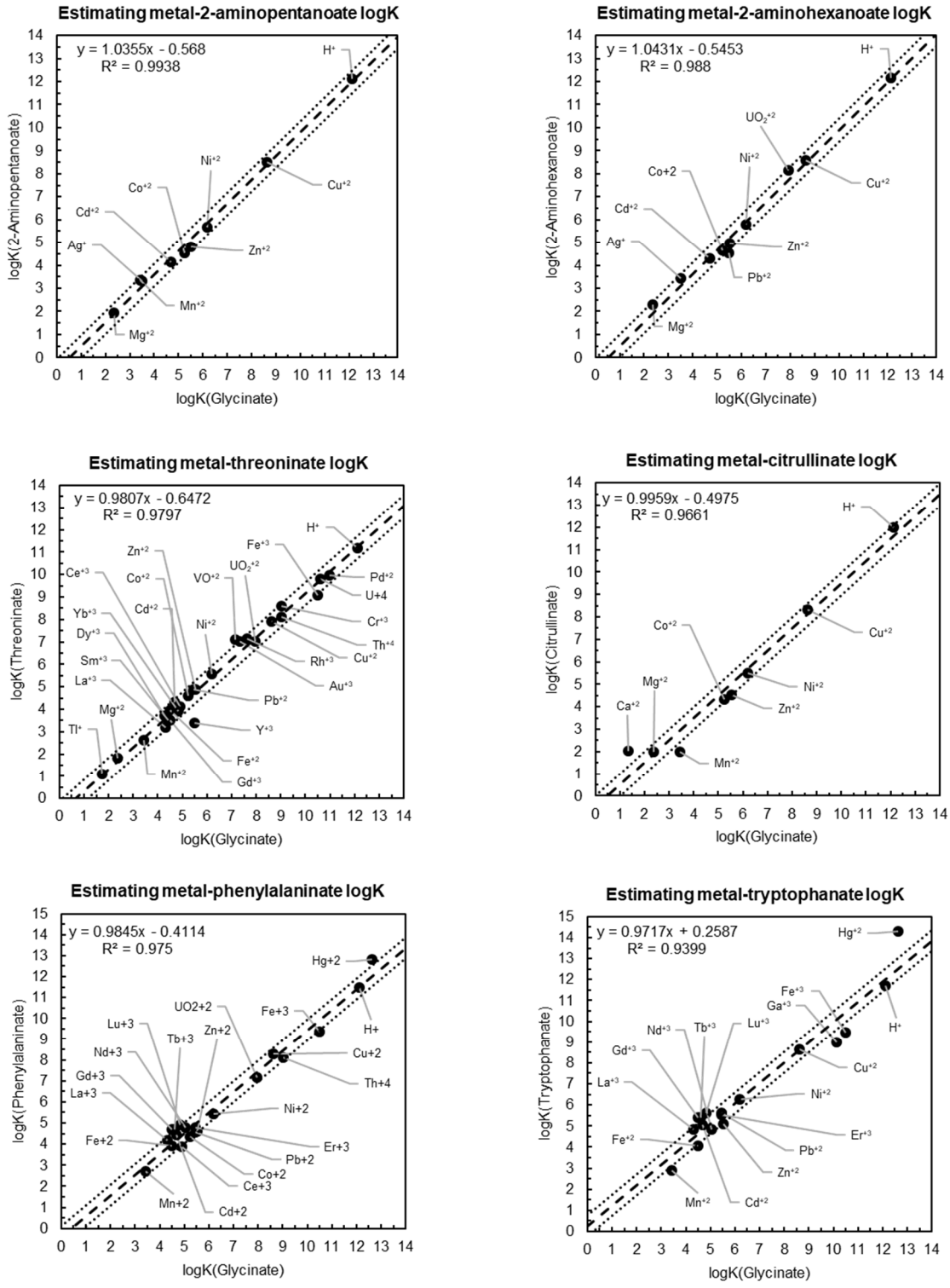

Fig A1. Amino Acid LFERs.

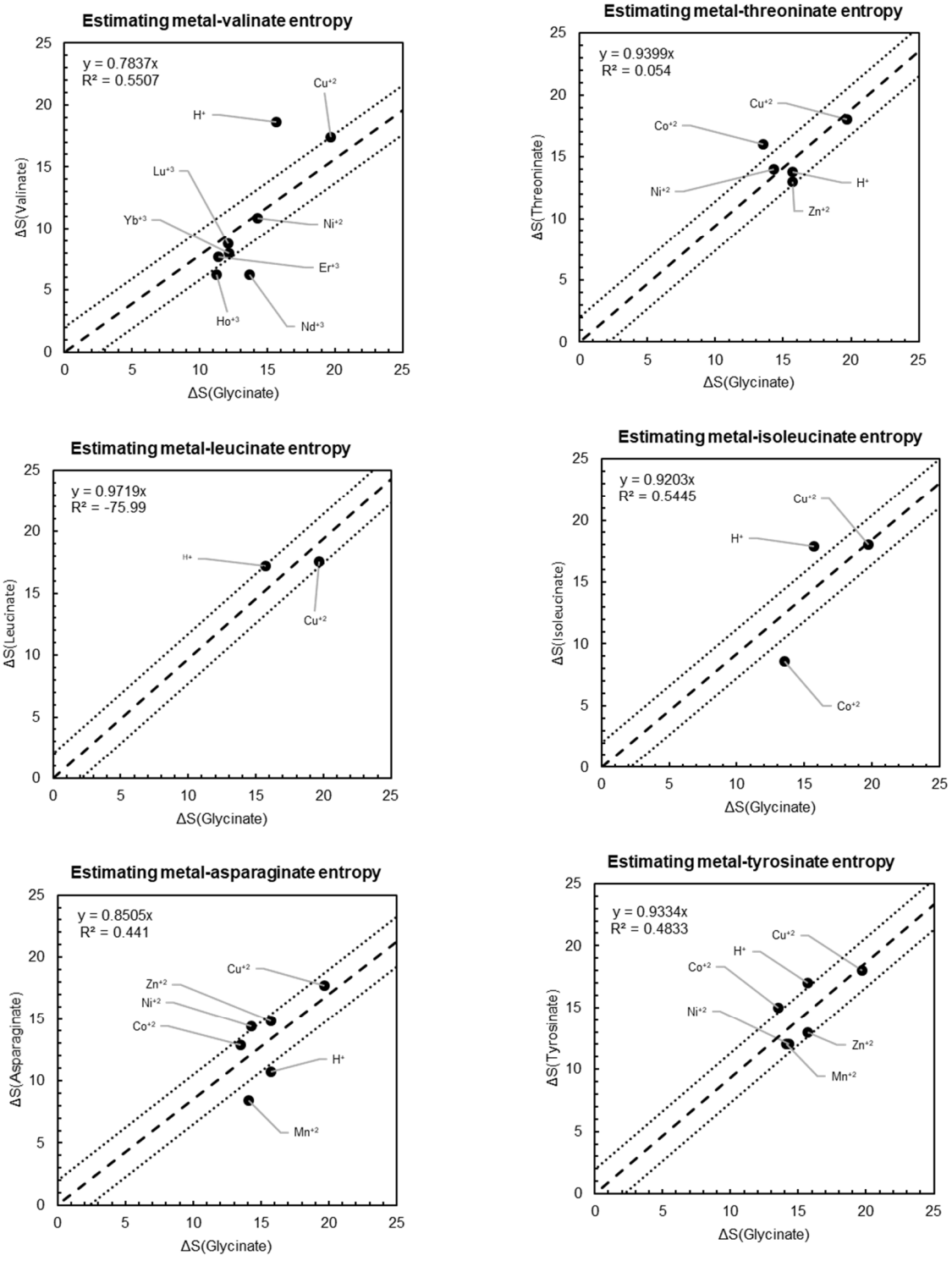

Fig. A2. Amino Acid entropy correlations (contd.)

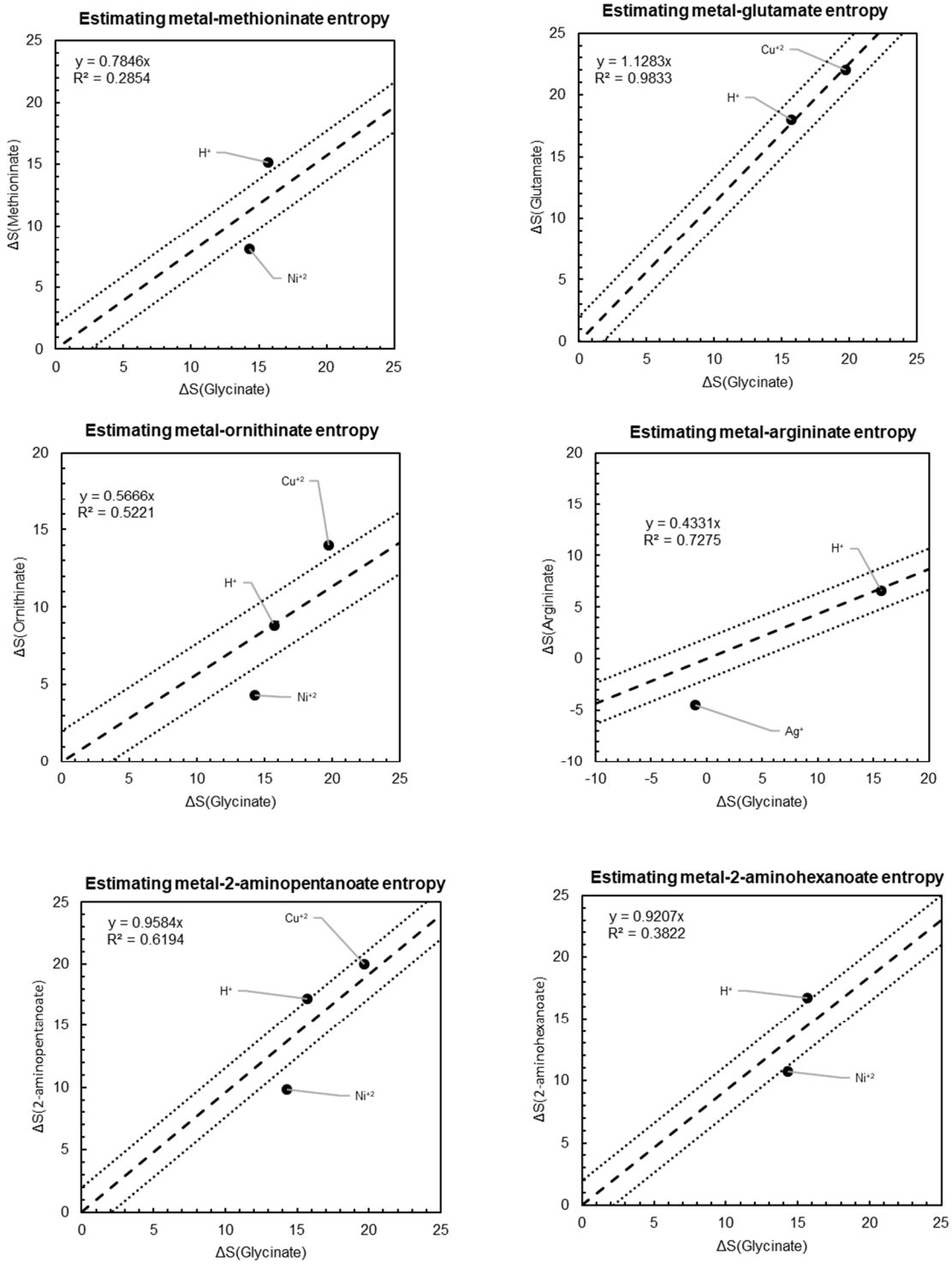

(contd.) Fig. A2. Amino Acid entropy correlations (contd.)

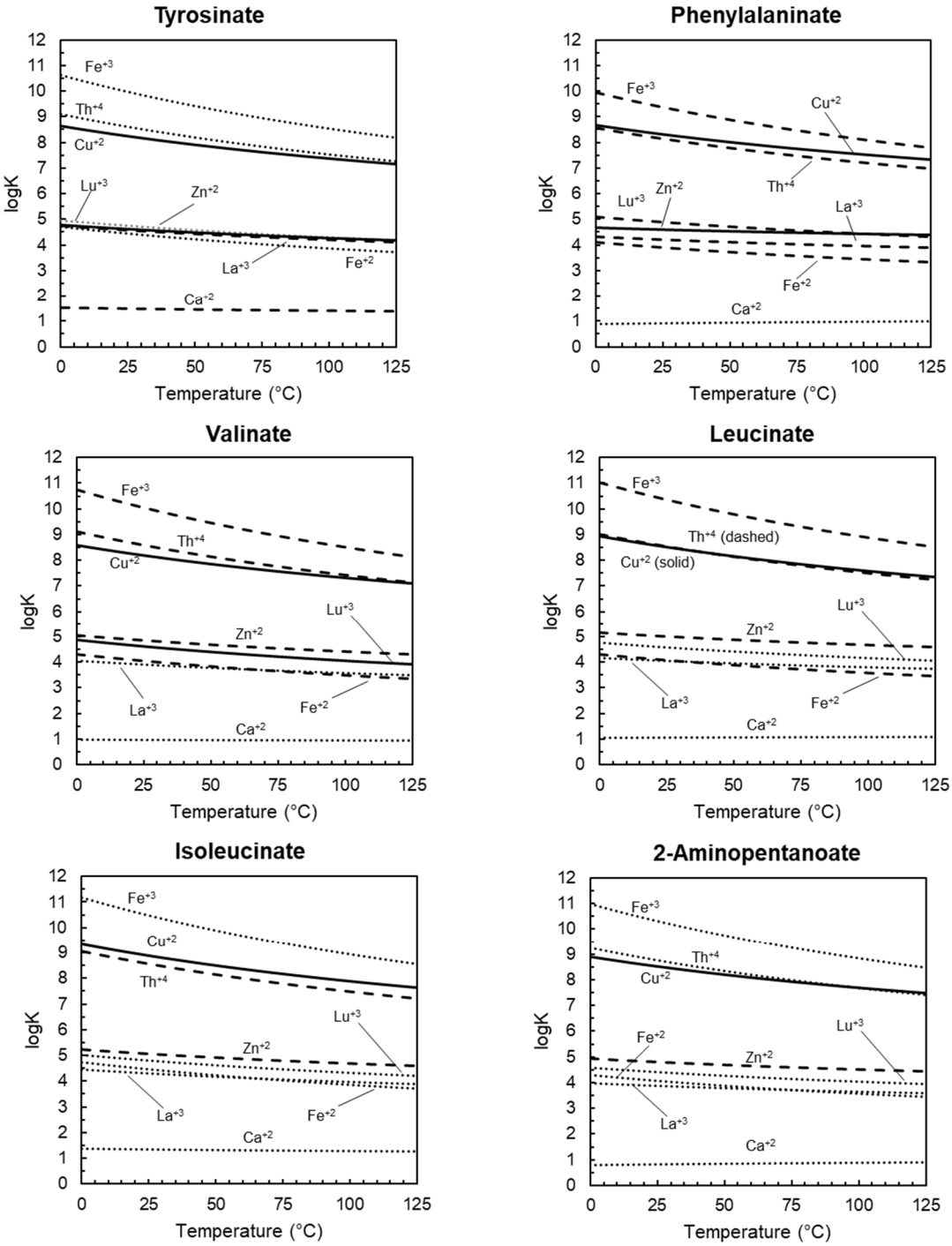

Fig A3. van't Hoff plots for metal-ligand complexes over biologically relevant temperature range. Solid curves represent van't Hoff calculations generated from experimental logK & ΔS, dashed curves represent van't Hoff calculations from experimental logK and estimated ΔS while dotted curves represent van't Hoff calculations from estimated logK & ΔS. (contd.)

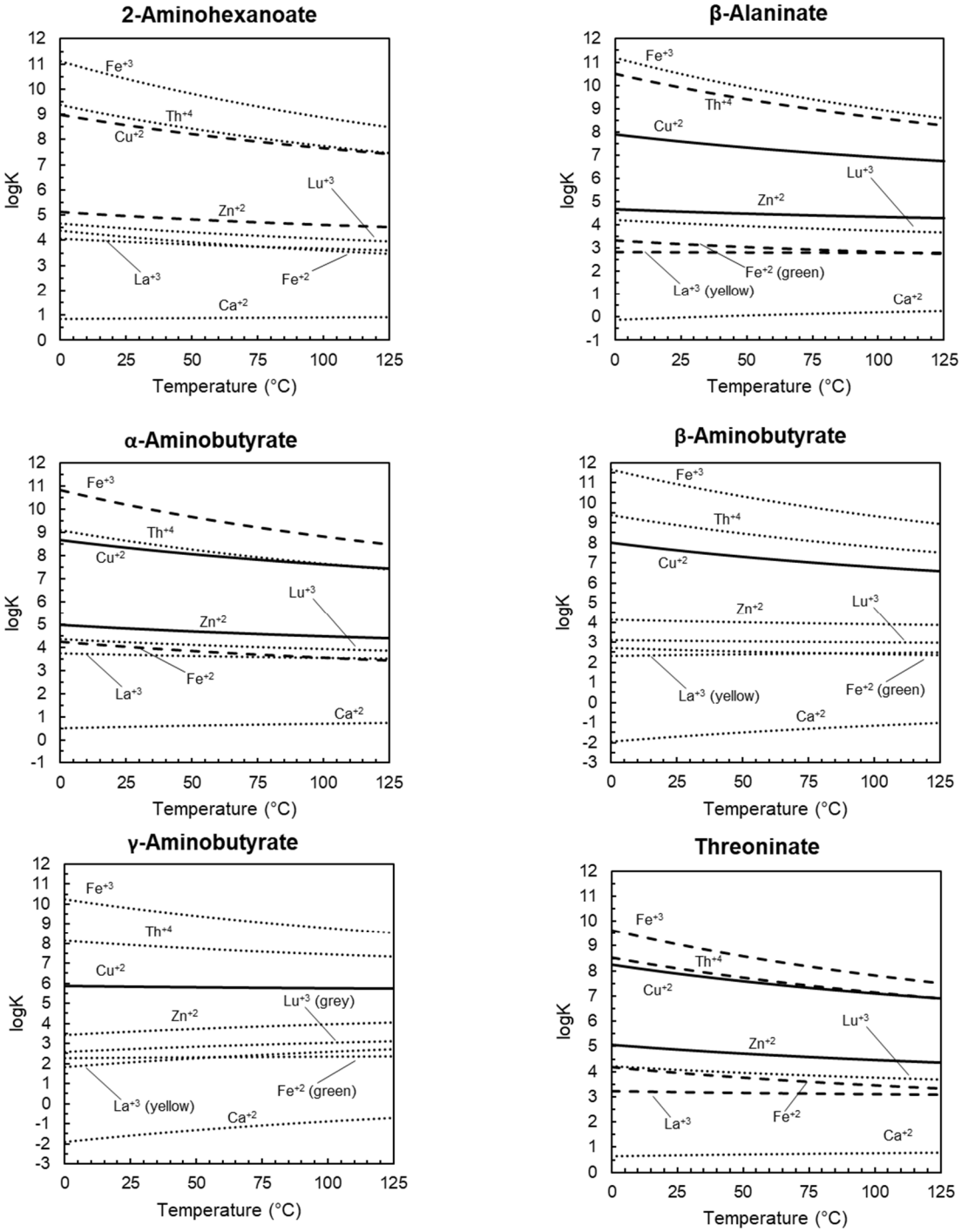

(contd.) Fig A3. van't Hoff plots for metal-ligand complexes over biologically relevant temperature range. Solid curves represent van't Hoff calculations generated from experimental logK & ΔS, dashed curves represent van't Hoff calculations from experimental logK and estimated ΔS while dotted curves represent van't Hoff calculations from estimated logK & ΔS. (contd.)

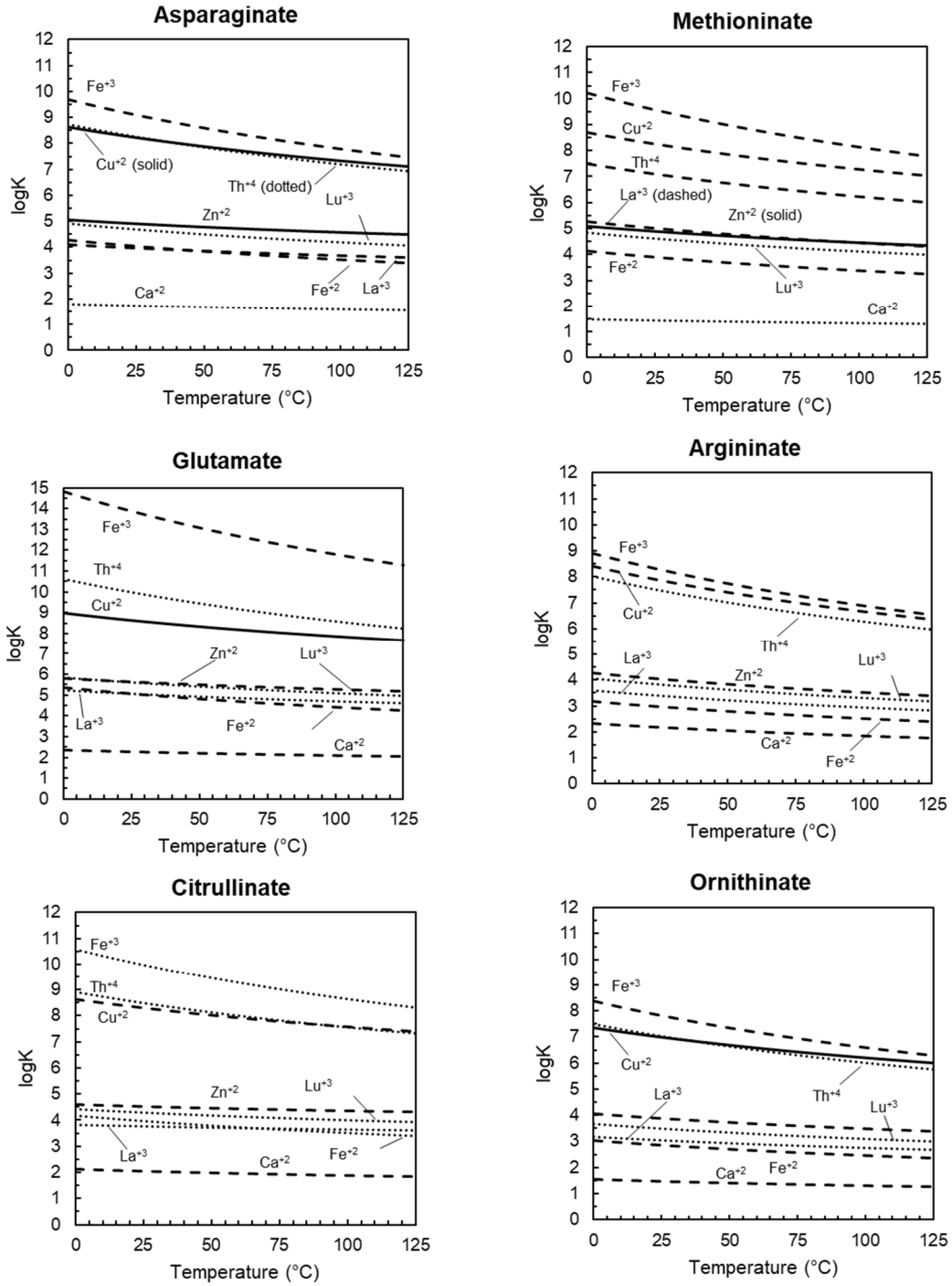

(contd.) Fig A3. van't Hoff plots for metal-ligand complexes over biologically relevant temperature range. Solid curves represent van't Hoff calculations generated from experimental logK & ΔS, dashed curves represent van't Hoff calculations from experimental logK and estimated ΔS while dotted curves represent van't Hoff calculations from estimated logK & ΔS.

APPENDIX B

COMPARISON OF OUR METAL SPECIATION CALCULATIONS WITH CORRESPONDING MEASUREMENTS FROM A SEMINAL MICROBIAL STUDY

In the 1976, Sunda & Guillard published the first study correlating metal speciation and bioavailability (Sunda & Guillard 1976) that eventually gave birth to the free ion activity model (Morel et al. 1978). In the study, the original authors performed copper toxicity experiments for a marine algae in a defined growth medium. They varied the free copper activity by primary altering pH and ligand concentration and measured algal growth rate. Owing to the compositional complexity of the growth medium, the free copper ion activity could not be measured using ion-selective electrodes and were instead obtained using equilibrium speciation calculations. They verified the validity of their calculations by comparing their calculated activity of free copper to copper activity measurements in a simple 'test medium' primarily composed of water, copper and the chelator Tris. We performed a similar comparison in Fig. B1 where the negative logarithm of free copper activity ($pCu= -\log a_{Cu+2}$) was calculated using the equilibrium speciation software EQ3/6 (Wolery 2010). As may be seen from the figure, our simulations are in excellent agreement with the corresponding measurements performed using ion-selective electrodes. The agreement is greater for high free copper activity (low pCu value) compared to low free copper activity (high pCu value) that is understandable owing to higher experimental uncertainty at lower free copper concentration. These results encouraged us to simulate other studies using our thermodynamic database and software.

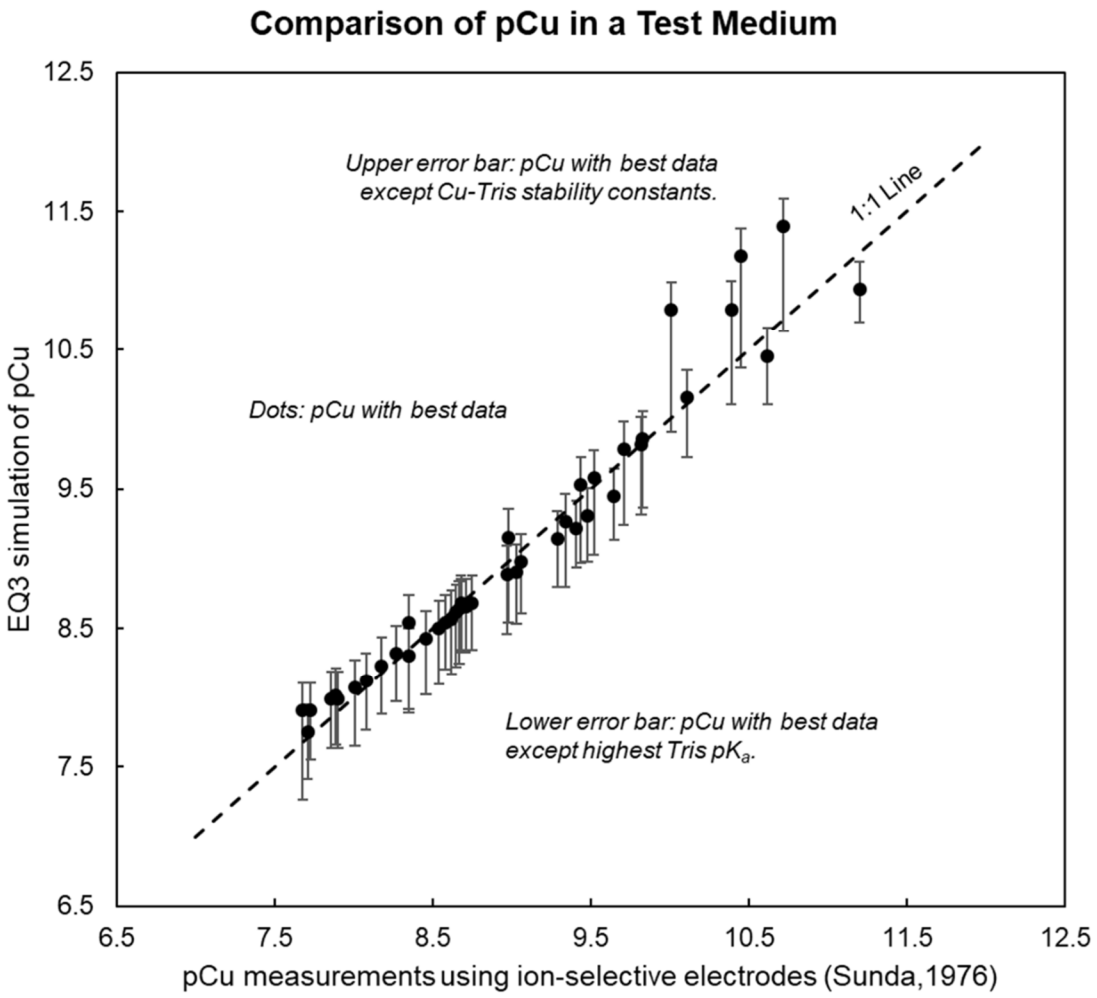

Fig. B1. Comparison of EQ3 calculation of pCu (pCu= -log a_{Cu+2}) with experimental measurements made by Sunda & Guillard 1976. Copper-Tris complexes accounted for over 99% of copper's speciation.

APPENDIX C

PROCUREMENT OF METAL-PROTEIN STABILITY CONSTANTS VIA REGRESSION OF METAL SPECIATION MEASUREMENTS FROM METAL-PROTEIN BINDING STUDIES

We validated our metal-protein stability constant data by regressing metal-speciation measurements of studies reporting metal-protein binding constants. This was primarily performed for the proteins human serum transferrin (hTF) and human serum albumin (HSA) as these are the two predominant proteins found in blood plasma. This regression was crucial for transferrin as several studies report pH-dependent 'stoichiometric constants' that deviates from pH-independent equilibrium constants used in our models. Additionally, many of these metal-binding studies for transferrin were performed before the measurement of the Tyr 188 pK_a at the binding site that was subsequently found to be considerably different from the pK_a of free tyrosine side chain (Sun et al. 2004). Incorporation of this pK_a value in our calculations enabled regression of experimental data with a pH-independent stability constant for several metals.

Equilibrium dialysis experiments of Aisen et al. 1978 were simulated to obtain stability constants of Fe(III)-Transferrin. In these experiments, a semi permeable membrane was used to constrain the large protein molecule to the 'protein compartment' followed by measurement of total iron concentration in the 'protein compartment' and the 'buffer compartment'. As the free ferric ion (Fe^{+3}) could move freely across this membrane, its concentration would be expected to be the same in 'protein' and 'buffer' compartments. As may be seen from Fig. C1, this was found to be the case for most experiments carried out at two different pH. The deviations from the 1:1 line occur at ferric ion molality which can be attributed to the higher measurement uncertainty associated with low concentration. A set of pH-independent stability constant values were obtained ($\log K_1$= 18.0, $\log K_2$= 16.7) that were different from the pH dependent values

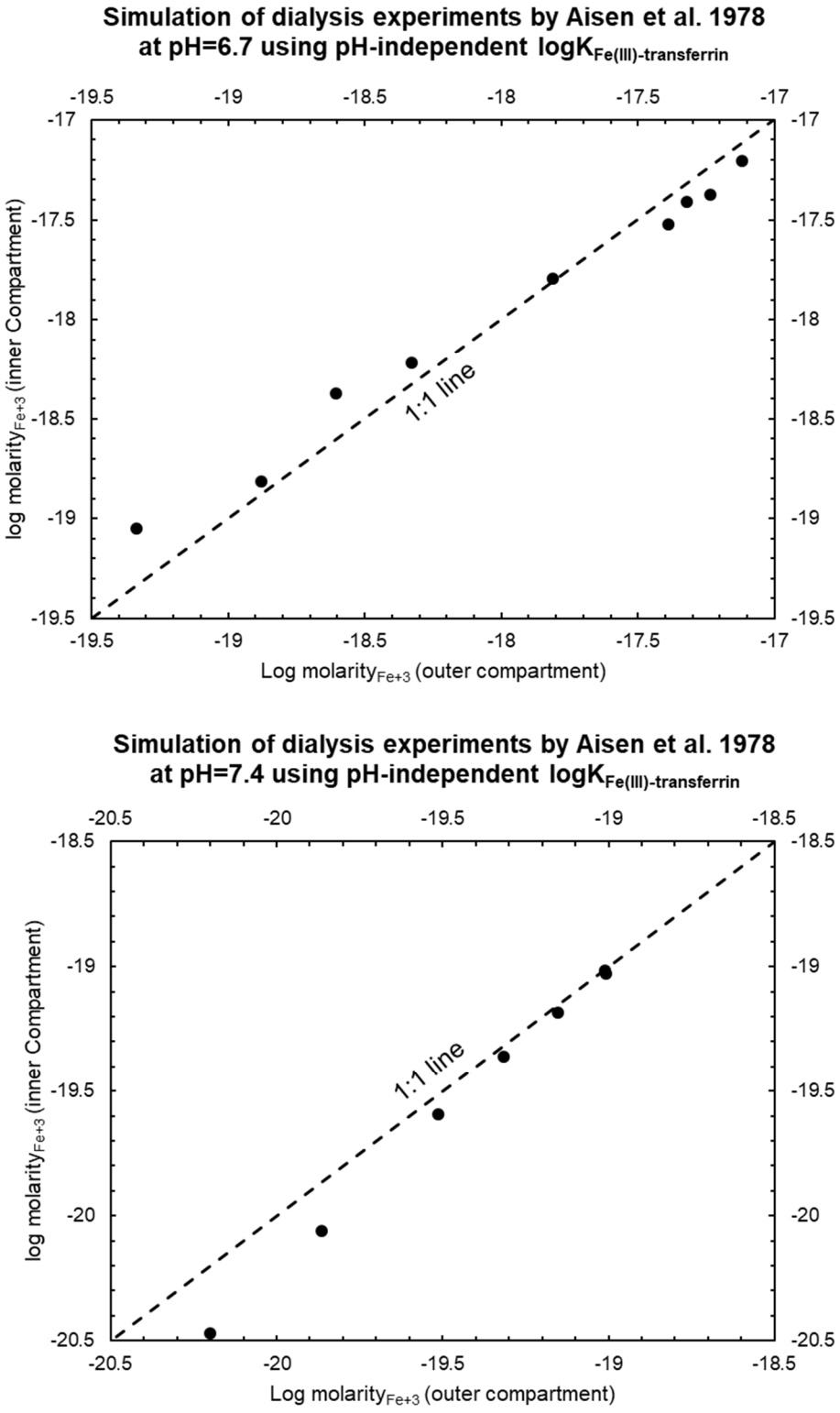

Fig C1. Analysis of dialysis experiments by Aisen et al. 1978 using pH-independent $\log K_{Fe(III)\text{-transferrin}}$ and subsequently published results on Tyr 188 pK_a by Sun et al. 2004.

reported in the original study ($\log K_1^* = 19.5$ & $\log K_2^* = 17.4$ at pH=6.7 and $\log K_1^* = 20.7$ & $\log K_2^* = 19.4$ at pH=7.4).

Analogous regression was performed for transferrin binding studies with Zn^{+2}, Bi^{+3} and Ga^{+3} and are shown in Fig. C2. In these studies, a metal chelator was used as a competitive ligand to control the abundance of metal-transferrin complex that was measured using UV or NMR spectroscopy. The standard state stability constant obtained were slightly different from the stoichiometric constants dependent on pH and concentration of bicarbonate ($\log K_1 = 4.0$, $\log K_2 = 3.0$ vs. $\log K_1^* = 7.9$ & $\log K_2^* = 6.5$ for Zn^{+2}; $\log K_1 = 17.2$, $\log K_2 = 16.4$ vs. $\log K_1^* = 20.1$ & $\log K_2^* = 19.3$ for Bi^{+3}; $\log K_1 = 17.5$, $\log K_2 = 16.2$ vs. $\log K_1^* = 20.4$ & $\log K_2^* = 19.4$ for Ga^{+3}).

Unexpectedly, ligand competition studies for metal-albumin studies were extremely rare (Kiss et al. 2017). Out of the 10 metal ions studied in this work, we only found ligand competition studies for Zn(II)-albumin binding wherein dipicolinate was used as the competing ligand (Bytzek et al. 2009). Zinc speciation was measured using capillary zone electrophoresis- inductively coupled plasma- mass spectrometry (CZE-ICP-MS). In this case, Zn-Albumin stability constants independently reported by Lu et al. 2012 and other relevant stability constants measured by the group (Kiss et al. 2009 and Enyedy et al. 2008) replicated the original experiments within 10% of zinc at high Zn-HSA concentration and within 15% zinc at low Zn-HSA abundance (Fig. C3).

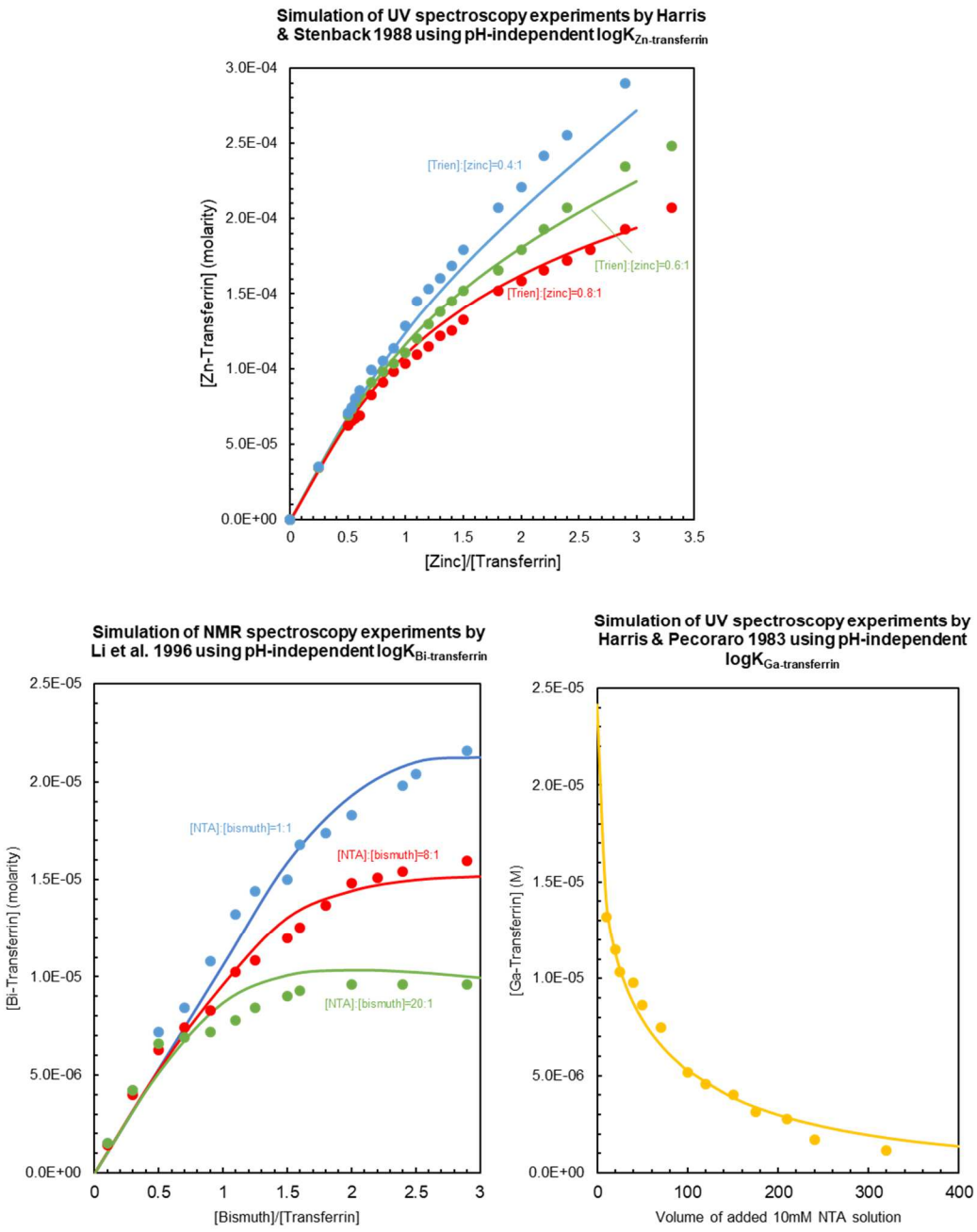

Fig C2. Analysis of UV and NMR spectroscopy measurements used to determine transferrin stability constants with zinc, bismuth and gallium performed by Harris & .Stenback 1988, Li et al. 1996 and Harris & Pecoraro 1983.

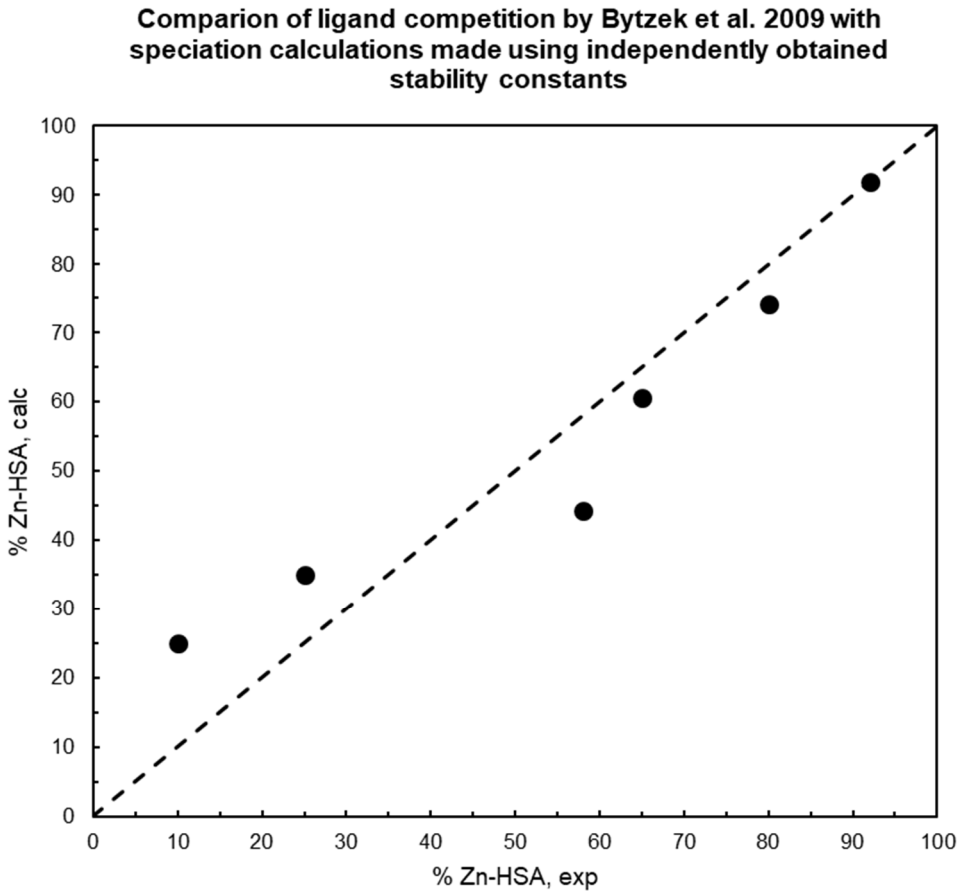

Fig C3. Analysis of CZE-ICP-MS (capillary zone electrophoresis- inductively coupled plasma- mass spectrometry) experiments by Bytzek et al. 2009 in zinc-human serum albumin-dipicolinate system with independently obtained stability constants. The $\log K_{Zn\text{-}HSA}$ used here was used in speciation calculations in this work.